High pressure in-situ combustion tube: commissioning and operation

El Ayadi, Omar Hussein

Award date:
2004

Awarding institution:
University of Bath

HIGH PRESSURE IN-SITU COMBUSTION TUBE : COMMISIONING AND OPERATION

Omar Hussein El Ayadi

Submitted for the Degree of Doctor of Philosophy of the University of Bath

Department of Chemical Engineering
University of Bath
BA2 7AY, UK

June 2004

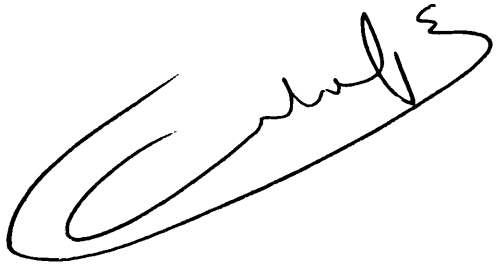

ProQuest LLC
789 East Eisenhower Parkway
P.O. Box 1346
Ann Arbor, MI 48106-1346

HIGH PRESSURE IN-SITU COMBUSTION TUBE : COMMISIONING AND OPERATION

Omar Hussein El Ayadi

Submitted for the Degree of Doctor of Philosophy of the University of Bath

Department of Chemical Engineering
University of Bath
BA2 7AY, UK

June 2004

DEDICATED TO

MY PARENTS (Hussein and Mabrouka)

MY WIFE (Salma)

MY CHILDREN (Hager, Nabeh, Nedal, and Nader)

MY FRIENDS.

(I lost My Father on 06 – 05 – 04, That is the destiny)

AKNOWLEDGEMENT

I would like to express my deepest gratitude to my supervisor, Professor Malcolm Greaves, who being most generous with his time, providing valuable guidance and encouragement throughout the project.

Gratitude is also extended to Dr.R.Rathnone for his useful discussion.I would like also to express my appreciation and my thanks to the secretaries, technicians and especially to Sally Barker and Mac Forsyth, in the Department of Chemical Engineering, for their helps.

I wish to express my appreciation to, the Libyan Secretary of Education for financial support.

Finally, I would highly appreciated my family for their continued support, help, encouragement and prayers.

Abstract

There are many air injection projects which are ongoing in various parts of the world, for both light and heavy oil recovery. Until recently, it was believed that the in-situ combustion (ISC) process was applicable only in heavy crude oil reservoirs, where the fuel for the process is generated by thermal cracking, and vis-breaking. However, in deep light crude oil reservoirs, air injection may be widely applicable if the process is auto-ignition stable, given that the oil and reservoir rock are sufficiently reactive.

A series of tests was carried using a High Pressure 'Combustion Tube' apparatus, first to test and improve the controlability of the system, and secondly, to carry out detailed combustion tube experiments on a light crude oil at high pressure.

Nine runs were performed using Ekofisk light oil. Mud Industry (MI) Calcium Carbonate was used as reservoir core, instead of Ekofisk chalk. The operation conditions were at 100 bar to 200 bar pressure, varying the air injection flux and oil saturation ranging from 30 to 70%.

Following initial trials, a number of successful combustion tube experiments were achieved, i.e. combustion front propagation was sustained with significant oil recovery of 40 to 95 % OOIP. Notably, steady combustion front temperatures were in the range 550-600 °C. The ISC process required high air injection flux, with the minimum being around $21 m^3/m^2 hr$. However, there were several occurrences of very high temperature (900°C) due, inpart, to accumulation of oxygen radicals in the oil ahead of the combustion front. The low temperature oxidation taking place in that region produced some severe alteration of the calcium carbonate matrix, causing dissolution of the matrix. This resulted in hollow cavities, of 'Conche shell'- like appearance, with a calcined, hard exterior.

Contents

NOMENCLATURE

Abbreviations:

Symbol	Definition
AAV	Air actuated valve
AIP	Air injection process
AOFMV	Air operated flow meter valve
AOP	Air operated pump
API	American Petroleum Institute
A_r	Air Requirement
ARC	Accelerated Rate Calorimetery
BV	Ball valve
CAR	Manual CPC
COFCAW	Combustion of forward Combustion and water flooding
COSH	Combustion Override Split-Production Horizontal well
CPC	Current to pneumatic converter
CPU	Central process unit
CT	Combustion Tube
DAQ	Data acquisition
DDP	Double displacement Process
DSC	Differential Scanning Calorimetry
EOR	Enhanced Oil Recovery
F	Filter
GC	Gas Chromatograph
GSGI	Gravity stabilized gas injection
GUI	Graphical user interface
HASD	Heated Annulus Steam Drive
HCPV	Hydrocarbon Pore Volume
HDC	Hydrocracking
HDM	Hydrodemetalisation
HDS	Hydrodesulphurisation
HIHP	Horizontal Injector Horizontal Producer
HPS	High pressure separator
HTO	High Temperature Oxidation
ID	Internal diameter
IOR	Improved Oil Recovery
ISC	In-Situ Combustion
ISC	In Situ Combustion
LD	Level detector
LED	Light emitting diode
LMF	Mass flow meter
LPS	Low pressure separator
LTO	Low Temperature Oxidation
MTO	Medium Temperature Oxidation

OD	Outside diameter
OOIP	Original Oil In Place
OWIP	Original Water In Place
PCGD	Pressure Controlled Gravity Drainage
PD	Pressure difference (shell-tube pressure)
PG	Pressure gauge
PID	Proportional integral derivative control
PPRV	Precise pressure reduction valve
PRVG	Manual PPRV
PT	Pressure transducer
SAGD	Steam-Assisted Gravity Drainage
STARS	Seam and Thermal Additive Reservoir Simulator
SV	Solenoid valve
TA	Axial thermocouple
TC	Thermocouple
TDA	Thermogravemetric analysis
TGA	Themogravimeteric Analysis
THAI	Toe-to Heel Air Injection
TL	Line thermocouple
TW	Wall thermocouple
U_a	Air Flux
U_b	Combustion Front Velocity
VAPEX	Vapor Extraction
VI	Virtual instrument GUI
VIVP	Vertical Injector Vertical Producer
WinProp	Window fluid properties simulator
WTM	Wet Test Meter

Greek Letter:

ρ	Fluid Density	Kg/m^3
μ	Fluid Viscosity	Pa-s
ϕ	Matrix Porosity	Fraction
α	Thermal Diffusivity	$m^2\ s^{-1}$
Γ	$\left(\frac{CO}{CO+CO_2}\right)$	Fraction
τ	Control time constant	

Variable Subscripts :

F	Field Scale
g	Gas
i	Reaction Regime
M	Model Scale
m	Reaction Order
n	Reaction Order
o	Oil
w	Water

Variable Symbol :

Variable Symbol	Definition	Dimensions
AFR	Air to Fuel Ratio	M^3/m^3
AOR	Air To Oil Ratio	M^3/m^3
C_f	Instantaneous Concentration of Fuel	
CO	Carbon Monoxide	
CO_2	Carbon Dioxide	
D	Distance	m
E	Activation Energy	J/gmol
h	Thickness	m
H	Heat of reaction	$Kcal/kgO_2$
H/C	Hydrogen to Carbon Ratio of Fuel	
k	Absolute Permeability	D
K	Reaction Rate Constant	t^{-1}
K_h	Horizontal Permeability	D
K_v	Vertical Permeability	D
l	Length	m
m	Molar Ratio $\left(\frac{CO}{CO+CO_2}\right)$	Fraction
P	Pressure	bar
P_{O2}	Partial Pressure of Oxygen	bar
R	Universal Gas Constant	J/K-gmole
R	Universal gas constant	
S_{gi}	Initial Gas Saturation	Fraction
S_{oi}	Initial Oil Saturation	Fraction
S_{or}	Residual Oil Saturation	Fraction
S_{wi}	Initial Water Saturation	Fraction
S_{wr}	Remaining Water Saturation	Fraction
T	Absolute Temperature	°C
t	Time	t
WAG	Water Alternating Gas	m/m^3
WAR	Water Air Ratio	m/m^3
x	H/C Ratio	

CHAPTER ONE

INTRODUCTION

Introduction

Petroleum plays a large role in providing the day-to-day energy needed to sustain economic development and quality of life. Its importance, as a major source of energy, is due to two main reasons ; Firstly, renewable resources, such as, solar and wind energy require further development to solve technical and practical problems before they can compete reasonably with oil. Secondly, nuclear energy needs further technical progress to overcome serious environmental and safety concerns. Therefore, oil and gas will remain by far, the main source of energy for the foreseeable future. The increase demand for oil and the decline in the discovery of new reserves has forced the petroleum industry to improve methods

In-Situ Combustion (ISC) is one of the Improved Oil Recovery (IOR) methods. ISC can be applied in many depleted reservoirs, or in viscous crude reservoirs. Recently, most of the pilot and or field projects utilize air as an injectant gas, instead of oxygen or enriched oxygen. Self, or induced ignition, can be used when air is injected , depending on several factors i.e. fluid properties, and reactivity at reservoir conditions (pressure and temperature). The factor that control and enhance oil recovery can be studied experimentally in the laboratory, or computationally, utilizing reservoir simulation.

The ISC process can achieve high performance in displacing light, medium and heavy crude oils. Air injection is a good candidate to improve oil recovery due to availability of the air. Depending on the crude oil and reservoir conditions, low, and high (LTO, MTO, and HTO) may be achieved. The main constituent of air, nitrogen, acts either to produce a miscible or immiscible gas displacement, depend on the operating reservoir pressure. Mostly, the immiscible displacement occurs, especially in depleted reservoirs.

Temperature increase due to oxidation generate heat, from combustion, reduce the crude oil viscosity, and even density, if any gas dissolved in the oil. Moreover, oil and water will evaporate, producing displacement gases. Water vapor acts as a steam drive ahead of

the combustion front, assisting the sweep efficiency especially in thick oil layer. Also, the condensed steam, acts to produce a hot water flood ahead of the combustion front.

The produced gases from combustion i.e. about 15% CO_2, will provide CO_2 displacement, mainly immiscible. This increased oil mobility is due to reduction of oil density and viscosity.

In the ISC process, many sub-processes occurs simulateously. ISC is therefore, a complex process, compared to other improved oil recovery (IOR) processes. There are no specific correlations, or formulas that can be used to predict oil recovery using the ISC process. There are several factors which influence the performance of the ISC process. One of the difficulties, is that is impossible to predict the type and the order of chemical reaction that may occur. Any variation in conditions, or experimental design, or procedure, can give different results. Different methods of ISC reaction occurs in: high pressure combustion tube, Small Batch Reactor (SBR), Accelerating Rate Calorimeter (ARC), thermogravimetric analysis (TGA) and Differential Scaning Calorimeter (DSC).

A high pressure combustion tube system was designed and built at the University of Bath, over 10 years ago. It was designed as a fully automated system. First commissioning runs were conducted by El Ayadi, 1993. However, the experiments were completely unsatisfactory, due to the low oxygen flux achieved. Moreover, the Macsym 260 was unable to handle the multitasking operations, resulting in poor control process (Computer system). During the course of 1997, the combustion tube facility was re-commissioned by Young, 1997, and four in-situ combustion tests were completed. The commissioning work involved the development of control and data acquisition software using LABVIEW, specifically IscVIEW. This enabled the experiments to be run automatically under computer control. A number of combustion tube runs were completed, on West of Shetlands Clair oil (19.7°API), at pressures of 50-100 bar. The results indicated that very high oil displacement could be achieved in areas of the core that were swept by the combustion front, thus demonstrating the potential improvements in recovery which can be achieved using ISC.

Prior to the processed investigation, the high pressure combustion tube facility had been used for a number of research projects. For example, in 1998, tests were carried by Greaves *et al*, 2000 on West of Shetlands Clair Oil and also a Light Australian Oil, at pressures of between 70 bar and 100 bar. In the case of the Clair Oil, it was found that, combustion front temperatures of around 400 °C were typical, indicating HTO was occuring. Temperatures were much lower, however, in the case of the Light Australian Oil, with the combustion zone typically reaching 250 °C.

Further studies have been carried out by using the combustion tube for investigations i.e. El-Usta, 1998, who, examined the feasibility of air injection into deep light oil reservoirs. It was found that most of the light oils tested were sufficiently reactive to allow the Low Temperature Oxidation process to take place.

Before commencing any investigation, extensive recommissioning work was needed in order to achieve adequate controllability, and also to extend operation to 200 bar pressure.

It was decided to design a series of experiments to fulfill the following objectives:

- Successfully start up the combustion tube system.
- Carry out work to ensure full integrity of the system, i.e all components functioned properly.
- Identify the optimum method for controlling the shell/tube ΔP, particularly during transient pressurisation.
- Minimise the venting of gas from the system, particularly during the pressurisation stage to minimise operating costs and prolong experiment time.
- Test the system backpressure control.
- Test the control of liquid level in the high and low pressure separators.
- Test the accuracy of the combustion tube thermocouples, axial, wall, line pressure.
- Test temperature control for the ignitor and band heaters (BH).
- Test overall multitasking computer control.
- Conduct actual runs using different crude oils.

The structure of the thesis is arranged by chapters : Chapter Two is literature review, Chapter Three, describes the equipment, commissioning tests, and experimental procedure, Chapter Four, presents experimental results, discussions and simulation part, Chapter Five, contains the conclusion and recommendation for the future work.

Objective of the Research :

The aim of the research was to investigate the in-situ combustion performance of a light crude oil at high pressure, simulating actual reservoir conditions, similar to the Ekofisk field. In addition, it was considered important that initial reservoir fluid state i.e. fluid saturation, was varied, as was the air injection flux. To gain further understanding of the process involved, numerical simulation studies of the experiments were undertaken using the STARS reservoir simulation.

CHAPTER TWO

Literature Review

2.1: AIR INJECTION:

Gas injection into petroleum reservoirs is an established technique for maintaining the initial reservoir pressure. For economic reasons the source of suitable gas to inject is very important.

Hydrocarbon associated gas with produced oil is recycled into the reservoir for economic and safety reasons, especially, if the transportation cost is too great. Generally the gas injected into the reservoirs should not creat problems such as formation fracturing, cooling or freezing of the wet gas in injection well.

The first application of air injection as a gas-drive dates back to 1911, near Merietta, Ohio. Air was compressed to 2.7 bar and injected into one well 4248 m^3 /day, to drive oil to near-by surrounding wells, Uren, L.C. 1939.

Underground combustion was discovered accidentally, when air was injected and oil production increased due to heating in the reservoir. However, neither of the effect was attributed to a subsurface fire, Schumacher, 1980. In the Soviet Union in the late 1930's, the first experiments on the in-situ combustion (ISC) was conducted. Mobil and Sinclair oil companies carried out tests in 1952. Mobil's work concentrated on tar sands, while Sinclair targeted unrecoverable light oils left in the reservoir after a waterflood.

During the period 1950-1965, considerable laboratory work was performed, especially by Mobil and Gulf Oil Companies. In 1962, the first field test of simultaneous air/water injection was conducted in the Loco field of Southern Oklahoma. The process is known as a combination thermal drive (CTD). In 1967, Amoco, Exxon and Shell published papers on a modified process of in-situ combustion called " Combination of Forward Combustion and Water Flood" (COFCAW). This was a major break through for ISC. During 1965-1975, mature projects experienced many operational difficulties and

problems. Since 1975, interest in in-situ combustion has been ebbing because of the previous problems associated with it (Farouq Ali., 1994), but there is now renewed interest in air injection for application in light, medium and heavy oil reservoirs.
So far, more than 160 in-situ combustion pilot tests of various types have reported Turta 1994. There are now more than sixteen active commercial projects worldwide and wider acceptance of the process is anticipated, as previous problems are now understood and great gains have made in new proving technologies. Air injection now embraces all previous oxidation processed in an oil reservoir.

Over the years, Gulf Coast operators have injected flue gas, nitrogen, natural gas and carbon dioxide to improve recovery in light-oil salt dome reservoirs. Each of these gas injection is more expensive than air. This is because air is free, and available everywhere. Operators avoided air injection due to concerns associated with the presence of oxygen in the reservoir (bacterial growth, emulsions) and in production equipment (severe corrosion, risk of explosions).

The benefits of air injection in low-pressure oil reservoirs include: 1) additional oil recovery as a result of the Double Displacement Process, 2) repressurisation, and 3) repositioning the oil rim in close proximity to existing wells. Each of these benefits contributes to improved oil recovery.

Air injection can also improve gravity drainage, if the pressure is high enough. Carbon dioxide is released by combustion and is absorbed by the reservoir oil. The carbon dioxide swells the oils and lowers the oil's viscosity, thereby improving the gravity drainage. The combustion process consumes almost no mobile oil. Laboratory and modeling results show that the process consumes only the immobile oil found (Gillham *et al*, 1997).

Air injection offers unique economic and technical opportunities for improved oil recovery in many candidate reservoirs. Concentrating on the economically-advantaged class of light oil reservoirs, potential process benefits include:

1) Excellent displacement efficiency of gravity stabilition, i.e dipping reservoir,
2) Rapid reservoir pressurization,AMOCO Report, 1997
3) Flue gas stripping of the reservoir oil,
4) Oil swelling,
5) Injection gas substitution.
6) For air injection into high pressure, hot reservoirs additional benefits may accrue,
7) Spontaneous oil ignition and complete oxygen utilization,
8) operation above the critical point of water, with possible super-extraction benefits, and
9) Near-miscibility of the generated flue gas and the oil.

Items 1-5 have received much attention in the technical literature, while 6-8 have been highlighted by Fassihi *et al*, 1994.

The Air-Oil Ratio (AOR) characterizing incremental oil production form air injection can vary typically in the range of 4000-9000 scf/bbl (about 700 to 1600 vol/vol), Surguchev *et al*, 1999.

The objective of air injection in light-oil reservoirs is the complete consumption of the oxygen at reservoir temperatures. In high-temperature oxidation (HTO) or in-situ combustion with heavy oils, CO_2 and H_2O are produced. LTO of heavy oils generated hydrocarbons, such as aldehydes, ketones, carboxylic acids, alcohols, and hydroperoxides, as well as small amounts of CO_2 and CO, Greaves *et al*, 1999.

2.2: In-Situ Combustion Process:

In-Situ Combustion, is a one of a number of thermal processes, including hot water drive and steam injection, Don *et al*, 1998. In the ISC process, thermal energy is generated in the reservoir by oxidation reaction, which may be initiated with either an electric heater or gas burner or may be spontaneous. Oxygen, as air or enriched air is compressed at the

surface and continuously injected into the reservoir; either dry (dry process) or together with water (wet process). The heat generated in the reservoir, causes the lighter components of the oil to vaporise and move ahead. Depending on the combustion and maximum temperature attained, thermal cracking may occur, and vapor products from this reaction also move downstream. Through cracking of the oil part of the oil is deposited as a coke-like material on the reservoir rock, and this solid material serves as the fuel in the process. Thus, as oxygen injection is continued front slowly propagates through the reservoir. The process of in-situ combustion is illustrated in Figure 2.1.

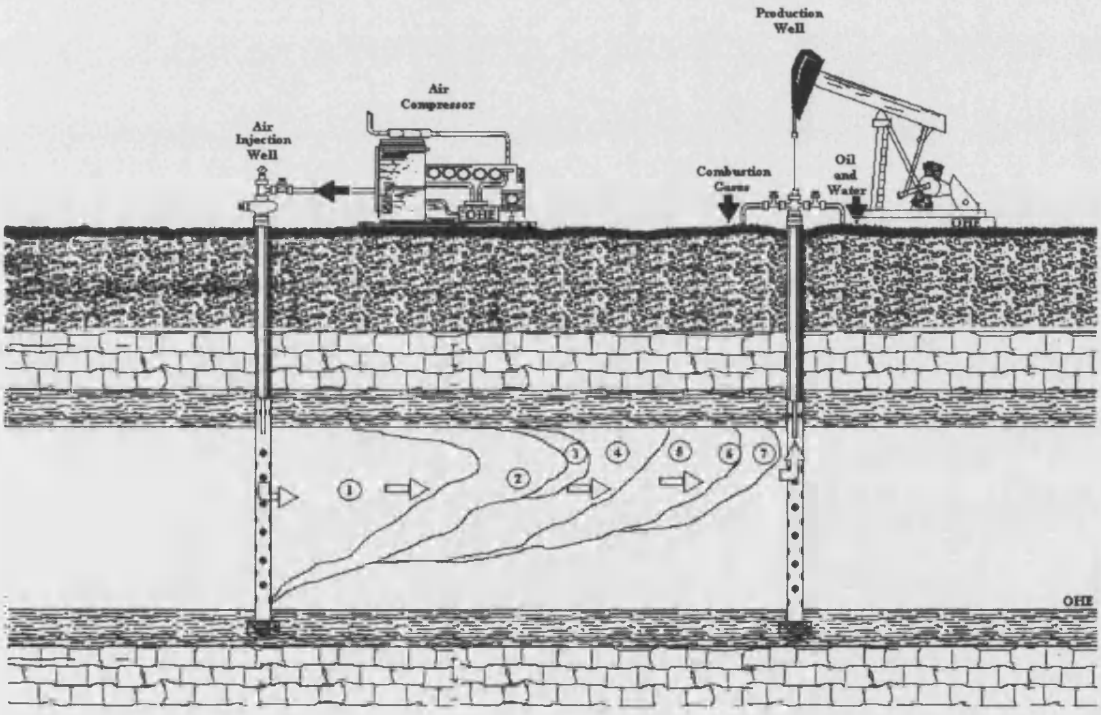

① Injected Air and Water Zone(Burned Out)
② Air and Vaporized Water Zone
③ Burning Front and Combustion Zone (600° – 1200°F)
④ Steam or Vaporizing Zone (Approx. 400°F)
⑤ Condensing or Hot Zone (50° – 200°F)
⑥ Oil Bank (Near Initial Temperature)
⑦ Cold Combustion Gases

Figure 2.1: Combustional Heavy Oil, In situ Combustion Process

2.3: Limitations and Disadvantages of In-Situ Combustion :

A major problem with the in-situ combustion method is to control the movement of the combustion front. Depending on reservoir properties and fluid distributions, the combustion front may move in a non-uniform manner through the reservoir, with resulting poor volumetric sweep. Also, if proper conditions are not maintained at the combustion front, the combustion reaction can weaken and cease completely. The process effectiveness is lost if this occurs. Finally, because of the high temperature generated, significant equipment problems can occur at the wells. Pollutant emission control also can be of concern in some cases.

Other problem with the combustion process include formation plugging by swelling clays contacted by fresh, condensed water ahead of the combustion front, by over-burning of the reservoir as the injected air tends to move toward the top of the formation, and by preferential up-dip burning in the titled patterns of steeply dipping beds. Mechanical problems include severe corrosion in producing wells and the formation of oil-water emulsions, which may require extensive and expensive treating.

Once any well or reservoir exposed to in-situ combustion and failed, it will be difficult to predict future recovery, especially if the same process repeated, or to establish any further improving oil recovery method.

2.4: Classification of Air Injection processes:

Air Injection Processes (AIP) were classified by Turta *et al*, 1998, into four categories. The type of AIP used depends mainly on the reservoir temperature and pressure, and the oil and rock properties, Turta *et al*, 1998. The main basis of this classification is their spontaneous ignition potential and gas miscibility at reservoir conditions. Thus the following different categories of air injection process may apply:

1. Immiscible air flooding (IAF) with intensive oxidation (HTO)
2. Immiscible air flooding (IAF) without intensive oxidation (LTO)
3. Miscible air flooding (MAF) with intensive oxidation (HTO), and High Pressure Air Injection process (HPIA)
4. Miscible air flooding (MAF) without intensive oxidation (LTO), and High Pressure Air Injection process (HPIA).

Hence, classic in-situ combustion is an immiscible air flooding process dominated by high temperature oxidation (HTO) and can be applied in light, medium and heavy oil reservoirs, when the reservoir and oil characteristics are beneficial. Failure to apply the process correctly in the past, i.e. in good candidate reservoirs, has been one of the biggest factors mitigating against success. The renewed interest now , is driven either because air is seen as a cheap, available source of gas or because of thermal and oil recovery efficiency.

2.5: In-Situ Combustion Principles:

In-situ combustion is a thermal recovery process, in which air, oxygen, or oxygen-enriched air is injected into the reservoir in order to burn part of the oil (coke) to improve the flow of the unburned part. This coke is a product of chemical reactions between the injected oxygen. The chemical reactions are triggered by an ignition device, or spontaneous ignition (some times called autoignition) when the injected oxygen contacts the oil near the wellbore. This temperature heats the zone surrounding the well to a significantly high temperature, so that continuous air injection causes a high peak temperature wave, or combustion front to propagate through the reservoir. For heavy oils, and also some light oils, usually the temperature reached at the combustion front is much greater than the saturation temperature of water, in most cases between 400 to 600°C Burger *et al*, 1985. Light oils can also operate effectively in low-temperature mode (150 to 300 °C), whereas heavy oils and bitumens operating in this temperature range are dominated by oxygen-addition reactions that immobilise the oil and must be avoided. Heavy oils and bitumens must react above 450 °C to achieve oil-mobilizing bond scission

reactions. Under certain conditions, both oil types can operate under high-temperature (>700 °C) gas-phase combustion, Moore *et al*, 1998. However, these temperatures are too high to be applied safely in many reservoirs, especially carbonate which can decompose.

The combustion temperature depends on to oil type, density and the composition of oil, as well as the air injection rate. The heat generated in the combustion zone causes distillation and vaporization of the oil and water. The lighter fractions of the crude oil are transferred downstream and condense in the cooler zones, and may form an oil bank. The heavier fractions of the oil remain behind and are converted to a semi-solid residue or coke. The amount of solid residual on fuel depends on the cracking reactions, which is dependant on the combustion front temperature achieved.

2.6: Reaction Kinetics of In-Situ Combustion :

The kinetics of in-situ combustion are important because accurate kinetic models can aid in the prediction of oil recovery economics. The reaction kinetics are intimately coupled with fluid flow and heat transfer in the reservoir, and therefore make ISC a very complex process. Reaction kinetics data is also to understand ignition and combustion front propagation. Although extensive work has been carried out for this purpose, a complete understanding of the complex physical and chemical changes taking within the combustion zone is yet to be achieved.

Numerous physical transitions and chemical reactions occur in an in-situ combustion process. Modeling of such a complicated process requires not only a detailed description of the fluid flow characteristics but also insight into the physical and chemical reactions involved, using a reliable kinetics model capable of predicting the progress of these reactions within the process. One solution would seem to simply isolate each component and study its kinetics behavior under all conditions of temperature, oxygen partial pressure, and time; however, this idealistic approach is not practical because of the complex chemical nature of crude oils and the multitude of components involved.

Therefore, kinetic studies should be aimed at groups of reactions rather than individual ones.

There are basically two approaches practiced to obtain kinetic models for use in-situ combustion reservoir simulation. They are: (1) evolved gas analysis (EVA), and (2) thermal analysis techniques such as thermogravimetric analysis and differential scanning calorimetry (DGC). Application of kinetic equations derived by both approaches to ISC reaction modeling requires knowledge of activation energies and frequency factors used in Arrhenius equations, along with the effects of the specific surface are and composition of the rock matrix. Values of activation energies and frequency factors used are average values (needed as input to reservoir simulation) over the temperature range of a given reaction regime, and their accuracy is often low Vossoughi *et al*, 1992.

Figure 2.2 illustrates two main regions of crude oil oxidation. The low temperature oxidation (LTO) region applies up to 300°C for heavy crude oils, but may be much lower for light crude oils, less than 200°C, and a high temperature oxidation region (HTO), above 300-350°C (heavy oil). There is also a intermediate region, MTO or medium temperature oxidation. This is aligned with the produced gases from thermal cracking reactions. Moore *et al*, 1998 has stated that bond scission reaction (thermal cracking) can take place at 200-250°C for light crude oils.

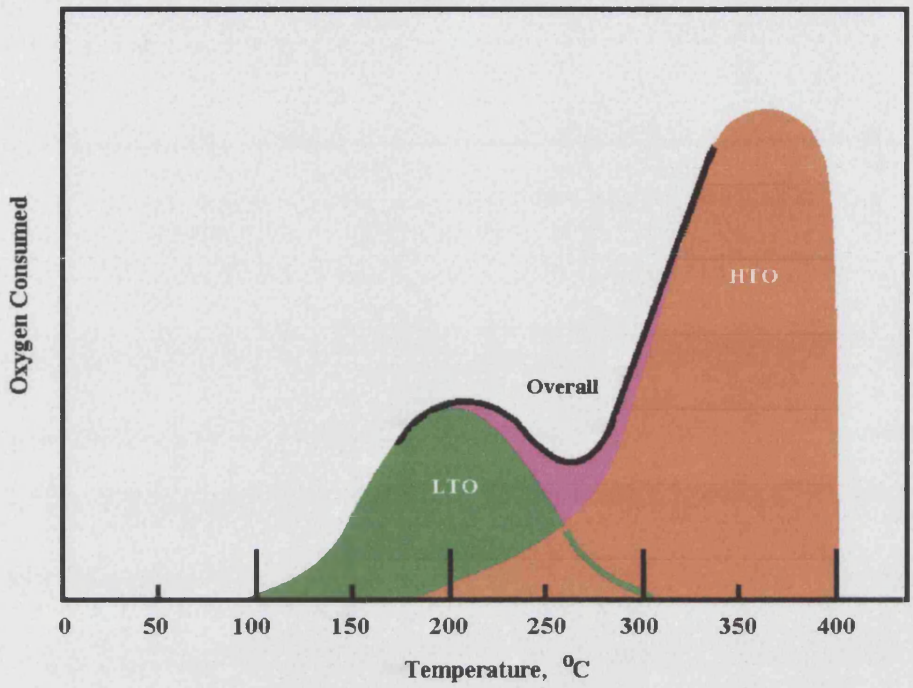

Figure 2.2: LTO and HTO Regions

The combustion kinetics of Maya crude oil was investigated by Greaves *et al*, 1988. They stated that activation energies and reaction rate constants show that dry combustion is kinetically controlled, whereas the wet combustion process is oxygen diffusion limited. The effect of oxygen enrichment appears to be mainly through its effect on combustion peak temperature, leading to an increase in combustion front velocity.

A kinetic study of the combustion of Athabasca tar sand was made by Dubdub *et al*, 1990. Their results indicated the occurrence of several consecutive reactions at different temperature. Both the extent of the LTO reactions and the rate parameters obtained for the high temperature combustion reaction are influenced by the oxygen partial pressure of the feed gas.

Soodhoo *et al*, 1988 studied the kinetics of non-catalytic thermal hydrocracking of Athabasca asphaltenes over the temperature range 350-425°C, in a batch autoclave reactor. The activation energy for asphaltene consumption are found to be 161 kJ mol^{-1}.

In the second, more complex model, four pseudoproducts were used [asphaltenes, maltenes (oil + resin), coke and gas]. The activation energies were found to be in the range 8-200 kJ mol^{-1}. Asphaltene hydrocracking reactions were found to have first-order kinetics.

The oxidation reaction kinetics of bitumen from Athabasca Tars sands have been investigated by Philips *et al*, 1985. Ronther They observed in the first model, that the Athabasca bitumen is considered to be a single react and the oxidation reaction a single irreversible reaction. The activation energy for the overall reaction was found to be 80 $kJmol^{-1}$. This model is limited to calculating the overall conversion of oxygen. Because the fraction of oxygen reacting to form carbon monoxide and carbon dioxide increases with temperature, a more sophisticated model was proposed to take this into account. The second model assumes that the bitumen is a single reactant and that the oxidation of bitumen may be described by two simultaneous, parallel reactions, one producing oxygenated hydrocarbons and water, the other producing CO and CO_2. The activation energy for first reaction was found to be 67 kJmol-1, and for the second, 145kJ mol-1. This more sophisticated model explains the result that at higher temperatures more oxygen is consumed in the oxidation of carbon, because this reaction has a higher activation energy than the reaction leading to the production of oxygenated hydrocarbons and water.

Kok *et al*, 1998 investigated the pyrolysis behaviour and kinetics of six crude oils by DSC and TGA/DTG. The crude oil pyrolysis indicated two main temperature ranges where loss of mass was observed. The first region, between 400 and 600°C, was visbreaking and thermal cracking. Arrhenius-type kinetics was used to determine the kinetic parameters. It was observed that as crude oils gets heavier (°API decreases) the activation energy of cracking reactions increases.

The effect of the oil composition, characterized on the basis of light hydrocarbon, resin and asphaltene contents, on the pyrolysis kinetics of the oil and combustion kinetics of

the fuel, was studied by Ranjbar *et al*, 1991. The results show that the composition of oil and also the heat transfer characteristics of the pyrolysis medium have a pronounced influence on the fuel formation and composition.

Fassihi *et al*, 1984, analyzed crude oil oxygen reactions at different temperatures. The results in LTO region appear to occur between the gas and liquid phases. MTO fuel deposition reactions appear to be homogeneous. The latter were found to be the rate-determining step in clean sands. Natural cores from reservoirs were found to have different kinetic behavior to the clean sands for the following reasons : (1) metallic additives lower the activation energy of the combustion reaction and hence shift the rate-determining step, and (2) clay and finer sands adsorb more fuel.

As reported by Greaves *et al*, the study of crude oil oxidation kinetics is important for following reasons :

- To obtain modeling parameters such as Arrhenius activation energy, order of reaction and pre-exponential factor. Such values are needed for numerical modeling studies of reservoirs.
- To identify the reaction regimes for a particular crude oil, i.e. LTO and HTO . LTO starts at the 'ignition' temperature of the oil and extends up to 300 to 350°C HTO approximately (for combustion) follows LTO and can extend up to 400 to 500°C for light oils.

Tsuzuki, *et al*, 1999 studied the kinetic modeling of oil cracking by hydrothermal pyrolysis experiments using a Japanese oil. They found that the apparent activation energy for cracking of heavy saturates was 76 kcal/mol, which is close to a value published on hexadecane cracking under high pressure in anhydrous conditions. Application of the model to geological conditions shows that the cracking of heavy saturates occurs within a temperature range of 190 to 230°C, which is higher than that usually accepted in petroleum geochemistry.

Coke is a solid material that deposits on the sand-grain surface area and is eventually burned as a fuel during an in-situ combustion process. Coke combustion is the main source of energy to sustain the combustion front. Vossoughi *et al*, 1989, state that the rate of coke combustion was proportional to the coke concentration yet to be burned, oxygen partial pressure, and sand-grain specific area.

Fassihi *et al*, 1984 studied continuous analysis of the produced gases from a small packed bed reactor, isothermally and with a linearly increasing temperature. They showed that the combustion of crude oil in porous media follows several consecutive reactions. They concluded that (1) at low temperatures, the crude oil undergoes oxidation reactions without generating carbon oxides. For some reactive oils, the heat released during this period may lead to spontaneous ignition. (2) as the temperature is increased, distillation, coupled with pyrolysis, produces little hydrogen gas and some light hydrocarbons in the gas phase. A part of these hydrocarbons are produced without being oxidized. However, oxygen reacts with the remainder of these hydrocarbons and, hence, MTO occurs. (3) at higher temperatures, this reaction is completed and a heterogeneous reaction begins. Here, the reactants are oxygen in the gas phase and a heavy residue of oil deposited on the solid matrix.

Tedama, 1959 studied the reaction kinetics by DTA method (DTA). He reported two different combustion reactions, one at about 270 °C and one at 400 °C. Analysis of produced gases showed that oxygen was taken up near 270 °C. A small fraction of oxygen was consumed to form CO and CO_2, while, the majority of oxygen reacted with hydrogen to form water. At 400 °C, mainly CO_2 and CO were formed, with little water and no hydrogen residue. He concluded that, during the first reaction, near 270 °C, mainly hydrogen is burned off, leaving a coke-like residue. This residue can only burn above 400 °C to produce CO_2 and CO. He also reported that the atomic hydrogen/ carbon ratio of burned fuel decreased with temperature.

Weijdma, 1968, identified three successive stages in oxidation of oil, (1). At low temperature oxygen is taken up in the oil molecules, presumably without any particular degradation of these molecules, (2) at increased temperature oxidative cracking occurs accompanied by the production of CO_2 and H_2O, which leaves coke residue; (3) at still higher temperatures the coke, which consists of partially pure carbon, is burnt.

Bousaid and Ramey, 1968 have found that the oxidation rate of crude oil in porous media depend on the carbon concentration, combustion temperature and oxygen partial pressure. The specific reaction rate constants related to combustion temperature by the Arrhenius equation. They also found that the activation energy decreased as a result of the addition of clay and it was not sensitive to the gravity of the crude oil.

The combustion rate (Rc) of crude oil in a porous medium was expressed by Wilson *et al*, 1963, Bousaid and Ramey, 1968, Burger and Sahuqet, 1972 and Fassihi *et al*, 1984 as follows :

$$\mathbf{Rci = Ki\ P_{O_2}^{mi}\ C_f^{ni}}$$

Where,

C_f = instantaneous concentration of fuel

K = reaction constant

P_{O2} = Partial Pressure of oxygen

m = reaction order with respect of oxygen

n = reaction order with respect of fuel concentration

i = reaction regime

The reaction rate is often assumed to be first order with respect to fuel for each reaction concentration, (i.e. n=1) Fassihi *et al*, 1990.

The reaction constant (K), is normally expressed as a function expressed as a function of temperature , T, by the Arrhenius equation :

$$K = Ar \exp\left(-\frac{E}{RT}\right)$$

Where :

Ar = Arrhenius constant

E = activation Energy

R = universal gas constant

T = absolute temperature

It is believed that the reaction mechanism between fuel (coke) and oxygen is a heterogeneous flow reaction and the oxidant gas must pass through the burning zone to make the combustion front move. Within the burning zone, four known transport processes occur Fassihi *et al*, 1980:

- Oxygen diffuses from the bulk gas to the fuel interface.
- Oxygen then adsorbs and reacts with fuel.
- Combustion products, CO_2, CO, and water.
- These products transfer into the bulk gas stream.

If any of these steps is inherently much slower than the remaining ones then it will be the rate determining step.

Hughes *et al*, 1987 investigated the effect of oxygen partial pressure and sand surface area on the overall activation energy of the process as well as on the peak temperature. They found that an increase in oxygen partial pressure and specific surface area of the porous media caused decreases in both the activation energy and the peak temperature.

It is important to recognize that the hydrocarbon fuel is different for the three reactions. For the LTO it is the unreacted crude oil, for the MTO it is oxygenated oil and for the HTO it is the products of pyrolysis and oxidation, Shallcross *et al*, 1991.

2.7: Thermal Cracking Kinetics:

Behar *et al*, 1988 studied oil cracking kinetics in a closed reactor system, over a large range of heating times (few minutes to 1 month) and temperatures (335 to 540°C). Their results show that :

- Molecular hydrogen is presented in negligible amounts,
- The cracking of condensate fractions is reached at 450°C, and 3hr, while the cracking of the C2-C5 compounds occurs at 500°C, and 9hr.
- As thermal cracking increases, asphaltenes disappear rapidly, followed by saturates and unsaturates ($C14^+$). Consequently, the residual $C14^+$ fraction is composed mainly of polyaromatic structures.

2.8: Air Injection: LTO Technique:

A new air injection technique, low temperature oxidation (LTO) process, is described, improved oil recovery from deep, light oil reservoirs is achieved by removing the oxygen in the injected air by LTO reactions with the residual oil in the reservoir. For light oils, LTO does not significantly effect the volatility, the carbon number distribution or the viscosity Fassihi *et al*, 1985,and Meyers *et al*, 1986. Air injection LTO is therefore applicable to light recovery.

The zones that are created in the reservoir during LTO are illustrated in Figure 2.3. The oxygen in the injected air is depleted in the oxidation zone. This leaves nitrogen and carbon oxides which strips light components from the oil, eventually culminating in a nitrogen 'flue gas' front, ahead of which builds up associated water and oil banks.

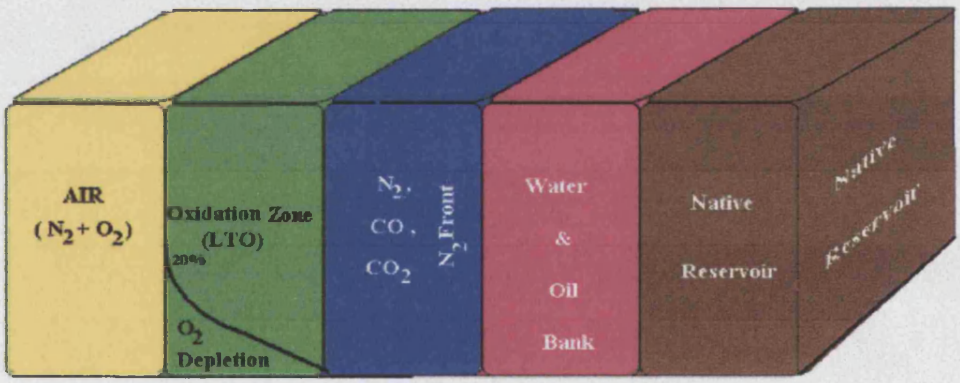

Figure 2.3: Air Injection LTO process

In the oxidation zone, homogeneous LTO reactions take place, where oxygen first diffuses in to the hydrocarbon phase. The oxygen consumption rate is linear and therefore not affected by oxygen partial pressure, the rate determining step being the oxygenation reaction and not the mass transfer of oxygen into the oil.

The oxygen consumption rate in the oxidation zone is between 0.15 and 0.25 g(O_2)/hr.kg(oil), or 27 to 40 O_2 % HCPV injected consumed/day, Greaves,1997. However this rate is very dependent on the reservoir temperature (very little oxidation

has been found to take place below~ 80°C). Sakthikumar *et al*, 1995, showed that the oxygen is depleted to very low levels with certain oils. Interestingly, considerable amounts of CO_2 are produced (when water is present), between 5 and 12%. This is most probably due to de-carboxylation reactions Wichert *et al*, 1995, the carboxylic acids having been produced by successive oxygenation reactions. This mechanism is further confirmed by low levels of carbon monoxide produced. There is also a lag time between initial oxygen consumption and initial CO_2 production. This suggests the following overall reaction for the air injection LTO technique :

$$\text{Oil} + O_2 \xrightarrow{\text{Oxygenation}} \underset{\text{Hydrocarbon}}{\text{Oxidised}} \xrightarrow{\text{de-carboxylation}} CO_2 + CO$$

For both adiabatic and iso-thermal experiments at reservoir conditions no measurable heat release has been observed. Any temperature rise in the reservoir is very dependent on the air flux used. Below a reservoir specific "Critical Flux" the temperature rise will be very small (see Figure 2.4), a reservoir temperature profile for a typical post-water flooded reservoir) but not insignificant. This is because of the very small amount of oxygen reacting with the large excess of hydrocarbon molecules and the large reservoir area (volume) over which these oxygen molecules react Greaves, 1997. Above a critical flux, however, the reaction will move along its particular exotherm, so that the temperature of the oxidation zone increases above that of the initial reservoir temperature. Depending on how the reservoir is operated, the critical flux may, or may not, be important.

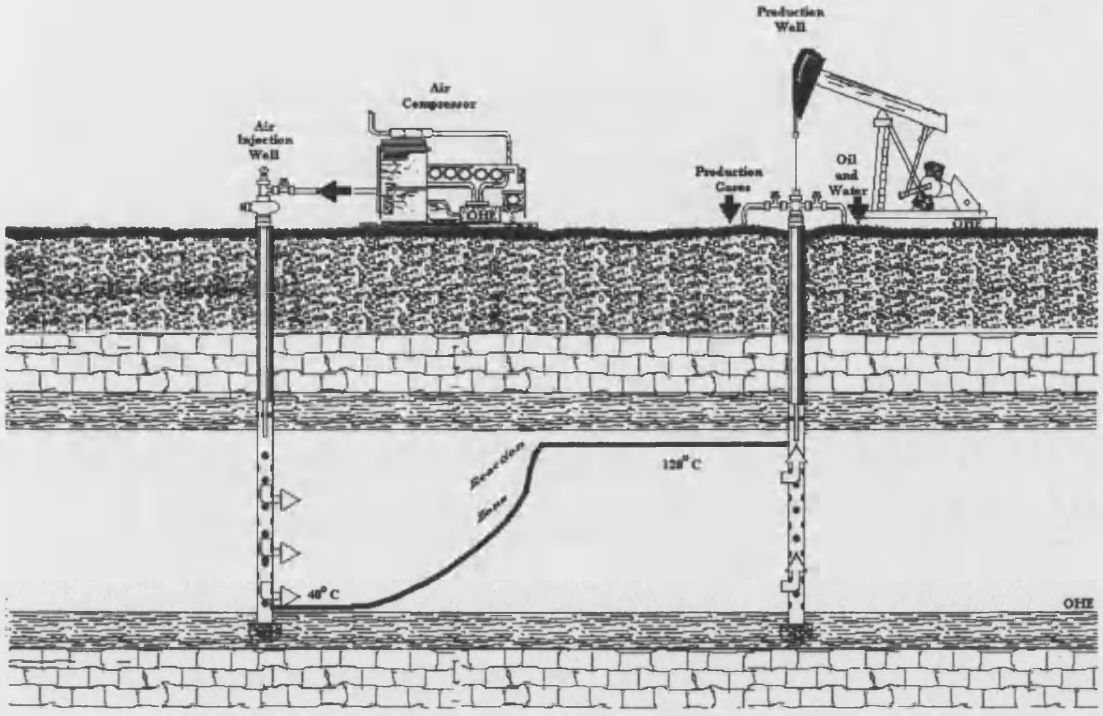

Figure 2.4: Air injection LTO, A reservoir temperature profile

The application of the LTO process should be considered where nitrogen or flue gas injection is appropriate, for example, Where gas is needed to pressurize the reservoir, or maintain its pressure during depletion. Additionally, it can be used for horizontal WAG (Water Alternative Gas) or GSGI (gravity Stabilized Gas Injection) . The advantage over nitrogen or carbon dioxide injection is that the cost of compression is generally cheaper for air Fassihi and Gilham, 1993 since no separation costs are involved.

Low temperature oxidation reactions are exothermic reactions which take place between the gas and liquid phases at temperatures less than that required for complete combustion (< 300°C). It is characterized by the absence, or low levels of carbon oxides in the effluent gas and yields water and oxygenated hydrocarbons such as carboxylic acids, aldehydes, ketones, alcohols and hydroperoxides.

Many papers have been published about LTO reactions for heavy crude oils, Alexander *et al*, 1962 investigated the effect of LTO on fuel formation. They reported that if crude oil is subjected to prolonged LTO reactions, the fuel content is increased especially in light oil reservoirs. It appears that oxygen is partially consumed at the combustion front. As a consequence, oil ahead of the front is subjected to some LTO, particularly when the temperature exceeds (93-121°C). They concluded that LTO reactions have a pronounced effect on fuel deposition and composition. Pottman *et al* 1967 have demonstrated that if the crude oil is subjected to low temperature oxidation then fuel content is increased as much as 100 per cent over what it is if no LTO occurs. Also, they established that fuel content is a function of the reservoir rock and oil properties.
In a combustion tube study carried out by Dabbous and Fulton, 1974, reaction rates were measured for two types of crude 19 and 27.1 °API. Their results indicated a higher oxidation rate under similar reactions for the higher API gravity crude. Light crudes appear to be more susceptible to LTO.

The products of the LTO reactions is a "flue gas", which displaces the oil . Preliminary results of LTO reaction kinetics and oil recovery have been obtained using four North Sea light oils by Greaves *et al*, 2000. They conclude for most of the oils, complete oxygen utilized was achieved over 10-20 days. This produced up to 9% CO_2 and some CO (around 1%). Significant oil recovery varying between 74-71% was obtained under the low rate LTO conditions using both crushed reservoir core and sandpacks. They recommend that the air LTO process should be considered for application to all light oil reservoir possessing sufficiently high reactivity.

Measured reaction rates for a 19.9°API and a 27.1°API crude indicated higher oxidation rates under similar reaction conditions for the higher API gravity crude. Light crude appear to be more susceptible to partial oxidation at low temperatures because of their relatively high hydrogen content as presented by Dabbous *et al*, 1974.

Fassihi *et al*, 1990 reported that, LTO increased oil viscosity and density. The rate of increase depend on an oil's API gravity, origin, and composition. LTO is shown to increase the asphaltene content of the oxidation oils significantly. They observed that physical and compositional property changes are consistent with the LTO mechanism proposed in the literature and confirmed also by Verkoczy *et al* :

Oil → Resins → Asphaltenes / Coke.

The kinetic parameters determined (K,EA,Ko) by Ranjbar *et al* indicate that the reactivity of the oil towards oxygen increases almost linearly with the content of resin and wax in the oil at temperature, up to 450°C . Above 500°C, however, the fuel formed from oil is rich in asphaltenes is more reactive than that originating from samples rich in wax and resins.

2.9: In-Situ Combustion of Light Crude Oil:

In-situ combustion behavior in light oil reservoirs (i.e. API > 25°API) is not as well documented as combustion of heavy oil and bitumens. The usual concerns expressed are that the light oil will be swept away by the gas flood to a residual level that is too low to sustain combustion, or that the process will be unable to deposit sufficient amounts of coke (i.e. fuel) to make the process self sustaining. Results by Tzanco *et al*, 1990 on her study showed that light Countess B oil did appear to be burning a coke-like fuel. Rather, it appears to be burning an oxidized asphaltene fraction. The low rate of coke deposition observed for this oil provides an important explanation of the difficulties reported in sustaining high temperature combustion in this light oil reservoir.

Abegbesan *et al*, 1983, studied the kinetic of LTO reactions of Athabasca bitumen. The studies were carried out in a temperature range of 60 to 149 °C at an oxygen partial pressure of 7.3 to 324 psi. The bitumen used was free of water and minerals.
They concluded that the overall rates of the oxygen consumption by LTO reactions are relatively small when compared with rates characteristic of high temperature oxidation.

Also they found that total pressure had no influence on the LTO reactions and they depend on oxygen partial pressure.

Turta *et al*, 1998 defined the spontaneous ignition as when air is injected in oil reservoir, slow oxidation (LTO) reactions occurs at the reservoir temperature, and in some cases the heat given off can initiate the in-situ combustion process. In general, an ignition delay of 10-20 days is seen in oil reservoirs whose reservoir temperatures are 50-60 °C. Spontaneous ignition can take place even at law reservoir temperature as 30°C, but can be as long as 100-150 days, and for light oil target it becomes impractical for various reasons, such as an increase in oil viscosity.

Islam, 1989 reported that LTO may result from incomplete oxygen consumption in the combustion zone, or air channeling into down stream zones, or tilted combustion front surface.

Fassihi *et al*, 1990 also attributed LTO reactions to oxygen channeling which results from both reservoir heterogeneity and insufficient combustion rate. They reported that LTO tends to be more pronounced when oxygen is injected into reservoir.

Belgrave, 1990, has shown that LTO is an important fuel forming step in in-situ combustion, especially for heavy oil recovery.

Yannimaras *et al*, 1995 have tested the oxidation characteristics of North Sea Maureen oil with air in the presence of reservoir rock and brine by using an accelerating rate calorimeter (ARC).

2.10: Procedure to Identify LTO Reaction Regime:

To distinguish between overlapping LTO and HTO, Al-Saffar *et al*, 2000 highlighted the following points :

a. In Isothermal runs using the same cores and crude oils, the onset of LTO reaction was identified. However, for the present non-isothermal experiments, while some show the occurrence of LTO reactions, in other experiments, LTO reactions appear to persist into HTO region so that LTO and HTO peaks merge into each other. It is belived that the characteristic of the consolidated core (similar to the real reservoir element) such as thickness, surface area, permeability, have a major effect in determining the extent of the LTO region.

b. The presence of LTO reaction regime will characteristically yield an apparent H/C ratio that is high.

c. LTO will generally give a relatively high molar carbon ratio $\frac{CO}{CO+CO_2}$, This means low CO_2 . Also, as the combustion regime changes from LTO to HTO, carbon dioxide becomes increasingly the dominant product of carbon oxidation.

d. During LTO reactions, some oxygen is consumed to produce carbon oxides, but the combined production of these gases is less than the oxygen consumption. The differences in oxygen consumption and carbon oxides production indicates that some oxygen is consumed on other reactions under LTO conditions. On the other hand, at high temperatures (i.e. the HTO region), nearly all of the oxygen is consumed to produce carbon oxides (the combined production of carbon oxides should equal oxygen consumption if the fuel is composed of carbon only and this is completely combusted).

2.11 : Medium Temperature Oxidation (MTO/Fuel Deposition) :

At temperatures above 300°C, the residual oil cracks into volatile fractions and a nonvolatile heavy residue consisting of coke, which constitutes the primary fuel for combustion. Both cracking reactions produce hydrogen gas and some light hydrocarbons

in the gas phase. In an oxygenated environment, a portion of these hydrocarbon is oxidized; hence medium temperature oxidation occurs. It is assumed that the pyrolysis of crude oils takes place by chain reactions Abu-Khamsin, 1988.

These reactions include the breaking of C-C bonds, H-C bonds, polymerization, condensation and alkylation. As a result, the reaction kinetics of this cracking can be extremely complex. Also, it is almost impossible to describe the mechanism precisely, even for a pure component because it not only produces solid like coke but also upgrades the remaining oil which affect the vaporization behaviour of crude oil Lin *et al*, 1984.

The reaction may be represented as :

Heavy Hydrocarbons $\longrightarrow$ Light Hydrocarbons + Heavy Residue

There is an assumption that crude oil does not crack into coke and gas, but it goes through an intermediate step of visbreaking, then cracking into coke.

Crude Oil $\xrightarrow{Heat}$ Visbroken Oil + Gas

Visbroken Oil $\xrightarrow{Heat}$ Coke + Gas

The amount of fuel deposited, is very important factor in in-situ combustion project design because the maximum oil recovery is the difference between the initial oil-in-place and the amount of fuel deposited. A high fuel concentration will reduce the combustion front velocity and increase air requirements, a high increase the overall cost of the project. On the other hand, if the fuel concentration is too low, heat generated may be insufficient to propagate a self-sustaining combustion Mamora, 1994.

Wu and Fulton, 1971 identified that thermal cracking occurs in both the cracking zone and the evaporation zone, while coke is produced in the cracking zone. Therefore, the mechanism of fuel deposition is controlled by two important factors; the kinetics of the cracking reaction and the evaporation of crude oil components (i.e. displacement

processes). These processes, determine the amount of fuel that will be deposited and how much fuel will be consumed. The displacement processes are hot water drive, gas drive, vaporization, miscible displacement, fluid and gravity drainage Fassihi *et al*, 1984.

Because of the light oils contain more volatile components and are vaporized to a large extent, vaporization and miscible gas displacement processes play a more important role in light oil reservoirs.

2.12 : High Temperature Oxidation (HTO) (Fuel Combustion):

Temperature oxidation reactions are the main source of heat for the in-situ combustion process. They are a heterogeneous reaction occurring between the oxygen in the gas phase and the coke at temperature above 343 °C. These reactions produce carbon monoxide, carbon dioxide and water.

To evaluate or study the performance of in-situ combustion laboratory or field test, the data typically available include :

(1) Gas injection and production rate and
(2) Gas analyses (CO_2, O_2, and CO_2) .

Evaluating the performance of the combustion project in terms of the following parameters is desired.

1. Average gas analysis.
2. Apparent H/C ratio.
3. Oxygen utilization efficiency.
4. Total combustion rate, Mscf/D.
5. Total fuel burned, Ibm/D.
6. Heat generation rate, Btu/d.
7. The concepts of fuel available, air requirement, and heat of reaction can be applied to analyze the performance of in-situ combustion project.

The detailed equations used to calculated these parameters are showing in Appendix A.

The effectiveness of HTO depends on the rate of heat generated by combustion and the efficiency of heat utilization, which depends on reservoir fluid distribution, and thermal properties of the reservoir rock and the adjacent formation.

One of the earlier studies to investigate the combustion reaction was done by Bousaid and Ramey, 1968. A total of 48 runs were made wherein a stationary thin layer of coke, unconsolidated sand was burned isothermal in a combustion cell. Individual runs were made at various temperature levels to permit determination of the effect of temperature upon the reaction. They concluded that the carbon burning rate of the crude oil in a porous medium was found to be dependent on carbon concentration, combustion temperature and oxygen partial pressure. They found that activation energy decreases significantly with the addition of clay to their sand matrix and it appeared to be insensitive to the oils used. Their results showed first order reaction rates in both partial pressure and carbon concentration.

Dabbous and Fulton, 1974 observed that the combustion reaction is first-order with respect to oxygen partial pressure and second-order with respect to carbon concentration. Greaves *et al*, 1988, found that the combustion kinetics is dependent on fuel concentration, oxygen partial pressure and combustion peak temperature. The reaction rates for carbon concentration were found to be first order. For dry combustion, the oxygen partial pressure was found to have an approximate first reaction rate, while for wet combustion, the value was less than half, due to the limiting factor of oxygen diffusion.

As heating rate increased the reaction temperature increase. Also, as the °API gravity of crude oil decrease in high temperature oxidation, the activation energy value produced will be higher Kok and Keskin, 1999.

The apparent activation energy of the high temperature oxidation reaction was observed by Hughes *et al*, 1987 decreases with increasing surface area of the substrate and was also affected by the partial pressure of oxygen over the range employed.

2.13: Effect of Matrix Surface Area and Clay :

Many oil reservoir formations are known to contain substantial amounts of fines (size of the grain < 1/256 mm) including considerable amounts of clay minerals. Because of the large surface area involved and the high reactivity of such surfaces, the response of the formations to various recovery processes may be dominated by reactions at the clay surface, Wilbur *et al* 1980.

For in-situ combustion process, the specific surface area of the porous media is one of the most important factors to achieve smoothly advanced combustion front. Many studies have been carried out on the effect of surface area and associated material on the ISC performance. The main conclusion is that surface area and fine solids materials may significantly influence combustion kinetics and fuel deposition.

Bousaid and Ramey, 1968 presented kinetic data from an isothermal combustion reactor in which a 13.9 °API crude oil was combusted at temperature ranging from 266 to 671 °C. They observed a decrease in activation energy from 61,887 to about 148,394 Joules/gram when the porous media containing 20% wt clay.

Hardy *et al*, 1972 have reported that combustion could not be sustained when clean sand was used instead of the actual reservoir rock. They attributed that to the lower fuel adsorption on the sand surface.

Fassihi *et al*, 1980 performed combustion tube tests on different crude oils in sandpacks containing clay. They reported that the average front temperature for the sandpack containing clay was about 510°C, whereas in the clay-free sandpack the average temperature was 343°C. They concluded that clay particles and fine sands enhance deposition of more fuel because of the adsorption characteristic on a high surface area.

Vossoughi *et al*, 1982, investigated the effects of surface area on in-situ combustion using thermogravimetric analysis (TGA). The experiments were done in the absence of clay by using silica sand with variable specific area. They concluded that for low specific surface area experiments (1120 cm^2/gram), the oil content immediately ahead of the front reduced below its original level, while the opposite affect occurred for high specific surface area experiments (3330 cm^2/gram). Their results show a minimum specific surface area is required for any particular crude oil in order to establish a self-sustained combustion front in clean unconsolidated sandpacks.

In another study, Vossoughi *et al*, 1984 investigated the effect of clay on dry ISC process. Sand mixtures of varying clay content were saturated with crude oil and water.
They found that more fuel was deposited as the clay content of the mixture was increased, as a result the combustion peak temperature increased. They reported a significant reduction in the activation energy resulting from the addition of clay. This phenomenon may be attributed to the composition of the clay minerals mostly consisting of silica and alumina which is classified as solid acid catalysts. Their catalytic activities are related to their acid site density and strength. Activation energy decreases with an increase in the acidity.

Greaves *et al*, 1987 investigated ISC behaviour in dry and wet modes using different crude oils (36.6, 32.4, and 22.1 °API). They found that with light crude oil, it was not possible to sustain a stable combustion front using a clean silica sand, without first incorporating a clay additive, or other combustion surface promoter. It has also been found that clay content in the range 5 to 10% wt did not significantly effect level of oxygen utilization.

Shallcross et al, 1991, performed experiments to study the effects of various additives on the oxidation kinetics of Californian and Venezuelan oils. They concluded that the presence of iron, tin, and aluminum enhanced fuel deposition for Huntington beach oil (density = 943 kg/m^3). In contrast, the presence of copper, nickel, and cadmium had little

or no effect. They found the presence of a ketal did not reduce the amount of fuel deposited by Venezuelan oil (density =996 kg/m^3).

Mamora and Brigham, 1993 have reported results similar to that observed by Fassihi *et al*, 1980. They attributed higher combustion temperature associated with the use of clay or fine sands to the reduction in permeability, which increase residual oil saturation and hence fuel concentration resulting in higher combustion temperature.

The presence of clay enhanced the LTO reactions by shorten the oxidation time and increase the amount of deposits on the sand grains. This greatly increased the compressive strength, but at the expense of larger permeability losses. When interstitial water was present with clay, the permeability loss was increased further while the compressive strength was slightly reduced. Acid treatment had no effect on the residue on the sand grains.

Decreasing the crude oil/surface area ratio enhanced the low-temperature oxidation (LTO) peak. It also was noticed by Drici and Vossoughi, 1985 that additives with large specific surface are shifted a large portion of the exothermic heat from a higher to a lower temperature range , The fractional shift correlates with the crude oil/surface area ratio of the mixture. Activation energies calculated for the crude oil combustion of the samples with a low crude oil/surface area ratio were significantly lower than those of samples with a high value of crude oil/surface area ratio . The surface area of the additives seemed to affect the crude oil combustion regardless of the composition of the additives.

The thermo-oxidative and thermal cracking reactions of Athabasca bitumen were examined qualitatively and quantitatively by Yoshiki *et al*,1985. They conclude that when sand was used as the support material there appeared to be a catalytic effect in both low temperature oxidation (LTO) and High temperature cracking (HTC) reactions.

The effect of clay on crude oil combustion where reported by Vossoughi *et al*, 1981. They observed that the large surface area of clays was a major contributor to the fuel

deposition process. Moreover, the activation energy reduced, caused by the addition of kaolinite clay to the crude oil indicates both catalytic and surface area effects on combustion / cracking reactions.

The use of different lithology (sandstone and lime stone) can give different combustion reaction results as presented by Bagci *et al*, 1987. They observed that considerable differences were obtained in atomic H/C, molar CO_2/CO ratio and activation energy in HTO region.

Core mineralogy played an important role in the generation of CO_2 , Belgrave *et al*, 1994 and the amount of H_2S produced was dependent on oil composition, mineralogy, and time, as stated by Belgrave *et al*, 1994.

Particle size effects were studied by Lukyaa *et al*,1994, They found that decreasing particle size of the sand increased the extent of LTO and thus favoured fuel lay down.

The role of clay in reservoirs and its possible influence on kinetics of crude oil burning is not entirely clear Rashidi and Bagci. However, it is known that

a. Clay fractions of the reservoir matrix possess the highest surface area per gram.
b. Clay fractions are the most chemically reactive of the inorganic consistent present in the reservoir and
c. Clay minerals generally possess catalytic properties toward various organic liquids.

Clay content of the matrix influenced the amount of the fuel deposited on the limestone. Increasingly more fuel was deposited as the clay content was increased. Addition of clay also increased the combustion peak temperature. Also, with addition of 10% of clay in the limestone tend to increase the average molar ratio from 3.71 to 5.97. He recommend to use natural core in studying in-situ combustion to represent the physical conditions and minerals in a sand pack are close to reservoir conditions as possible.

2.14: Effect of Pressure :

Air injection can offer economic and technical opportunities for improved oil recovery in many candidate reservoirs. Air injection is an efficient oil recovery process since only a small amount of the in-place oil is consumed, while the rest is displaced, banked, and eventually produced. Light oils at high pressure offer many unique advantages for the air-injection process including

(1) Excellent displacement efficiency,
(2) Near-miscibility and associated enhanced hydrocarbon extraction capability of the flue gas ,
(3) Spontaneous oil ignition with complete oxygen utilization, and
(4) Operation above the critical point of water with possible super-extraction benefits, Tiffin and Yannimaras, 1997.

Commercial application of ISC was mainly in heavy oil reservoirs, which were characterized by low initial pressure. The effect of pressure on the process performance has been studied by number of investigators. Wilson *et al*, 1963, conducted combustion tube tests to study the effect of pressure on forward and reverse combustion. They used five types of crude, test pressure ranging from 1 to 69 bar. In forward combustion, they found that increasing the pressure increases peak temperature, decreases combustion front velocities, but did not affect oil recovery. In reverse combustion, they found that increasing the pressure resulted in decreasing peak temperature, oil recovery and increasing the rate of advance.

Bae, 1977 observed that the effect of pressure is oil dependent, but in general, increase in pressure causes the low temperature heat generation to increase.

Prasad and Salter, 1986 conducted combustion tube runs at pressure up to 207 bar. They found some benefits not observed at low pressure. Immiscible displacement of oil by carbon dioxide was found to be an important mechanism for both dry and normal wet

combustion accompanied by an associated increase in oil production rate. This was caused by gas at its high partial pressure, dissolving in oil, swelling it and also reducing its viscosity.

Adegbesan *et al*, 1987 studied the effect of pressure LTO reaction kinetics. The pressure applied in the study ranged from 22 to 44 bar. They concluded that the total pressure had no influence on LTO reaction but the reaction rates were found to depend on oxygen partial pressure.

Moore *et al*, 1990 studied the effect of pressure on Athabasca oil cores in combustion tube runs by using enriched-air (95%O_2). They found that increasing the operating pressure caused a significant rise in the oxygen and fuel requirements. They observed that the pressure effect with air is not effect to the same extent as for oxygen.

Tiffin and Yannimaras, 1997 investigated the effect of pressure on the combustion behavior of two light crudes. Experiments were conducted at pressures ranging from 6.9 to 37.2 Mpa using an automated high pressure combustion tube. They concluded that the air/fuel ratio was relatively constant with pressure, while fuel deposition and air requirements increased slightly with pressure. They also reported the need for a high injection rate to operate the runs under high pressure. In the field, this can be a very limiting factor for sustaining HTO, or a propagating combustion front pattern, if the oxygen flux declines in the reservoir (limited air compression capacity) the process will drop into LTO mode. However, a high temperature front (<300°C) can still propagate.

Kisler and Shallcross, 1997 have studied the oxidation kinetics of a light Australian crude oil by using Evolved Gas Analysis technique (EGA). They reported that high pressures increased oxygen consumption throughout the oxidation and pyrolysis reactions.

Rashidi and Bagci presents results indicating that the oxygen consumed increases with increasing operating pressure. This means more fuel is burned by increasing the pressure; which is due to the effect of pressure on the volatility of the oil components. Because,

increasing pressure will depress oil volatility and so the fuel availability would increase. This also suggests that distillation might be the dominant mechanism for fuel deposition.

The main effect of pressure is that higher air injection rates are required to propagate a self-sustaining high temperature combustion front. However, air/fuel ratio was fairly constant with pressure, but air requirement varied with pressure, oil and sand. Stated by Tiffin and Yannimaras, 1995.

2.15: Effect of Air Flux:

The concept of minimum air flux is simply the minimum flow rate of air per unit cross-sectional area of the reaction zone which will maintain the combustion in the HTO mode. It relates mainly to the heat capacity of the formation (sand and fluid), which has to be heated to the over 350°C temperature required for high-temperature oxidation of a typical Canadian heavy oil . The minimum air flux is higher for Canadian heavy oils than for many light oils, because of the higher temperature required to operate in the HTO mode.

By definition, flux is the air flow rate unit area . The air flux is related to the combustion zone velocity by the relation .

$$U_b = \frac{U_a}{A_r}$$

Where: U_b is the combustion front velocity, U_a is the flux and A_r is the air requirement.

Nelson and McNeil, 1961 suggest a minimum burn front velocity of 0.125 ft/day (0.038 m/d) for successful operation of an in-situ combustion process.

Once the line drive has formed, the minimum required injection is given by the following equation. Prior to establishing the line drive, less air is required and air injectivity is lower .

$$\text{Air Injection} = 2.5\, U_{min} \,.\, a \,.\, h$$

Where : U_{min} is the minimum air flux, a is the distance between wells, and h is the reservoir thickness.

It should be emphasized that linear drive can be found in case of locating two wells parallel to two barriers i.e. two faults. However, the important feature to be considered when selecting air injection flux such as radial flow. The combustion front velocity will be much lower ahead of the injection area due to the expanding displacement.

2.16: Effect of Oxygen Enrichment :

A great deal of attention has been directed for using oxygen enrichment since 1980 as many of its potential advantages have been recognized. For reservoir that require a large volume of high pressure gas, oxygen is cheaper than air simply based on compression costs. Addition process benefits with oxygen include as suggested by Shahani and Gunardson, 1994:

- Faster oil production
- Lower Injection Pressure
- Greater Well Spacing
- Increased Carbon Dioxide Partial Pressure, to decrease oil viscosity and density, and recycle it into the same reservoir Hansel *et al*, 1984.
- Lower Gas-Oil Ratios
- Purer Production Gas
- Reduce Compression cost per unit injection oxygen.
- Ability to sustain combustion under reservoir conditions of low permeability, due to a decrease volume of gas that needs to be injected to sustain combustion White and Farfield, 1982.

These feature provide a compelling case for oxygen, once the safety Hvizdos *et al*, 1983 and materials compatibility issue are properly addressed.

The use of oxygen-enriched air at high pressure, results in increased low-temperature reactions between the oxygen and the oil, resulting in an increase fuel load and decreased burn stability Moore *et al*, 1990.

Shahani and Hansel, 1987 found that a high coke loading alone was not adequate to ensure satisfactory in-situ combustion. The relative reactivity of the coke with O_2 also appeared to be critical. Nevertheless, some crude oil did not burn in air ; however the same flux of contained O_2, high levels of O_2 enriched could sustain combustion.

By using three dimentional (3-D) scaled model. Garon *et al*, 1986 indicated that the sweep of fireflood was similar for both oxygen and air combustion; water results in a small decreases in the sweep of the fireflood; wet combustion required less oxygen or air and increased the oil recovery rate; fireflooding a medium-gravity crude oil reservoir results in a large sweep than a heavy oil reservoir; and higher injection rates improved the sweep efficiency.

Oxygen injection may substantially increase oil productivity so that projects may be completed more rapidly in productivity-limited reservoir. However, Oxygen/Oil ratio (OOR), or cost per barrel of produced oil, is also higher with oxygen injection. Wet combustion may reduce OOR, Especially for oxygen injection and high pressure reservoirs.

Lukyaa *et al*, 1994 found using an Differential Scanning Calorimeter (DSC), that with increase of oxygen concentration there was increased heat evolved up to 50% oxygen; further increases in oxygen had no effect

Moss and Cady, 1982 reported combustion tube results using oxygen concentration up to 95%. They concluded that the peak temperature and oxygen utilization were found to be similar for both oxygen and air. The apparent fuel lay down was 20 to 10 % higher over air dry and wet combustion.

Hansel *et al*, 1984, conducted combustion tube experiments by using oxygen enrichment to evaluate the combustion characteristics of light oil. They used low initial oil saturation under different percentage of oxygen enrichment (21 to 95% O_2) at constant gas influx. They concluded that combustion with 40% to 95% oxygen was vigorous, whereas combustion with air and 30% oxygen was unsatisfactory. Also they reported that front velocity increased and faster production was obtained with oxygen enrichment. The H/C ratio, peak temperature, oxygen utilization and CO/CO_2 ratio were found to be the same under both oxygen enrichment and air.

Hughes *et al*, 1990 reported that an increase of partial pressure of oxygen give better use of the fuel laid down in the combustion process and related to the virtual completion of LTO reaction at 377°C with high concentration of oxygen (30-40 %). They also added that increase oxygen concentration also produced a decrease in the activation energy for high temperature oxidation reaction.

Petit, 1997 studied the effect of total pressure, oxygen partial pressure and oxygen flux on the combustion kinetics of two crude oils having API gravity of 25.7 and 16°. He reported that at constant oxygen flux and increased oxygen partial pressure, there was a less than a proportional increase in combustion front velocity. At low pressure (10 bar), he observed that fuel availability and the air requirement at the front are slightly affected by the oxygen partial pressure. For 16°API crude oil, he reported a slight increase in fuel availability and air requirements with oxygen enrichment. The opposite effect was observed for the lightest oil.
At high pressures (70-100 bar), there was no effect on the combustion of the heaviest oil, but there was a reduction of approximately 40% in the oxygen requirement at front for the lightest oil.

2.17: Porosity Effect:

Iin-situ combustion does not appear feasible in extremely low porosity reservoirs. The porosity requirement is directly related to heat losses within the matrix, Turta and Singhal, 1998.

CHAPTER THREE

EQUIPMENT, COMMISSIONING AND EXPERIMENTAL PROCEDURE

The high-pressure combustion tube facility is shown in Figure 3.1. The system was originally constructed 12 years ago. There have a number of adaptations to the original system, especially concerning the control and monitoring systems. The most resent modification were not undertaken by T.Young, 1997. It is designed as a physical simulator of the in-situ combustion process, and is capable of operating up to 240 bar pressure.

The combustion tube system is housed in a self-contained safety containment area, which is located outside of the main chemical engineering laboratory. The combustion tube is contained inside a pressure shell, because it can support only a very low pressure (< 3 bar).

3.1: Flow Sheet of Combustion Tube System:

Compressed air injected through the inlet system, which consists of two inlet lines, one contain high mass flow rate calibrated meter, and the other with low flux. Gas supplied to the combustion tube (air) and pressure shell (nitrogen), from high pressure cylinders. Produced fluids exit from the bottom of the combustion tube. Gas is separated from the oil and water in two stages, via a high pressure separator (HPS) and a low pressure separator (LPS), and at the simultaneously they are cooled down. The produced cumulative gas and any hydrocarbon gases are send to the vent extract system, after the volumetric flow was measured by a wet test meter (WTM). Oil and water samples are collected from the additional atmospheric separator (Figure 3.1).

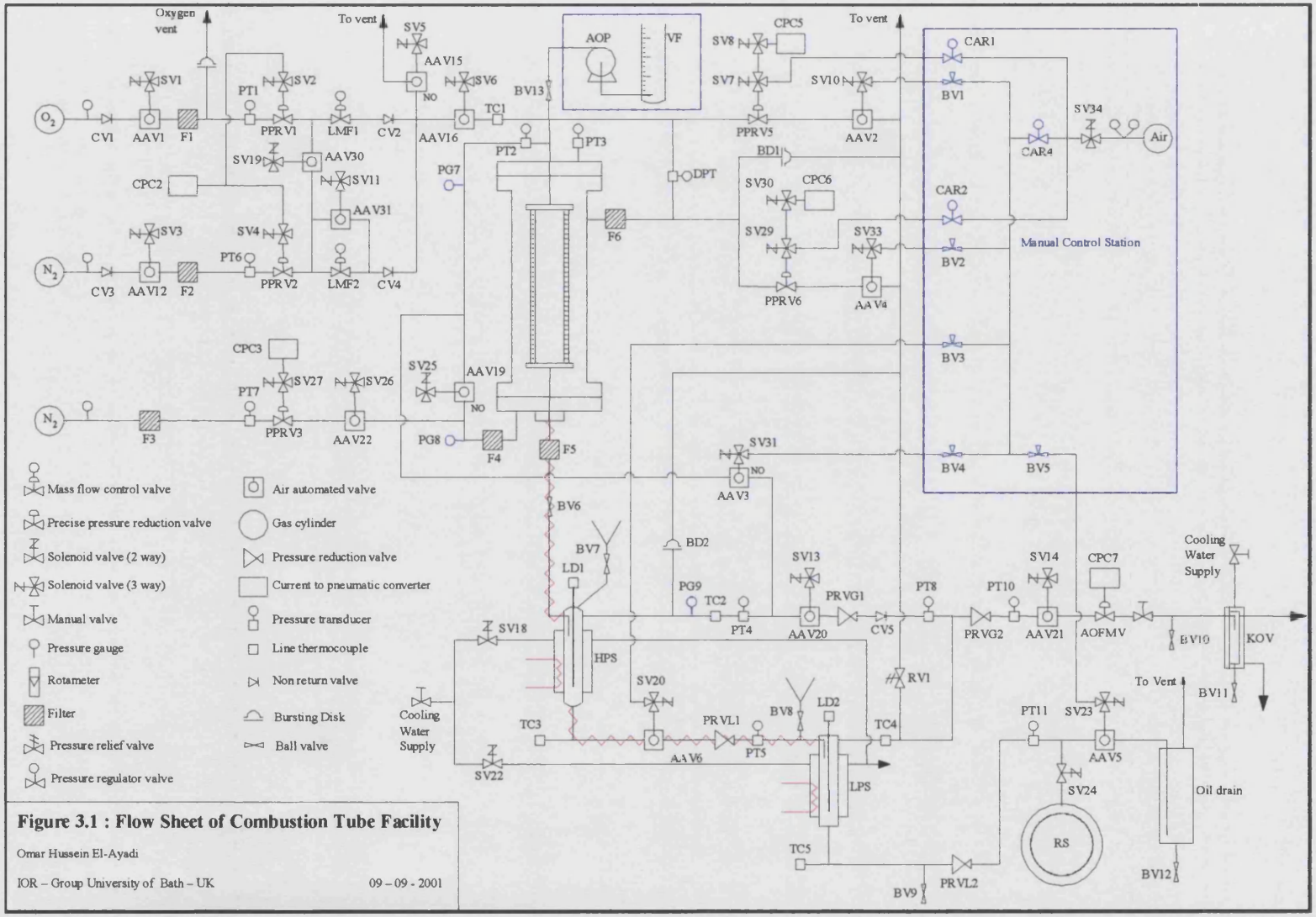

Figure 3.1 : Flow Sheet of Combustion Tube Facility

Omar Hussein El-Ayadi

IOR – Group University of Bath – UK 09 – 09 - 2001

3.2: Equipment:

3.2.1: Combustion Tube :

A diagram of the combustion tube and surrounding pressure shell assembly can be seen in Figure 3.2. A photograph of the combustion tube can be seen in Figure 3.3. The combustion tube reactor is a cylindrical tube 0.1 m in diameter, 1.25 m long and 1.75 mm thick, constructed from Inconel 625. Inconel 625 was chosen due to its outstanding corrosion resistance, superior mechanical properties and lower thermal conductivity. The thin wall reduces axial heat conduction. The end flanges are sealed with high pressure/temperature gaskets, and secured into position with eight bolts.

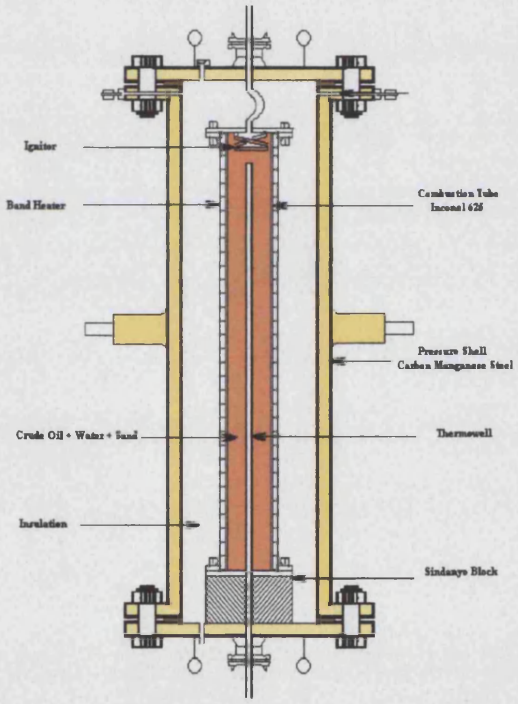

Figure 3.2 : Pressure shell and combustion tube assembly.

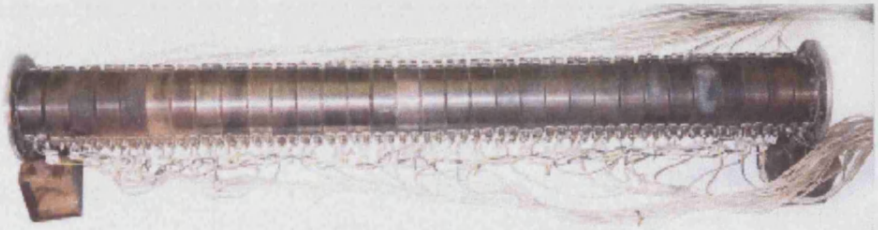

Figure 3.3 : Photo of Combustion Tube.

An electrical ignitor is located at the top of the tube to initiate combustion. It is fixed to the top flange by two Connax MK-250 glands. The ignitor is a tubular heater shaped into spiral rated at 500 W.

The combustion tube is surrounded by a stack of 32 circular band heaters (BH), to heat the tube, and reduce heat loss from the core. A near adiabatic condition present in a reservoir. Each BH is 3.9 mm wide, 2 mm thick and has a maximum power rating of 800 W. Between the tube and the band heaters is a thin layer of ceramic paper which protects the band heaters from any large increases in temperature. However, one additional purpose of band heaters is that it provide some support to the tube from bursting pressure.

A thermocouple probe is mounted to monitor the sand pack temperature along the central axis of the tube. It contains 32 thermocouple (K-type, mineral insulated, floating signal) equally spaced along its length. They are welded to insert clips and placed at equal distances from one another. The thermocouple assembly is contained inside a removable stainless steel tube, of diameter ¼ in. When the axial thermocouple probe is positioned correctly, the position of the thermocouples corresponds to 32 similar thermocouples located on the tube wall. The wall thermocouples measure the temperature of the band heaters. The wall thermocouples are held in place by heat conducting collars positioned beneath each BH.

At the base of the combustion tube a specially constructed filter support plate holds the limestone core in place. It has holes through its centre to allow the axial thermocouple to pass.PT2 and PG7 monitor the pressure at the top of the tube.

3.2.2: Gas Injection System :

As mentioned previously this system consists of Gas source (Figure 3.4) and gas input system Figure 3.5. The injection gases is provided from high pressure (~ 300 bar) horizontal lay, nitrogen cylinders and vertical lay, oxygen (~ 230 bar) cylinders and filtered via filters F1 and F2. The gas is reduced via precise pressure reduction valves

PPRV1 and PPRV2, down to 12 bar above the required reservoir pressure. LMF1 and LMF2 are precision mass flow meter controller, which control the flow rate of oxygen and nitrogen respectively. They are ratio controlled to maintain the required concentration and total flux of the injected gas. Air actuated valves AAV1 and AAV12 are used to shut off the gas supply during shout down procedure. Pressure transducers PT1 and PT2 monitor the gas supply pressure. The oxygen injection temperature is monitored by TC1 in case a reverse burn condition should occur. AAV15 has a normally open valve state. In an emergency, Therefore, it vents any injection gases, as the AAVs return to their normal states.

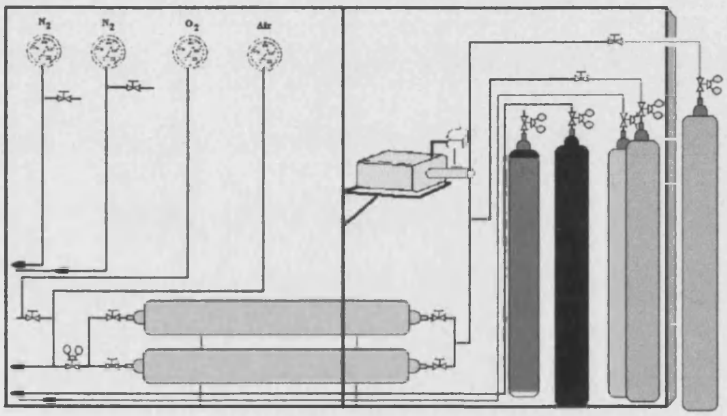

Figure 3.4: Gas Supply system.

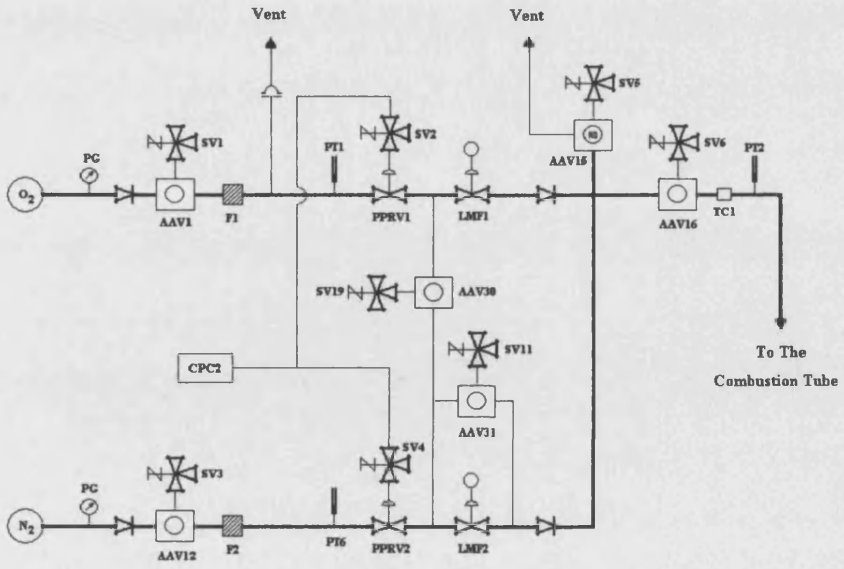

Figure 3.5: Gas Injection System

Manual control panel consists of pressures gauges of in-situ combustion tube In and Out, shell and gas injection. This set of gauges are main pressures around the combustion tube (up, down, surround the tube) . In case of manual shut down or emergency shut down, this control panel will be the only monitor available to the system. A manual control of bleed tube and shell valves are also on the panel as illustrated in Figure 3.6.

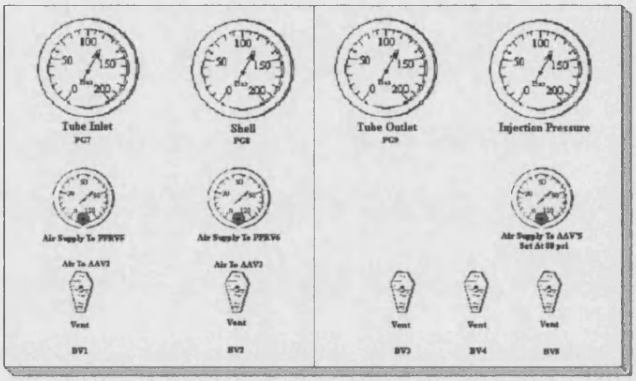

Figure 3.6: Manual Control Panel

3.2.3: Pressure Shell :

The pressure shell contains the combustion tube, providing small overpressure, compared to operating pressure for combustion tube. A photograph of the pressure shell is shown in Figure 3.7. The shell was designed for 330 bar at 100°C. It is constructed from carbon manganese steel in accordance with BS5500, 1988. The annulus between the combustion tube and the shell is filled with Vermiculite, a high efficiency insulation.

Figure 3.7: Pressure Shell

A "Sindanyo" insulating block is placed at the bottom of the shell to minimize heat transfer from the combustion tube to the shell. Thermocouple and band heater connections pass through a series of high pressure "Conax" glands. The inlet and outlet connections pass through a series of high pressure " Conax" glands. The inlet and outlet line of the combustion tube are held in place with two sets of carbon reinforced PTFE Crane "Tetrvee" pneumatic compression rings (piston rings). These are contained in a stuffing box on each end flange of the pressure shell. The inlet line to the tube has an expansion band to allow for thermal expansion.

The pressure difference between the pressure shell and the combustion tube must be maintained below a maximum of about 2 bar, since the Inconel tube is 1.75 mm thick. Any overpressure of the combustion can cause it to collapse. Nitrogen gas is used to pressurize the shell and also prevent corrosion of the BHs. The shell is filled by operating PPRV3 and AAV22. Gas vented via PPRV6 and AAV4, as shown in Figure 3.8. If the 2 bar safety limit is exceeded, AAV19 and AAV3 are opened to allow pressure equalization through the high pressure parts of the system.

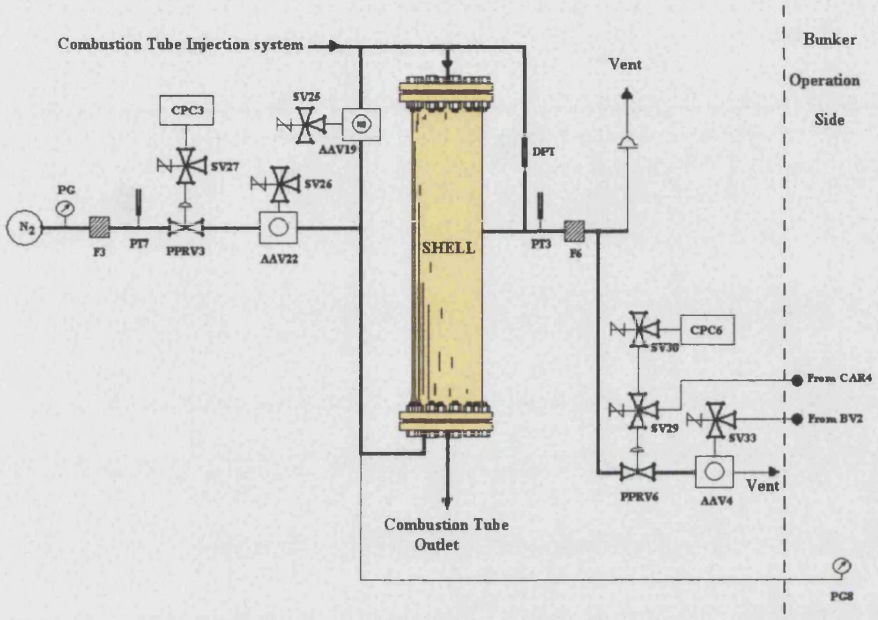

Figure 3.8: Gas Injection for Pressure shell.

PT3 measures the shell pressure. F6 filters any insulating material from the vented gas. A bursting disk is fitted to the shell in case exceed 240 bar, maximum safe working pressure.

3.2.4: Separation System :

In the separation process, the produced fluids from the combustion tube are passed to the high pressure separator (HPS), where they are separated into liquid and gas (Figure 3.9). When the HPS is full, AAV6 is opened and the liquid flows via PRVG1 into the low pressure separator (LPS). PRVL1 reduces the pressure to 3.5 bar.

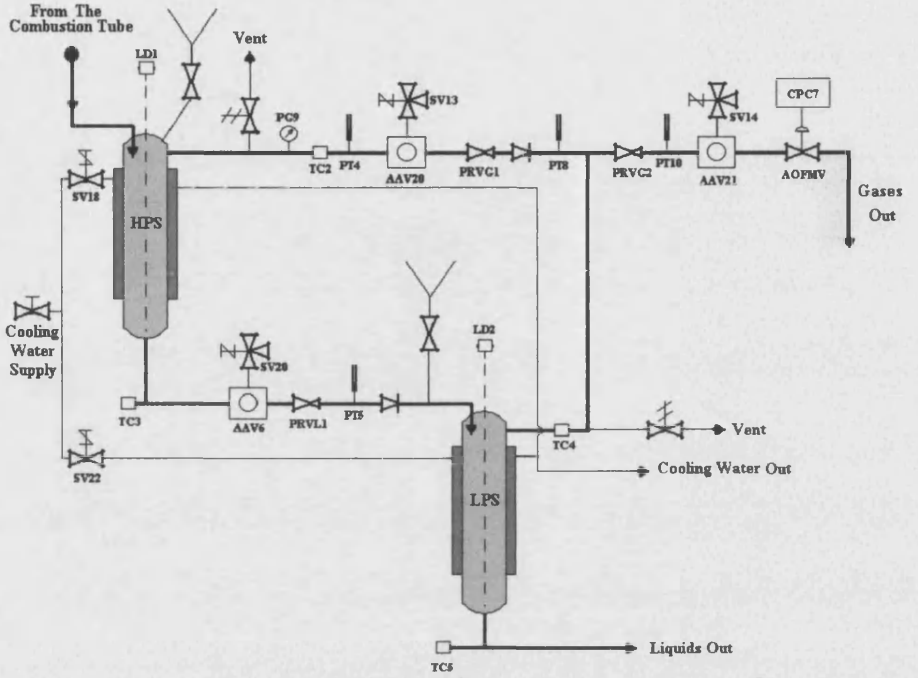

Figure 3.9: Separation system.

PRVG1 reduces the gas pressure from the HPS to 3 bar, allowing liquid to flow from the HPS to LPS at a controlled rate when AAV6 is open. The pressure of LPS depend on two requirements. Firstly the importance of the mass balances. A lower the final separation pressure mean more complete separation of liquid from gas. Secondly, pressure is set too low, control become too difficult. 3.5 bar was found in practice to be satisfactory.

The argument for the use of one separation stage (flashing instantly to 3.5 bar) fails on two counts. Firstly, accurate measurement of the tube exit pressure would have to be made on a multiphase line. Secondly, the composition of the products is not constant, leading to varying gas flow rates.

PT4 and PG9 measure the HPS pressure. TC5 monitors the HPS gas temperature in case of auto ignition. TC3measures the HPS liquid temperature. The temperature is controlled with cooling water via SV18 and a trace heating element with an independent controller. TC5 provides the same control measurement input for the LPS and LD2. PT5 measures the LPS inlet pressure and is used to set PRVL1. PT8 is used to set PRVG1 and PT10 is

used to set PRVG2. PRVL1 and PRVL2 may need to be adjusted during an experiment, as the composition of the produced liquid has a small effect on the pressure at which they are set to deliver. This in turn can affect the rate of draining of the two separators.

Both separators are protected by pressure relief valves. AAV20 is used in an emergency to shut in the high pressure part of the system.

The air operated fine metering valve AOFMV is used to control the back pressure on the tube. This is a very critical control operation. Interestingly, it is positioned at the low pressure side of the system.

3.2.5: Gas Analysis:

The gas was analysed continuously for CO_2, O_2, and CO using analyzers, it can detect full range of the products. This can be seen in Figure (3.11).

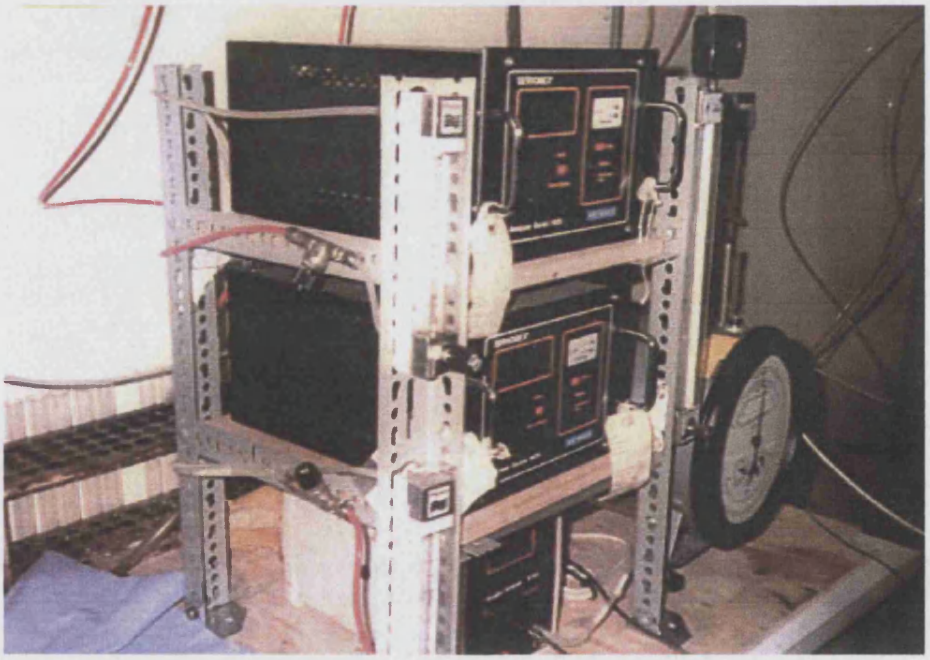

Photo 3.10 : CO_2, O_2, CO analysers

The gases are first passed through the knock out vessel (KOV) where any condensable components are captured (Figure 3.11). The manual control valves ensure that the pressure to the analysers and the wet test meter (WTM) is kept below about 2 psig (Normally less than 1 psig for the WTM). A side stream is dried in a silica gel drier and passed via rotameters R1, R2, and R3 to oxygen, carbon dioxide and carbon monoxide analysers. The analysers exit stream is then mixed again with the main gas stream before entering the WTM, which measures the cumulative volumetric gas flow. The non-return valves prevent a reverse pressure gradient on the analysers.

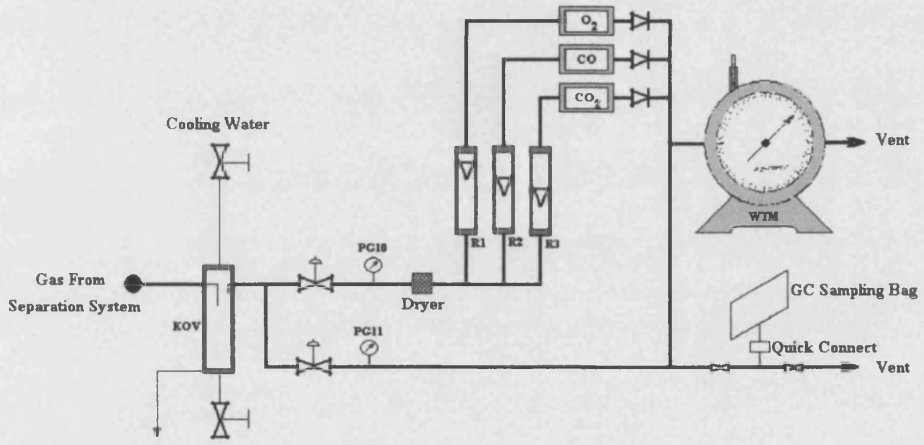

Figure 3.11 : Gas Analysis Unit.

The produced gases can be also collected in a PTFE sample bags for off-line analysis, either gas chromatography (GC) or sample analysis tubes. The small amount of light hydrocarbon (C1-C4) can be measured.

3.2.6: Liquid Sampling :

The liquid from the LPS is passed through PRVL2 to reduce its pressure to a slightly above atmospheric. Liquid is then sampled via SV24. The rotating sampler is capable of accommodating 30 samples of 125 ml. During shut down the oil is drained via AAV5 to the oil drain as presented in Figure 3.12.

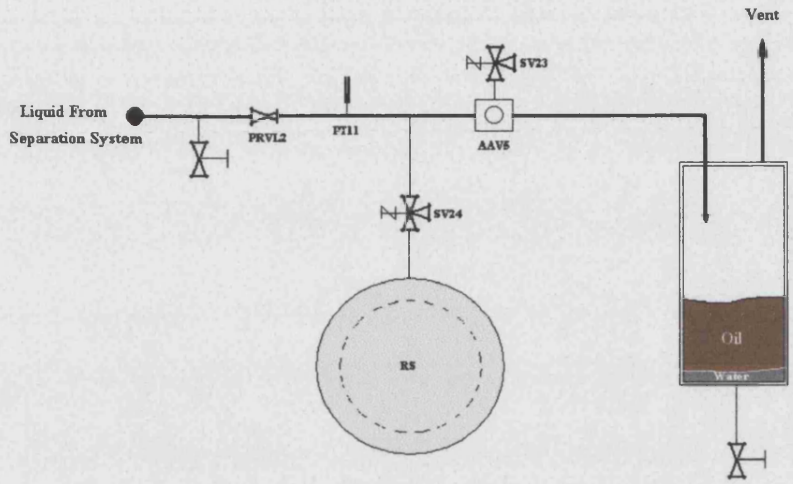

Figure 3.12: Liquid sampling and Collections Unit.

3.2.7: Instrument Air Supply:

This comprises a network of pneumatic (80 psi) lines (1/4 in nylon) servicing the AAVs. The air flow is directed via a combination of solenoid valves (SVs) and current to pneumatic converters (CPCs).

3.2.8: Power and Electronic System:

This works in two distinct ways. First by providing the power necessary to drive the SVs, CPCs, PTs, and LDs. Secondly, to convert signals from the PTs and the LDs to signals that can be inputted to the control computer. Whole wires, connection and the inter-face between the computer and the equaipment are shown in Figure 3.13.

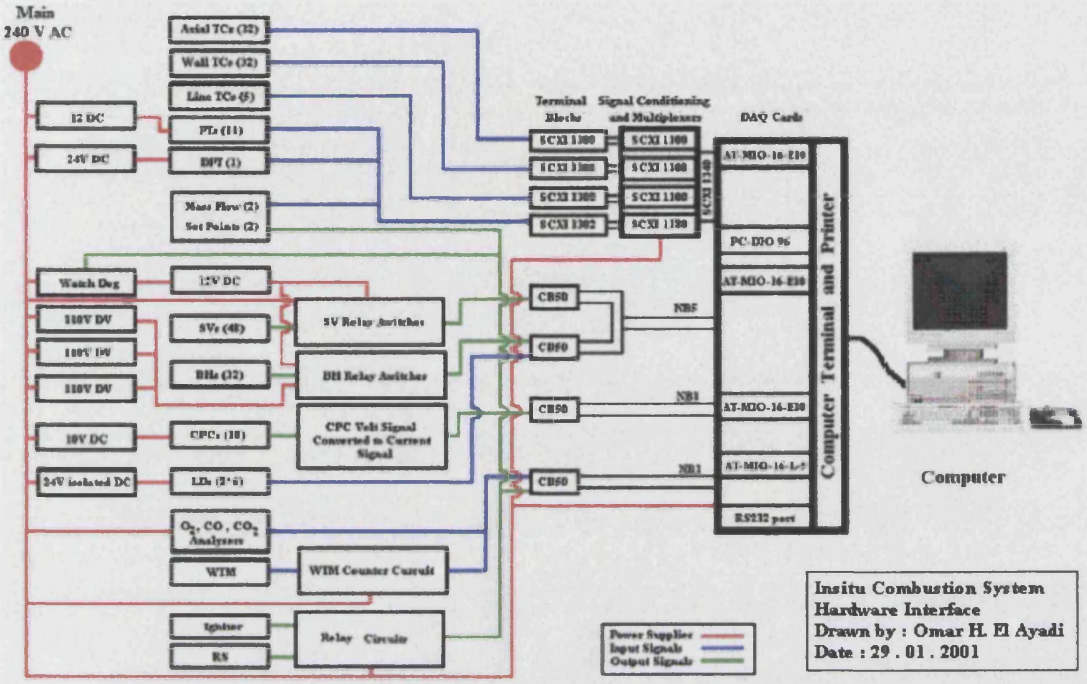

Figure 3.13: Electrical Connection and the Interfacing between the Combustion Equipment and Computer.

3.2.9: Computer:

The signals from the various transducers are monitored and recorded. Control signals are signals are sent out in response to these inputs for overall control of the system.

The combustion tube facility is housed in a concrete safety cell. This is constructed in two sections. The main process and pneumatics in one half (the operations area) and the electronic and computer functions in the other half (the observation and control area).

3.2.10: Shut Down :

This is accomplished using AAV19 and AAV3 (Figure 3.1). When open (their normal positions) they allow pressure equalisation between the shell, and combustion tube and also to HPS. A controlled pressure let down under the control of the computer, takes place by opening AAV6 and AAV5. Note that the large volume of nitrogen in the shell

flow through the combustion tube, and this acts to dilute oxygen in the system at any point during shut down.

The system can also be shut-down manually (Figure 3.1), by opening AAV6 and AAV5, using BV4 and BV5, respectively. CAR4 is reduce the back up cylinder air pressure down to the normal pneumatic line pressure of 80 psi.

If a blockage occurs along the liquid line from the HPS, PPRV6 and AAV4 can be controlled via CAR2 and BV2. Here the path is via the shell vent line. If a blockage occurs between the shell and the tube then PPRV5 and AAV2 (via CAR1 and BV1) must be used in conjunction with PPRV6 and AAV4 to let down the pressure in the shell and the tube separately. This process is monitored using PG7, PG8 and PG9.

3.3: Preparation of Core Material for Combustion Tube:

The following amounts illustrate the volume and weight used in Run 2:

- Prepare 14.796 kg of Lime Stone (MI Calcium Carbonate) needed as rock sample unconsolidated or crushed core.
- Prepare 2.048 liter of water needed (50%) as initial or current water saturation.
- Prepare 2.048 liter (1.757 kg) of oil required (50%) as initial or current oil saturation. Due to gravity effect and deposition of heavy residue at the bottom of the drum. The drum should be rolled few times to be sure homogeneous mixture in the drum before collecting samples.
- Mix water, oil and lime-stone. Then pack it inside the combustion tube, which is placed inside the shell outside the bunker. Then place it in the right position inside the bunker and make the top and bottom connection of the tube and shell.
- Full-up the cylinders with the gases required for the test (nitrogen, oxygen and/or air).
- Before initialising conditions for an experiment, check the reservoir and drain-off any accumulation water inside the air compressor. Start the compressor and adjust the pressure to 80 psi. Switch-on all of the electrical supplies. Next, follow the prompts displayed on the computer.

3.4: Experimental Procedure:

Automatic control and operation of the combustion tube is achieved by computer. LabVIEW, uses the computer language "G". The data acquisition and control of the combustion tube is achieved using a special program called IscView. IscView Controls every aspects of an experiment, from start-up to shut down. Any manual changes that need to be made are prompted by the program. The original IscView program was developed by T.Young , 1997.

The computer program controls Four main tasks simultaneously:

1. Control of pressures.
2. Control of temperatures.

3. Control of flow.
4. Control and detect of liquid level in the separators.

Each of these is a critical routine that the computer needs to control precisely . Failure in control, or inability to achieve the desired set point requirement will result in experiment being terminated.

3.5: Computer Program:

IscView program was written using LabVIEW© (Appendix D) software graphical programming language. It performs unlimited multitasking control and monitoring programs. IscView controls the ISC equipment and also monitors, the collection of data and as well as saving input/output data.

3.6: Commissioning:

Prior to commissioning, extensive checks were made to ensure that all equipment line connections, instrumentation and valves were correctly installed, and working. Two major task were implemented:

1. Commissioning the IscView control program.
2. Commissioning of equipment.

Before an actual run can be performed, the following should also be checked:

1. Test all axial and wall thermocouples in-situ, and be aware that the BHs will oxidize if heated in air.
2. Replace faulty thermocouples.
3. Install the missing check valve in the oxygen line.
4. Replace the jackets on the separators.
5. Connect GC or GC sampling bag.
6. Replace silica gel in water drier (prior to analyzer).
7. Calibrate mass flow meters.
8. Wet test meters
9. Calibrate the CO_2, O_2, CO analysers.
10. Test the power supply needed to achieve adiabatic control in as fast as it can be.
11. Leaks

    Note: Appendix B contain equipment component and check results of solenoidals valves. Appendix C presents the check results of pressure transducers.

3.6.1: Commissioning Performance:

Initially, tests were carried out at 20 bar (Test 1), 50 bar (Tests 2), 100 bar (Tests 3 and 4). There was particular concern to see how the control of the shell-tube differential pressure varied during the experiment, with the most critical phase being the pressurisation.

3.6.2: Pressure Control of Combustion Tube:

Test No. 1:

The results of this test were very poor as the differential pressure greatly exceeded the 2 bar limit, and the control was inadequate as shown in Figure 3.16. It could have been due to the fact that the venting and filling duration (maximum 500 ms, minimum 250 ms) were too large, because dummy tube has a much lower volume. This was obvious by observation of the pressure gauges. In following tests the venting and filling times were reduced.

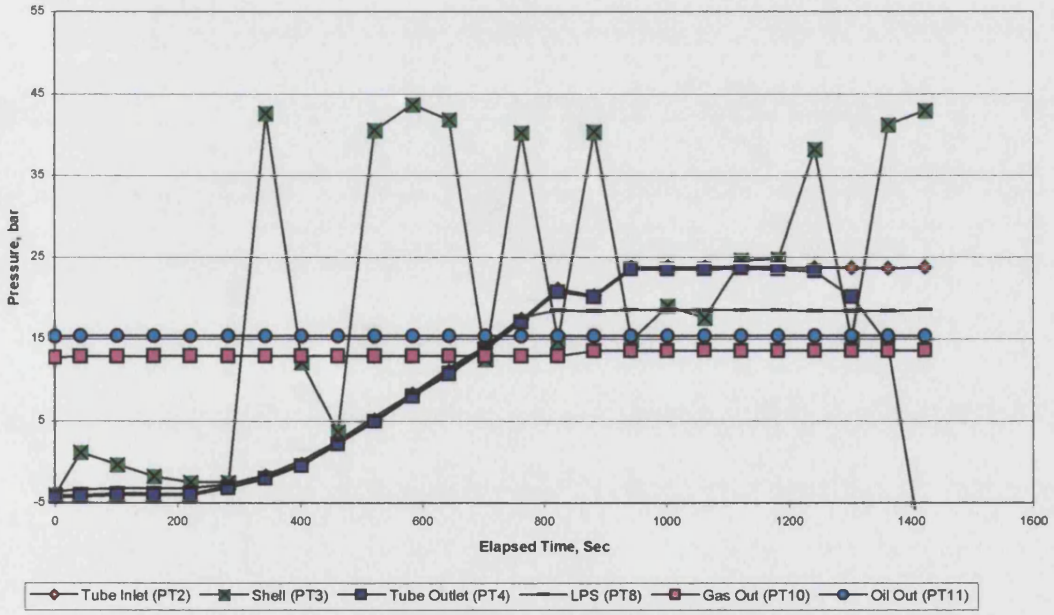

Figure 3.16: Commissioning Test No.1 at 20 bar Pressure.

Test No. 2:

The filling and vent times were reduced down to a maximum of 30 ms, and minimum of 5 ms. There was a slight improvement on Test 1, but the differential pressure still far exceeded the 2 bar limit. The backpressure of the system was also changed, the tube responded well to this but the shell pressure response oscillated in order to match this change (Figure 3.17).

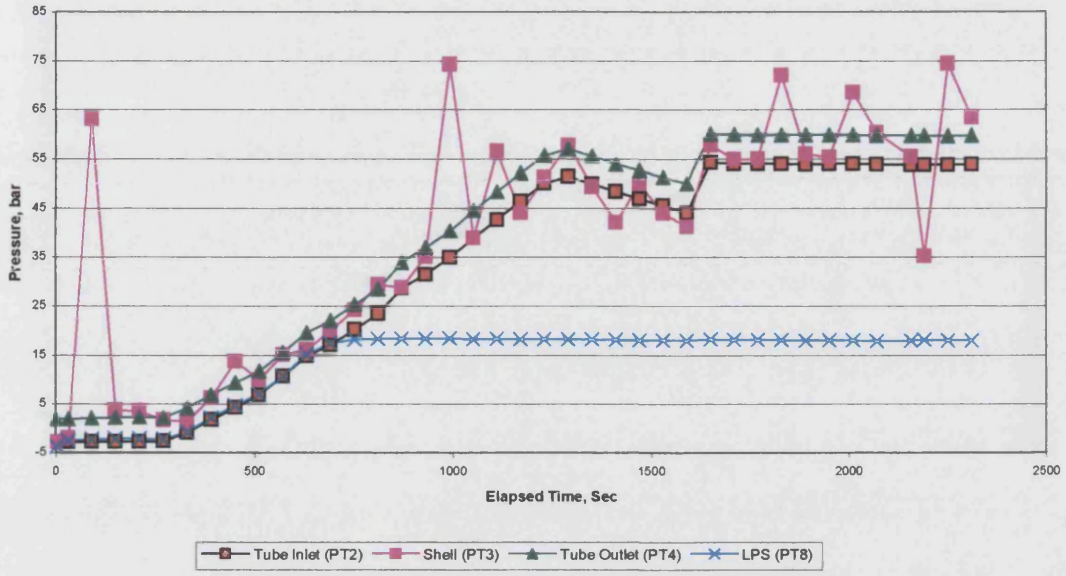

Figure 3.17: Commissioning Test No. 2 at 50 bar Pressure.

Test No. 3:

The same procedure for this test at 100 bar, was used as reported by T.Young, 1997 and S.El-Usta, 1998. Figure 3.18 shows a major improvement over test 2, but the results are still unsatisfactory.

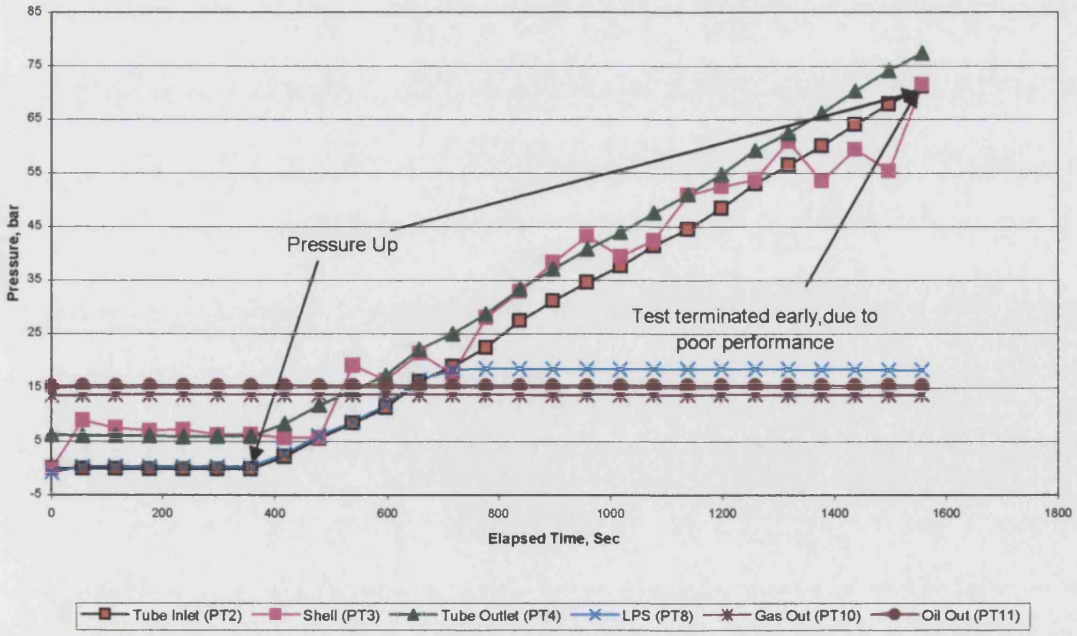

Figure 3.18: Commissioning Test No.3 at 100 bar Pressure.

Test No. 4:

Using the same equipment arrangement as previously, the operation was modified as follows:

1. Communication between the shell and tube was achieved by closing SV25, with AAV19 open (normal position).
2. Since flow into the system is equalized from the tube and the shell, pressurization is very fast.
3. When the pressure of the system is achieved, the SV25 is opened, isolating the shell and tube.

However, once the shell and tube were isolated by opening SV 25 the same variations occurred and exceeded the differential pressure limit. Once this was noticed the test was cut short and the pressure decreased as shown in Figure (3.19).

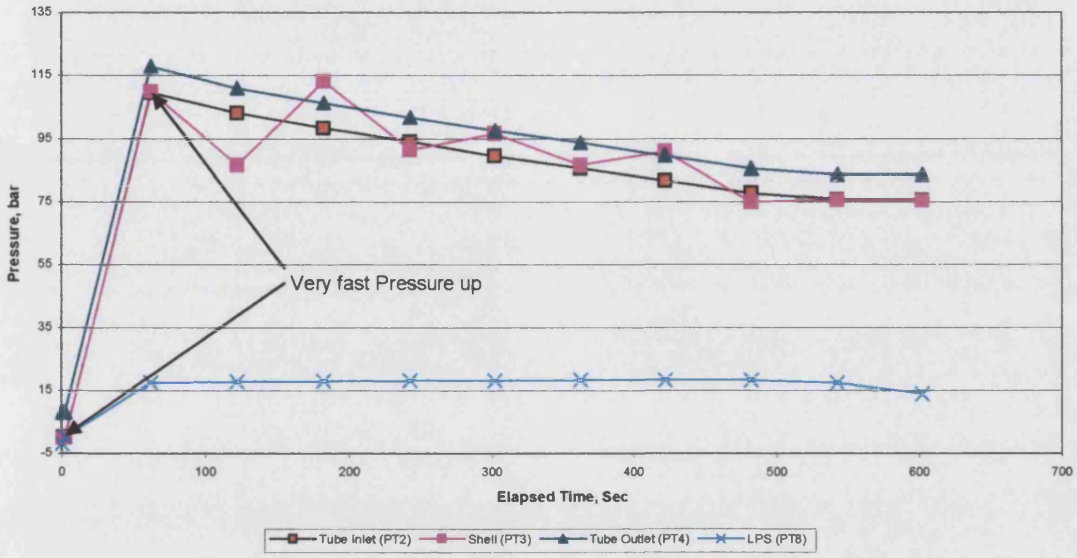

Figure 3.19: Commissioning Test No. 4 at 100 bar Pressure.

Test No. 5:

Referring now to Figure 3.20, some general conclusions can be drawn about the pressurisation of the system during flow operation stages. Firstly, it can be seen that PT3 (shell pressure) behaves erratically during the pressurisation stage (this is the cause of the instability in the ΔP control, already discussed). Control of PT3 settles down at around 2000s. This point denotes the time at which flow was achieved through the system. Initially, once the system had reached the desired operating pressure, there was no flow through the system. In order to detect when flow commenced, the gas outlet from the tube passed through a section of flexible hose (under actual experimental circumstances, this is routed to the gas analyser), into a beaker of water, such that bubbles would be formed when a flow of gas was present. After investigation, it was found that both PRVG2 and AAV21 were closed, shutting in the gas flow. Once these valves were opened (at 2000s), flow through the system was achieved.

PT2 (tube pressure), and PT4 (HPS pressure) increased steadily during the start up period, before leveling off, once the system had reached operating pressure. As expected, under flow conditions, PT4 recorded a slightly lower pressure than PT2, due to the pressure drop through the system. PT5 and PT9 remained at zero during the experiment,

as these instruments are positioned upstream and downstream of the LPS, respectively. The LPS was isolated during the course of this experiment. However, it can be seen that, at 3200s, the reading given by PT5 suddenly increased. This occurred because AAV6 and PRVL1, connecting the HPS to the LPS were opened as part of the system shut-down logic. Finally it is worth noting that all of the pressure transmitters, apart from PT9, were showing zero errors. This should be taken into account when considering the pressures recorded during the experiments.

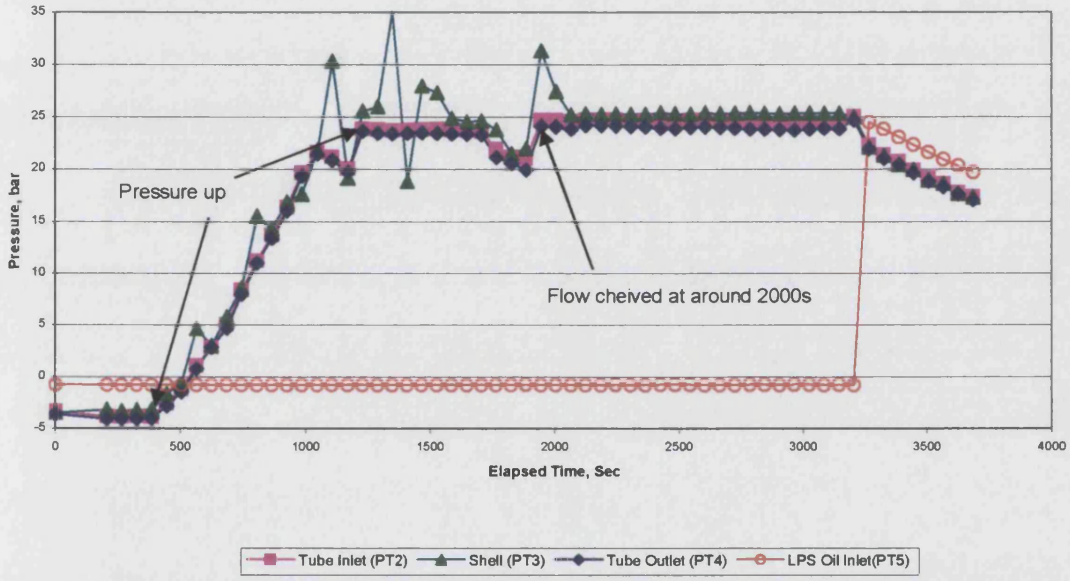

Figure 3.20: Commissioning Test No. 5 at 20 bar Pressure.

Test No. 6:

This was very similar to Test 5. However, more changes were made in the back pressure, and different venting and filling times were used in order to find an optimal setting. This showed that, despite the changes in shell venting and filling times, the response of the shell pressure to pressure changes was still extremely poor.

The conclusion was that significant disturbances in the pressure (resulting from using a small dummy shell), were leading to large calculated values for fill/vent times. This was caused the shell pressure to significantly overshoot/undershoot the desired value. Furthermore, the nature of the control algorithm means that if a calculated vent/fill time

is too high, the resulting sharp increase, or decrease, in shell pressure will result in another large value for the vent/fill time; thus the system becomes unstable.

Given the problems with the ΔP control, it was apparent that there was something wrong with the algorithm used to calculate the fill/vent times. However, there was concern , also about altering the algorithm itself, for fear of making changes that might have found hard to remove at a later date. In general, it was decided not save any changes to the computer control system.

Upper and lower limits exist for the shell fill/vent time.It was therefore decided to repeat the test, using smaller values for the maximum and minimum fill/vent times (20ms and 1ms respectively). This would act to restrict the venting and filling times, with the intention that this would result in more stable control. The pressure test was repeated at 20 bar, to allow a valid comparison with other tests.

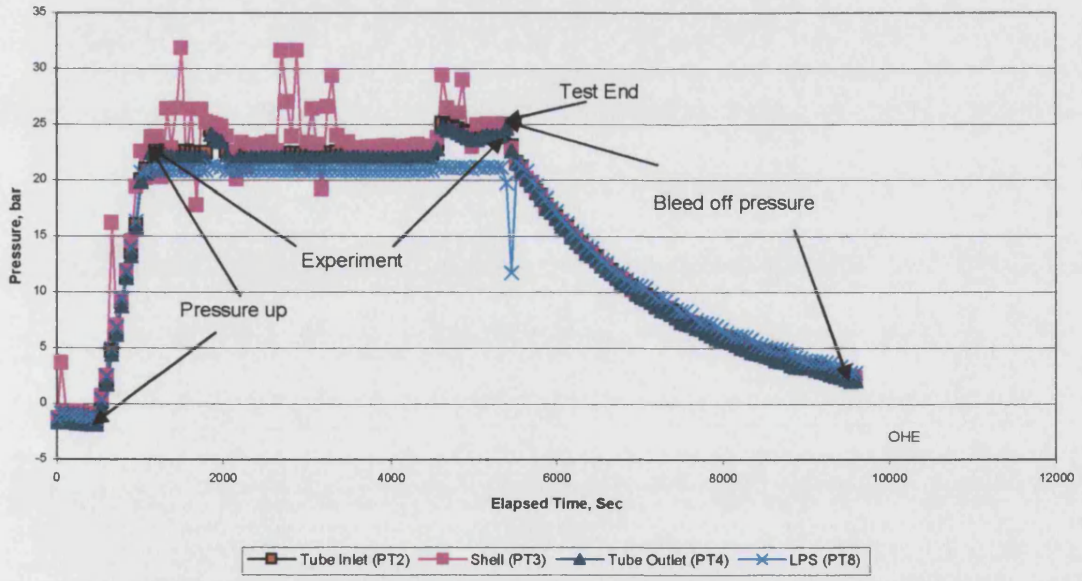

Figure 3.21: Commissioning Test No. 6 at 20 bar Pressure, some Disturbance Caused by Changing Control Parameters.

The results for this test are given in Figure 3.21. It can be seen that changing the limits for the fill/vent times resulted in no noticeable improvement in control, with the 'spikes' in the ΔP being of similar size in both cases.

Test No. 7:

It was clear from the results of the first tests, that there was a need for additional pressure tests to determine the best way of pressurising the system up. However, in addition to this, there was also a need to examine the back pressure control under normal steady flow conditions. Given that there was a possibility that new valve-trims might be required to achieve good back pressure control, it was decided to carry out two tests to determine the effectiveness of the back pressure control. The ΔP control during pressurisation was a secondary concern during these tests.

Two tests were carried out, one at 50 bar (test 7), and one at 90 bar (test 8), to determine the effectiveness of the back pressure control under different conditions.

The working of the back pressure control system can be described as follow:

- PRVG1 and PRVG2 are forward pressure regulators, i.e. they control the pressure on their downstream side by varying the amount of gas let through. In effect, they provide most of the pressure drop between the HPS and the AOFMV
- The Air Operated Fine Metering Valve (AOFMV) is designed to operate over a smaller range of pressures, and works as a back pressure regulator, adjusting the amount of gas leaving the system. In effect, this 'fine-tunes' the back pressure.
- If there were no adjustable PRVG's in the system, it would be necessary for the AOFMV to operate at a range of different pressures, and gas fluxes. This would require several different sizes of valve stem.

In this test, having pressurised the system, it was decided to examine whether the AOFMV could effectively maintain the system back pressure, whilst the PRVG's were adjusted to deliver differing pressures to the AOFMV. The control system for the AOFMV is a standard PID controller operating in a feedback mode. The pressure is measured at the tube, and the signal is sent to the PID controller, which determines the action to take. The controller produces an output signal, which is sent to the Current to

Pneumatic Controller (CPC) which acts on the AOFMV. This was an effective way to introducing disturbances into the system, to examine whether the PID control parameters and the valve trim size would give good back pressure control with varying pressures on the inlet to the AOFMV. In addition, it was possible to test whether PRVG1 and PRVG2 were operating correctly, e.g. to see whether they were blocked.

The test was carried out at 50 bar. The back pressure slowly reduced during the course of the experiment, from around 55 bar to 50 bar. However, since this decrease was relatively steady over the course of the experiment, it does not appear that changing the settings of either PRVG1 or PRVG2 was the cause of this decrease. Rather, it would appear that during the pressurisation stage, the system pressurises up to around 5 bar more than the set point back pressure (i.e. the system pressure rose to 55 bar initially, compared with a set point of 50 bar). During the course of the experiment, the control system slowly reduces the pressure back down to the set point.
The pressure downstream of PRVG1 (but upstream of PRVG2) is measured by PT8. The pressure downstream of PRVG2 is measured by PT10.

Test 7 showed a much better pressurization result than before, with fewer and smaller pressure 'spikes' in the shell. The pressure control of the LPS and the gas sampling system were also checked and showed that the back pressure of the separators can easily be controlled. Clear in Figure 3.22 that there are two sets of (PT8) pressure. This is caused by varying PRVG1 setting from fully open to half open. However, the pressure bleed-off time can be also controlled, as shown in the same figure.

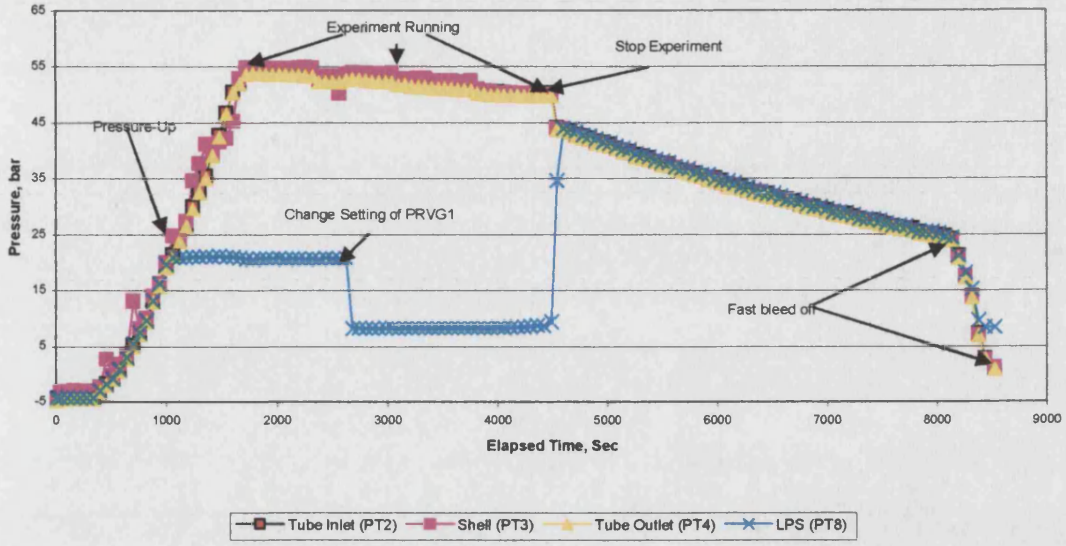

Figure 3.22: Commissioning Test No. 7 at 50 bar Pressure, Change Control Setting Between HPS & LPS (Gas Line).

Test No. 8:

Referring to Figure 3.23, which shows the results for Test 8 (90 bar), it can be seen that the setting on PRVG1 was reduced in stages during the course of the experiment. Since PRVG2 was positioned in between PRVG1 and the AOFMV, PRVG2 should have acted to maintain the pressure on its downstream side to its set value. This should have meant that the pressure at the inlet to the AOFMV would have remained constant. However, in order to maintain the downstream pressure constant, the flow of gas through PRVG1 and PRVG2 would have had to have changed, thus introducing a disturbance to the AOFMV and the back pressure control system.

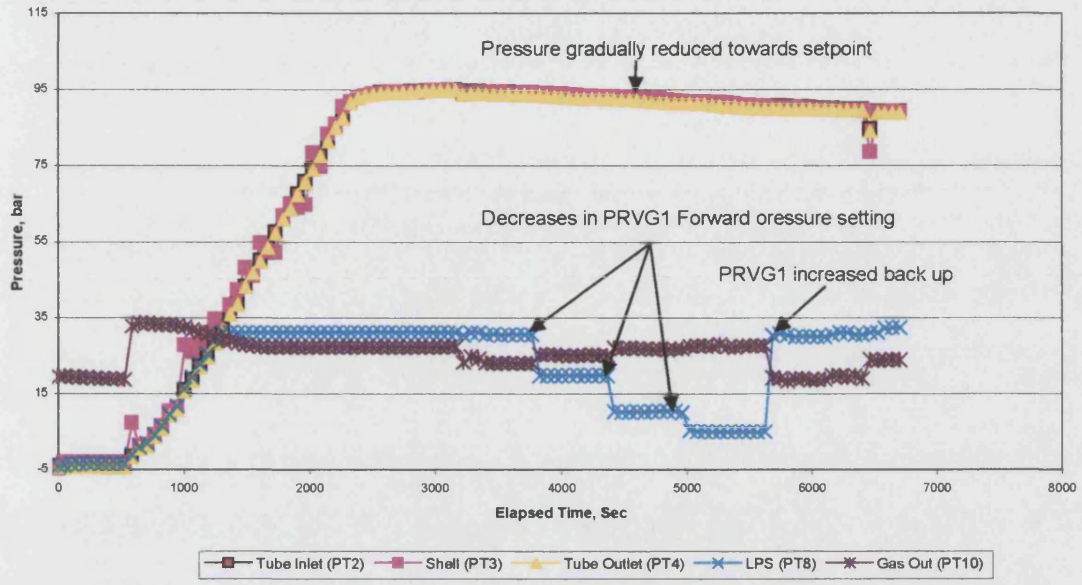

Figure 3.23: Commissioning Test No. 8 at 90 bar Pressure.

From the pattern of the results, the following conclusions can be drawn:

- Broadly speaking, comparing trends for PT10 and PT8, it can be seen that as the PRVG1 setting was varied, PRVG2 was nevertheless able to maintain a (relatively) steady pressure on the downstream side, i.e. at the inlet to the AOFMV. This provides evidence that both PRVG1 and PRVG2 remain in good condition.
- The setting of PRVG1 was varied in steps, from 30 bar to 20 bar, then to 10 bar and finally 5 bar. In order to maintain the set pressure on the downstream side of PRVG2, the flow through the system would have changed to compensate. This would have introduced a disturbance to the AOFMV. Furthermore, since it can be seen that the pressure downstream of PRVG2 varied slightly as a result of changing the PRVG1 setting, a disturbance was introduced to the AOFMV inlet pressure.
- Despite these changes, the system back pressure, as measured by PT2, remained relatively steady during the course of the experiment, dropping by only 5 bar during the period when PRVG1 was being adjusted.
- In addition to varying PRVG1 setting, PRVG2 was also changed, in one step, from 27 psi to 20 psi. Once again, this had no noticeable effect on the back pressure control.

A similar result as test 7 was obtained, where the set point back pressure was 90 bar. In this case, the pressure initially rose to 95 bar, but then reduced during the course of the experiment back down to 90 bar.

Originally, it was thought that in order to achieve good back pressure control, it would be necessary to tune the control parameters (proportional, integral, and derivative times) for the PID algorithm. However, given the results of these (and previous) tests, it was decided that the back pressure control was working perfectly well, and there was no need to change the controller settings.

In both tests, during the pressurisation stage, the shell-tube ΔP was very unsteady, with peaks of around 12 bar ΔP. The problem with this aspect of the control is addressed in the following experiments.

Test No. 9:

Following Tests 1-5, it was felt that the gas supply line pressure to the shell was too high, given the fact that a small-volume 'dummy' shell was used. Because the supply pressure was high, and the volume of space to be filled relatively small, the shell was pressuring up far too quickly, and the control system was unable to deal with the rapid increase in pressure. Of course, a rapid increase in pressure would lead to the control system calling for a large vent time, in order to reduce the pressur, thus leading to instability.

In this test, it was decided to decrease the supply shell gas pressure during the pressurisation stage. This can be accomplished in two ways:

- Reduce the pressure setting on the cylinder forward pressure regulators, thus reducing the nitrogen supply pressure.
- Reduce the 'Injection Pressure Margin'. This figure is the margin by which PPRV3 (shell nitrogen injection forward pressure regulator) is set to exceed the required

operating pressure. This is normally set at 20 bar, so if for example an operating pressure of 50 bar is required, PPRV3 is set to deliver 70 bar.

- Adjust the CPC ratio, i.e. the ratio of the controller output to the controller input, or adjust the time delay between the control determining the output, and the valve responding.

A further problem with the current control set-up, is that during pressurisation, PPRV3 is set to deliver a fixed pressure, determined by the required operating pressure, and the pressure margin. This means that the full supply pressure is available at all times during the pressurisation, even at the beginning of the experiment, when the system is at a low pressure. This results is a large pressure differential between the gas supply and the shell; this in turn results in extremely rapid filling of the shell, initiating the instability seen in the early stages of Tests 1-5.

It was therefore decided that, in addition to reducing the injection pressure margin, we would manually regulate the supply pressure by adjusting the pressure regulator on the supply cylinders themselves. It was decided to start off with the cylinders delivering only 20 bar pressure, and as the experiment progressed and the shell pressured up, the pressure delivered by the cylinders would be further increased. The idea was that this would allow PPRV3 to operate around the middle of its range, allowing for good control. Furthermore, the result of this would be that the shell pressured up more slowly, leaving more time for the control system to respond to changes.

Referring to the difference between the shell and tube pressure ΔP presented in Figure 3.24 and 3.25, it can be seen that during the first period of the pressurisation, until around 2000s had elapsed, the ΔP control was very good (successfully maintained within around $\pm$1bar). Unfortunately, it was not possible to plot superimpose the variation in gas supply pressure with time, due to the fact that PT7 (on the shell nitrogen supply line), was absent

from the system. By maintaining the supply pressure at just 20 bar initially, the shell pressured up more slowly, allowing for better control.

Test to try and improve the pressure up and pressure down of the system. The test begins well but there are still large pressure variations on the shell side of the equipment. The pressures of the low-pressure separator and gas sampling system are also varied again. There were also problems, with the pressure in the gas cylinders, hence the low-pressure spike at around 3000 s elapsed where this was switched to a different cylinder.

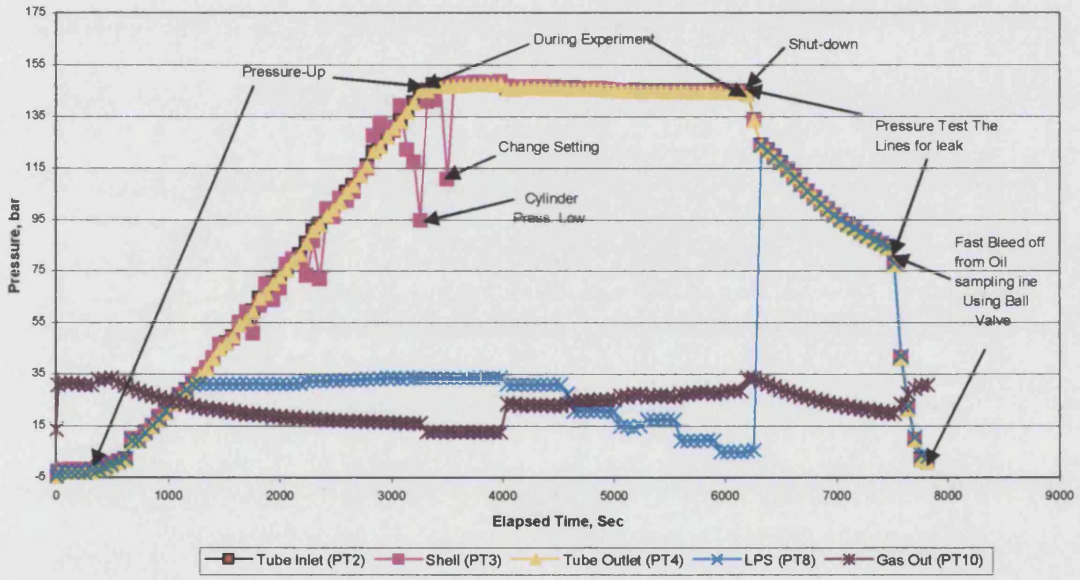

Figure 3.24: Commissioning Test No. 9 at 145 bar Pressure, Pressure Up and Down.

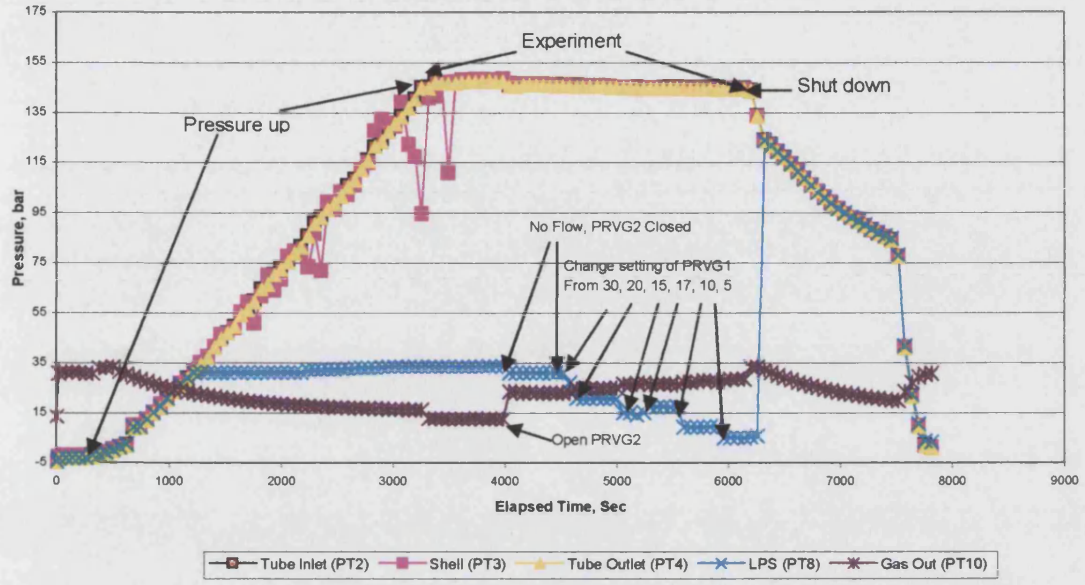

Figure 3.25: Commissioning Test No. 9 at 145 bar Pressure, Control Back Pressure by Varying PRVG1 & PRVG2.

However it can be seen that, towards the end of the pressurization stage, there are 'spikes' in the ΔP, reading up to 50bar, which is clearly an unacceptable performance. It is clear from Figure (5. 11- A and B) that the cause of these spikes were due to substantial decreases in the shell pressure. It seems likely that this resulted from the cylinder supply pressure (which was being manually adjusted at the cylinder pressure regulator) becoming too low in comparison with the pressure in the shell as we reached the end of the pressurisation. The effect would be that when the shell required filling, the supply pressure was only slightly higher than the required operating pressure. Since it was known that there were leaks within the system (which would have caused pressure reductions, necessitating opening the filling line to the shell), it seems likely that the low supply pressure meant that the shell was not 'topped up' quickly enough to avoid the reduction in pressure.

During the shut-down period, in order to speed up the depressurisation, a ball valve was opened on the line which would normally pass to the rotating sampler. This is the reason for the very rapid depressurisation of the equipment.

Test No.10:

The default control mechanism for the pressurizing during start-up is as follows:

- The tube pressure, as measured by PT2, is increased via the Oxygen/Nitrogen injection lines.
- The shell and tube are isolated from one another. During the start up, the shell pressure is controlled so as to maintain the shell/tube ΔP at a maximum of 2 bar.

Although, superficially, it would seem to be logical for the shell and tube to be in communication during pressurisation, allowing equalisation of the pressures during the transient pressurisation stage (when the ΔP is most difficult to control). Once the system has pressurised, the shell must be isolated from the tube. Previous researcher T.Young, 1997 has discussed this issue, and suggested that the self-tuning nature of the control system leads to problems when initiating the shell/tube ΔP control. It was therefore decided to conduct an experiment to investigate this further. The back pressure chosen was 60 bar. Vent and fill limits were set at a maximum of 20ms, and a minimum of 1ms, as before.

The control logic was altered such that AAV19 would remain open (communication between shell and tube) during the pressurisation stage, and would close once the system was up to operating pressure (isolating the shell and tube). In addition, it was decided to fill both the shell and the tube via the tube supply line, in order to enable the shell and tube to be pressurised together. Therefore SV27 was closed during the pressure-up (preventing filling via the nitrogen supply line). Once the tube had pressured up, SV27 was opened back up allowing flow via PPRV3 to the shell, i.e. the system was returned to its normal operating state. These changes illustrated precisely in description of computer programs in the previous chapter.

The results for this test are given in Figure 3.26. It can be seen that the ΔP control was excellent throughout the test. The greatest ΔP recorded was –2.5bar. This is slightly more than the target of ±2 bar, however in practice, the extra strength imparted to the combustion tube by the matrix of sand and oil means that a tube failure would be unlikely.

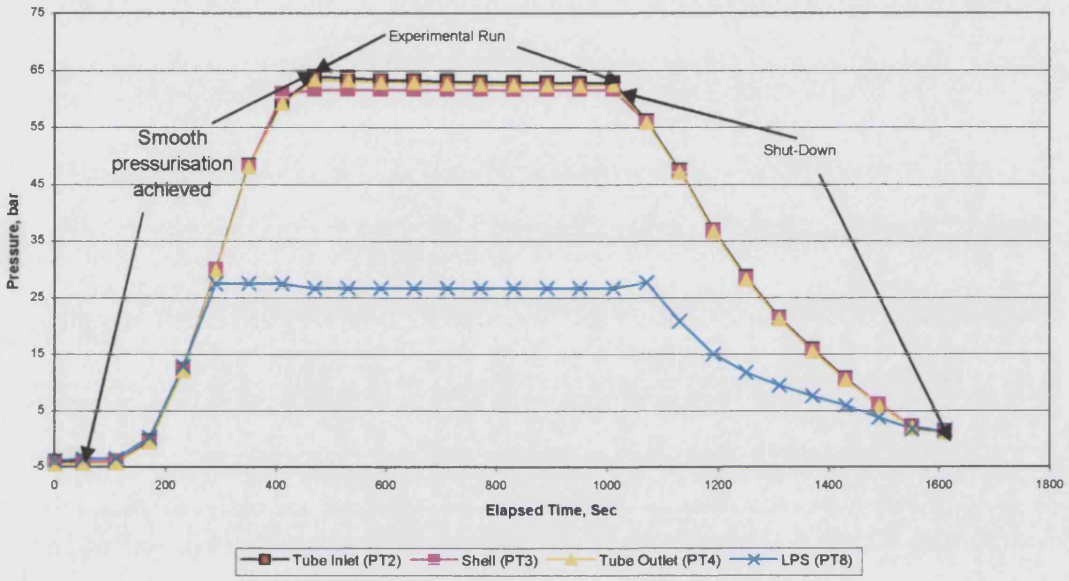

Figure 3.26: Commissioning Test No. 10 at 60 bar Pressure, Smooth Pressure-Up Control.

The largest change in ΔP in Figures 3.26 occurred at the same time as the pressurisation sequence was completed. The ΔP reduced from +1.5 bar to –2.5 bar. It is likely that the problem here was one of initialisation, as described by a previous researcher[138]. It is possible that because the control system logic isolates the shell from the tube (i.e. opens SV25) *before* PPRV3 is initialised to allow pressure control of the shell (i.e. SV27 is opened), there is a small time delay during which the shell is isolated from the tube, and it is not possible to fill the tube with gas. Under these circumstances, if any venting were to take place, or if there were any leaks on the shell side, the shell would lose pressure, and there would be no means of re-pressuring it (until PPRV3 was initialised). This

would cause the shell pressure to fall, accounting for the falling ΔP observed during this experiment.

Test No.11:

Following the successful test of the control system in Test 10, it was decided that Test 11 would consist of a further pressure test, to examine the effectiveness of the ΔP control at much higher pressures. 208 bar was chosen as the maximum pressure that ISC experiments might conceivably operate at.

The results are given in Figure 3.27. The pattern observed was similar to Test 10. ΔP control was excellent until the point (at about 4000s), when operating pressure was reached. At this point, a sharp drop in ΔP was recorded, down to –5 bar. This coincided with the initialisation of PPRV3 and the isolation of the shell from the tube. The explanation for this is exactly the same as for experiment 10, namely that the time delay between the shell and tube being isolated, and PPRV3 being initialised, allowed the pressure in the shell to fall. The effect is more pronounced than in Test 9, due to the higher pressure used in this test (which would have resulted in more rapid venting/leaking of air from the shell during the time delay period). It can be seen that once it was noticed that the pressure in the shell was falling rapidly, the supply pressure was step-increased to speed the recovery of the shell pressure. However, given that there was a significant time delay, of almost an hour, between the ΔP falling, and the ΔP recovering.

This problem would be less apparent if the actual shell were used; given that the volume is so large, venting of small amounts of gas would result in much less of a change in the shell pressure. In addition, the system would be less sensitive to venting and filling times.

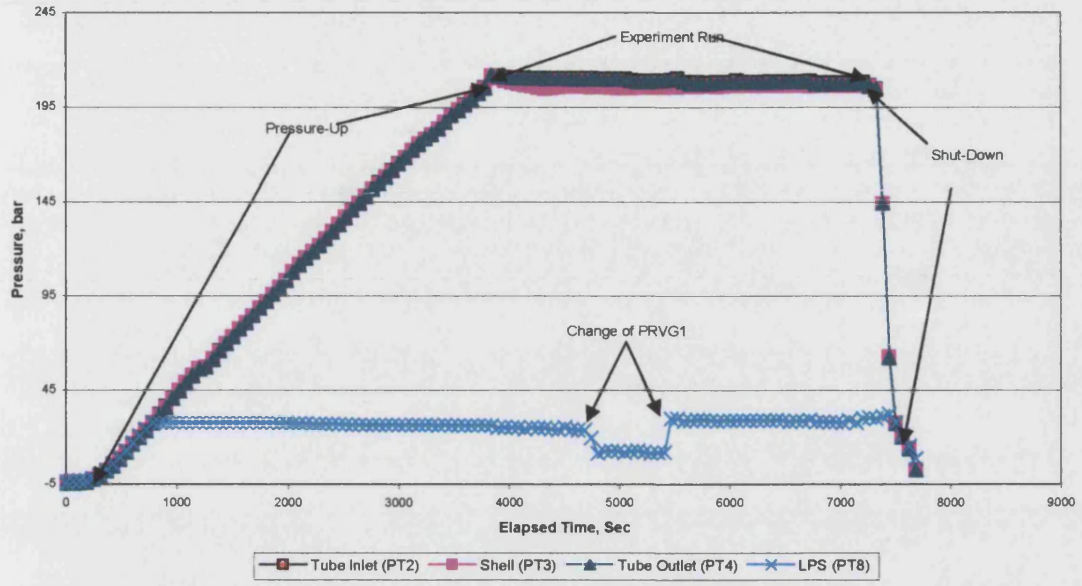

Figure 3.27: Commissioning Test No. 11 at 208 bar Pressure.

It is also worth pointing out that the time delay that occurs during the change over of the control at the end of the pressurisation stage, may well result from inadequate computer control power. Furthermore, switching from pressurisation to stable operation, several other tasks switched on simultaneously i.e. ignitor and B.H. control .. etc. However, the multitasking program will shares the process control time. If further processors were added to the system, it would be possible to enhance the multitasking of the different control loops.

The main problem, therefore with tests at very high pressure, is the response time required to reach an acceptable ΔP, following a disturbance. It is appropriate to compare the results of Tests 10 and 11 (which both experienced a disturbance caused by the isolation of the shell from the tube upon reaching operating pressure), on the basis of a response time.

Test No. 12:

The purpose of this test was to install an alternative AOFMV for regulating the system back pressure, under flow conditions, to determine whether the valve was operating correctly. In addition, this test gave us a further opportunity to look at the control of the ΔP, using a different pressure to those used so far (110 bar in this case).

Referring to Figure 3.28, it can be seen that a spike occurred in the ΔP at the point where the system isolated the shell from the tube (i.e. when the pressure had been achieved). This is a similar pattern to that observed during tests 10 and 11.

This pattern fits in with previous observations that the higher the system pressure, the greater the response time (due to the longer time taken for the pressure to recover in the shell).

Finally, after the system had pressured up, it was possible to check the spare back pressure AOFMV. Unfortunately it was found that the valve stem was jammed (the stem was stuck to the valve seat), and so we were initially unable to obtain flow through the system. Finally, the manually operated bypass around the AOFMV was opened, in order to allow flow to start. The AOFMV was taken out of service following this experiment, and replaced with the original valve.

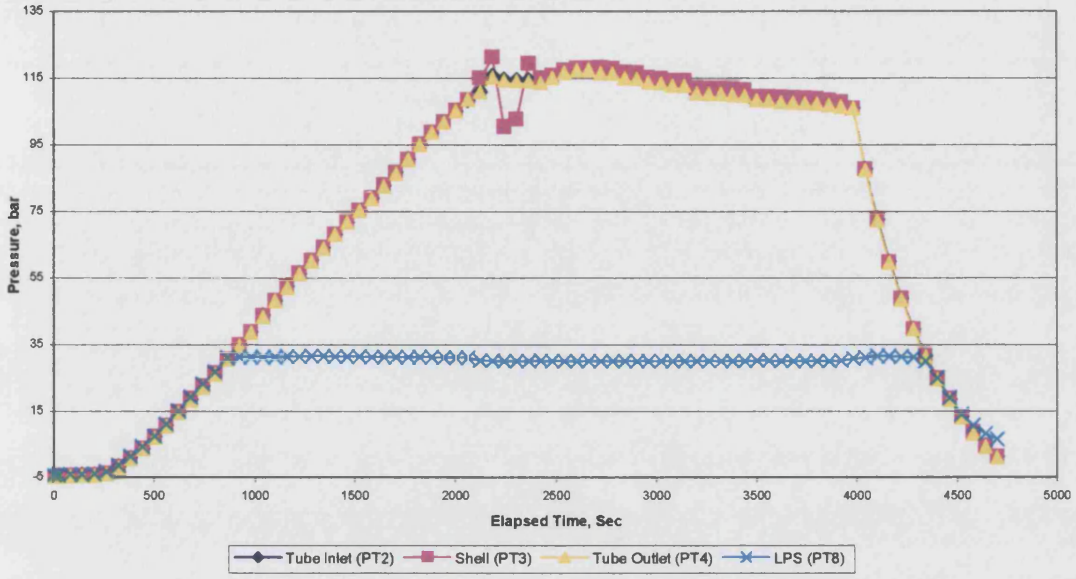

Figure 3.28: Commissioning Test No. 12 at 110 bar Pressure.

Test No. 13:

This test was in preparation for the level control tests that follow. Since it was necessary to connect together the shell and the tube in preparation for the level tests, it was thought necessary to ensure the pressure control worked correctly in this situation, before level tests were carried out. The results are shown in Figure 3.29. It can be seen that the ΔP control was excellent (no more than ±0.5 bar), as would be expected when operating with the shell and tube connected up (so that they pressure up together). Once the operating pressure had been reached, flow commenced, and the back pressure control successfully held the pressure at the set point of around 60 bar. No problems were experienced during this test, and so it was decide to proceed with the level control tests as planned.

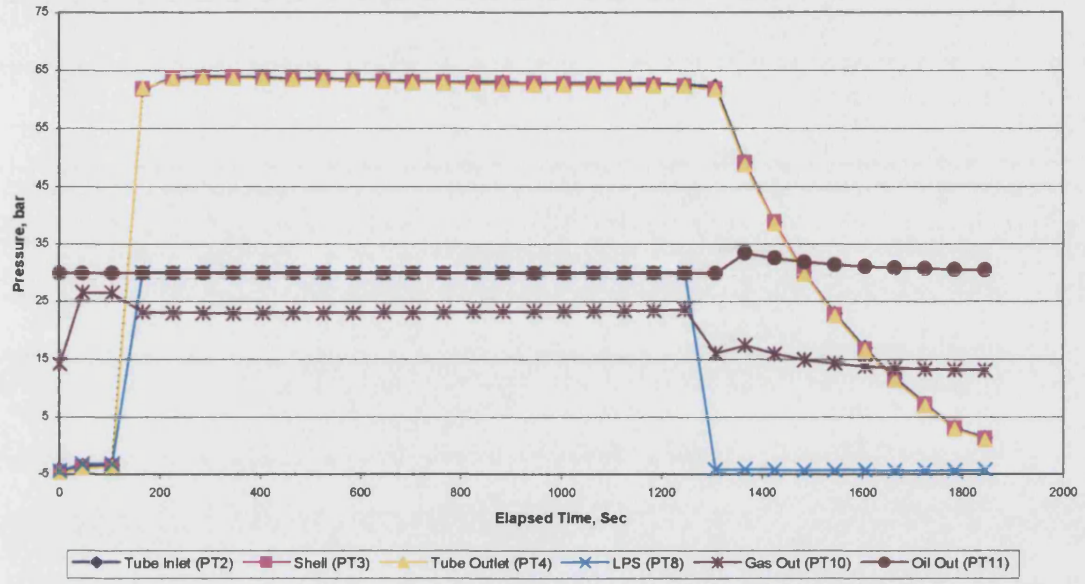

Figure 3.29: Commissioning Test No. 13 at 60 bar Pressure.

3.6.3: Level Control Tests :

Test No. 14:

Both the HPS and LPS separators use the same method for controlling the liquid level. A float device, which moves up and down with the liquid level, activates one of 8 switches placed at different vertical positions within the separator as programmed from total of 12. The level is thus indicated by a number between 1 and 8, with 1 being the lowest level setting, and 8 being the highest level setting. The signal from the level detector is sent to the computer software; the sub-vi 'Separator Control' opens a valve on the liquid outlet line, in order to drain the vessel, when the level reaches an operator-determined 'High Level', (HPH for the high pressure separator, LPH for the low pressure separator). The High Level is normally set to switch 8 on the level detector. When the level falls to reach the 'Low Level', (HPL for the high pressure separator, LPL for the low pressure separator), the valve on the liquid outlet line is closed, allowing the level to build up in the separator. The low level is normally set to switch 1.

The level control described above applies to both the HPS and LPS. The LPS is fed by liquid from the high pressure separator, and therefore the level control of the LPS is dependent upon the HPS level control working correctly.

Initially, it was discovered that the forward pressure regulator, PRVL1 was missing from the system. Under these circumstances, it would not have been safe to operate the HPS to LPS liquid line, since this pressure reduction valve was responsible for maintaining the pressure drop between the high and low pressure separators. The first task was therefore to locate and re-install the valve.

Once this had been done, the shell and tube were connected, and the system water reservoir was filled as illustrated in Figure 3.30.

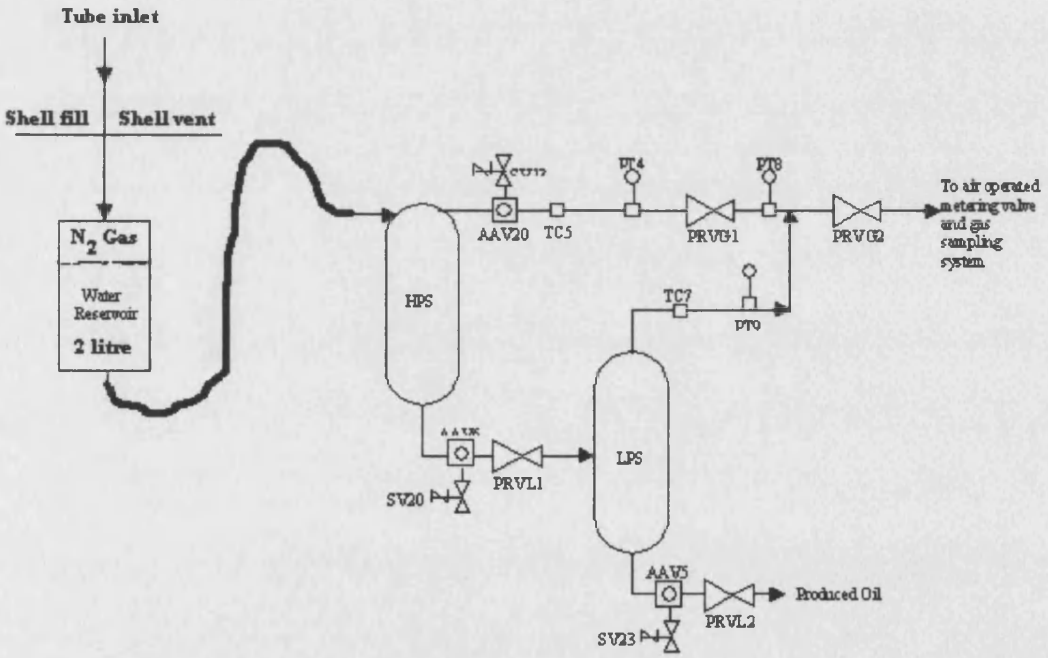

Figure 3.30: Line Connections for Testing of Separators.

The results of Test 14, are given in Figure 3.31. This first experiment was not a success. Initially, it was found that PRVL1 was plugged, since there did not seem to be any liquid passing from the HPS to the LPS. Secondly, we were unable to obtain any gas flow through the system, and this problem was traced to PRVG2, which was also plugged.

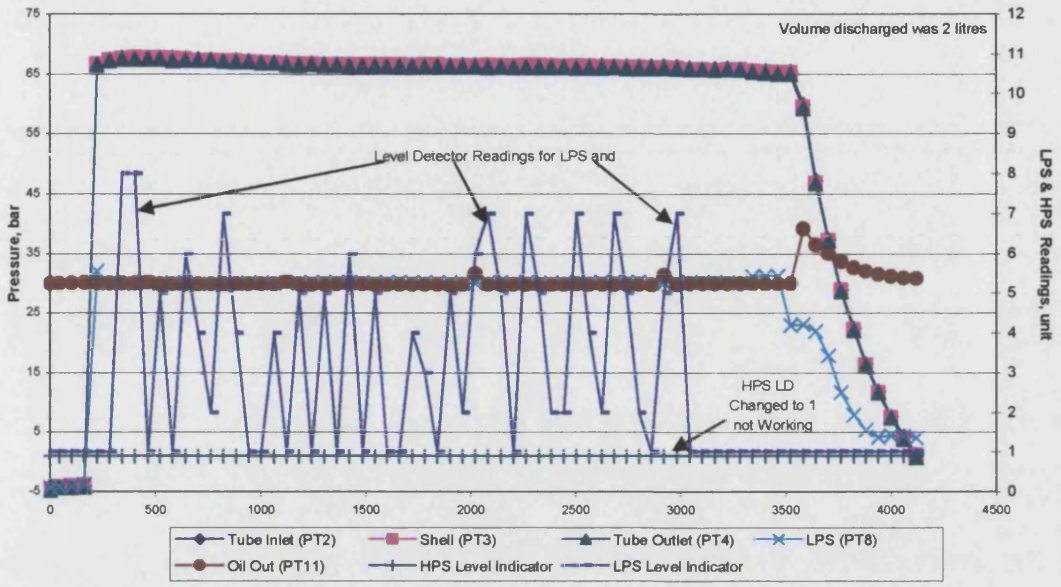

Figure 3.31: Commissioning Test No. 14 at 65 bar Pressure, Test HPS and LPS Level Detector.

The next step was to clear the blockages from PRVL1 and PRVG2. This was done by disconnecting the equipment, and blowing instrument air backwards through the valves. Once the blockages had been cleared, the valves were re-installed. It should be noted that due to the absence of the correct liquid pressure regulator (PRVL1), it was necessary to operate by using a gas pressure regulator for the purposes of these tests. This would not provide adequate control for liquid oil, as the regulator would foul up very quickly.

The results Figure 3.31 show that the level controller on the LPS successfully controlled the level between the Low and High level switches (switch 1 and 8 respectively). This indicates that the level control on the LPS is working correctly.

Test No. 15:

A second test was carried out, which was similar to the first. The results for Test 15 are given in Figure 3.32. Initially, it was noticed that the HPS level reading was stuck at the lowest position, i.e. switch 1. This presented a problem, as it meant that the control system would keep AAV6 (the HPS liquid valve) shut. This would have meant that no

liquid would be passed to the LPS, which in turn would have made it impossible to test the level control on the LPS. To overcome this problem, the 'Separator Level Control.vi' sub program was altered to set the High level on the HPS to switch 1, i.e. the lowest level position. This caused the control system to keep AAV6 open, (since the valve opens to drain the vessel when the high level switch is reached). This allowed water to pass between the HPS and the LPS. By adjusting PRVL1, it was possible to obtain a reasonably steady flow of water through the system to the LPS.

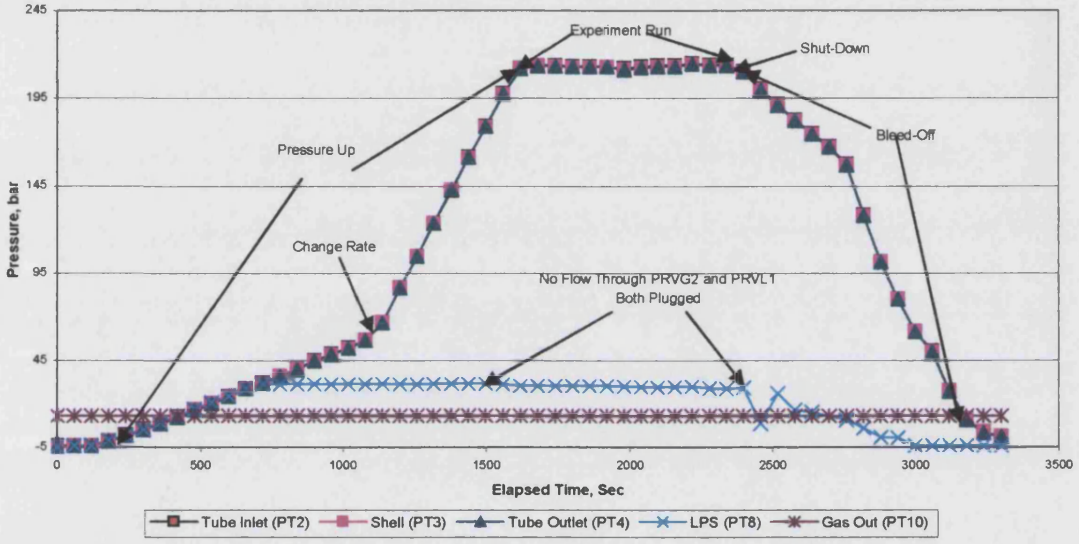

Figure 3.32: Commissioning Test No. 15 at 210 bar Pressure.

After the experiment, the HPS was opened in order to examine the problem with the level detector. When the level detector was removed, it was found that a section of the float was missing. It was therefore necessary to construct a new float, to allow the level tests to be completed. Unfortunately, the new float was not available in time to carry out any further tests.

However, given the successful recommissioning of LPS level control system, it was confidently anticipated that the HPS system would work equally well. The control of the system back pressure Figure 3.31 was excellent during these tests, which is encouraging, given that the disturbances in the level control will effect the volume of the vapour spaces in the separators, thus effecting the pressure control.

In addition to carrying out checks on the level control system, it was decided to calibrate the level detector position with the length of the level detector stem, for different positions. The tests were repeated three times in order to allow cross checking of results. The pattern in the results is clear, that is to say level detector reading increases with stem position, as one would expect. By carrying out a trend analysis on the data, it has been possible to calculate the equation of the straight line which best describes the data. This is as follows:

Computer reading = 1.7587 x length of needle – 13.071

In addition, it was possible to calculate the volume of the separator, by weighing before and after draining of water. The results were as follows:

Weight of Empty flask = 58.2 grams
Weight of flask + water drained from HPS = 323.8 grams
Weight of water drained from separator = 323.8-58.2 = 265.5 grams
Approximate volume of the separator = 265.5 cm^3 (since 1 gram ≅ 1 cm^3)

The total volume of water drained off between the level detector positions 1 and 12 was only 50 cm^3. This represents around 19% of the total volume.

The results for the High Pressure separator followed a similar pattern, with calibration as follows:

Computer reading = 4.094 x length of needle – 1.1865

The volume of the separator was found to be 289 cm^3, using the same method as before.

The total volume of water drained off between the level detector positions 1 and 12 was only 49 cm^3. This represents around 17% of the total volume.

5.5 : Thermocouple Tests:

Test No.16:

Results for the thermocouple tests are given in Table (5.1). It was found that thermocouples Numbers 1, 3, 5, 15, 20, 23, 26, 30, 31, 32 were missing. These were replaced with new thermocouples and tested along with the other thermocouples. In addition, thermocouples Numbers 6, 10 and 28 were found to be broken.

Table (3.2) : Calibration test of In-Situ Combustion Tube Wall Thermocouples Test Conducted In {26/02/2001} :

Thermocable No.	Length, mm	Room or Test Temperature, °C	Resistivity Tests, Rs, Ω	Note
1	**480**	**-**	**7.6**	**M (New)**
2	**510**	**23**	**11.7**	
3	**560**	**-**	**8.8**	**M (New)**
4	**590**	**23.2**	**13.5**	
5	**640**	**-**	**10.1**	**M (New)**
6	**650**	**23.1**		**replaced**
7	**690**	**23.2**	**16.3**	
8	**750**	**23.2**	**11.2**	
9	**770**	**23.2**	**17.8**	
10	**810**	**23.2**	**18.9**	**Replaced**
11	**840**	**23.3**	**18.9**	
12	**890**	**23.4**	**20.0**	
13	**930**	**23.0**	**21.3**	
14	**1030**	**23.0**	**15.3**	
15	**1020**	**23.0**	**14.9**	**M (New)**
16	**1040**	**23.0**	**23.0**	
17	**1080**	**23.0**	**24.7**	
18	**1120**	**23.0**	**25.3**	
19	**1160**	**23.0**	**26.9**	
20	**1240**	**23.0**	**17.5**	**M (New)**
21	**1460**	**23.0**	**20.5**	
22	**1450**	**23.0**	**20.4**	
23	**1320**	**23.0**	**19.6**	**M (New)**
24	**1120**	**23.0**	**17.0**	
25	**1610**	**23.0**	**22.4**	
26	**1440**	**23.0**	**21.1**	**M(New)**

27	1570	23.0	22.4	
28	1507	23.0		Replaced
29	1537	23.0	35.5	
30	1600	23.0	23.5	M (New)
31	1620	23.0	24.0	M (New)
32	1650	23.0	38.7	M (New)

Note :

- *M (New) : It mean the thermocouple was missing and it replaced with new ONE.*
- *The thermocouple No. 6, 10, and 28 replaced.*

Combustion Tube Experiment Commissioning

Commissioning Tests :

Extensive revamping of the combustion tube facility was carried out to replace defective parts of the system and to include a number of important modifications, mainly concerned with process control and the production system.

Upon completion of the revamp, a series of commissioning tests as made to test the operabily of the system. The operating conditions are reported in Table 4.1.

Table 4.1 : Combustion Tube Commissioning Tests.

Experiment Condition\Run Number	Run 1	Run 2	Run 3
Back Pressure (bar)	90 – 100	200	200
Reservoir Bed Temperature (°C)	60	60	60
Ignitor Temperature (°C)	350	400	350
Air Injection Concentration (%)	100		
Produced Gas Flux (m^3/m^2hr std)		27.1	62.3
Cylinder Supply Pressure Max.(bar)	230		
So_i (%)	70	50	30
Sw_i (%)	30	50	70
Band Heater Operation	Yes		
Dry Sand Pack	No		
Reservoir Core Material (Crushed)	MI Lime Stone		
Clay content (%)	0		
Porosity (%)	42.8		

Run One :

Run 1 was made to test the modified computer program (Appendix E) and to test all of the equipment and instrumentation.

Figure 3.33 illustrates the pressure control achieved when the combustion tube was pressurised up to 90 bar. Apart from the slight overshot, the pressure control is maintained with the desired limit. Important, the difference between the shell and tube pressure is excellent. The Figure illustrate only two stages. The first is pressure build up and the second is experiment combustion and displacement stage. The third stage is missing from the chart because it was not able to continue the experiment due to electrical failure.

There are three parts to the pressurisation profile. During the first 36 minutes, increasing of PPRV1 and PPRV2 by 0.01 mA, causing a high differential pressure between the tube and shell. There was a short period between the first stage and the second part when no N_2 gas was injected to the shell (also the tube). The small pressure increase was due to a compression caused by temperature effect. During the second part of pressurisation, the increment to PPRV1 and PPRV2 was decreased to 0.0025 mA. Excellent differential pressure control was achieved. It was not necessary to bleed-off any nitrogen from the shell to control the differential pressure.

During the second stage of pressurisation, approximate 36 min. Injection of nitrogen was continued in order to cool down the reservoir to a lower temperature. After 46 min., air injection was started and simultaneously nitrogen injection was stopped; auto-ignite was achieved at time 74 min.

Pressurisation of the tube was originally set at 100 bar, as a precaution against possible gas bypassing via the thermocouple probe. The control pressure reduced to 90 bar due to a change in injected N_2 gas rate.

Prior to combustion commencing, the pressurisation profile is different to that when shutting-down the equipment, i.e. reducing pressurisation. There are two resistances affecting the pressurisation, the porous media and also the screen located at the bottom of the tube. A differential pressure of about 6 bar is required to achieve flow through the tube. This depend on the porous media, it's porosity, permeability, method of packing and screen mesh size.

Fluctuations of 8 to 10 bar occurred during the combustion period. This required the shell to be continuously bled off and repressurized, requiring a large amount of nitrogen. Typically, 6 to 15 cylinders to complete an experiment, depending on Injection rate and pressure.

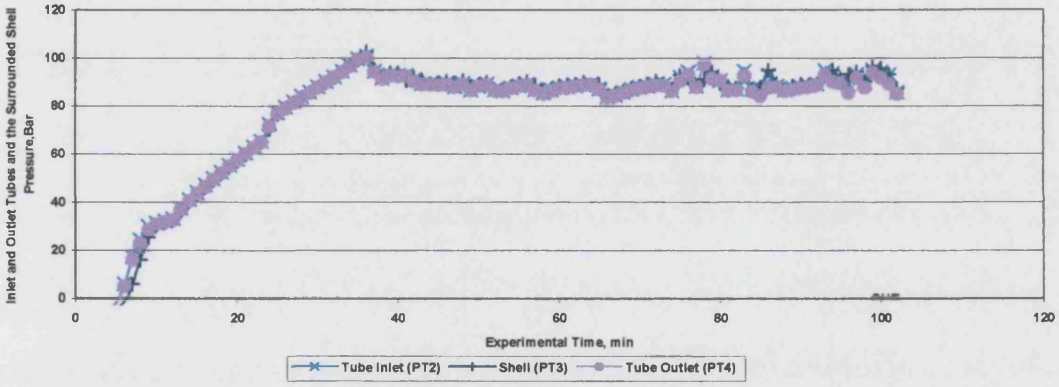

Figure 3.33 Run 1 : Inlet and Outlet Combustion Tube Pressures and Shell Pressure versus Experimental Time.

The back pressure on the liquid and gas moves from the separator were logged as a function of time, as shown in Figure 3.34. PT5 measures the pressure of the liquid passing from the High Pressure Separator (HPS) to Low Pressure Separator (LPS), as well as the outlet pressure and the adjusted pressure of PRVL1. At about 25 min., there was a decrease of pressure from 27 to 18 bar. This was due to the discharge of liquid from the HPS before it had reach the desired operating pressure. At about 95 min., the PT5 began increase. Although an attempt was made to lower the LPS pressure, it's increased to 90 bar. This indicated that first, AAV20 was not working properly (normally closed, but actually stayed open). Secondly, PRVL1 regulator failed to control properly. After testing by the supplier (Fluid Control Limited), the

problem was found to be a faulting stem seat and the spring. The gas line pressure (PT8) between the HPS and LPS, worked perfectly [permits gas flow to analysers and Wet Test Meter (WTM)].

PT9 shows the compressed air supply pressure to operate the pressure regulators, maintaining a set value of 6 bar. Indicating that the new compressor works perfect (50 litre and 150 psi delivery pressure).

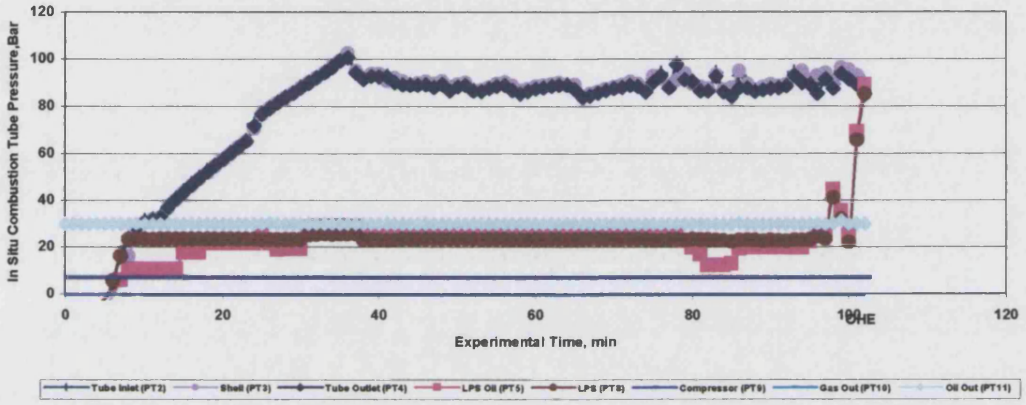

Figure 3.34 Run 1 : Combustion Tube Pressurization.

Figure 3.35 shows the pulsed frequency (PF) of band heaters (BH) sequence, controlling power. The maximum pulse frequency is 30 times in one minute, 1 sec "ON" and 1 sec "OFF". The number of pulses is very important for control of the following operations:

1. Establishing the initial reservoir core/tube temperature
2. Temperature lead of BH, 1 to 4, needed to support ignition.
3. Adiabatically temperature control of the combustion tube to minimize heat losses to the surrounding shell.

It is clear in Figure 3.34 that the BH "switched on" to heat up the tube to the desired reservoir temperature before injecting air. The BH "switched off" after about 17 min. when the reservoir temperature reached 60 °C. At 42 min, the BH "switched on" again to raise the temperatures in part of the core which were below 60 °C.

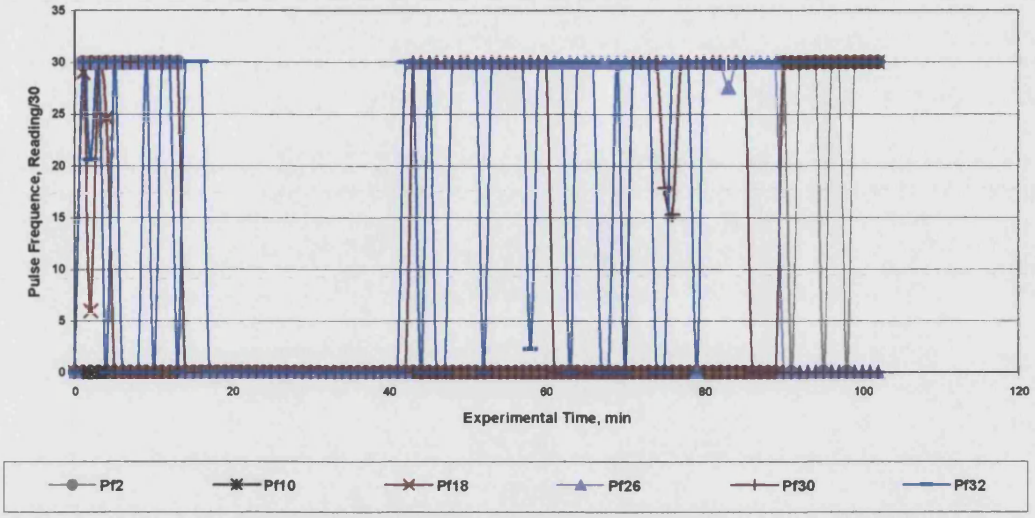

Figure 3.35 Run 1: Band Heaters Pulse Frequency .

Axial tube temperature at different BH location (number) is shown from Figs. 3.36 to 3.39. It shows that the ignition occurred at BH10 and BH11 (interpolation). BH's 10, 11, 17, and 25 were inactive during the test, due to electrical connection faults. The gaps in the Figure are due to misreading, or faulty axial thermocouples.

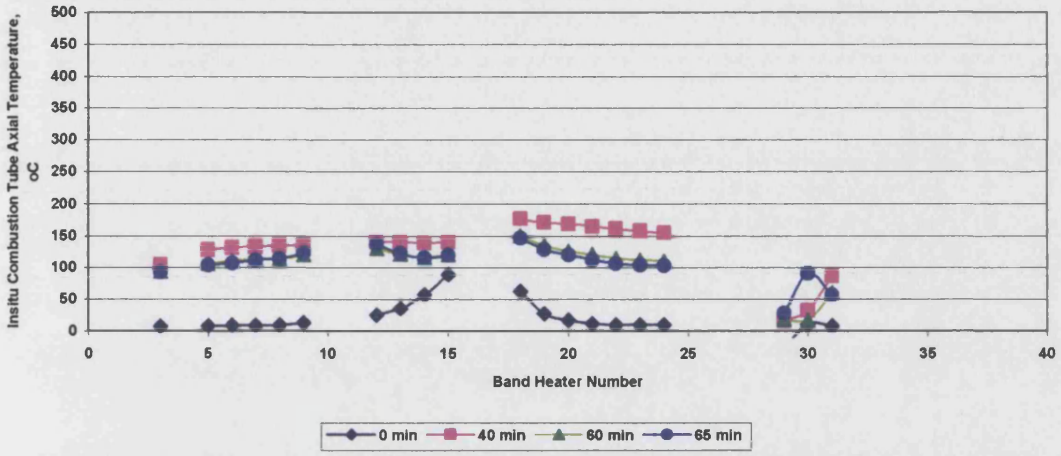

Figure 3.36 : Run 1 Combustion Tube Axial Temperature prior to ignition.

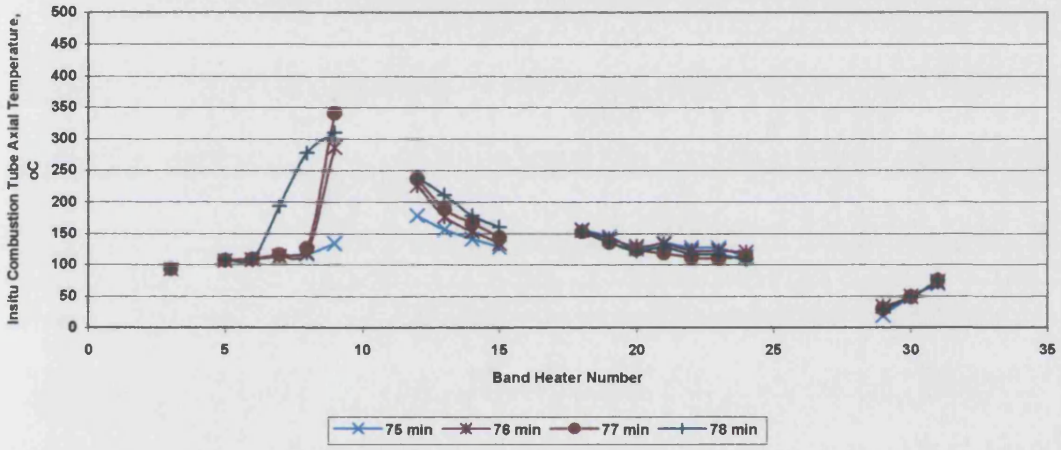

Figure 3.37 : Run 1 Combustion Tube Axial Temperature.

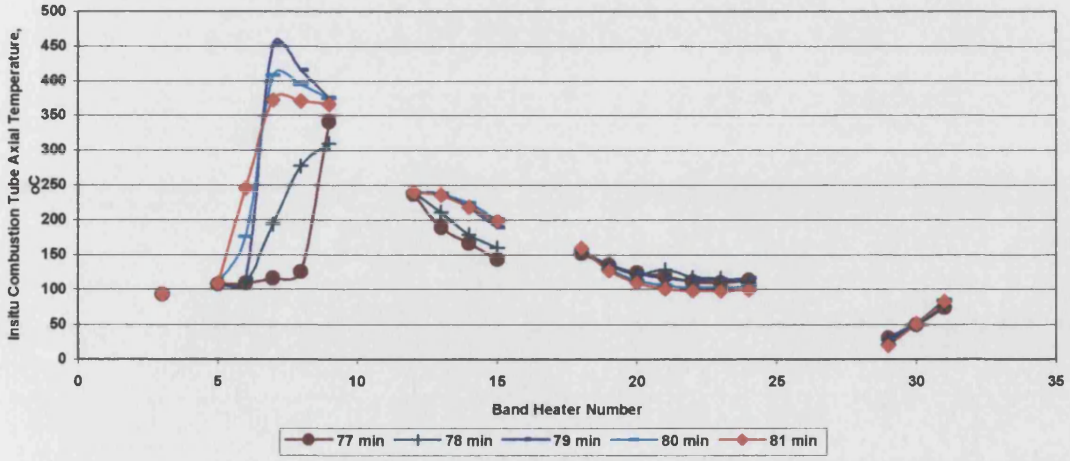

Figure 3.38 : Run 1 Combustion Tube Axial Temperature.

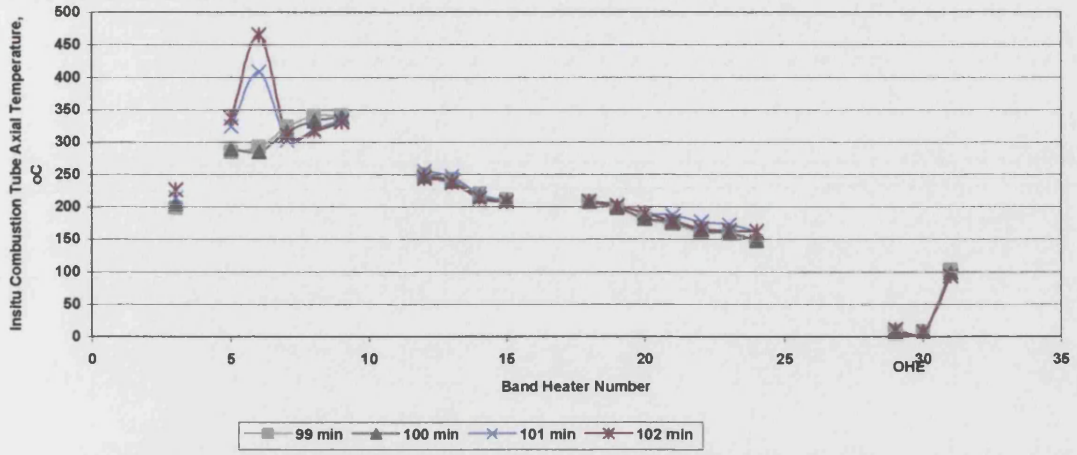

Figure 3.39 : Run 1 Combustion Tube Axial Temperature.

Figure 3.40 shows the percentage of produced gas time history. Gas production started 49 minutes after air injection. Oxygen that was shown (14.5%) for up to 40 minutes, was originally available inside the analyser before the test started and during pressurisation of the combustion tube. It drop to zero representing only nitrogen start produced. Initially, only about 0.7% of oxygen was produced, which increased slowly to about 1.1% after 32 min. Oxygen then increased dramatically to about 8.7% indicating channelling or bypassing around the axial thermocouples probe or along the tube. Autoignite occurs after 65 minutes because the increasing levels of CO_2 and CO at 74 min. Although CO_2 reaches more than 10% and CO to about 6.5%, the amounts fluctuated, indication unstable combustion.

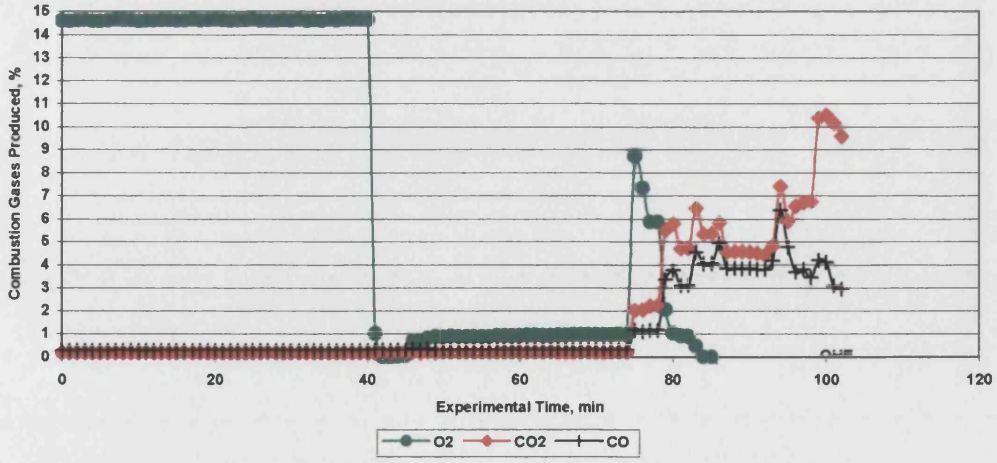

Figure 3.40 Run 1 : Produced Gas Composition.

Figure 3.41 shows the HPS and LPS level readings. A reading of 12 indicates that the HPS is full. Thus, there was flow the HPS to PRVL1. It was subsequents found that PRVL1 had become plugged due to a very viscous emulsion.

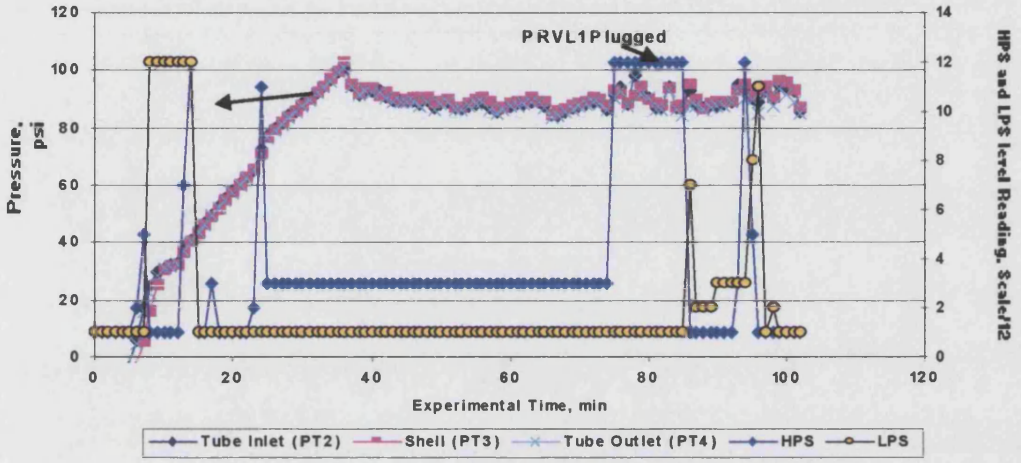

Figure 3.41 Run 1 : High and Low Pressure Separator Operation.

The only volume was recorded for liquid produced, because of a communication fault between the Wet Test Meter (WTM) and the computer. There was also an incorrect zero reading on the WTM. Moreover, the mass flow rate could be not achieved exactly due to the unsteady state flow regime.

As shown in Figure 3.42, combustion of 25.0 % of the combustion tube length realised a recovery of 31.5 % clear oil, 49 % of emulsion equivalent to 40.25 % of original liquid in place. Less than 1 % was clear water.

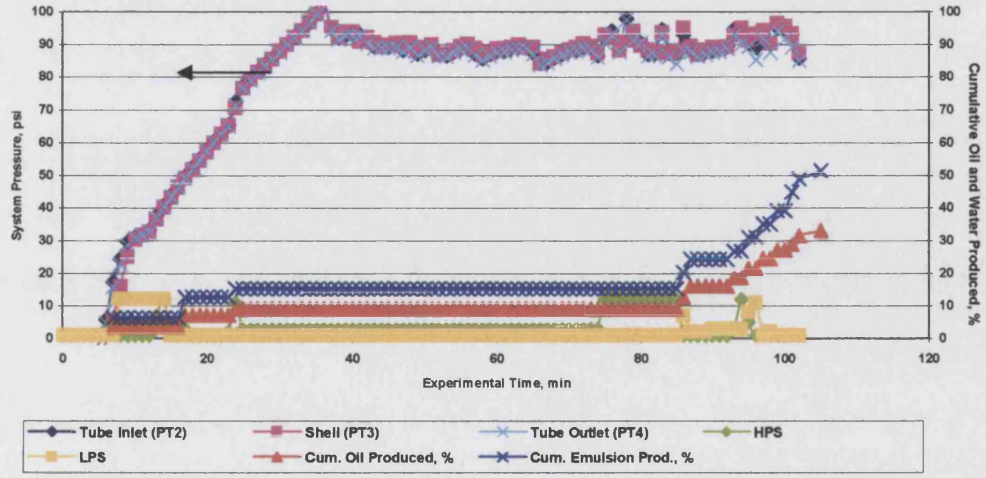

Figure 3.42 Run 1 : Cumulative Oil and Water Production.

Run 2 :

Run 2 was conducted at higher pressure (200 bar), but with the same oil and water saturation as Run 1. Many problems were experienced during pressure up of the system. First the computer sent an incorrect signal to the solenoiding valve, which opens the inlet gas pressure regulator. This resulted in the program switching-off and starting again. However, the signal to increment the opening of PPRV1 was very high, causing a sudden increase in the tube and shell pressures to about 50 bar, This inlet gas regulator (PPRV1) became stuck again. The start up sequence was restarted, but with a low incremental opening of the inlet gas pressure regulator, causing a delay of about 20 minutes before the full supply pressure was achieved. A smooth build up of pressure occurred, eventually reaching 209 bar. It is not possible to increase pressure more than this because of the pressure of the nitrogen source gas. Incrementation of the signal to the PPRV1 was stopped at the 206 bar, although it was originally set at 215 bar. The process then had to wait while the booster pump replenished the nitrogen supply cylinder (see Figure 3.43). The main injection pressure regulator (PT1) was set at 235 bar, limited by the optimum operating pressure of the air actuated valve (AAV). It is very important to have at least 30 bar above the required tube pressure, to effectively control the ΔP between the tube and shell. The set pressure of 215 bar was reduced to 200 bar after 125 minutes to allow air to displace the nitrogen used for pressurization. Simultaneously, air and ignitor switched on as it illustrated later.

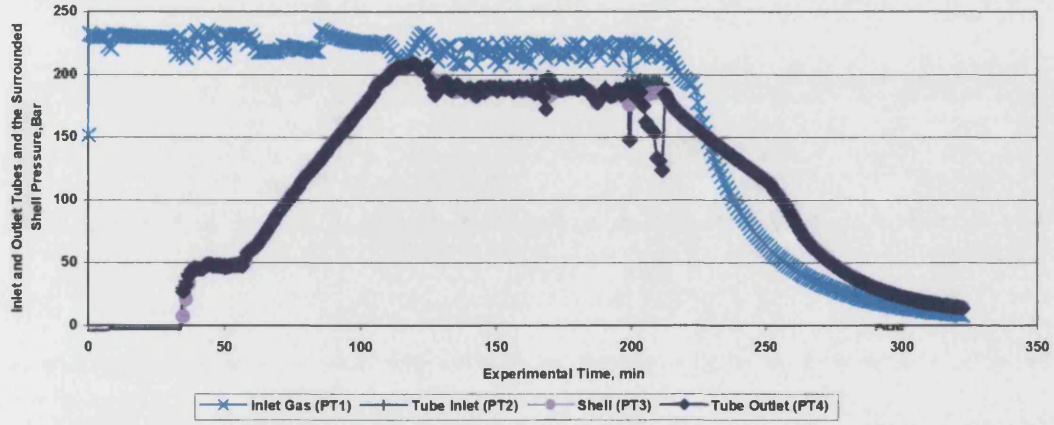

Figure 3.43 Run 2 : Inlet and Outlet Combustion Tube Pressures and Shell Pressure versus Experimental Time.

The back pressure was reduced to about 190 bar to allow increased flow through the combustion tube. At 222 min the experiment was terminated. It required about 100 minutes to reduce the pressure on the combustion down to atmosphere.

The problems incurred during this run was mainly the result of a partial fail of the back pressure controller liquid side only. Liquid discharges from the HPS to LPS via connecting line became completely blocked, and when the bypass valve was opened to discharge the high pressure separator, a leak secured.

When the back pressure readings PT4 became much less than the injection pressure PT2, the experiment was terminated. This differential pressure, caused by plugging across the screen at 200 minutes, as shown in Figure 3.44.

It is considered that the emulsion formed inside the chalk core, so that there was no fluid flowing through the screen. The high viscosity of the emulsion cause the pressure regulator to plug as well. Although the emulsion is easily broken outside of the combustion tube, it is much more difficult to do this inside the tube.

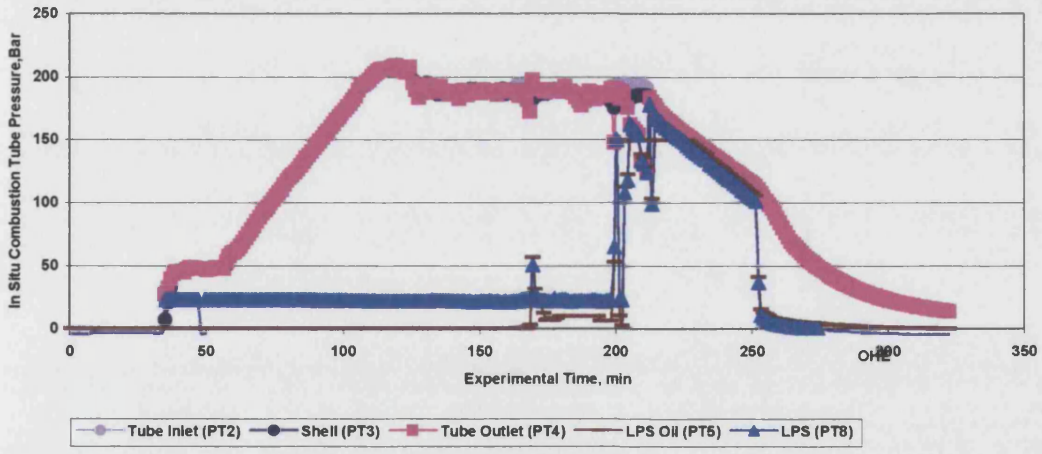

Figure 3.44 Run 2 : Combustion Tube Pressures.

The initial reservoir bed temperature was established at 60 °C, as shown in Figure 3.45, for about 125 minutes before ignition. All of the BH's were controlling except BH7 and BH27. There were switched off before the experiment, because of a fault. A manual switch was incorporated to control vent such problem with the control relays.

The ignitor was switched on when the first BH was set to reach 400 °C, However, due to delay in the BH respond, the temperature actually increased to about 590 °C. Between 145 and 150 minutes, the ignition occurred, causing the temperature at TC2 to increase to 540 °C (Figure 3.46). At 169 minutes, there is a rapid rise in temperature (BH5), reaching 826 °C. The temperature reduced down to 538 °C at 170 minures (Figure 3.47). The combustion front reversed so that burning took place in the unburned zone, shown in Figure 3.47.

The oil auto-ignited ahead of the main combustion front, as showing in Figure 3.48. At 200 minutes, second front started at BH12, and then advanced to BH15 only, taken 4 minutes. Another, separate small peak, as second and combustion front can be seen, a minute after the previous front occurred at BH15 (Figure 3.49).

The temperature of the main combustion front decreases from 600 °C as shown in Figure 3.50, but secondary front temperature begain to increase. Figures 3.50 to 3.52 show that the main combustion front becomes stalled at BH5. Downstream of this to temperature began to fall continuously after experiment is terminated, aud pressure is reduced.

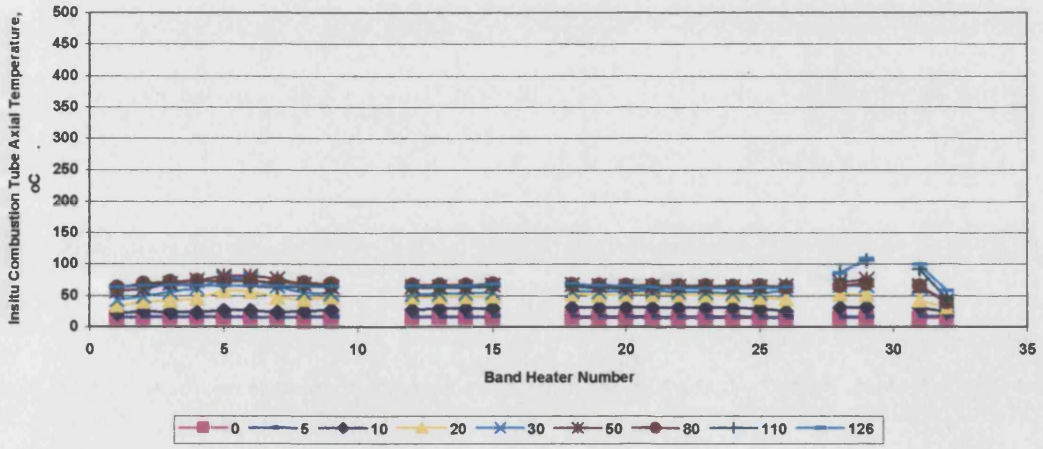

Figure 3.45 Run 2: In-Situ Combustion Tube Axial Temperature, During Pressurisation and prior Ignitor Switched ON.

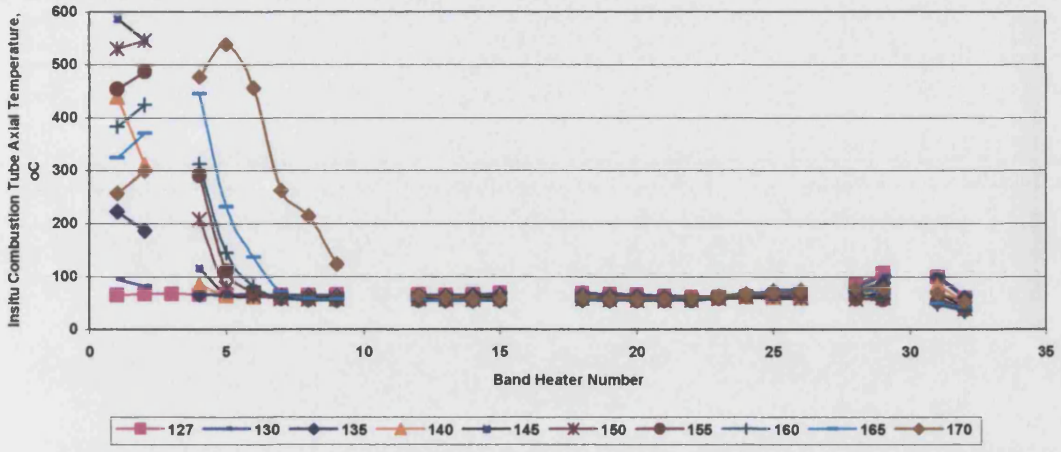

Figure 3.46 Run 2: In-Situ Combustion Tube Axial Temperature.

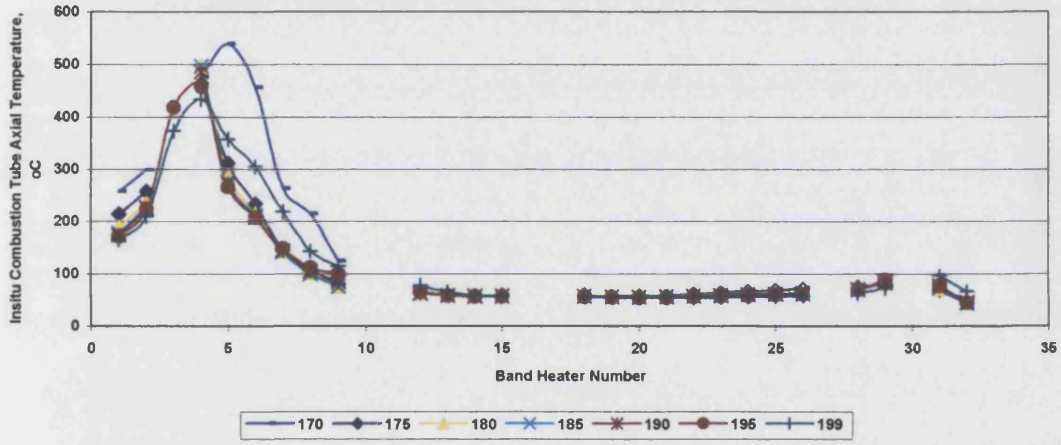

Figure 3.47 Run 2: In-Situ Combustion Tube Axial Temperature.

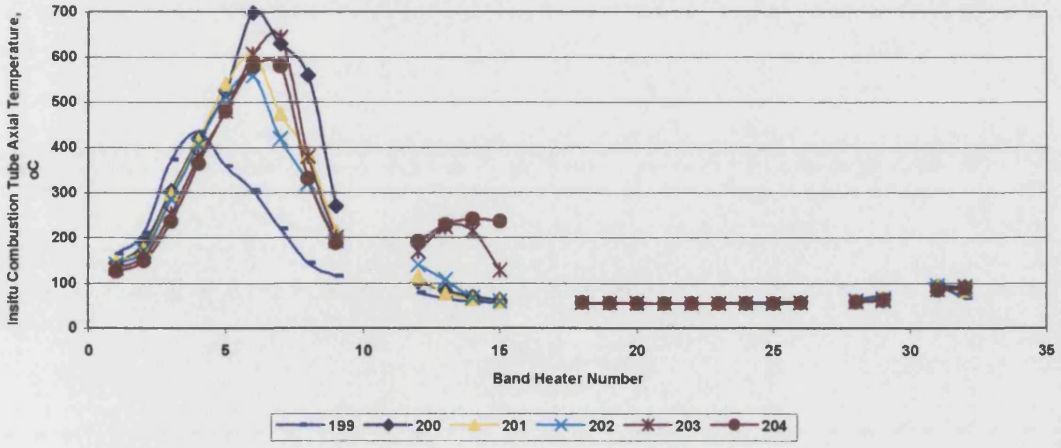

Figure 3.48 Run 2: In-Situ Combustion Tube Axial Temperature.

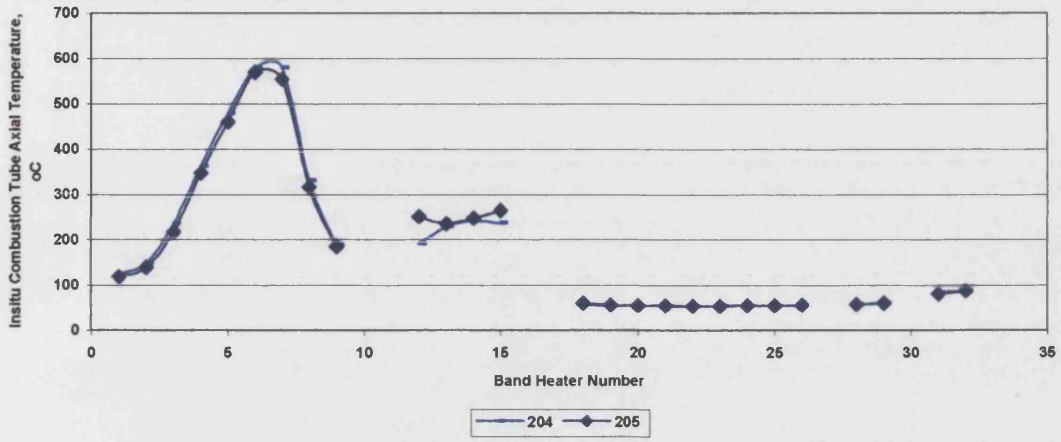

Figure 3.49 Run 2: In-Situ Combustion Tube Axial Temperature.

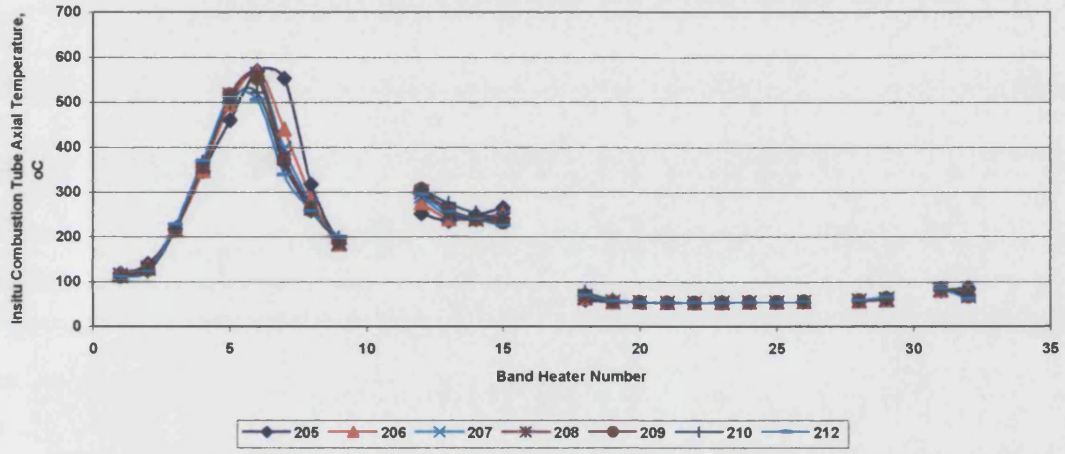

Figure 3.50 Run 2: In-Situ Combustion Tube Axial Temperature.

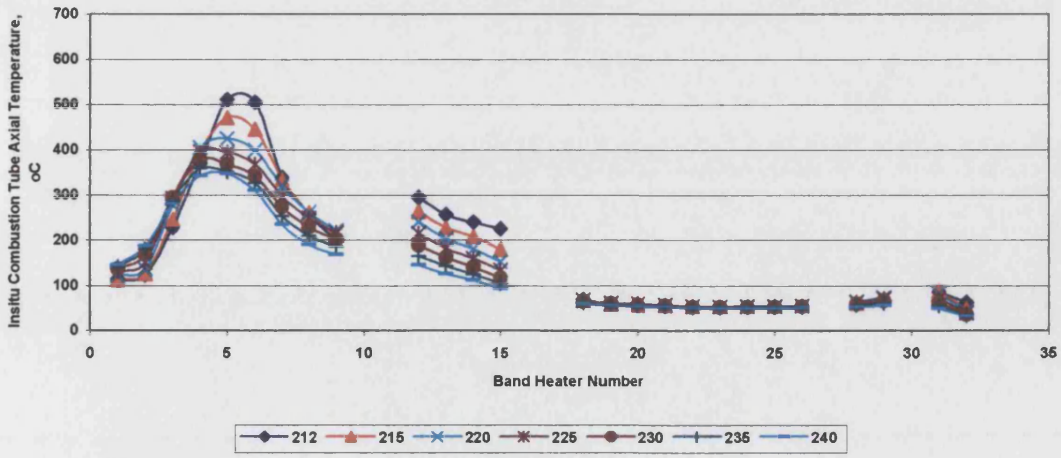

Figure 3.51 Run 2: In-Situ Combustion Tube Axial Temperature, Temperature Reduction in Both Peaks.

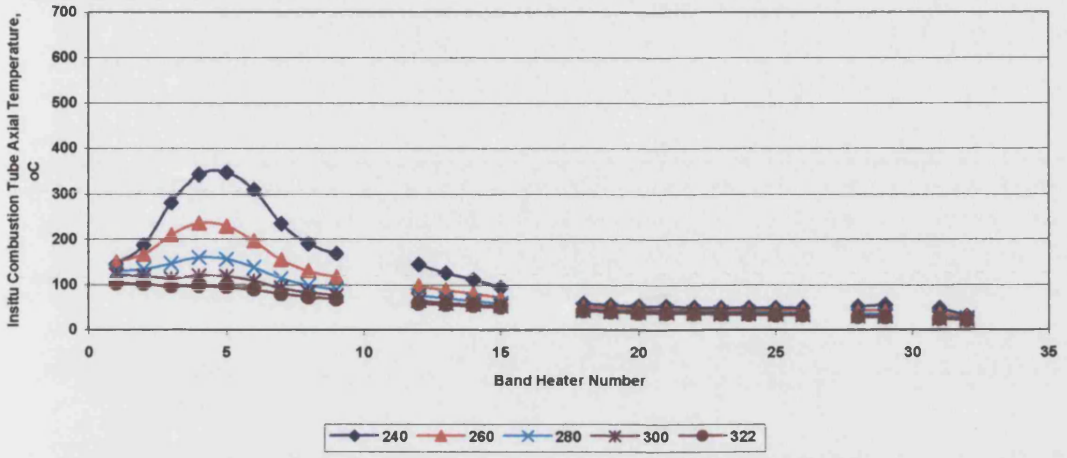

Figure 3.52 Run 2: In-Situ Combustion Tube Axial Temperature.

Produced Gas :

The produced oxygen is shown Figure 3.53. During start-up, the oxygen level reduced to 12% due to restarting of the computer control program. At 125 minutes, the produced oxygen fall to zero. The percentage of oxygen did not remained at zero but it increased with the other values of CO and CO_2 . This may indicate that the oxygen did not consumed 100% but about 50% consumed. Between time of 201 and 205 the percentage of oxygen drop from 11% to 4.4% . However, this due to the auto ignition, which utilizes more of the oxygen, remained not consumed by the first peak generated by the artificial ignitor. At time of 222 the experiment terminated and the percentage of CO_2 decreased and Oxygen increased.

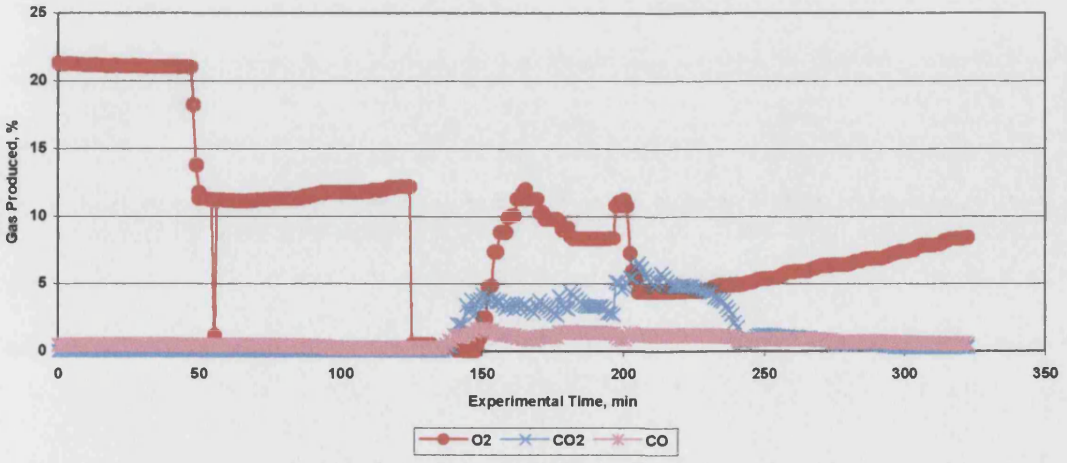

Figure 3.53 Run 2 : Produced Gas Combustion.

The cumulative volumetric flow rate of produced gas is given in Figure 3.54. The total amount of gas attributed to the effect of the main combustion front is 0.151 m^3. The increase up to 0.296 m^3 is due to LTO downstream.

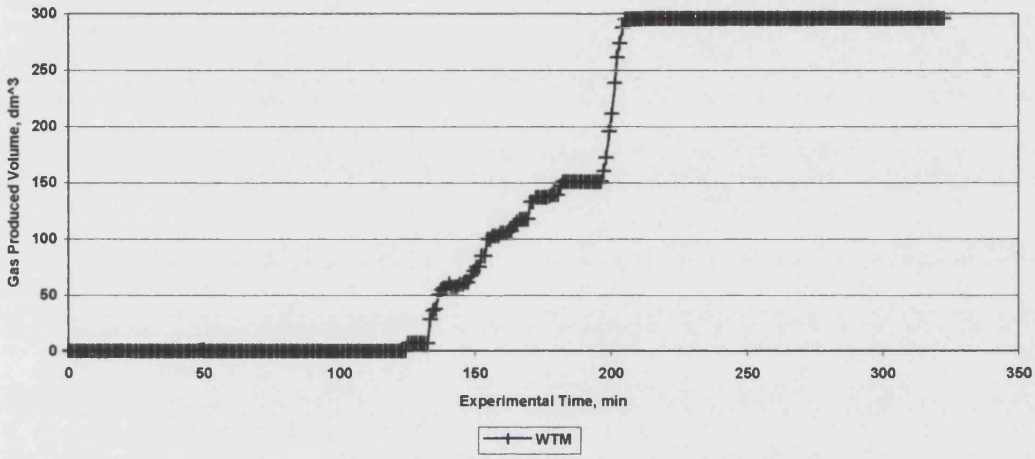

Figure 3.54 Run 2: Combustion Gases Produced Measurement.

Although the design flux for this run was set as 70 m^3/m^2hr, because the process essentially is unsteady state, it is not possible to fully realize this flux value, except at the end of the test where mainly gas flow through the combustion tube.

The recovery of oil and water was approximately 17% and 8%, respectively (Figure 3.55).

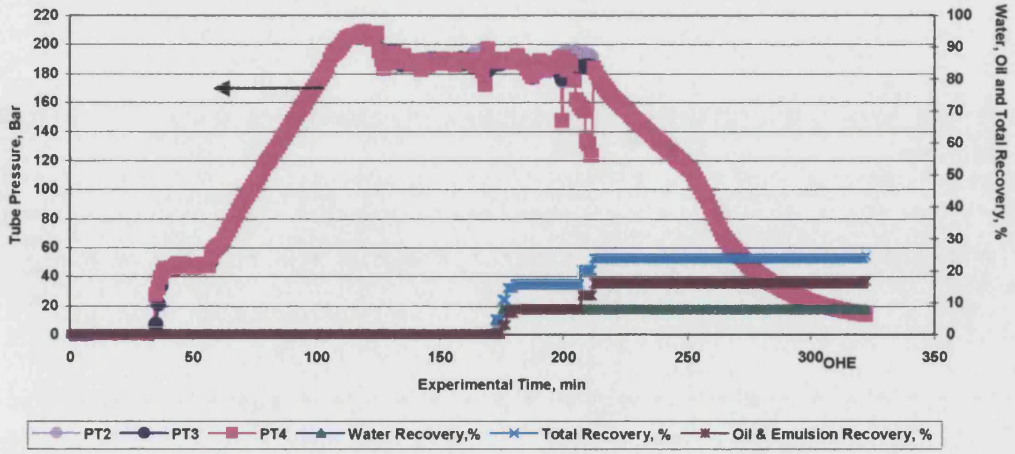

Figure 3.55 Run 2: Oil and Water Recovery.

Run 3 :

Run 3 was conducted at 200 bar, with 30% oil saturation and 70% water saturation. In this experiment, a valve was added ahead of the liquid pressure regulator (PRVL1), placed between the HPS and LPS. This was due to improved control of the process. Moreover, the liquid line between the two separators was wrapped with heating tape, controlled at about 60°C. Several tests where made initially to ensure that there was no affect on the AAV20, which is positioned in the middle of the connecting HPS and LPS line.

A modification was made to one task " Ignitor Control.vi" as the control program. Instead of starting off when the CO_2 level reached 5%, switched off the ignitor when the CO_2 level was 1% , at the same time start increasing the flux to the required value.

The BH27 found to be switched-on permanently, using the new manual switch board shown in Figure 3.56. It is very important to ensure that there are no overheating during pressure up period.

Pressurisation of the tube and shell required three attempts due to a problem reading the shell pressure (PT3), as shown in Figure 3.57. The problem was caused by insufficient time for the booster pump to pressurize the horizontal supply cylinders with nitrogen. The desired set pressure 217 bar was achieved after 148 minutes. The nitrogen flow was switched to air after isolating communication between the tube and shell. Simultaneously, the ignitor switched on. The back pressure reduced gradually to allow gas to flow through the tube porous media and the resident nitrogen. This displacement took place from 148 to 234 minutes.

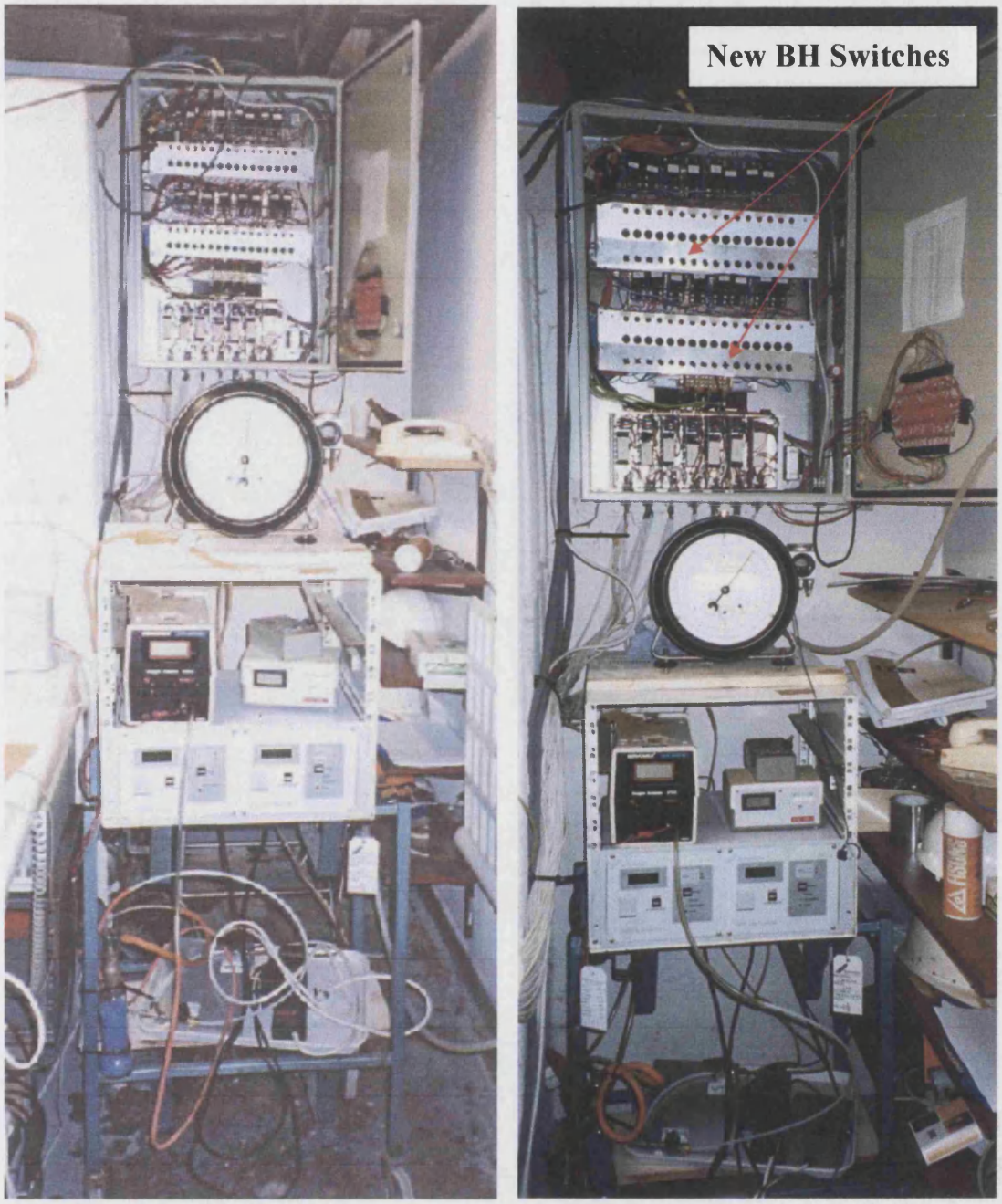

" Old " " New "

Figure 3.56 Run 3: New 32 Band Heater Switch Board.

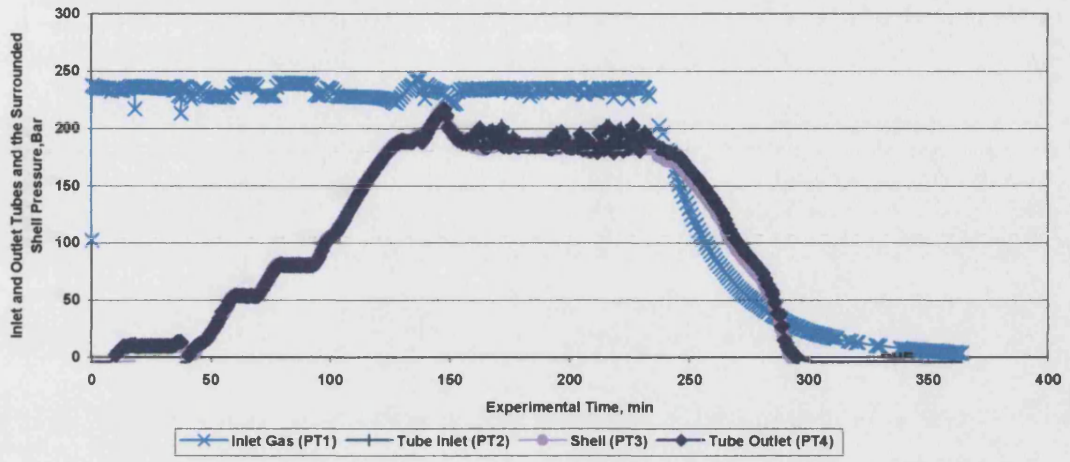

Figure 3.57 Run 3 : Inlet and Outlet Combustion Tube Pressures and Shell Pressure versus Experimental Time.

It was realized during the run as shown in Figure 3.58 that the HPS was plugged at the bottom. With this type of problem, there are only two options. The first was to switch off the system and shut-down the experiment. Alternatively it was possible to collect the oil produced after the HPS becomes full. However, this is not satisfactory, because any liquid passing through the gas line will cause plugging and also problems with the analysers.

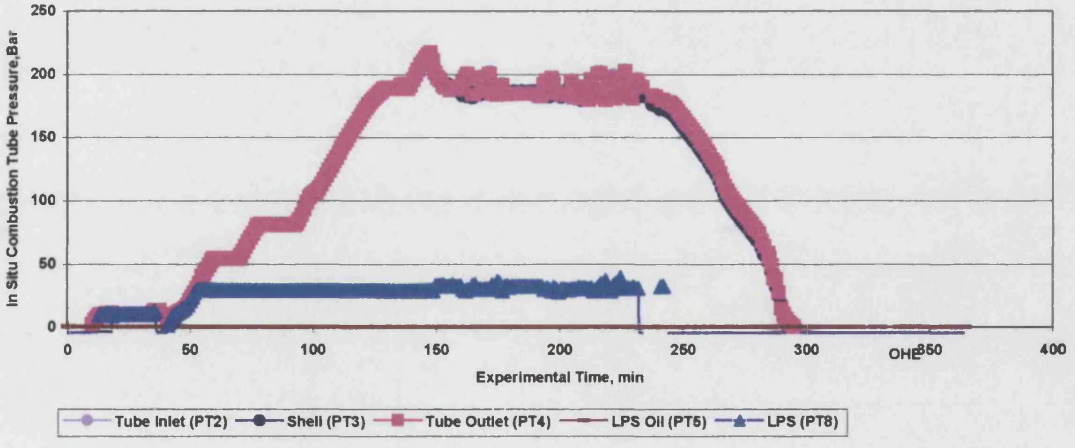

Figure 3.58 Run 3: Combustion Tube Pressurisation.

Axial Temperature Profile :

As shown in Figure 3.59, the temperature was initially about 60°C during pressure-up period. During the pressure-up period, cold nitrogen gas was injected at the top and at the bottom of the tube to maintain pressure. This explains why the temperature is lower in the first part of the tube.

The ignitor was switched on at 148 min, and then switched off at 158 minutes, after the ignitor had reached 350°C . However, ignition failed to occurr before 158 minutes, and then was no response at TA2 (Figure 3.60).

Rapid ignition occurred between times 162 and 164 minutes, as shown in Figure 3.61, reading more than 500 °C. Between 164 and 166 minutes, indicating that the combustion front moved from BH1 to BH2. The combustion front temperature then decreased to around 350°C, with the combustion front advancing to BH3. Two secondary LTO reaction zones occur at 176 minutes, the first peak between BH9 and BH12, and the second peak at BH24 (Figure 3.62).

The main combustion front is stailed 14 minutes and the temperature increased slightly from 340 to 370°C (Figure 3.63). The secondary two self ignition (LTO reaction zone) peaks increases in temperature to 125°C. At 196 minutes, the main combustion front temperature was increased from about 370 to 415°C.

At time 206 minutes, the combustion front start advances to BH4, with the temperature reaching to 420 °C. The two LTO zone down stream are stationary, but shown an increase in temperature to 160°C (Figure 3.64).

The combustion front then advances to BH5 at 218 minutes. The secondary LTO now appear to be start at 214 minutes as shown in Figure 3.65.

The combustion front moves advances to BH7 (232 minutes). The first LTO reaction zone begin it's increased temperature compared with any temperature ahead of it, when the temperature reaches to about 250°C, thus exhibiting combustion front property. The

second LTO zone peak moves ahead to the end of the tube (Figure 3.66), reaching a maximum temperature of 190°C. The experiment was terminated after 234 minutes due to safety reasons (BH32 reached 110°C). The maximum temperature of the main combustion front was 540°C.

Figure 3.67 shows the temperature variation along the core during pressure reduction (Bleed-off) the tube. It took more than 2 hours for the main combustion front to be extinguished.

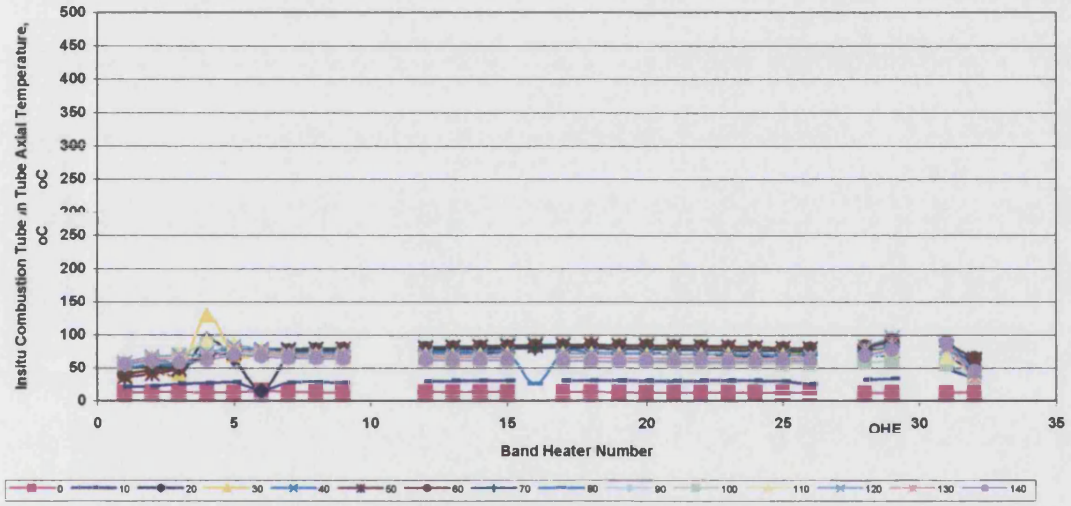

Figure 3.59 Run 3: In-Situ Combustion Tube Axial Temperature, During Pressurisation and Prior to the Ignitor being "Switched-on".

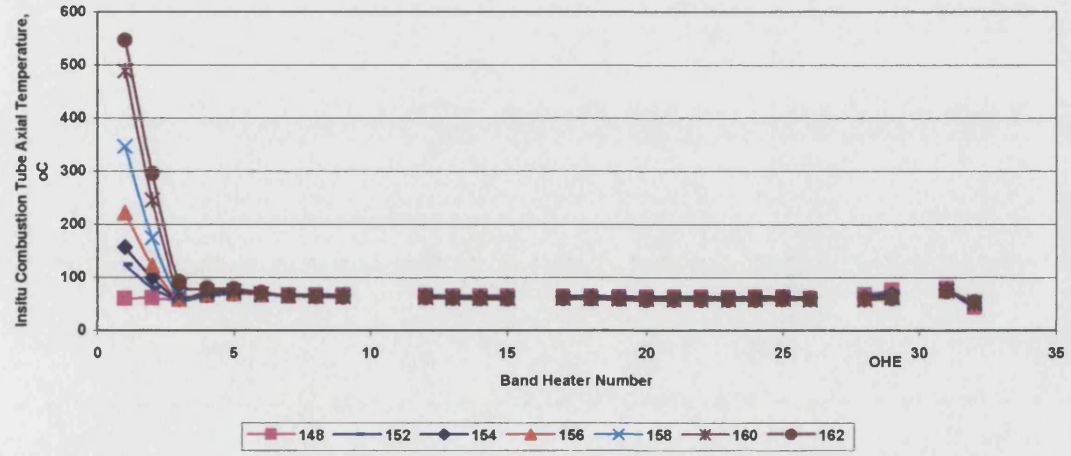

Figure 3.60 Run 3: In-Situ Combustion Tube Axial Temperature, after Ignitor "Switched-on".

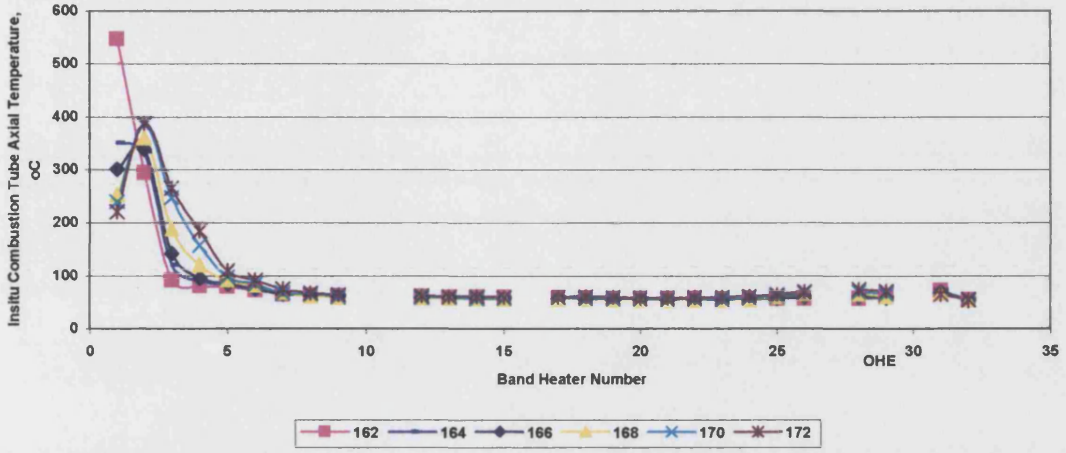

Figure 3.61 Run 3: In-Situ Combustion Tube Axial Temperature.

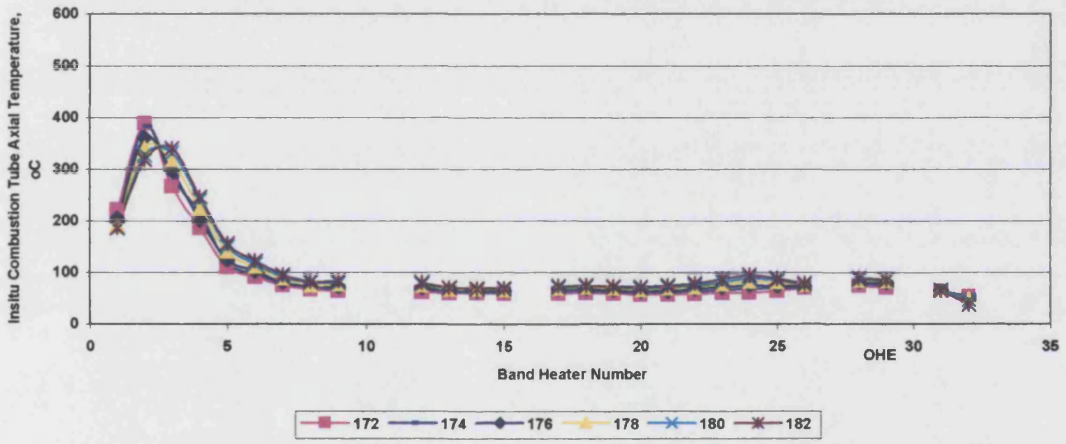

Figure 3.62 Run 3 : In-Situ Combustion Tube Axial Temperature.

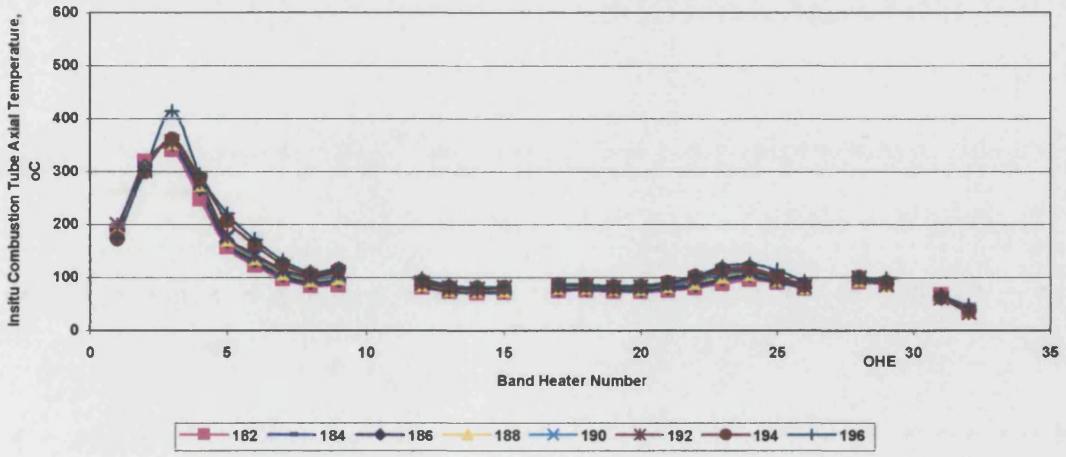

Figure 3.63 Run 3: In-Situ Combustion Tube Axial Temperature.

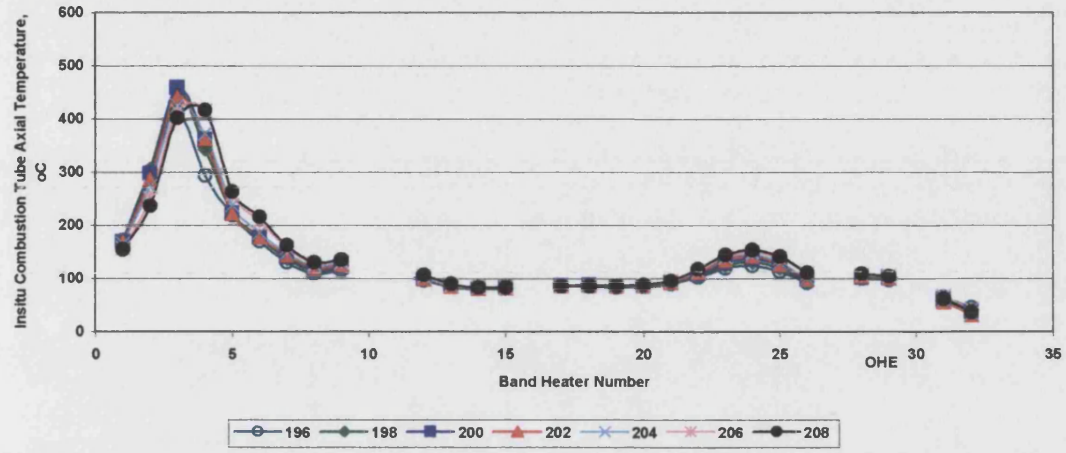

Figure 3.64 Run 3: In-Situ Combustion Tube Axial Temperature.

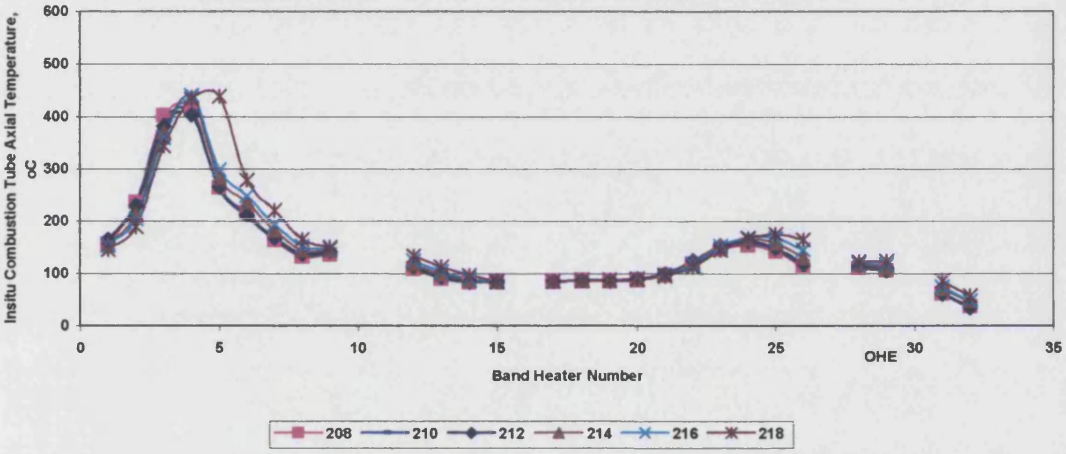

Figure 3.65 Run 3: In-Situ Combustion Tube Axial Temperature.

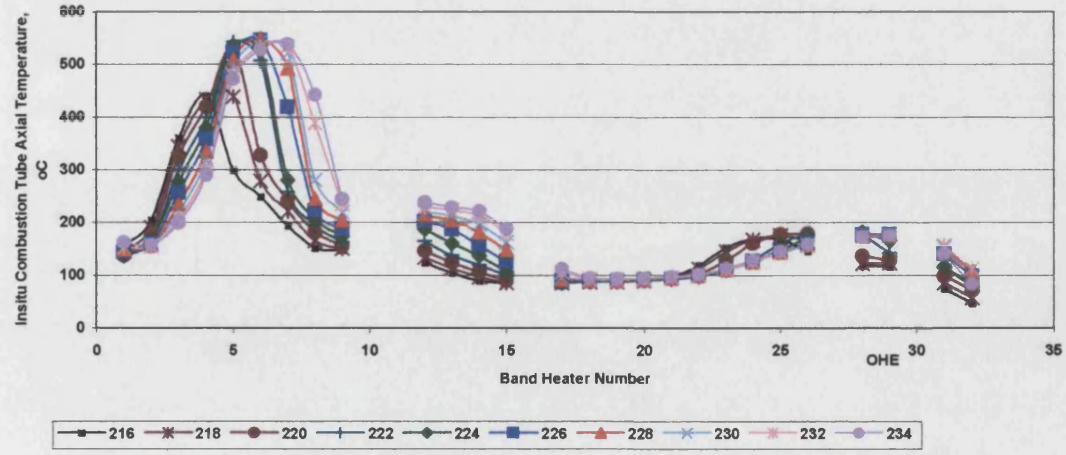

Figure 3.66 Run 3: In-Situ Combustion Tube Axial Temperature.

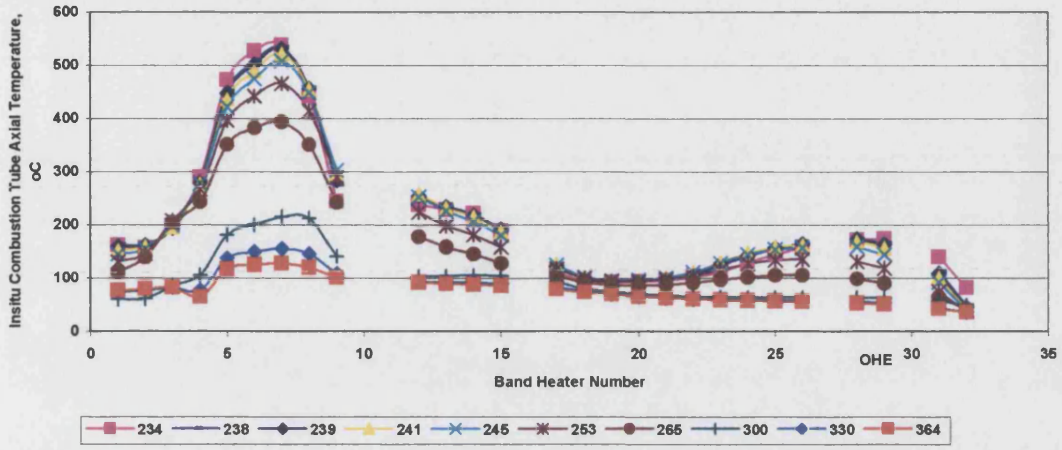

Figure 3.67 Run 3: In-Situ Combustion Tube Axial Temperature.

Produced Gas:

The produced gas analysis is given in Figure 3.68. At 164 minutes, the injected air flux increased to the set value, and the oxygen produced began to increase-up to 8%, and maintain this level for over 40 minutes. The produced CO_2 remains At quit low values for most of the test (172-212 minutes), but then increases to around 10%. However, this increases caused when the LTO reactions occurs and causing oxygen to fall down to about zero. CO produced show only average of (1.8 to 2 %) all the way to 212 minutes. The value increase to 3.6% at the 221 minutes, then reduced gradually to about 2.3% at the end of the experiment.

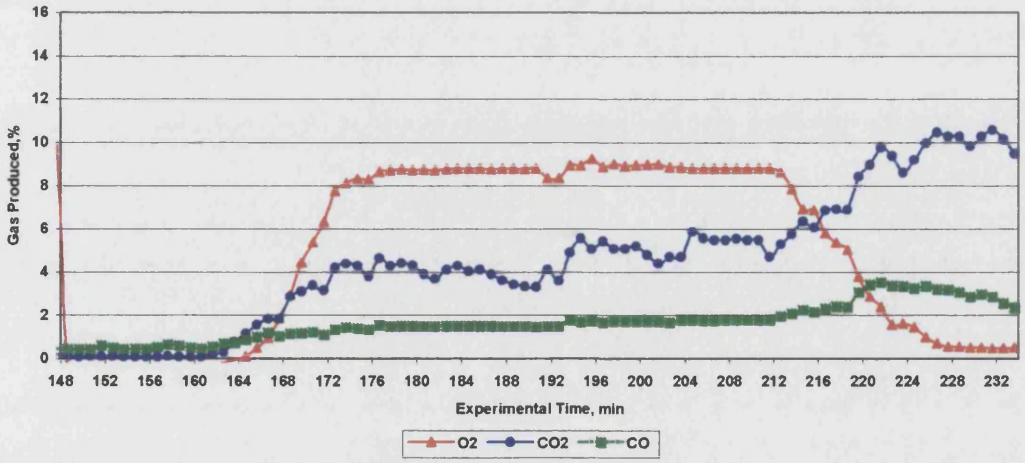

Figure 3.68 Run 3: Produced Gas Composition.

Figure 3.69 shows the Wet Test Meter (WTM) readings. The total volume of gas produced was about 700 litres. That there are three different rates. The rate during the first period was 12.7 litre/min, and the second 2.5 liter/min, and the third 14.2 liter/min. The overall average volumetric flow rate for the test, was 8.23 litre/min, which is equivalent to average flux of 62.3 m^3/m^2hr.

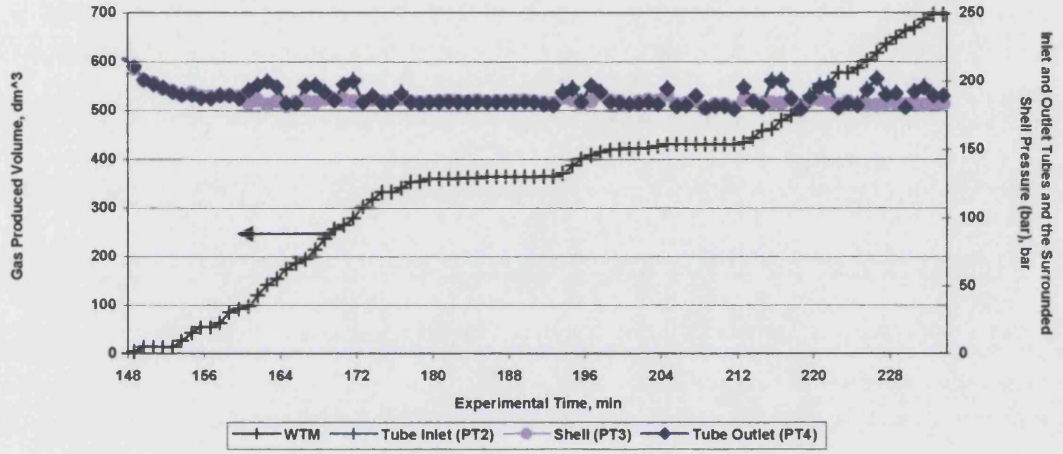

Figure 3.69 Run 3: Gas Wet Test Meter Measurement.

Post-Mortem Photographs of Burned Core from Combustion Tube:

The complex effects resulting from the burned cores from Run 1, 2, and 3 are treated individually, run by run.

Run 1:

The top layer of MI limestone was loose, and easily fell off of the tube when the top flange was disconnected as shown in Figure 3.70. The thickness of this sand went to about 4.5 cm (All Band Heater No. 1). The soft sand colour look like oxidised sand and no oil or fuel or coke withon the sand. At distance of 4.5 cm a small black coke can be seen in the centre of the core (Figure 3.71).

The post-mortem sequence in Figure 3.71 to 3.75 reveals the change which occurs in the shape of the residual carbon layer Originally accumulated in the central zone of the core. Figure 3.71 pressents the basics of the tube flange and it's contents with a post mortem photo taken at 5 cm from the tube top. Point (A) present little coke deposited, point (B) shows not complete combustion occurrence, point (C) illustrate burnt media, and point (D) with high amount of fuel deposited. Figure 3.72 illustrate different shape of coke. The combustion went in a circular form, where the highest combustion occurred and shows a Polynomial (egg) shape of coke. The inner side of the tube shows burned porous with moderate fuel remained compared with the whole cross section. The joint of two Band Heaters halfs located exactly in the outer side of the combustion tube, where there are less/no heating.

The shape of the coke enlarged in size with the same thickness as seen in Figure 3.73. Highest combustion occur at distance 7 cm. Some point shows high percentage of fuel left after combustion. This fuel may be deposited after the combustion generated. The shape of the coke layer enlarged more to the tube sides. Moreover the coke stick into the tube inner wall where it is presumed less heat generated in the same cross section.

The In situ combustion tube cross section at a distance of 8 cm shown in Figure 3.74. It is very obvious in this photo that the inner combustion portion enlarged more than in Figure 3.74. Some point shows that the coke layer reached and stick into the wall. It is believed that the reason was due to less heat generated around the tube [where the wall thermocouples placed] compared to [Below middle half of Band Heaters] .

Coke shape changed in the cross section at distance 11 cm as shown Figure 3.75. A vertical layer of combustion performed along the tube. High percentage of fuel and some coke presented as a thick layer, surrounded by two straight lines of coke.

The inner combustion thickness is small in Figure 3.76 [distance 13 cm] compared with Figure 3.75, where high fuel and moderate coke were available. Figure 3.77, taken at 18 cm distance. It shows two communicated burned portions.

Figure 3.78 presents a cross section taken at 20 cm distance of combustion tube. No deposition occurred beside the inner wall of the tube and in the centre where the axial thermocouples pipe located. The shape of the combustion portion is closed to square.

Combustion layer appeared clear at distance of 26 cm as shown in Figure 3.79. However, no more fully combustion media appeared at this distance. The distribution of coke was completely uniform in the cross section. This coke went all the way to about 30 cm. Then, some coke was found stuck on the wall [Half Bow of Band Heater] at about 33 cm as shown in Figure 3.80.

The unburned soft calcium carbonate media found from 33 cm to the end of the combustion tube as shown in Figure 3.81.

Soft and/or crushed calcium carbonate retrieved from the combustion is shown in Figure 3.82. It is very obvious that there are sequence in colour. The carbonate get darker with distance, this mean the percentage of fuel and coke increase with distance away from the inlet air injection portion even if the combustion performance is not in consistency.

Figure 3.70 Run 1:Ignitor

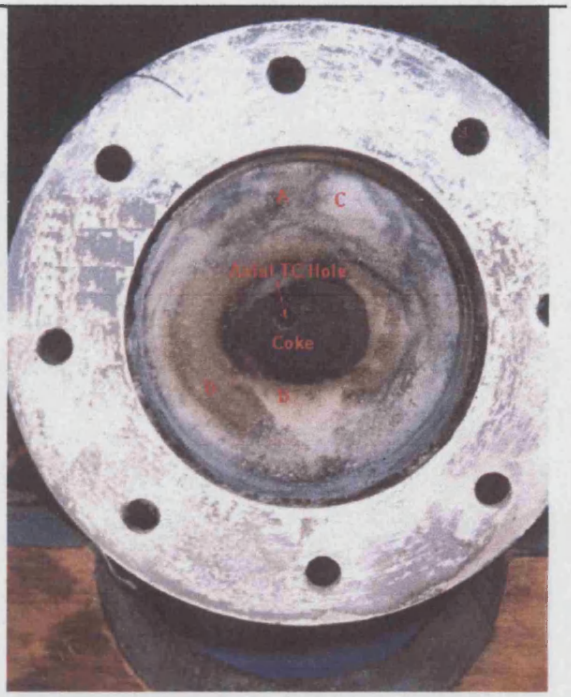

Figure 3.71:Top of Combustion Tube, 5 cm into core.

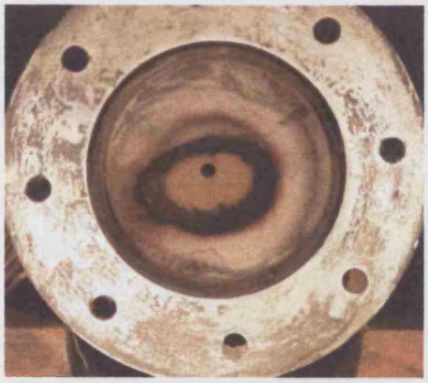

Figure 3.72 Run 1:Combustion Tube at 6 cm.

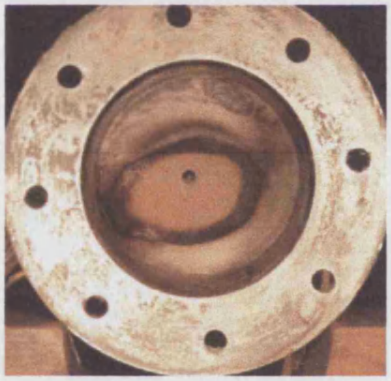

Figure 3.73 Run 1:Combustion Tube at 7 cm.

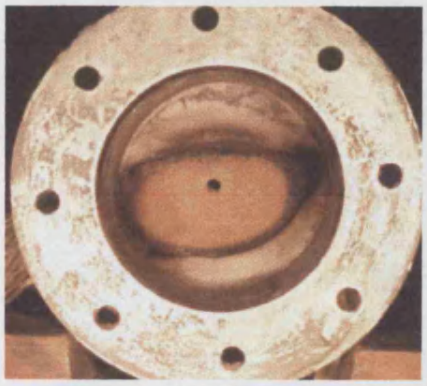

Figure 3.74 Run 1:Combustion Tube at 8 cm.

Figure 3.75 Run 1:Combustion Tube at 11 cm.

Figure 3.76 Run 1:Combustion Tube at 13 cm.

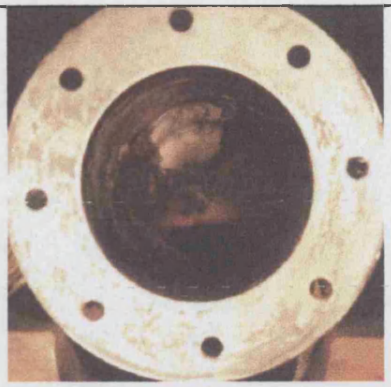

Figure 3.77 Run 1:Combustion Tube at 18 cm.

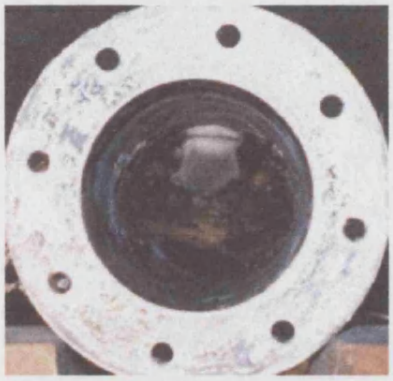

Figure 3.78 Run 1:Combustion Tube at 20 cm.

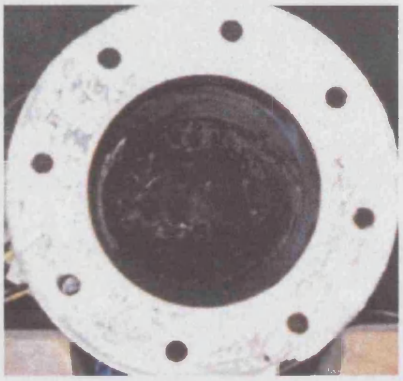

Figure 3.79 Run 1:Combustion Tube at 26 cm.

Figure 3.80 Run 1:Solid Coke at 26 cm.

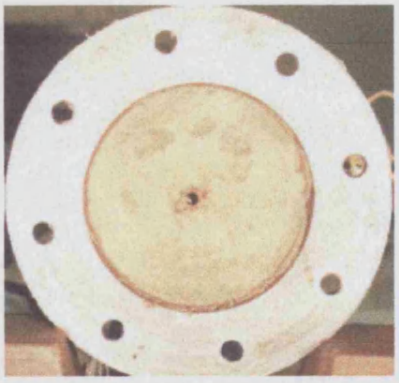

Figure 3.81 Run 1:Bottom of the Combustion Tube.

Bottom Figure 3.82 Run 1: Core samples shows extent of carbon deposition. *Top*

Post-Mortem Photographs of MI Limestone from Combustion Tube (Run Two):

The first photo taken for the second run and from the combustion tube media is shown in Figure 3.83. Soft sand came out of the tube when the ignitor released. The depth of the soft and loss sand ranged to about 6 cm as shown in Figure 3.83. The soft sand removed, and the shape and the colour of the media at 6 cm exactly is shown in Figure 3.84. Some coke left behind more in the middle more than the tube. Zones burned show white colour than unburned. Figure 3.85 which represent the tube cross-section at distance of 7 cm. Overall clearance of complete combustion occurred in this section. None considerable coke where left. The most clearance of sand indicated complete burnt zone. This clearance did not found ahead or behind this cross section.

At distance of 9 cm long of the tube cross-section as presented by Figure 3.86. Very loose sand fall down in the middle, making a bigger hole than the original axial thermocouple ¼" hole. Some coke can be seen inside the tube and closed to the wall. Figure 3.87 represent the shape of the very soft sand enlargement at 10 cm. Most of the fuel and the coke burned in some locations. Thin area shown, very thin film of coke unburned partially across the tube, this may be due to the availability of high amount of fuel, caused by packing. However, during the packing, the oil moves up to the top of the packed sand due to compression. The combustion occurs in the middle more than in the edges of the cross-section at 12 cm long of the tube as shown in Figure 3.88.Dark rings of cokes presented in Figure 3.89, taken at 15 cm long of the tube. The highest bunt zone can be seen radially. High amount of coke deposited beside the inner side of the tube wall. Figure 3.90 show small consolidated coke placed in the middle with a hole in the middle (Axial thermocouple pipe place). The shape of the coke is shown in Figure 3.91 which is located at 21 cm distance. At 22 cm the burnt portion appear in Figure 3.92, with unburnt zone obvious as half circuit. Figure 3.93 at 25 cm show the two separate major sections. Thick solid Coke start appearing at distance of 30 cm as shown in Figure 3.94. Figure 3.95 show the cracked coke at distance of 36 cm. The piece of coke retrieved is shown in Figure 3.96. This coke piece elongated to 40 cm as shown in Figure 3.97. Figure 3.98 taken at 50 cm, show a radial combustion occurred, surrounded by coke.

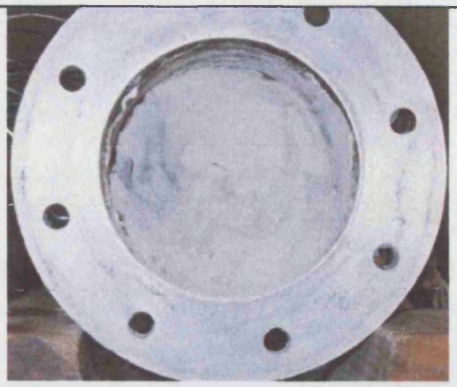

Figure 3.83 Run 2:Combustion Tube at 0-6 cm.

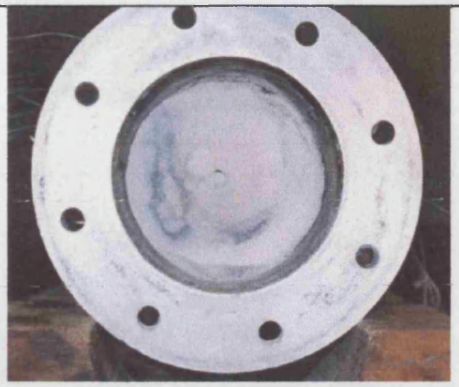

Figure 3.84 Run 2:Combustion Tube at 6 cm.

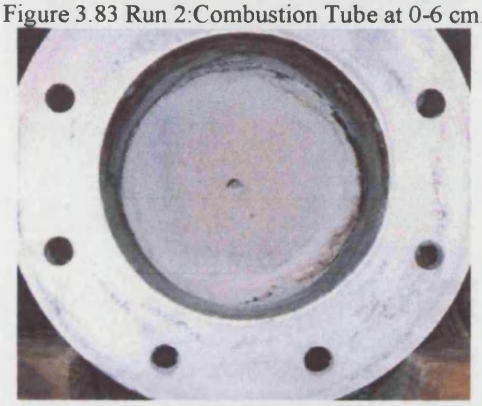

Figure 3.85 Run 2:Combustion Tube at 7 cm.

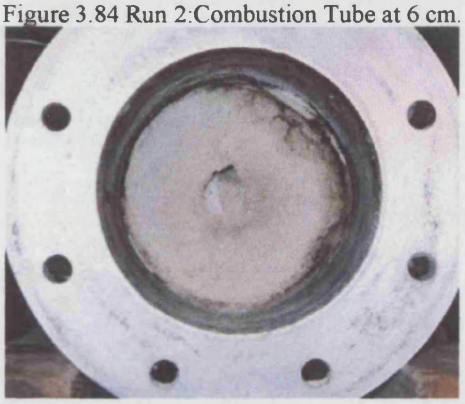

Figure 3.86 Run 2:Combustion Tube at 9 cm.

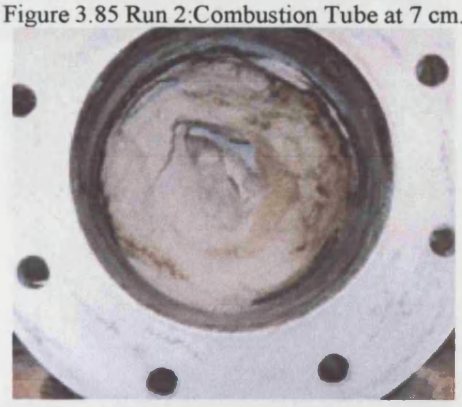

Figure 3.87 Run 2:Combustion Tube at 10 cm.

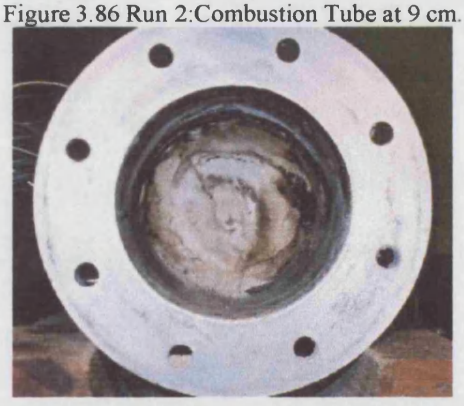

Figure 3.88 Run 2:Combustion Tube at 12 cm.

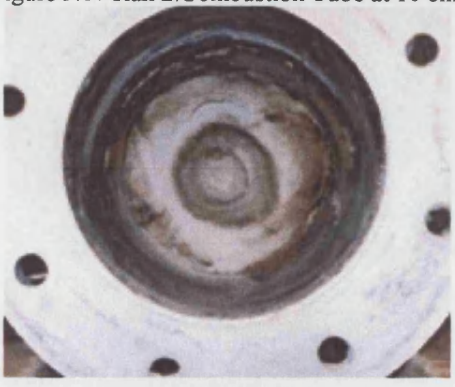

Figure 3.89 Run 2:Combustion Tube at 15 cm.

Figure 3.90 Run 2:Combustion Tube at 21 cm.

Figure 3.91 Run 2:Solid Coke at 21 cm.

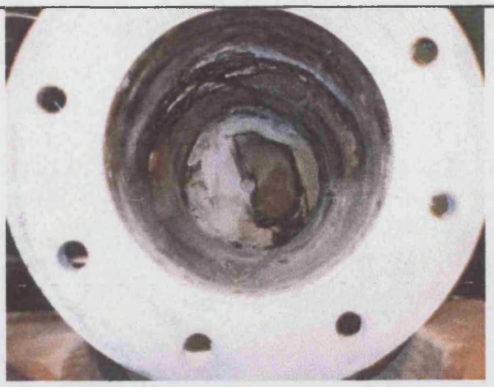

Figure 3.92 Run 2:Combustion Tube at 22 cm.

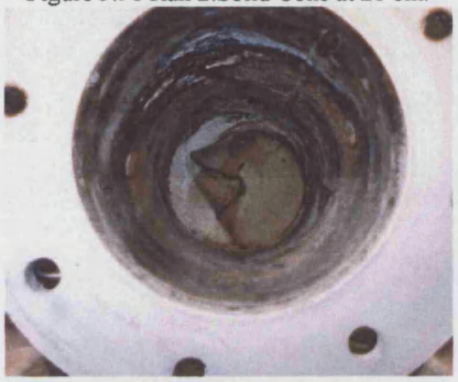

Figure 3.93 Run 2:Combustion Tube at 25 cm.

Figure 3.94 Run 2:Combustion Tube at 30 cm

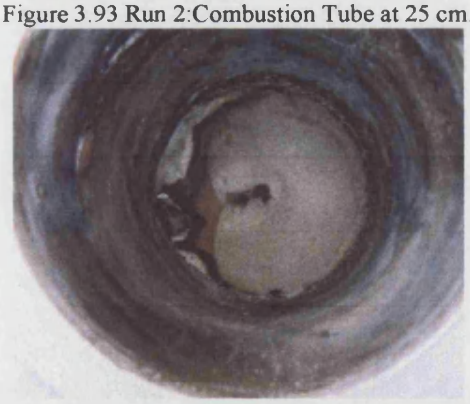

Figure 3.95 Run 2:Combustion Tube at 36 cm.

Figure 3.96 Run 2: Solid Coke at 30 – 40 cm

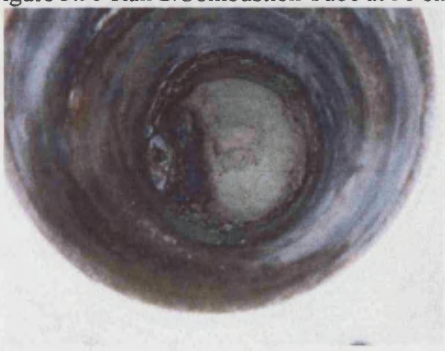

Figure 3.97 Run 2:Combustion Tube at 40 cm.

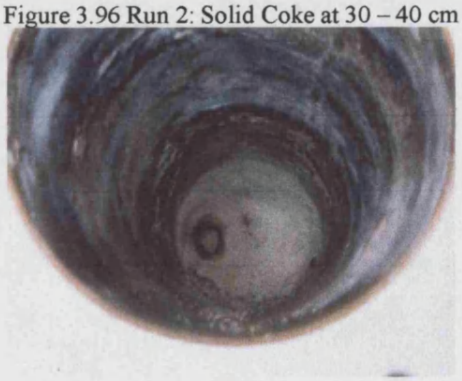

Figure 3.98 Run 2:Combustion Tube at 50 cm.

Post-Mortem Photographs of MI Limestone from Combustion Tube (Run Three):

To analyse the photos taken from the combustion tube run, it should be emphasized that these photos represent the last minute of the shut down and after cooling and the tube and it is contents. As it was realized that once the run terminated or completed, there will be no more movement of the combustion fronts. But, temperature reduced to the room condition. All the crude burned and form loose sand from the ignitor to about 11 cm. No any dark colour appeared, it mean no even a small coke left behind the combustion front. Figure 3.99 represent the tube cross section at 12.5 long of the tube. No coke left behind the combustion front and all the formation burned completely even closed to the tube wall. Figure 3.100 represent cross section taken at 14.5 cm, it show dark color of formation comes from little amount of fuel left behind not burned. Overall others are whites colour.

Some points went darker than before as shown in Figure 3.101 taken at 17 cm. The darkness appears to have round or circular form. Another inner circle appear inside the old big fuel deposited circle as seen in Figure 3.102, taken at 21 cm. As what it can be seen that the inner pipe has no effect into the size and the shape of the fuel remaining. Tangent of the inner circle reach to the axial thermocouples pipe hole with no change in the circle. Also it clear that the inner and the outer circle of the fuel deposited have or sharing same tangent at some points. This cross section taken at 23 cm (Figure 3.103). Very clear burned zone still can be seen after 25 cm as shown in Figure 3.104. The shape of the remained fuel enlarges uniformly. The inner tangent of the circle takes place in the middle of the TA pipe hole. Another third circle start appear inside the first two as shown in Figure 3.105, taken at 29 cm.

The outer formation burned completely.Another radial fuel deposited on the top of the old one is shown in Figure 3.106, taken at 31 cm. Only one circle remained at 32 cm as shown in Figure 3.107. Little (about 20%) of the cross section taken at 34 cm was

burned as shown in Figure 3.108. At 36 cm [see Figure 3.109], a thick coke layer appeared and small hole can be seen beside the wall surrounded with very solid coke. It is believed that this hole induced by reaction fluids and the media. Specially when CO_2 and water react and form carbonic acid, which will be easily to react with carbonate sand, creating induced or secondary porosity. Figure 3.110 presents high percentage of coke closed to the tube wall at 40.5 cm. At 45.5 cm as shown in Figure 3.111 the hole and coke start disappear. At 50 cm [see Figure 3.112] the cross section continue to show a very small differences between light and little dark area. Figure 3.113, still show a fuel deposited, the other cross section taken at 56 still show wavy colour dark to light. At very deep of the tube and at 97 cm a small dark area appeared as shown in Figure 3.114.

Figure 3.99 Run 3:Combustion Tube at 12.5 cm

Figure 3.100 Run 3:Combustion Tube at 14.5 cm.

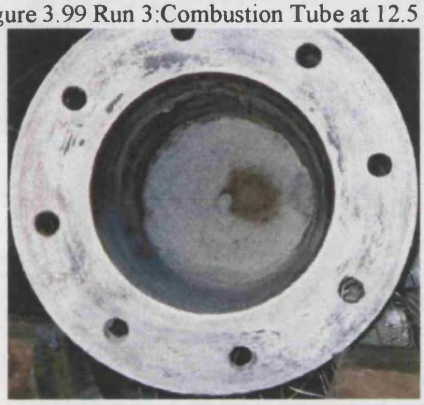

Figure 3.101 Run 3:Combustion Tube at 17 cm.

Figure 3.102 Run 3:Combustion Tube at 21 cm.

Figure 3.103 Run 3:Combustion Tube at 23 cm.

Figure 3.104 Run 3:Combustion Tube at 25 cm.

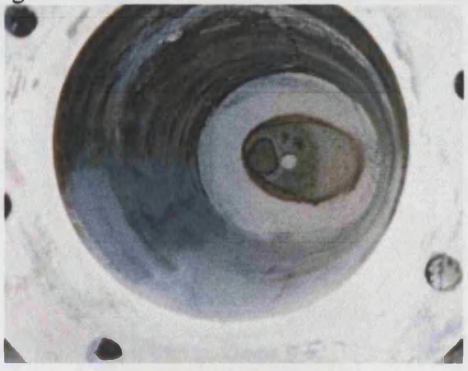

Figure 3.105 Run 3:Combustion Tube at 29 cm.

Figure 3.106 Run 3:Combustion Tube at 31 cm.

Figure 3.107 Run 3:Combustion Tube at 32 cm.

Figure 3.108:Combustion Tube at 34 cm.

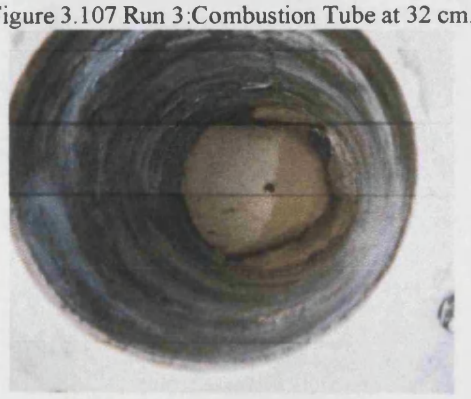

Figure 3.109 Run 3:Combustion Tube at 36 cm.

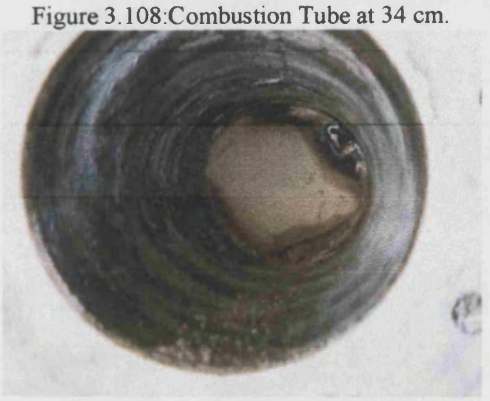

Figure 3.110 Run 3:Combustion Tube at 40.5

Figure 3.111 Run 3:Combustion Tube at 45.5

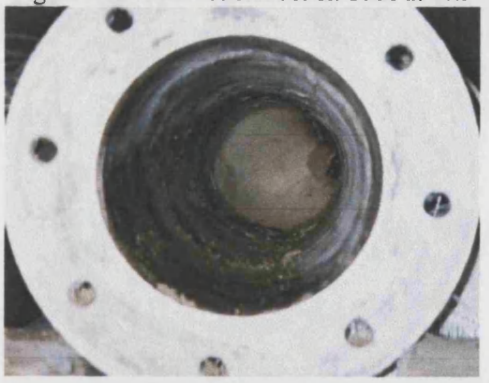

Figure 3.112 Run 3:Combustion Tube at 50 cm.

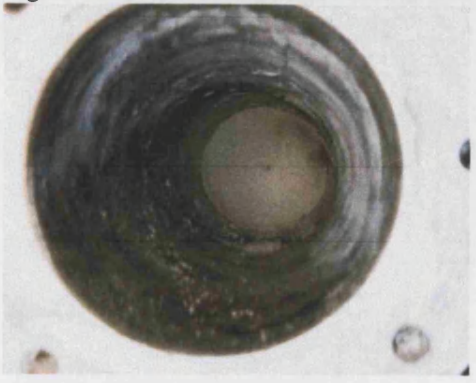

Figure 3.113 Run 3:Combustion Tube at 56 cm.

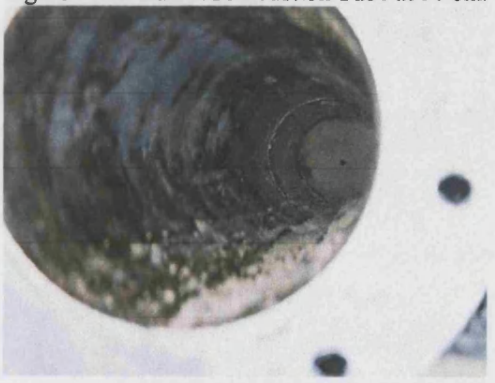

Figure 3.114 Run 3:Combustion Tube at 97 cm.

Oil and Water Production:

The oil produced from Run 1 appear to be less viscous than that produced from Run 2. Figure 3.115 present generally good separation between oil and water phases i.e. the emulsions were nor a problem.

Figure 3.115: Oil and water produced from Run 1.

The oil and water produced from Run 2 is shown in Figure 3.116. Large amount of emulsion were produced. Oxidised oil also appears to be produced, because Channelling of oxygen and cooling of steam inside the oil. The milky, oil in water emulsion is formed during the ends stage of the experiment, whereas a 'chocolate' make in oil emulsion formed during the rest of the run.

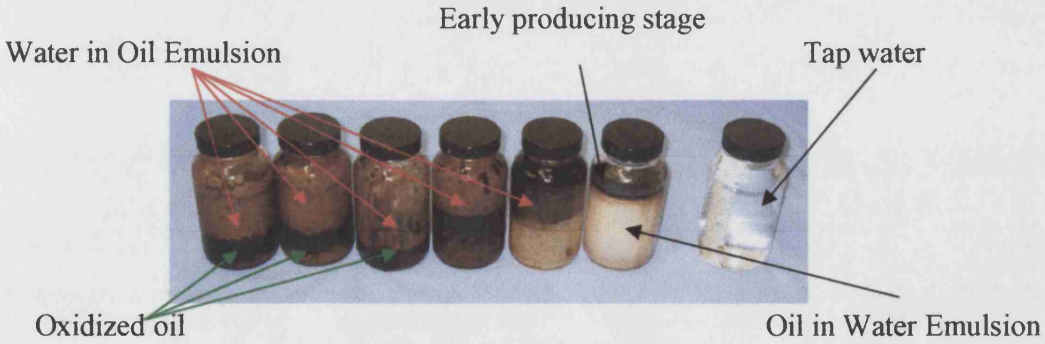

Figure 3.116: Oil and water produced from Run 2

Figure 3.117 and 3.118, illustrate the degree to which emulsion and oxidized oil are formed. In Figure 3.117, the surface of the oxidised oil seems to be smooth, and shining in appearance, the emulsified oil is more 'hetrerogeneous', or much less smooth. Figure 3.118 presents the difference in thickness between the emulsified and oxidised oil, the emulsified oil with thicker particle.

Figure 3.117: Oxidised and Emulsified Oil (Top View)

Figure 3.118: Oxidised and Emulsified Oil (Side View)

The same particle of emulsified oil was placed on a stainless steel screen (24 mesh),the oil failed to pass through, evidencing a very tight emulsion (Figure 3.119). This kind of emulsion could easily have pluged the liquid pressure regulator (PRVL1), between HPS and LPS.

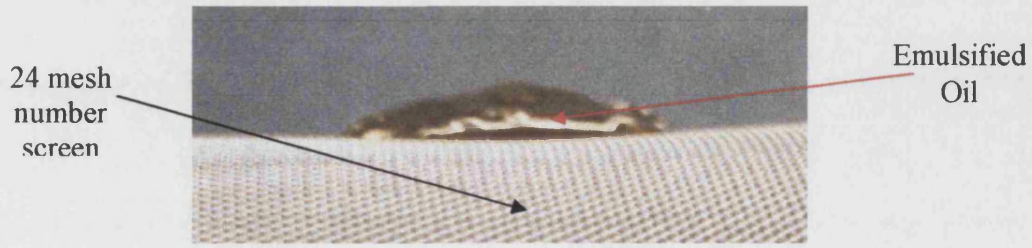

Figure 3.119: Emulsified Oil on 24 mesh Number screen.

3.7: In-Situ Combustion Tube System Modifications:

The second run performed with more accuracy and control. A new Thermocouple axial probe built and tested, providing a better measurement response. The 32 thermocouples were inserted inside a ¼ inch tube, then was clamped with bolt ferrules at the end of the tube. Figure 3.120 shows the old axial thermocouples, where expoxyed into place at the bottom of the tube connector, which did not allow any damaged ones to be repaired.

Figure 3.120: Old Axial thermocouple pipe and connection.

Figure 3.121 and 3.122 shows the new set of axial thermocouples and the way how it is installed. As mentioned before, any damaged thermocouple can be replace.

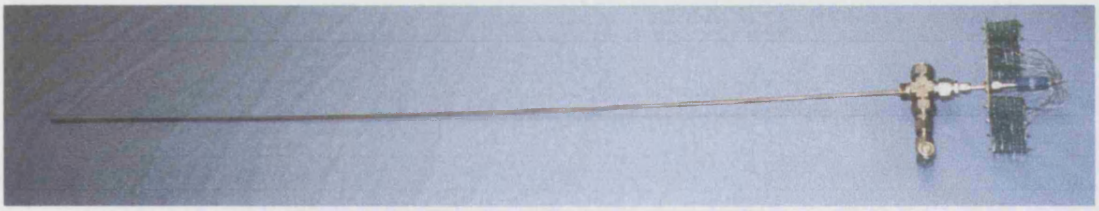

Figure 3.121: The new axial thermocouple robe.

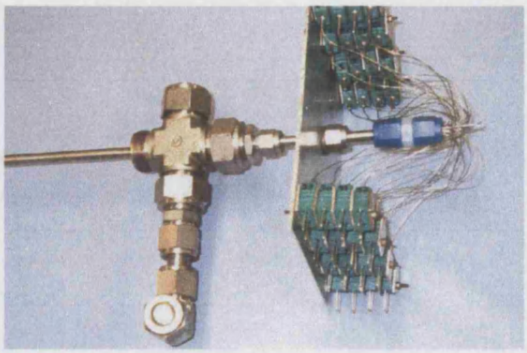

Figure 3.122: Axial thermocouple connections

Band Heaters:

The new band heater indicator box is shown in Figure 3.123, it consists of 32 lamps to indicates the activation of the 32 band heaters. The benefits of this arrangement are:

1. Indication that all band heaters are properly connected.
2. Indicate the active state of each band heater.
3. Test the ability to pulsing frequency and multitasking operation of each BH.
4. Test the operation of the ignitor connections.

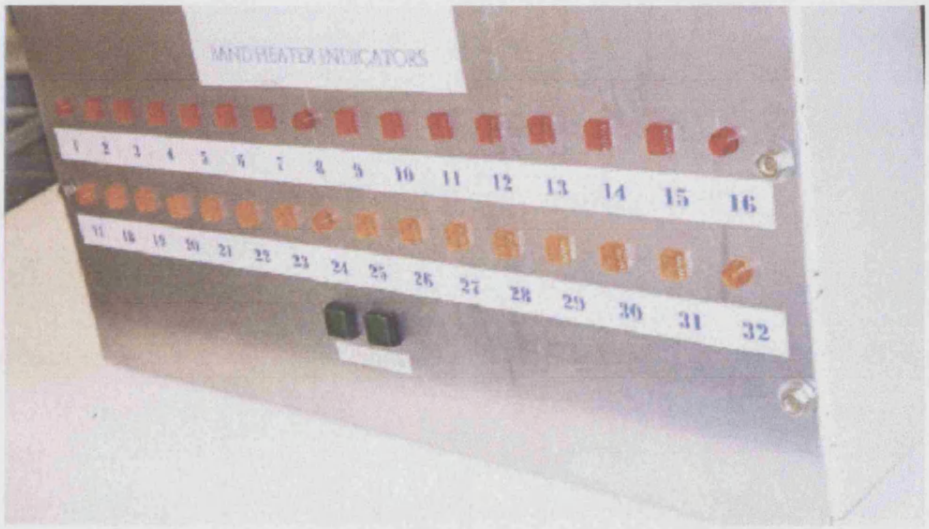

Figure 3.123: New Band Heater Indicators

During run No. 1, it was concluded that there the band heaters arrangement affected the combustion process. The old sequence of BHs as performed and used in run No. 1, is shown in Figure 3.124. It was found that more heat was generated in the middle of the half of band heater than at the join of two halves, where the wall thermocouples was inserted.

Figure 3.124: Old Sequence of Band Heaters

The modification is shown in Figure 3.125. Moreover, this is to insure and guaranty better distribution of temperature and heat all around the combustion tube. The odd numbers joints from 1 to 31 placed horizontally, and the even numbers from 2 to 32 placed vertically on them.

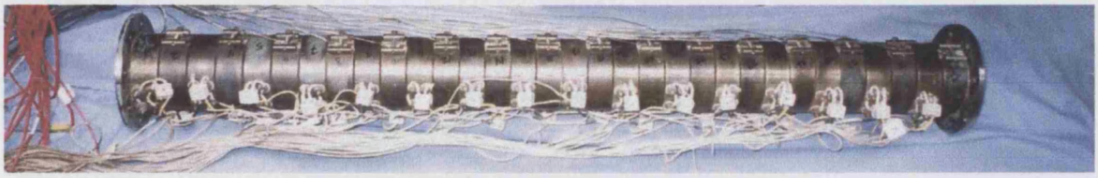

Figure 3.125: New sequence of Band Heaters

Gas Knock-Out Device:

A gas knock out was added to the system in run 3. Another temporary line was added as well to replace the liquid exit line, as shown by the arrangement in Figure 3.126 disengage from the oil via LPS. Elimination or minimization of liquid carried over was achieved.

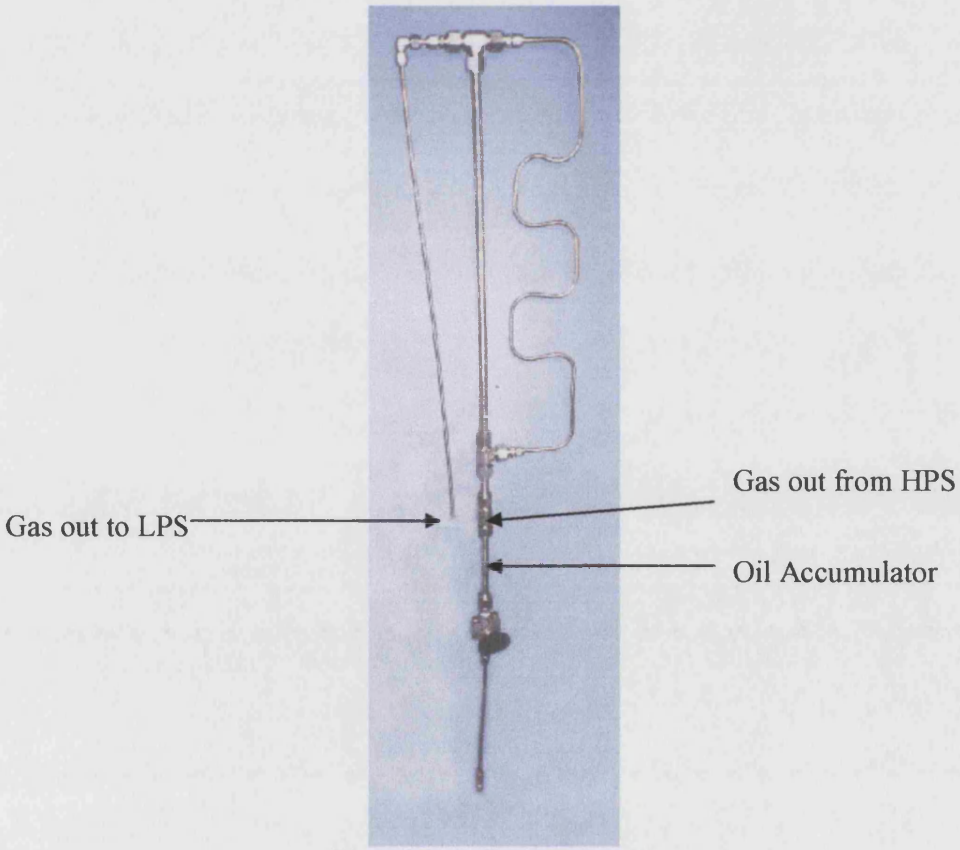

Figure 3.126 : Gas Knock-out.

In Run No. 3, no major modification was made to the system, except adding a valve ahead of liquid pressure regulator (PRVL1), placed between HPS and LPS, to insure control the process during the run. Moreover, the liquid line between the separators wrapped with heating tape, controlled at about 60°C. Several tests where conducted to estimate the voltage required to heat up the tape to desired set temperature (see Table 3.4). However, this test was made to ensure that there are no damage to the Air Actuated Valve (AAV20), placed in the middle of the line, due to its limited operating conditions from –23 to 65°C. Type of potential voltage used is blue colour (ZENITH) type V-3H M, output, 270V.

Table 3.4 : Tape temperature maintained at different variant supply power.

Temperature, °C	Varian reading, %	Varian output, Volt
70	40	108.8
60	35	96.9

Computer Program:

Only the " Ignitor Control.vi" was modified. Originally, it was programmed to switch-off the ignitor when the CO_2 % level reach 5%. Run No. 3, conducted the produced CO_2 was allowed reach each to 1%, before switch-off the ignitor, and increasing the air flux to the required value.

Additional Separator:

A third stage separator was added to the system in run No. 4. This was added to control separation of gas from the produced oil (Figure 3.127).This unit was operated at atmospheric pressure and room temperature.

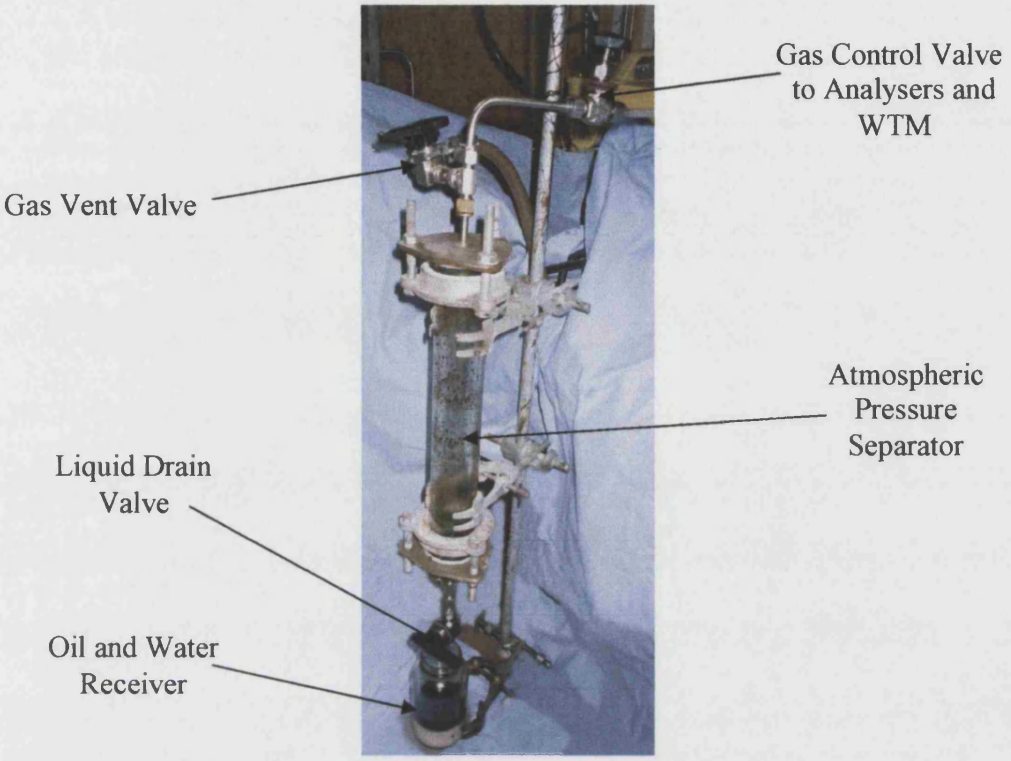

Figure 3.127: Atmospheric Pressure Separator (Third Stage).

Crude oil passes from the LPS to the atmospheric pressure separator (APS), and separtated gases are sent to the analysers (CO, CO_2, and O_2), and finally to the WTM.

Flange Bolt:

A particular difficulty in achieving pressurization to 217 bar in Run No. 4, was due to failure of one the pressure shell top flange bolts. As shown in Figure 3.128, one of the bolts had developed a severe stress crack, and had to be replaced with new bolt with the following specifications:

- M45 x 250 8.8 Bolt S/COL (High Tensile Bolt)
- M 45 GR.8 Nut S/COL
- M 45 Washer – S/COL

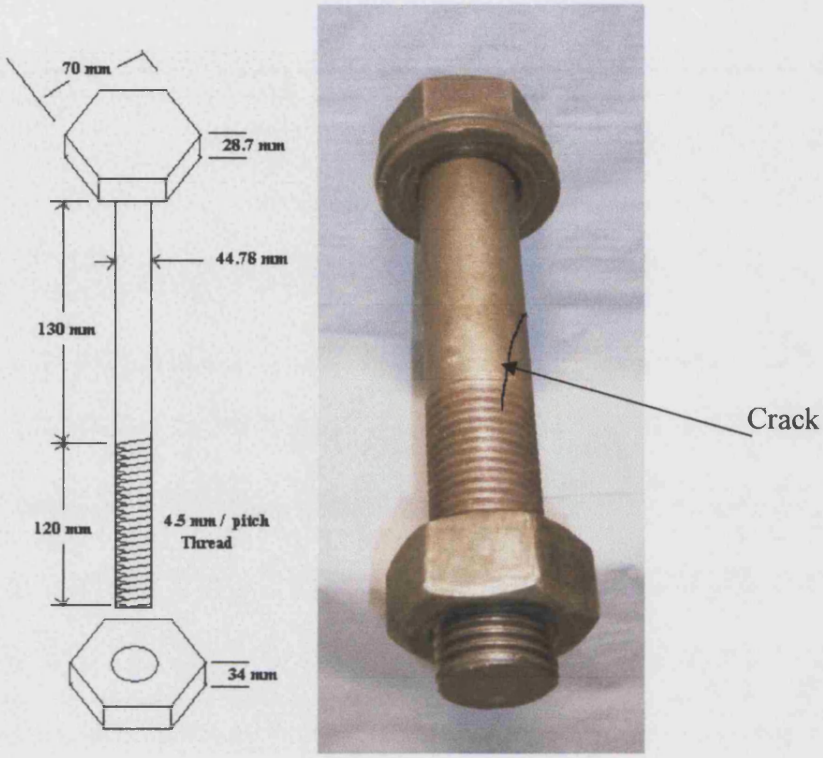

Figure 3.128: 70 mm High Tensile Shell Flange Bolt, Showing Stress Cracking

CHAPTER FOUR

RESULTS AND DISCUSIONS

Results and Discussions

The results of five combustion tube runs are presented in detail. The main conditions for these experiments are given in Table 4.1. Run 4 and 5 were operated without band heater control. Run 6, 8, and 9 were oprated with full BH control, but for certain periods, the BH's were not fully active, because of multitasking limitation (see *Axial-Wall Temperature Difference*.

Table 4.1 : Combustion Tube Experiments:

Experiment Condition\Run Number	Run 4	Run 5	Run 6	Run 8	Run 9
Back Pressure (bar)	200	200	200	200	100
Reservoir Bed Temperature (°C)	30-40	18-22	19-25	17-29.5	19-25.6
Ignitor Temperature (°C)	250				
Air Injection Concentration (%)	100				
Produced Gas Flux (m^3/m^2hr std)	83.9	30.8 93.8 36.4	21.0 104.0	42.0	62.65
Cylinder Supply Pressure Max.(bar)	230				
So_i (%)	30	27.6	30	70	30
Sw_i (%)	70	64.4	70	30	70
Band Heater Operation	No+	Yes++	Yes		
Dry Sand Pack	No	Yes+++	No		
Reservoir Core Material (Crushed)*	MI Lime Stone				
Clay content (%)	0				
Porosity (%)	42.5				
Permeability of MI Lime Stone	600 md (estimated)				

Run 7 was excluded, due to communication between tube and shell.

+ Band heaters 20-32 operational when set pressure attained, prior to ignition, to equalize tube temperature.

++ On when the combustion front did not propagate properly.

+++ Dry sand at the bottom of the tube (10 cm).

4.1: Run 4 :

General Observations:

Run 4 is an example of combustion tube operation without band heater control. Normally, a tolerance of 20 °C (below the sand pack axial temperature) was employed to ensure a near adiabatic control condition, as in Run 1, 2, and 3. This because it was suspected that the BH's could be artificially energized, due to specious currents, or earthing connections.

It was noted in the preliminary experiments (Runs 1, 2 and 3) that there was a particular shape of the coke layer that remained after the combustion front advanced ahead, circular, rounded or oval. There are three main factors that can affect the shape of the coke zone:

1. Heat distribution around the band heater from each half-section.
2. The combustion tube
3. The axial thermocouple probe.

Others factor that could contribute to the coke effect indirectly, are:

1. Porous media geometry
2. Flow regime.
3. Fuel distribution
4. Fingering through the porous media
5. Channeling around the porous media and beside the tube wall.
6. Channeling around the internal axial thermocouple pipe.
7. Presence of multi media inside the porous voidages Liquid (Oil, Water and acid) and gases (LTO, and HTO products)

The main factor determining coke laydown, i.e. LTO and thermal cracking.

Startup/ Pressurisation:

The pressure was incremented at a continuous rate, (0.0025 mA) opening with PPRV2, until the pressure reach to 169 bar after 59 minutes. Farther pressurization was then halted. This allowed process equallisation between the tube and shell, as well as enabling the high pressure gas supply cylinder to be repressurised to 234 bar. The pressure held constant for the next 47 minutes, giving time to the horizontal cylinders to pressurize from 200 bar to 234 bar. It is necessary to maintain at lest 30 bar higher pressure than the tube operating pressure of 200 bar. Pressure up continued at 107 minutes at same incremented rate. When the tube and shell pressure reached 204 bar, there was a problem in the pressure. It was decided to reduce the back pressure from 217 bar to 200 bar, to allow liquid displacement in the tube. Nitrogen flow to the sand pack was switched-off and air was switched-on at 134 minutes. off at time of 134 minutes. There was no flow until ball valve (BV6) opened at time 142 minutes, causing the pressure to drop to 194 bar, equalizing PT2 and PT4, as shown in Figure 4.1. At 167 minutes the combustion tube pressure reached 200 bar, but then reduced to 192 bar. The pressure disturbance is an indication that combustion had commenced.

The pressure during the experiment averaged 198 bar. At time of 247 minutes, the air supply started decreasing gradually until the end of the experiment, down only to 205 bar. The experiment terminated at 285 minutes, and shut-down commenced.

At 147 minutes, the gas exit line was closed using a needle valve placed after PT4 . This was to ensure that no bypass of leaking occurred through the main control gas exit valve. The latter closes only gradually and take a short time to close completely (PT8 in Figure 4.1). The surge in Pressure (PT8 at 230 minutes) is because of the slow pressure regulator action (PRVL1) caused by slightly viscous oil production.

Note that PT5 reading the liquid exit line pressure, was not working during the run. It has since been replaced with high accuracy pressure gauge.

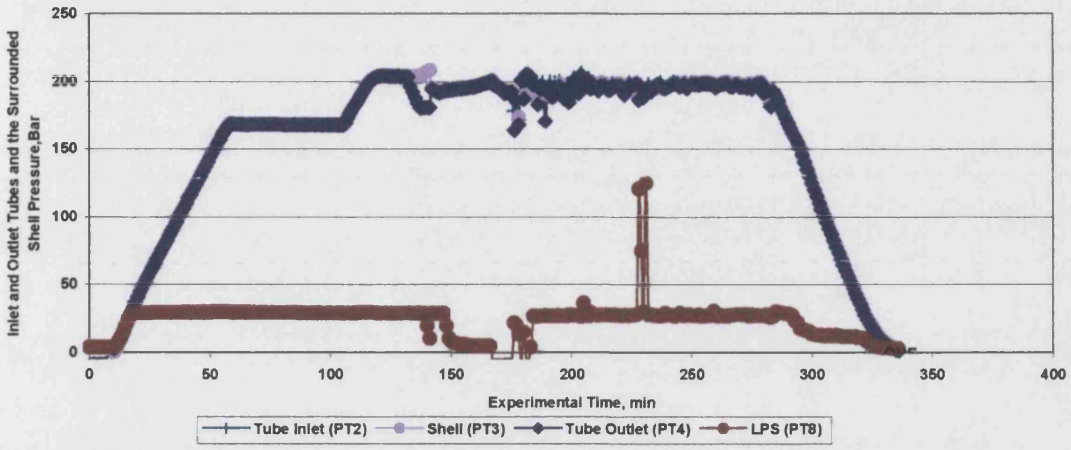

Figure 4.1 Run 4 : Combustion Tube Pressurization.

The tube was pressurized only from the top. This is important, because more difficulties are experienced in temperature interpretation if the tube is pressurized simultaneously from the top and bottom. Pressurising from the top compresses the fluid that is expanded by heat the core to its initial reservoir bed temperature. The best procedure to establish communication between top and bottom of tube is to pressurize from both ends, particularly if the crude oil used has a high density and viscosity.

The effect of pressurizing the combustion tube on the reservoir bed temperature can be seen in Figure 4.3. The average temperature when nitrogen injection started was 18.22 °C. After 60 minutes, the temperature at axial thermocouple number one reached 30 °C. The effect is due to a combination of higher external gas temperature and compression heat.

There is progression cooling along the tube due to heat 'drain-off' by the end flange, and to some extent also because the shell is pressurized by nitrogen flow from the bottom end.

The malfunction of axial thermocouple No. 10 is due to a computer connection problem.

The set pressure was achieved at 133 minutes, and the electrical ignitor switched-on. The lower part of the core was also heated-up using BH 19 to 32. The temperature rise in the core is shown in Figure 4.4. The maximum axial thermocouple reached was about 42 °C then lowered to about 34 °C at time 176 minutes. The ignitor heating rate lowered less

than what used in the previous tests as it can be seen in Figure 4.4. With this low heating rate criteria, good and farther heat distribution can be gained as it can been in the figure, it reach band heater number two.

After 178 minutes (Figure 4.5), BH 1 reached 215 °C. At this time, nitrogen flow was stopped and air injection started. Immediate ignition occurred, causing the temperature to rise to 614 °C with in 2 minutes. There is a very rapid increase to 765 °C at 182 minutes. Since igniton took place at 215°C , low temperature oxidation probably occurred first, before achieving high temperature oxidation 614°C. It is always recommended that the ignitor temperature is raised to the desired temperature (> 215°C) before air injected. Otherwise, there is the possibility of detonation, an explosion, if peroxides are formed first from LTO.

A further observation from Figure 4.5, is that the combustion front moved to BH 2 at time 184 minutes. At time 185 minutes, the combustion front temperature reduces and it advances to BH 2. A cooling effect occured at BH 1 causes the combustion front to move ahead.

In Figure 4.6, the combustion front has reached BH 3 after 191 minutes, but the maximum peak temperature is reduced to 400 °C. Then, the peak temperate then increases to 428°C at 197 minutes reaching BH 4. At 197 minutes, the temperature ahead of the combustion front has increased to 74°C, (BH 16) due to temperature of heat from upstream. It should be noted that the band heaters were switched-off at 52 minutes, so there was no possibilities of forcing the process.

At 198 minutes, (BH 21), the temperature increases very rapidly, from 28.7 to 152.4 °C due to LTO. The LTO zone advances at an average temperature between 200 to 220 °C, as shown in Figure 4.7.

Auto-ignition occur between BH's 9 and 11. There is gradual increase in temperature from 68 to 184 °C. At time 207 min., the combustion front reaches BH 5. Although, the

ignitor switched-on accidentally for about 5 minutes, it no longer had any effect on the combustion ignition on BH 1.

The combustion front stalled at BH 5,(Figure 4.8 and 4.9). Since the maximum peak combustion temperature remain constant at 465°C, because the oxygen consumed even in other places in the combustion tube.

The average maximum temperature of the second LTO zone, was about 250°C at BH 25. Two small peaks were first initiated, at BH 20, (213 minutes), and then at BH 23, (215 minutes), Figure 4.8. The temperature increased from 30 to 40 °C, during the next 5 minutes. The second LTO zone increased in temperature to 280°C, just after BH 26, but the first LTO (zone) only increased to 260 - 275°C, between BH's 9 and 11. The combustion front then moved forward to BH number 6 at 219 minutes. A new cycle of LTO started between BH 20 and 21, causing the temperature to increase from 144 to 250°C, as shown in Figure 4.9.

The second LTO front continues moving to the bottom of the tube. At 229 minutes, the combustion front has moved to BH 7, the peak combustion temperature remaining at about 460°C. Ahead of the combustion front, the average temperature has increased along the tube to 250 °C (Figure 4.10).

The combustion front becomes more active when it reaches BH 8, and the zone of combustion becomes wider, reaching to BH 12 in the next 5 minutes. The increase in temperature ahead of the combustion (380 to 465 °C) could be due to increased fuel availability, caused by the formation of LTO products (see Figure 4.11).

The burned zone extends from BH 6 to BH 16, a distance of 0.4 m. At 241 minutes, a new LTO zone initiated at BH 21, and another LTO peak also occurs at BH 25, at 243 minutes, as shown in Figure 4.12.

Those two LTO zone initiate a very large temperature rise, the first zone increases to approximately 900 °C at BH 21, and the second zone went up to 700°C at BH 26. The

reason for this very rapid rise in temperature, is possibly the accumulation of oxygen radicals in the oil, which causes an explosive, or rapid oxidation.

High Temperature Zone:

The two high temperature zone in Figure 4.13, reaching 900°C and 700°C. Figure 4.2 (Photo) shows the effect of the very high temperatures on the 316 stainless steel axial thermocouple probe. They show typical tempering colours for this temperature range.

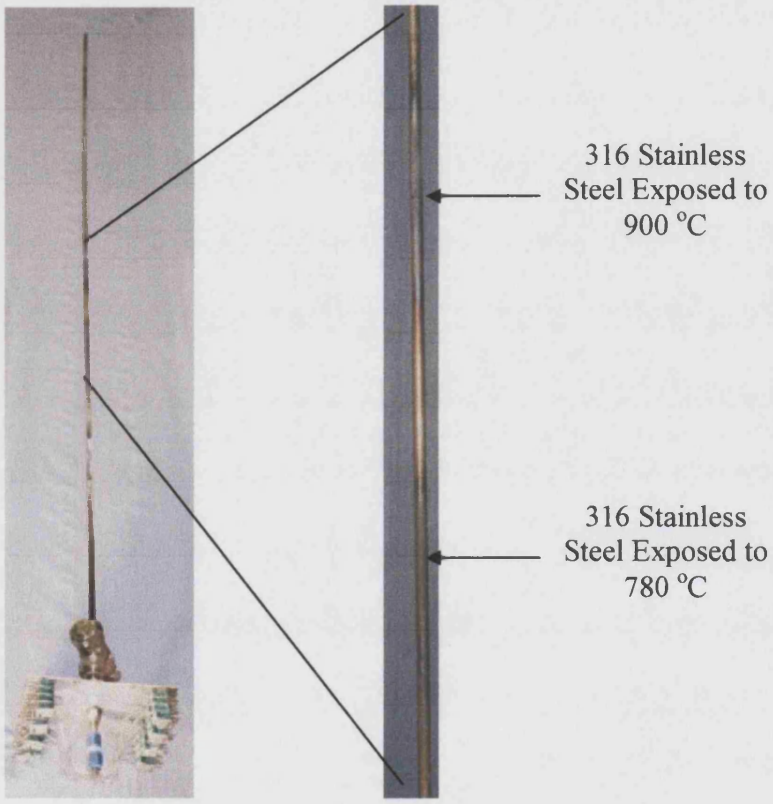

Figure 4.2 : Photograph of tempering on Axial Thermocouple Probe.

The burnt region of the core continuously cooled by the injection of cold air (Figure 4.13 and 4.14), down to 50 °C, up to BH 4.

The combusted zone front comprises two separate entities, one extending to BH 24, and another downstream of this. At 261 minutes, the two combustion region join together, with temperature of 450 °C.

Another high temperature front startes near the bottom of the combustion tube (BH 32), but the main combustion front is still moving towards it (Figure 4.15). The combustion front continues moving down until it merges with the very high temperature (807°C) region at BH 32. The experiment was terminated at time 285 minutes (Figure 4.16). Only in this test, the combustion front allowed to continue to the bottom of the tube.

The combustion tube system was depressurized over a period of 50 minutes, down to atmosphere. When the pressure reaches zero, the computer program terminates the executing of all tasks, including data saved to disk. Figure 4.17 show the decline in temperature when air injection is stopped, and the system pressure is reduced.

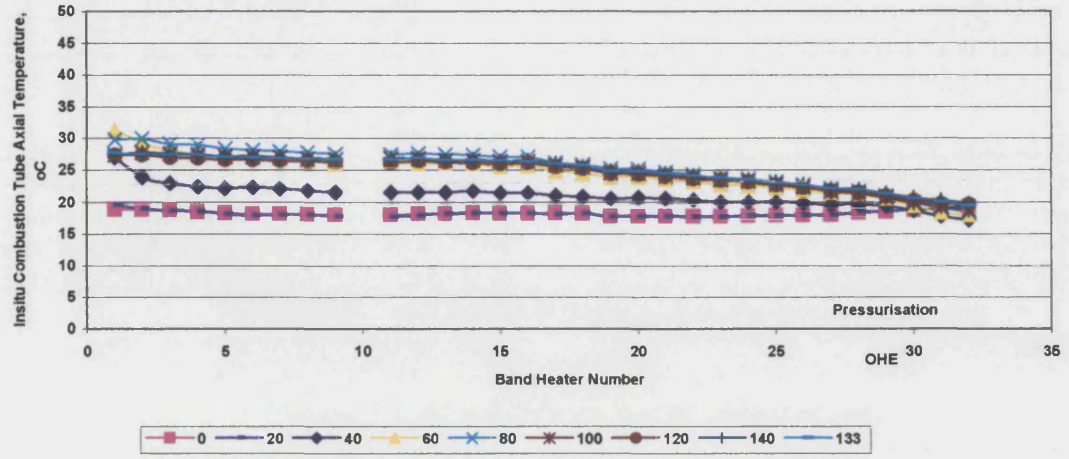

Figure 4.3 Run 4: In Situ Combustion Tube Axial Temperature,

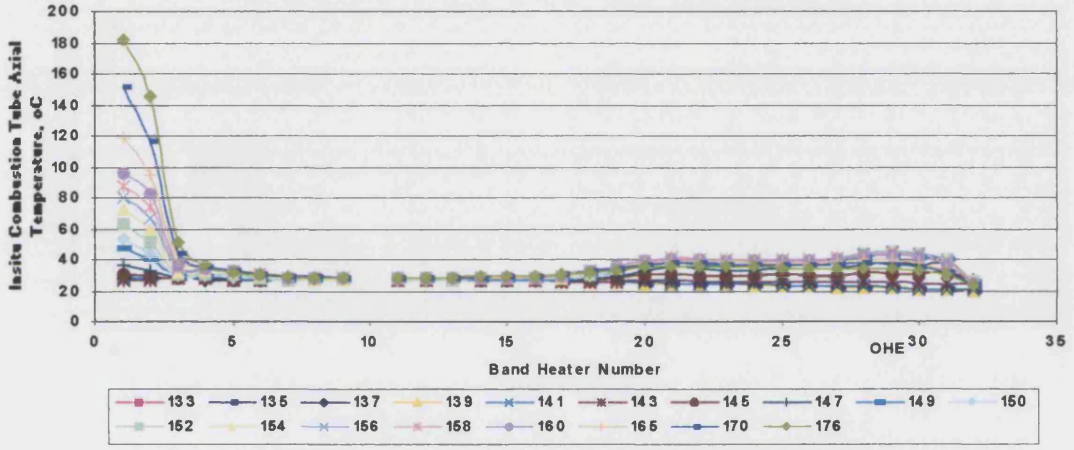

Figure 4.4 Run 4: In Situ Combustion Tube Axial Temperature.

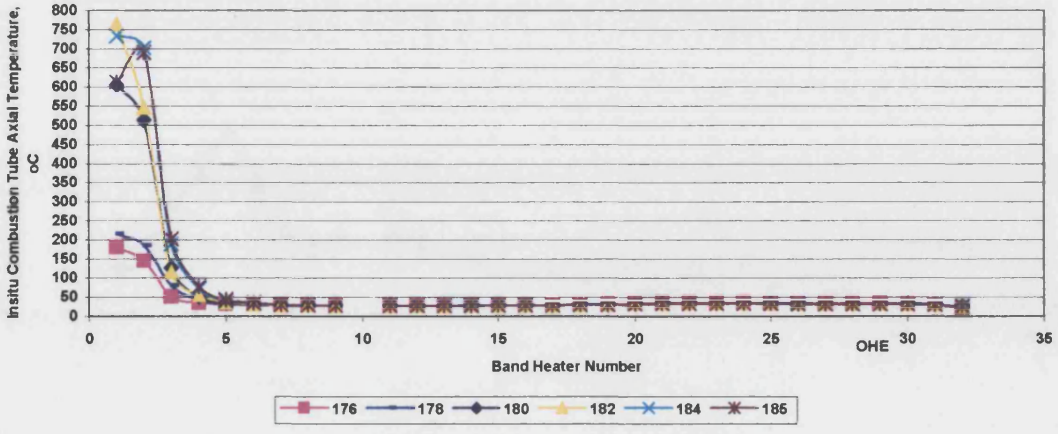

Figure 4.5 Run 4: In Situ Combustion Tube Axial Temperature.

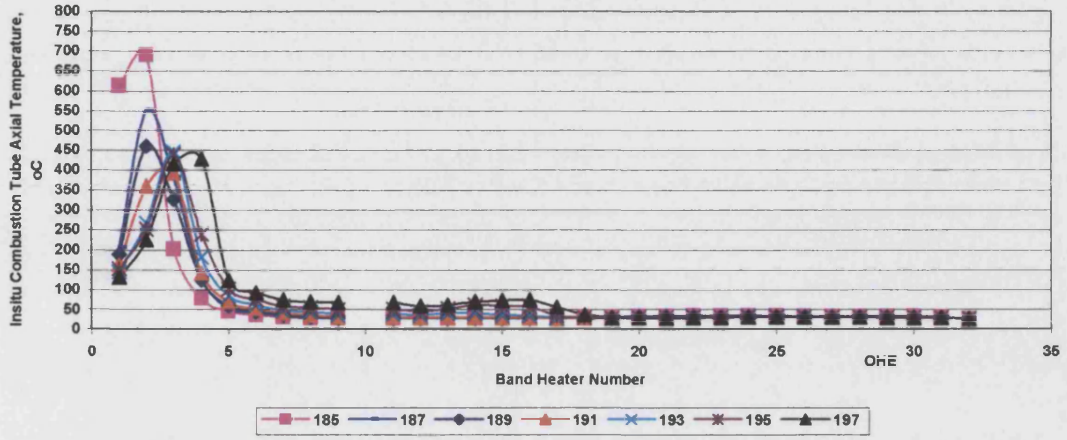

Figure 4.6 Run 4: In Situ Combustion Tube Axial Temperature

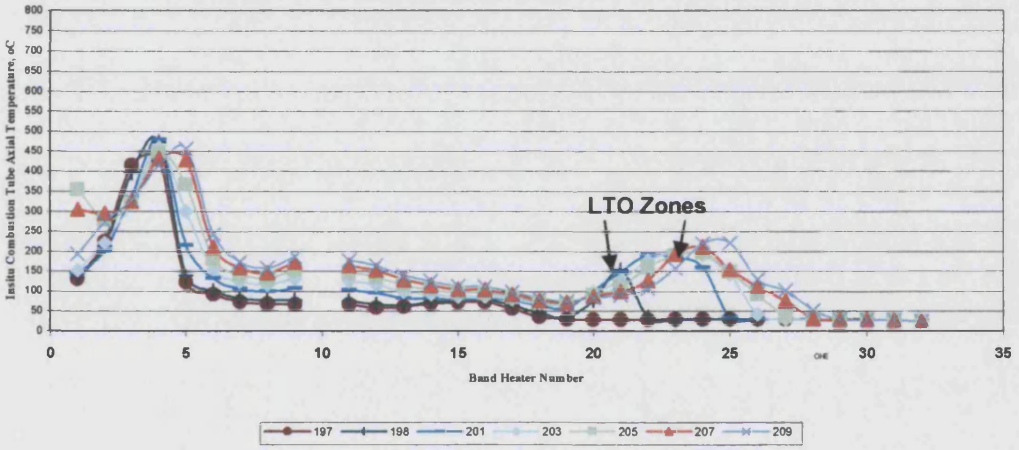

Figure 4.7 Run 4: In Situ Combustion Tube Axial Temperature.

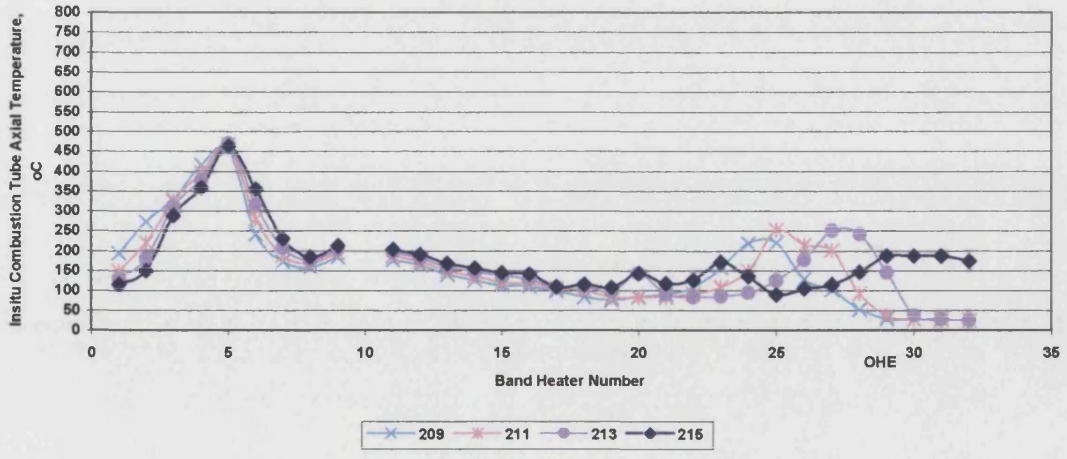

Figure 4.8 Run 4: In Situ Combustion Tube Axial Temperature.

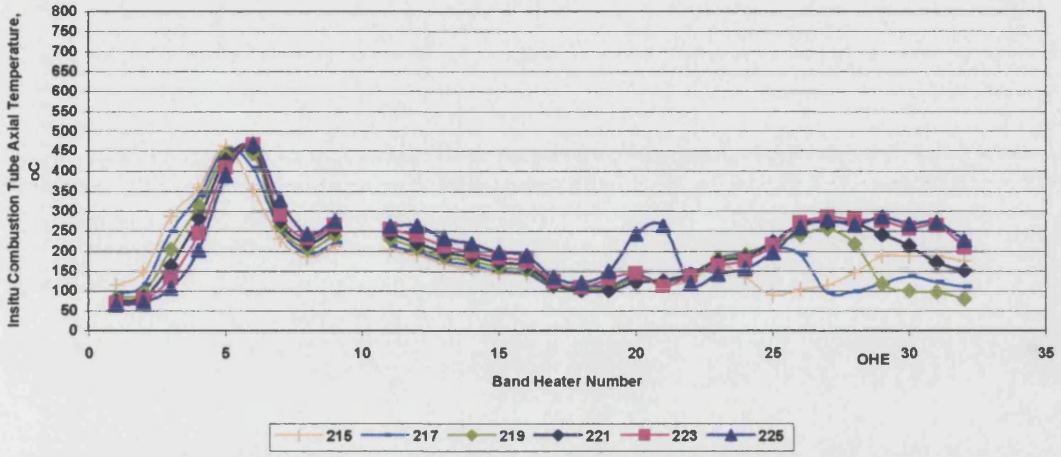

Figure 4.9 Run 4: In Situ Combustion Tube Axial Temperature.

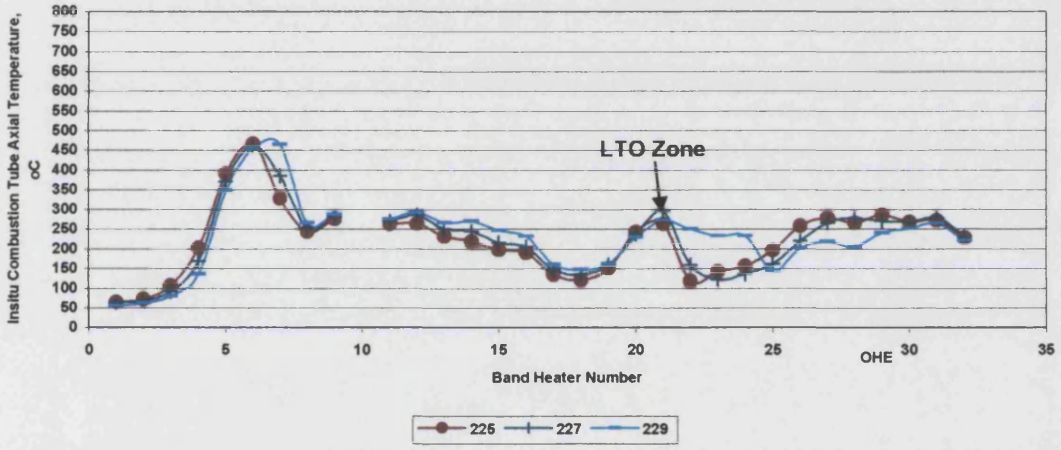

Figure 4.10 Run 4: In Situ Combustion Tube Axial Temperature.

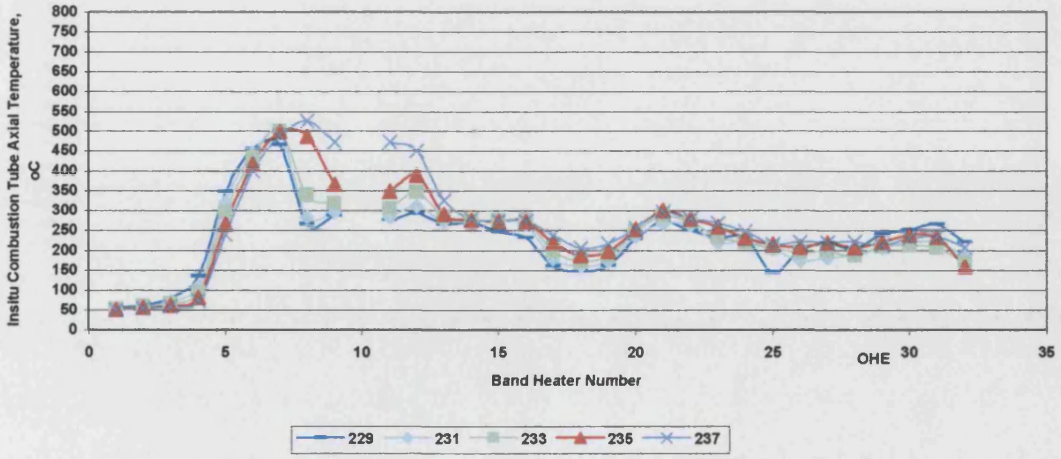

Figure 4.11 Run 4: In Situ Combustion Tube Axial Temperature.

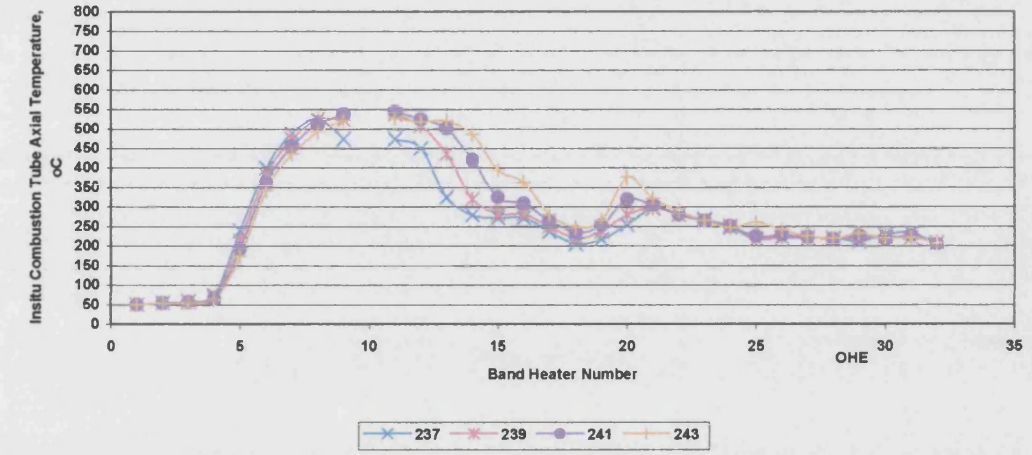

Figure 4.12 Run 4: In Situ Combustion Tube Axial Temperature.

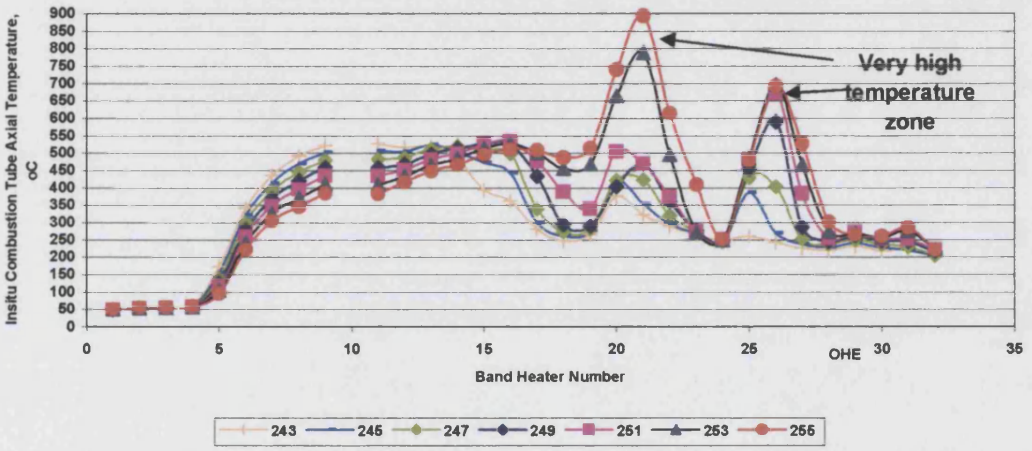

Figure 4.13 Run 4: In Situ Combustion Tube Axial Temperature

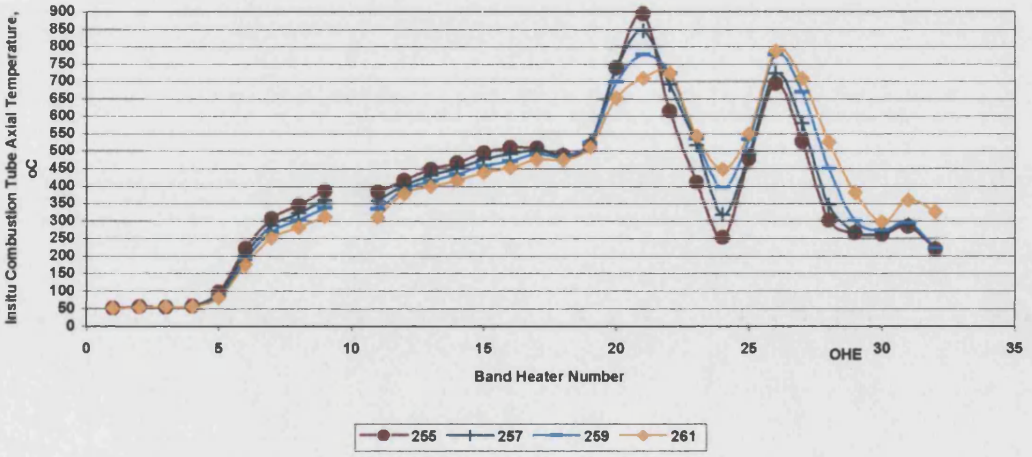

Figure 4.14 Run 4: In Situ Combustion Tube Axial Temperature.

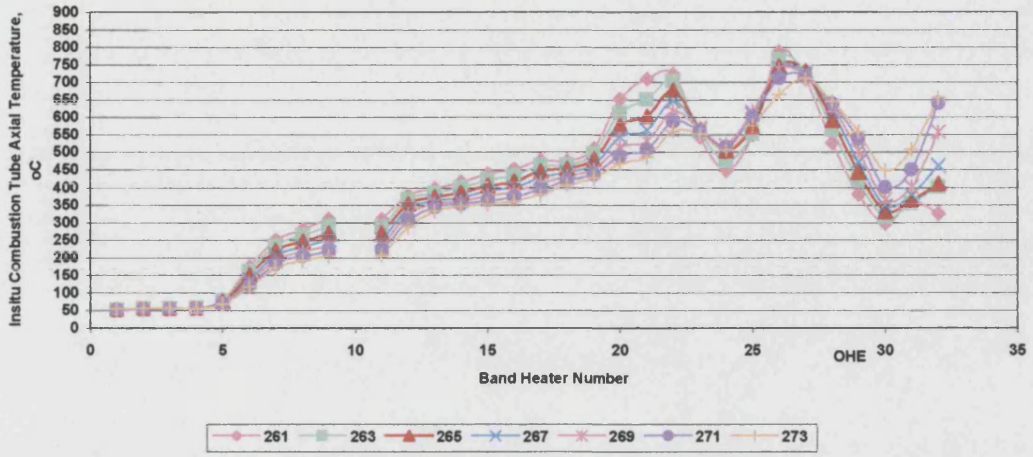

Figure 4.15 Run 4: In Situ Combustion Tube Axial Temperature.

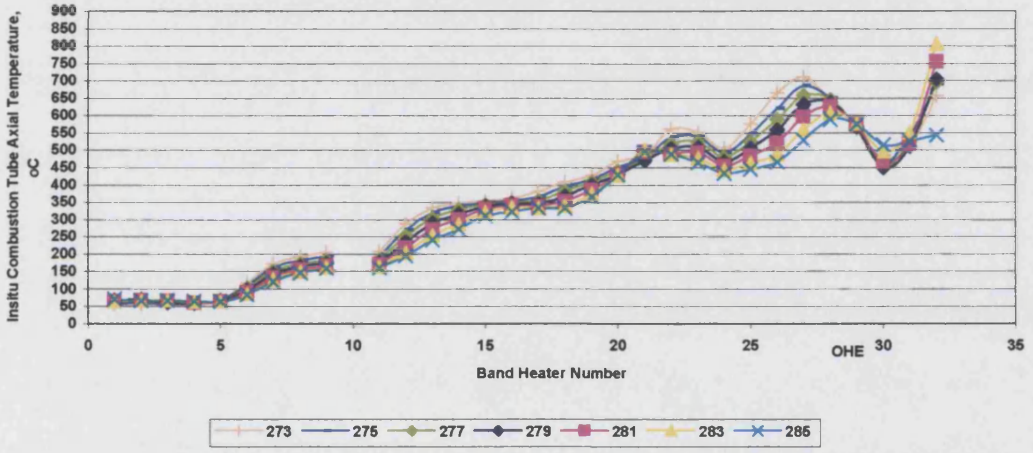

Figure 4.16 Run 4: In Situ Combustion Tube Axial Temperature.

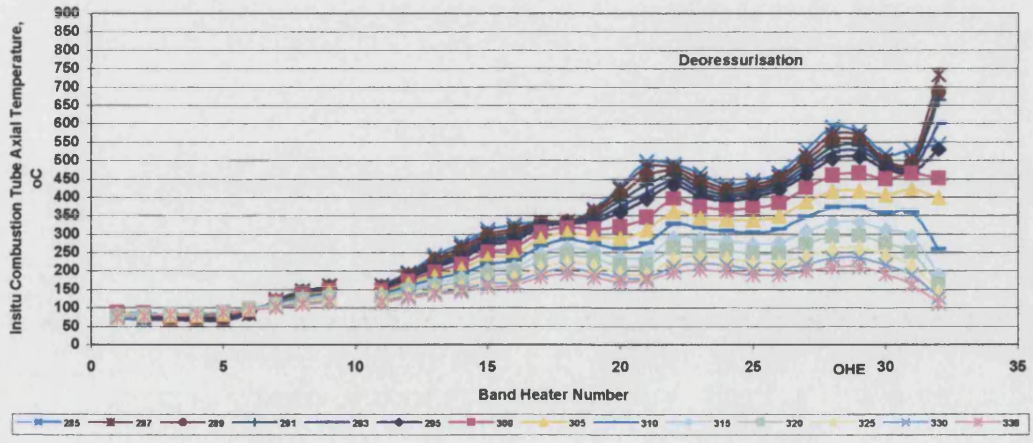

Figure 4.17 Run 4: In Situ Combustion Tube Axial Temperature.

Combustion Front Movement:

The movement or advance of the combustion front is well demonstrated in Figure 4.18. However, as shown by Figure 4.19, this combustion front moves more slowly as it advances downstream.

This trend is summarised in Figures 4.20 and 4.21. The period of steady combustion front propagation exists over the period 190 to 240 minutes, with an increase rate period at the end due to LTO induced effect.

Steady combustion front of 0.3 to 0.5 cm/min are very high compared with much lower value for heavy oil (typically less than 0.1 m/hr).

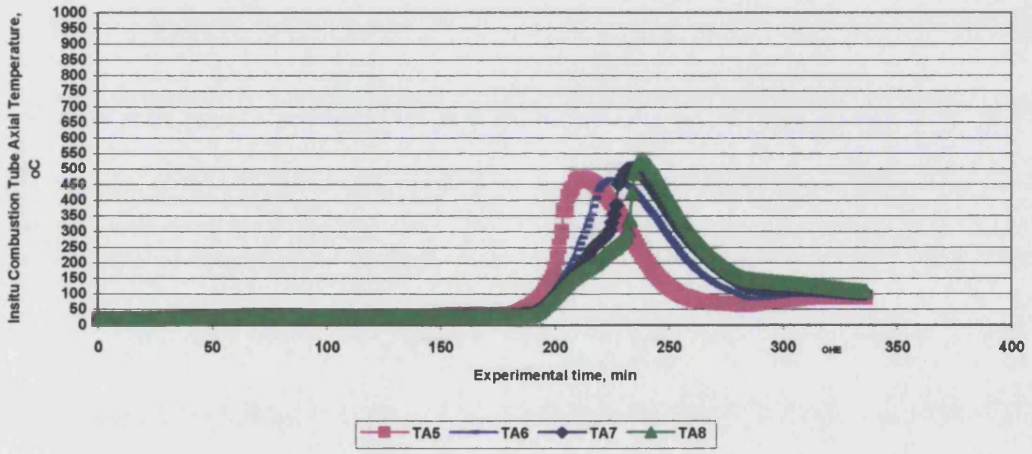

Figure 4.18 Run 4: In-Situ Combustion Tube Axial Temperature, Band Heaters 5 to 8.

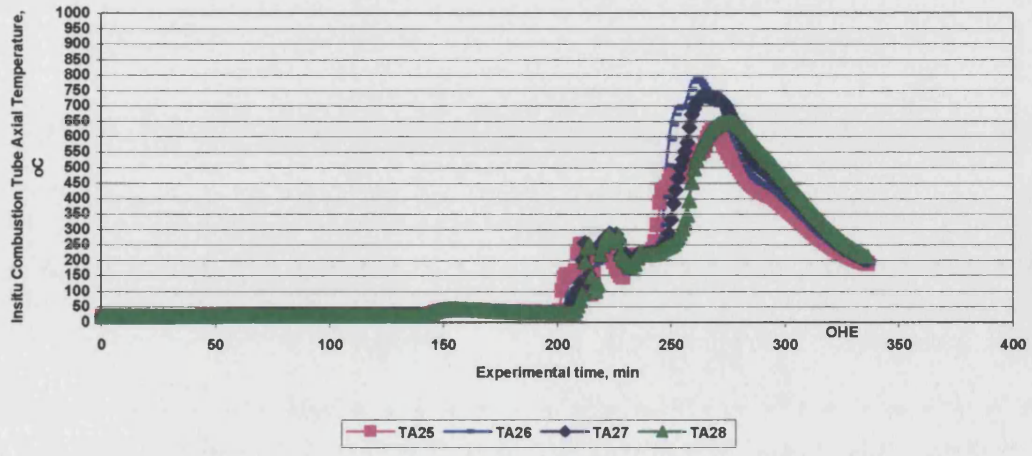

Figure 4.19 Run 4: In-Situ Combustion Tube Axial Temperature, Band Heaters 25 to 28.

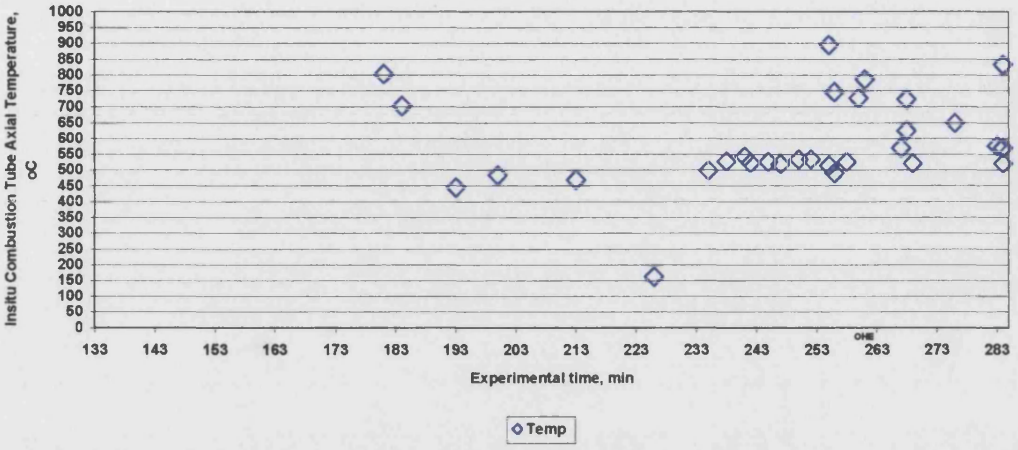

Figure 4.20 Run 4: Combustion Front Temperature.

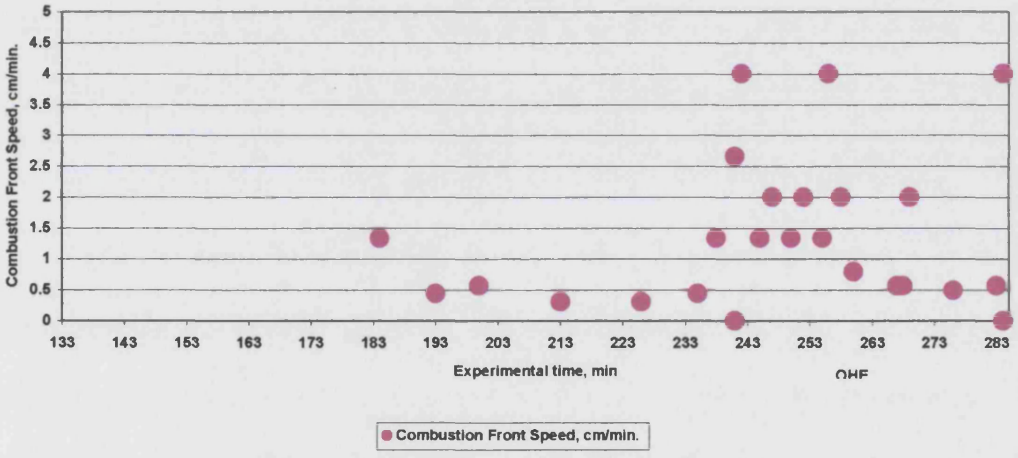

Figure 4.21 Run 4: Combustion Front Velocity.

Produced Gas Composition:

Figure 4.22 shows the variation in the gas composition during Run 4. Gas production commences at 177 minutes, exactly when the oxygen reads zero. CO_2 is produced gradually 183 minutes, reaching to 14.2 % at 195 minutes, and then from 198 minutes reduces to 10 %, at 214 minutes. The level of CO_2 remains constant at 12 % from 216 to 233 minutes, but increases to 15.1 % at 254 minutes. CO initially increases rapidly to a very high value of 21.7% at 189 minutes, but decreases quickly to 7.2% at 192 minutes. For most of the rest of the experiment, CO average around 2%. The very high CO level is due to LTO (215°C) and this occurred before any HTO. This effect not observed in any of the three previous experiments, because ignition was started above 350 °C. The general trends of CO and CO_2 in the produced gas are similar to those simulated by STARS. There is an inverse relation between CO and CO_2, in particular, when no oxygen is produced (241 minutes to the end of the experiment).

The first occurrence of oxygen occurs at 195 minutes, and then continues to increase to over 5%, eventually decreased to zero at 241 minutes. Oxygen channeling ahead of the combustion front is responsible for the auto-ignition and development of the LTO zone ahead of the combustion front reached at BH 21. Part of this oxygen is consumed in the LTO zone and the remain produced, with a value of about 5%. The combustion front was stalled at BH 5 during this period.

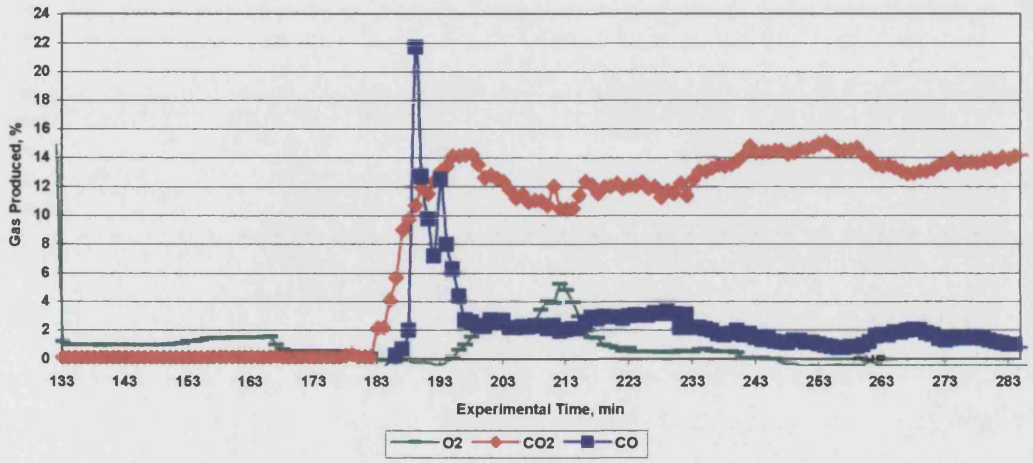

Figure 4.22 Run 4 : Produced Gas Combustion.

Figure 4.23 shows the cumulative amount of gas produced, the initial rate is higher at approximately 5 litre/min, but continue at a lower rate for to the end of the test (~3litre/min).

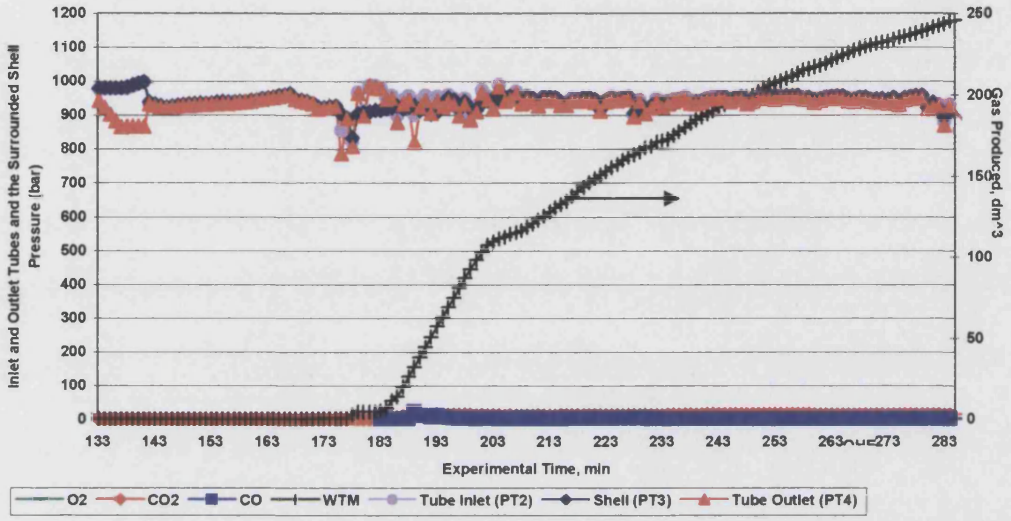

Figure 4.23 Run 4: Gas Wet Test Meter Measurements.

Oil and Water Production:

The ultimate oil recovery was 42.7 % of OOIP. The incremental oil rate after 219 minutes caused possibly by the effect LTO induced. The large amount of water produced, 84% of OWIP, is no doubt due to supplementation for water formed from the combustion and LTO reactions. The total amount of liquid recovered reached to 71.65 % from the original liquid in place as plotted in Figure 4.24.

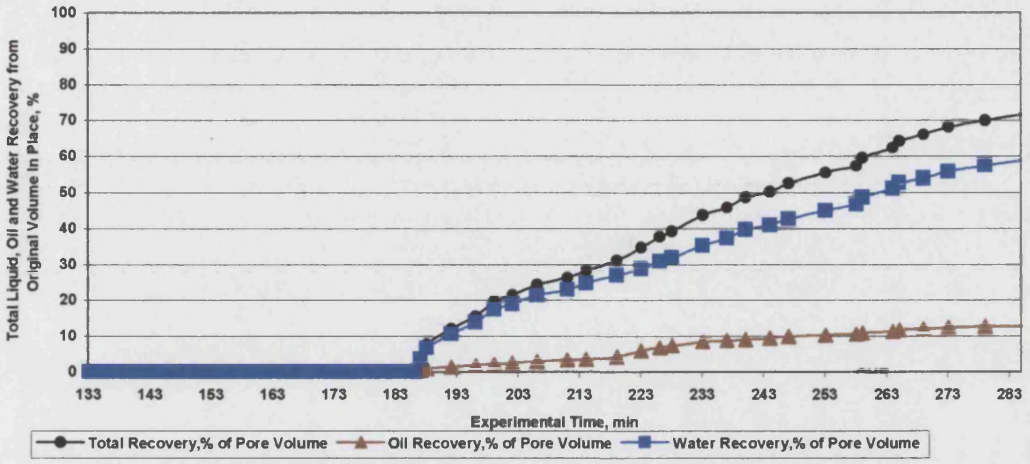

Figure 4.24 Run 4: Liquid Recovery From Pores Media.

In Figure 4.25, at time 219 minutes, colour of the water changed from clear to yellow. Therefore, the yellow coloured water produced had been affected by the combustion proven, and also, possibly, any LTO reaction occur downstream. The oil produced at this time appears to be oxidized oil, since it was very viscous.

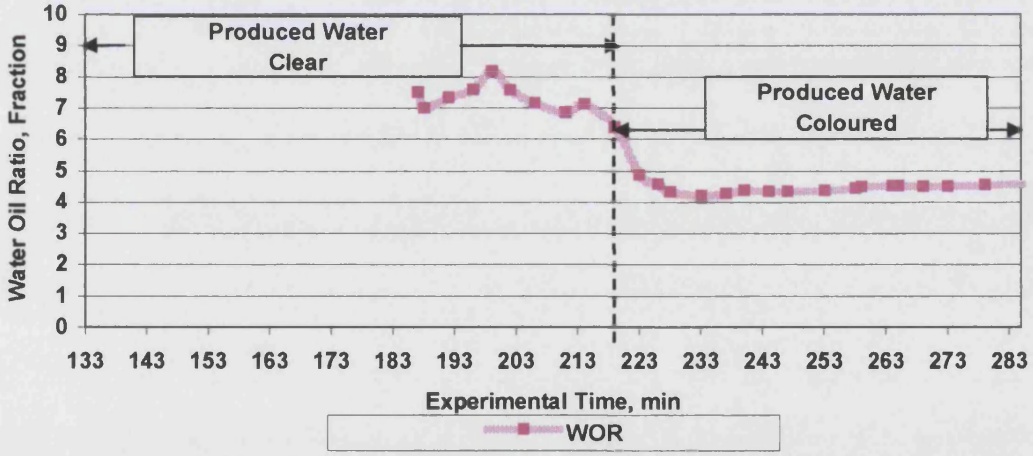

Figure 4.25 Run 4: Water Oil Ratio (Run Four).

The clear (Original) water displaced from the core achieved a water cut of 89%. The water cut reach to value 89%, a value considered to be quite high for primary recovery. This could have important implication for the process.

The pH of the water produced is shown in Figure 4.26. The colour of the produced water appears to be related to the water acidity. The clear produced water has a pH of between 7 and 8, which is normal. After 219 minutes, when the water changed to a yellow colour, the pH value reduced gradually to 4.2, steadying, but then reducing farther to 3.

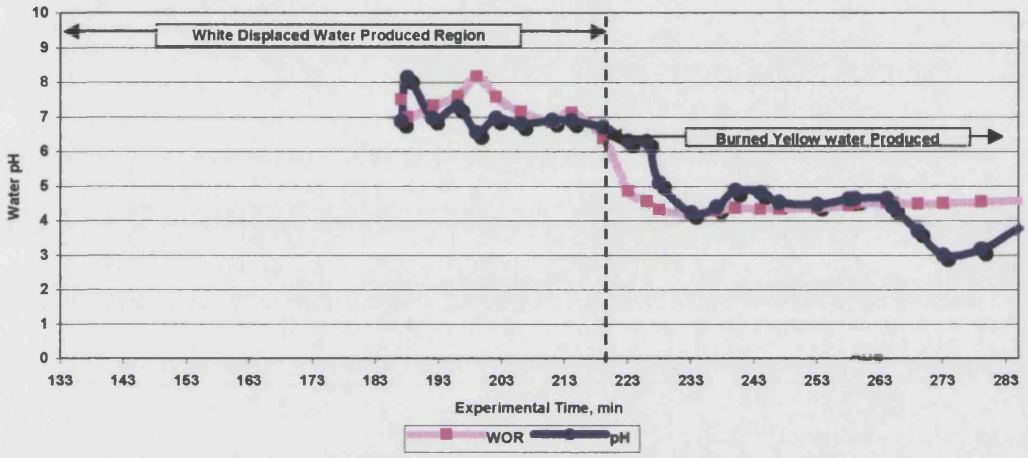

Figure 4.26 Run 4: Water pH.

4.2: Run Five :

Run 5 was conducted under the similar conditions to Run 4 but a lower flux, oil saturation 27.6% and water saturation 64.4%. However, it is very valuable to know the limitation of lower gas injection rate that can be used in laboratory and field scale, to perform good in-situ combustion process.

Generally, the air injection rate will contribute directly, to perform ignition and combustion. If the air injectivity is low then the process will not proceed. If the air injectivity is higher than the optimum, then the process becomes not economical and oxidized oil may be able to influence the recovery efficiency.

It should be emphasized that run 5 is the only run which conducted with 10 cm of dry sand (W-50) located in the bottom of the tube. This was used to protect the bottom sealing and gasket from high heat as it has been seen in Run 4. Pressurisation of the tube took 97 minutes, experiment terminated at 356 minutes.

The Ignitor switched on 97 to 130 minutes. The iqnition and combustion gained as shown in Figure 4.27. The rate of heat generation at this flux was not sufficient to maintain tube temperature and front stalled after ignition and died when fuel was exhausted (204 minutes). Combustion was reiqnited by switching on all BH for 15 minutes. The whole tube heated to between 100 and 150°C before an ignition was observed at BH5. The combustion then moved back towards the top of the tube and peak temperature of about 550°C was observed at BH3. A secondary LTO region of elevated temperature also developed between BH12 and BH16 with a maximum temperature of 300°C at BH12 (Figure 4.28).

When falling temperature and rising oxygen indicated that this combustion was also dying, the flux was increased to get production changed from 30.8 m^3/m^2hr to 93.8 m^3/m^2hr, similar level to that used in the previous run. Simultaneously, the combustion moved downstream in both LTO and HTO peaks (364 min.). After the flux was returned

to its original setting, temperatures again declined, oxygen breakthrough increased and the run was terminated.

Some propagation of these temperature features was observed during the high flux period, but the peak temperatures remained below 400°C and did not achieve the levels recorded at the same flux in Run 4. When the flux was returned to its original value, the tube cooled and the combustion died.

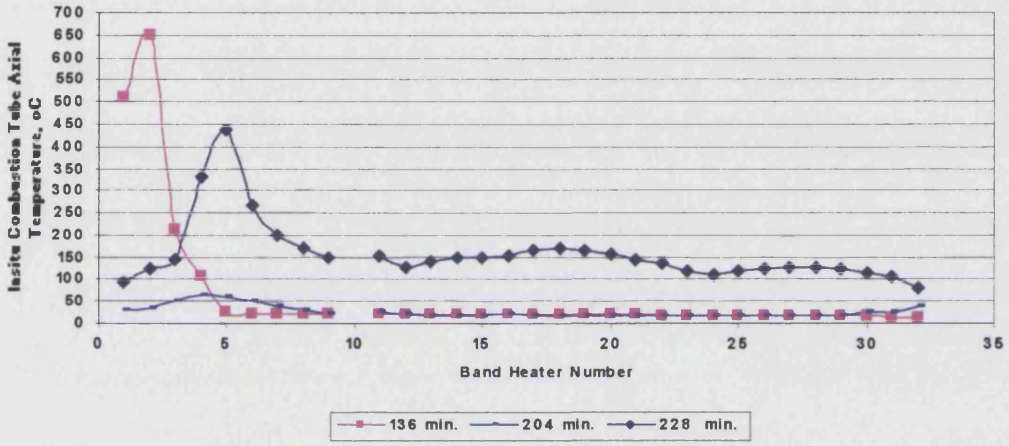

Figure 4.27 Run 5 : Axial Temperature Profile, Post-Ignition.

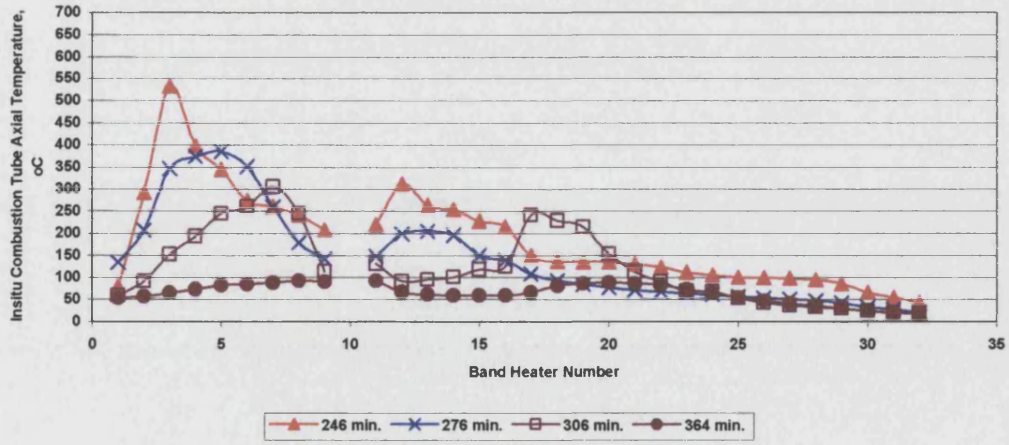

Figure 4.28 Run 5 : Axial Temperature Profile, Post-Ignition.

Produced Gases:

Oxygen breakthrough occurred throughout the run. Following ignition, the oxygen concentration in the produced gases dropped to 2% and then increased to 21% as the tube cooled. CO_2 production peaked at 7% and CO at 1.5% in this period (Figure 4.29). After the reignition by the band heaters, oxygen production dropped to 4%, CO_2 increased to 11% and CO increased to 2%. The period of increased flux resulted in decreased oxygen and increase CO_2 production. However, it did not effect CO which continued to decline and was about 1% when oxygen breakthrough was at its minimum.

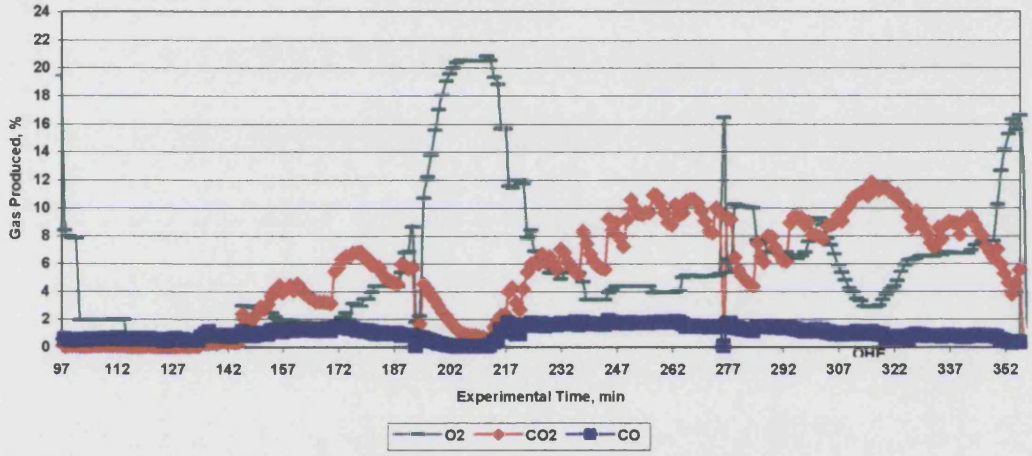

Figure 4.29 Run 5 : Produced Gas Combustion.

Figure 4.30 presents the volume of gas produced during the experiment. It show clearly the effect of changing production rate with the injection. It shows also all the operation and the changes made on the band heater.

Oil and Water Production:

Oil recovery was 9% of the original oil in place. The majority of this oil was produced during the period when the entire tube warmed by the band heaters. Water recovery was 40% of original water in place. Water production was also significantly increased during the period when the entire tube had been warned. The ultimate liquid recovered from the test did not exceed 31.3% as shown in Figure 4.31.

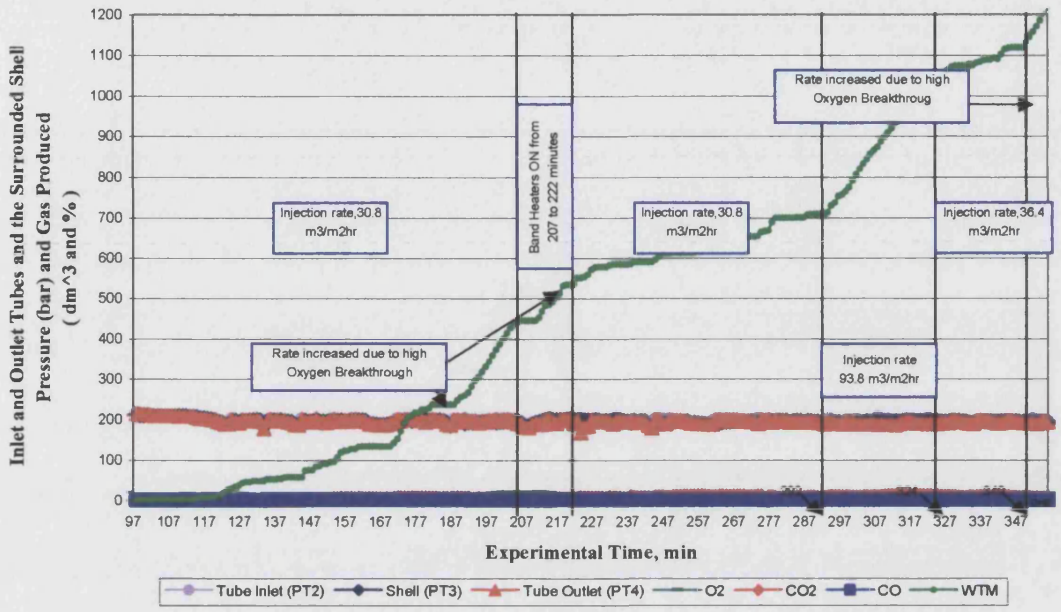

Figure 4.30 Run 5: Gas Wet Test Meter Measurement.

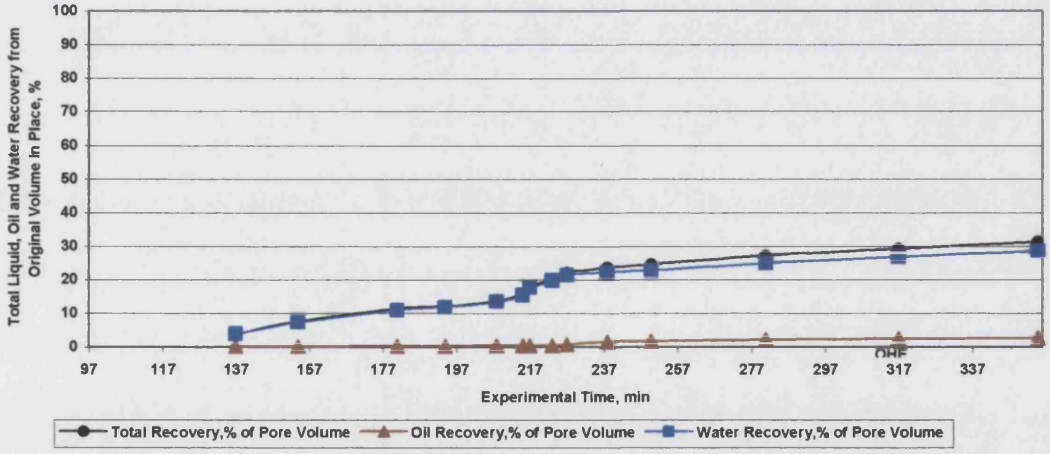

Figure 4.31 Run 5 : Liquid Recovery From Pores Media.

There where no major changes between the water produced in pH as it can be seen from Figure 4.32.

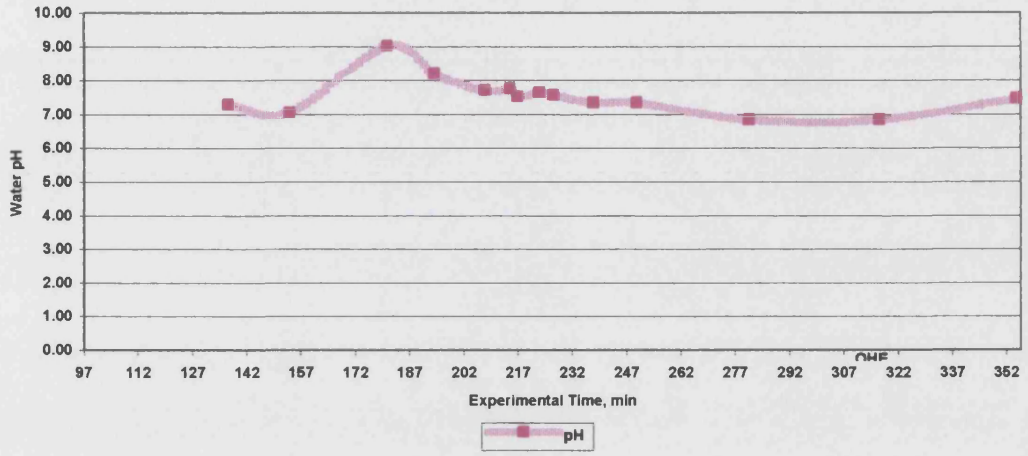

Figure 4.32 Run 5 : Water pH.

4.3: Run 6:

Run 6 was a repeat of run 5 but with band heater used for adiabatic control, oil saturation 30% and water saturation 70%. Following the pressurisation which took 89 minutes, the ignitor switched on for 27 minutes from the beginning of the run. The ignitor switched off when BH1 reaches 250°C.

Following ignition, the peak temperature recorded between 400 and 450°C. The temperature profile is shown in Figure 4.33. The peak temperature normally remained steady but showed sensitive to flux specially when a high flux was used for half an hour at the end of the run. LTO region occur just ahead of HTO peak between BH6 and BH12, where the temperature fixed at 255°C. Other LTO reaction occurred at BH22, enlarged with time to the bottom of the tube.

Following the increase in flux at 340 minutes, temperatures down stream of the front rose rapidly and multiple peaks developed. At the conclusion of the run there were peaks at BH15, 18, and 24 with temperatures of 560, 630 and 320oC respectively as can be seen in Figure 4.33.

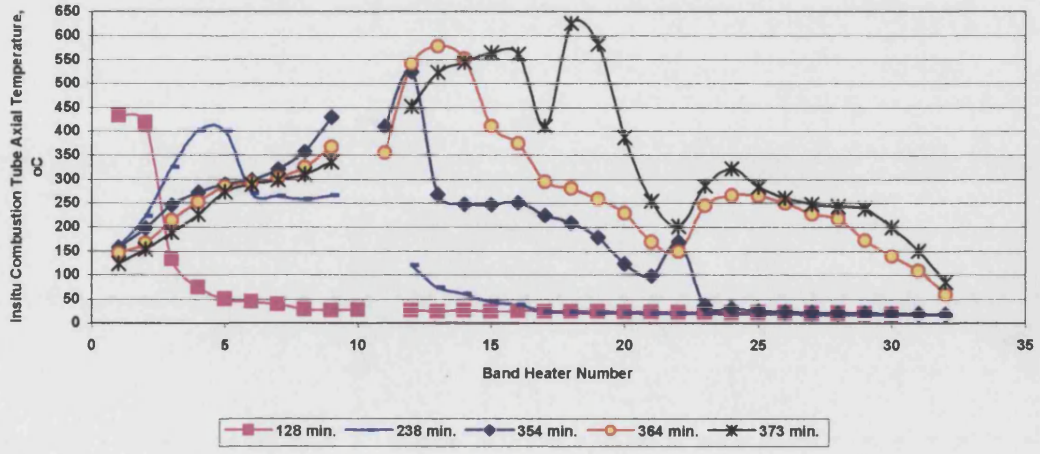

Figure 4.33 Run 6 : Axial Temperature Profile, Post-Ignition.

Figure 4.34 is one of the most important figure used to calculate the velocity of combustion front and also to estimate maximum peak temperature. The figure Shows stable movement and steady progression of the combustion front between BH5 to BH8 at about 10 cm/hours.

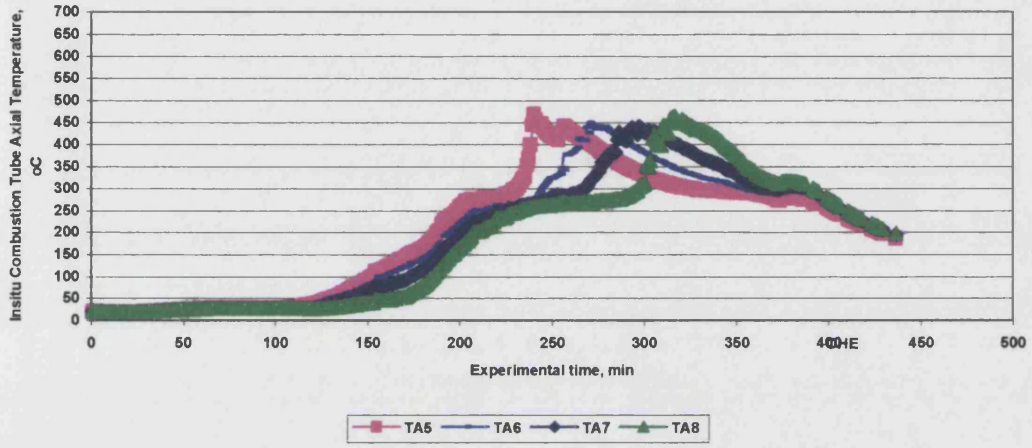

Figure 4.34 Run 6: In Situ Combustion Tube Axial Temperature, Band Heater 5 to 8.

The estimated maximum peak temperatures obtained were plotted as shown in Figure 4.35. Utilizing the low air injection flow rate at early period of production gives maximum peak temperature of 457.7 °C. Due to increase air injection rate at the late period, and after 352 minutes, the average maximum peak temperature estimated was 573 °C.

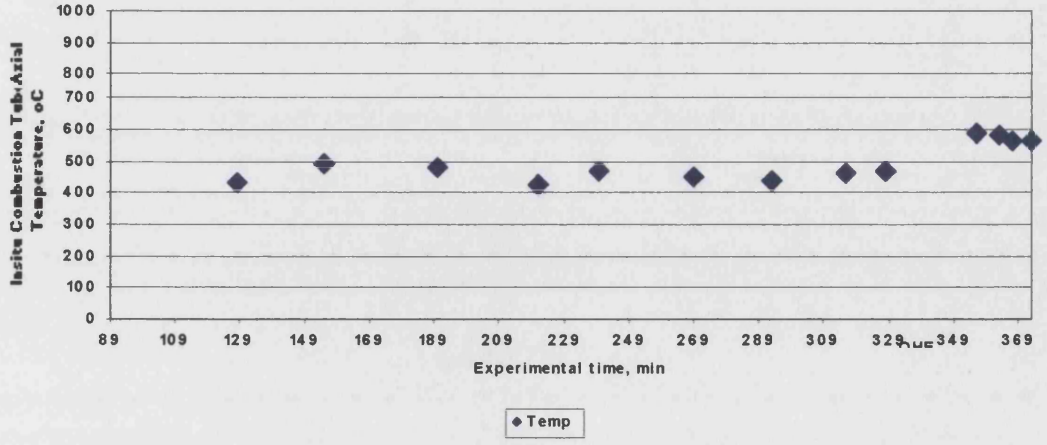

Figure 4.35 Run 6 : Combustion Front Temperature.

The calculated combustion front velocity was plotted as shown in Figure 4.36. At the early period the combustion front speed range from 0.1 to 0.35 cm/min. At the late period the speed went up to 1 cm/min.

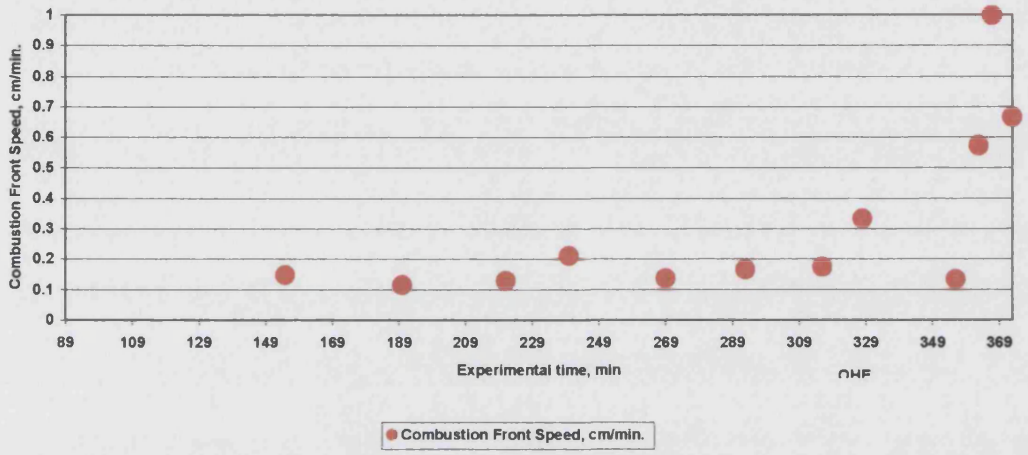

Figure 4.36 Run 6 : Combustion Front Velocity.

Produced Gases:

Oxygen production was initially low, increased to about 6% after 90 minutes of air injection and then fell for the remainder of the run, reaching 2% after 150 minutes and 1% after 240 minutes. At this time the flux was increased and oxygen production quickly fell to 0%. Carbon dioxide production was observed earlier than oxygen, and increased towards 11% during the low flux period. During the final high flux period CO_2 levels reaches 13%. Carbon monoxide levels were steady at about 0.8% prior to the oxygen peak, then followed a similar pattern to CO_2, reaching 1.6% during the low flux period and 2.3% in the high flux period. The measured gas concentrations are shown in Figure 4.37.

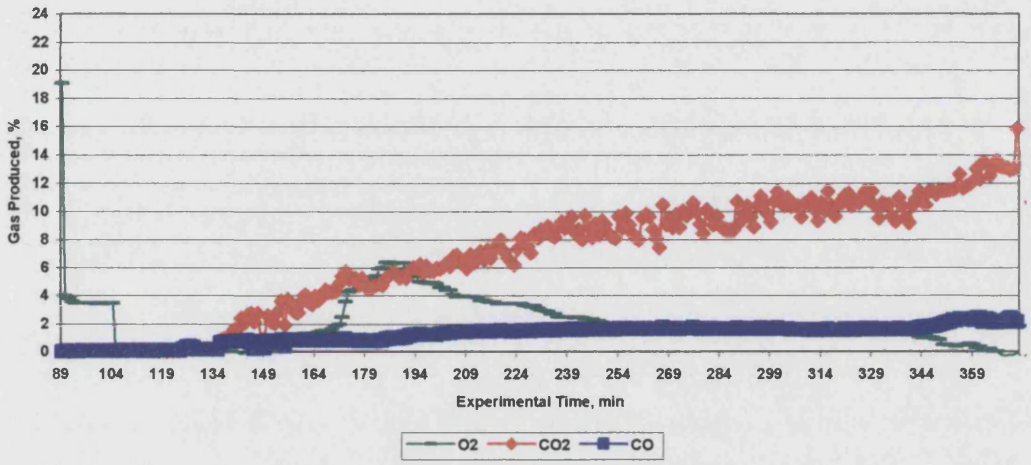

Figure 4.37 Run 6 : Produced Gas Combustion.

The average gas produced rate was estimated and plotted in Figure 4.38. During the period from 104 to 340 minutes, the gas was produced with average flux of 21 m3/m2hr. Due to increase in the air injection rate the produced gas during the period from 340 minutes to 373 minutes was 104 m3/m2hr.

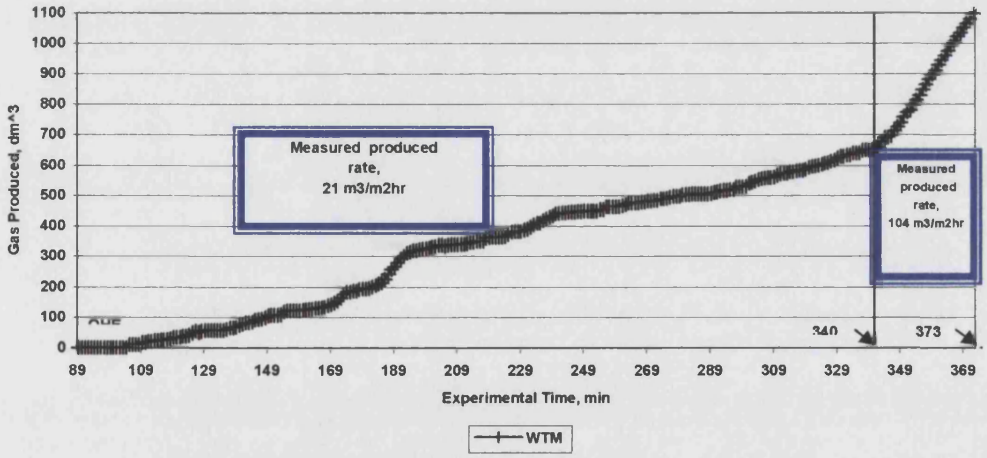

Figure 4.38 Run 6 : Gas Wet Test Meter Measurement.

Oil and Water Production:

It was decided to increase the air injection rate during the experiment, because only 5% of OOIP was recovered during the whole first period (350 minutes). The total oil recovery was 64% of the original oil in place. Most of this was produced during the final high flux period. Water was produced throughout the run with 63% of the original water

in place being produced by the end of the run. The production history are shown in Figure 4.39.

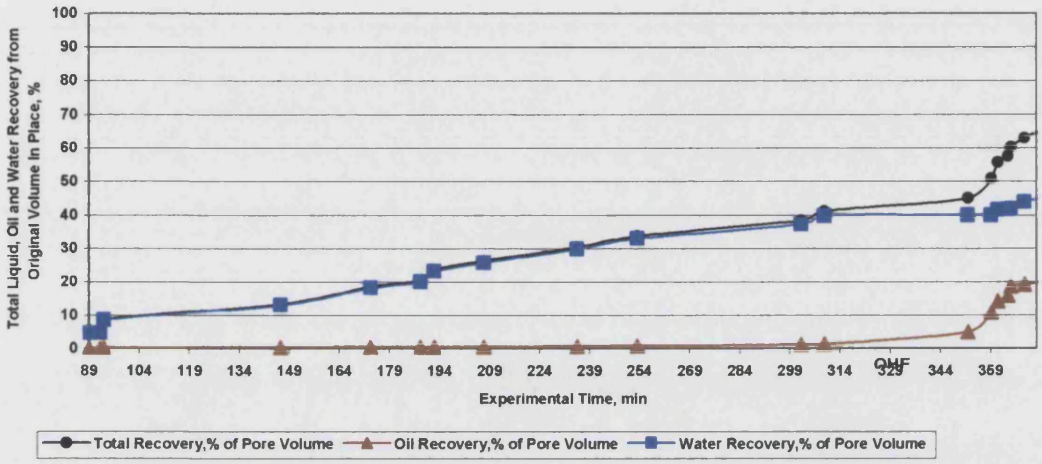

Figure 4.39 Run 6 : Liquid Recovery From Pores Media.

Oil bank was formed ahead of the combustion front due to occurrence of LTO and experiment low air flux. While the air injectivity increased, the oil displaced down stream.

The Water pH did not show major changes during combustion and displacement. The value remains between 6.5 to 7, to the end of the experiment (Figure 4.40).

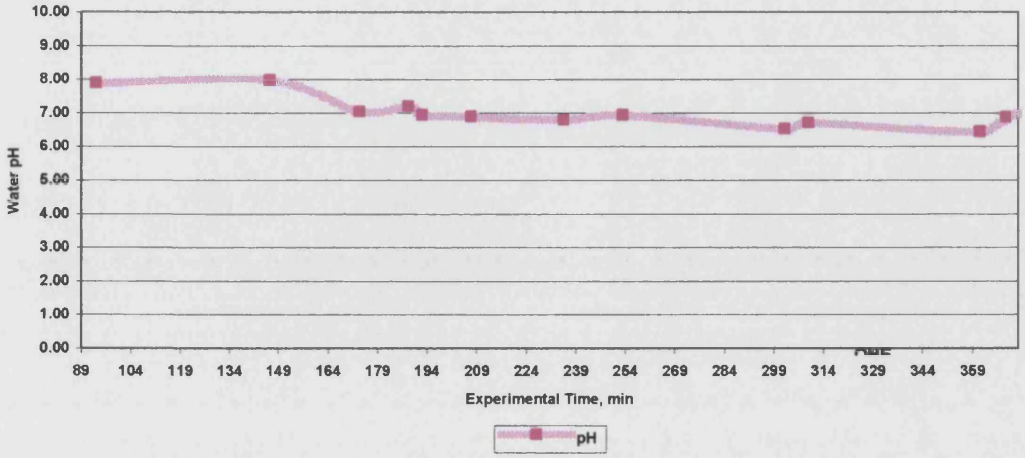

Figure 4.40 Run 6 : Water pH.

4.4: Run 8:

Run 8 was conducted at high oil saturation (70%), and low water saturation (30%). This run conducted to get better understanding on whether advanced LTO occurred, and converting the unconsolidated media to solid rock at low water saturation.

The ignitor was switched on at 114 min., with ignition occuring at 220°C after a further 25 minutes. This was followed by an initial, very rapid combustion front propagation, reaching a temperature of 840°C (146 min.), but then falling to 520°C at 180 min. Heat transported ahead of the combustion front can also been seen in Figure 4.41. More wider and enlarge in the combustion front zone continues , with LTO reaction occurred ahead of the combustion front peak, then HTO peak (820°C) induced downstream as shown in Figure 4.42.

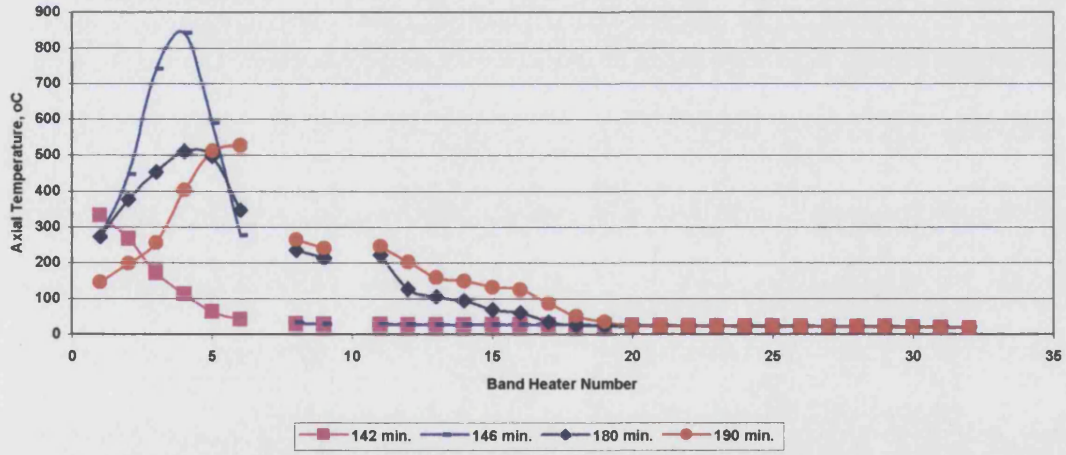

Figure 4.41 Run 8 : Axial Temperature Profile Post-Ignition.

Figure 4.43 shows the changes occurred in location of BH 13, 14, 15 and 16. It also show the constant differences between them, which mean stable combustion front movement.

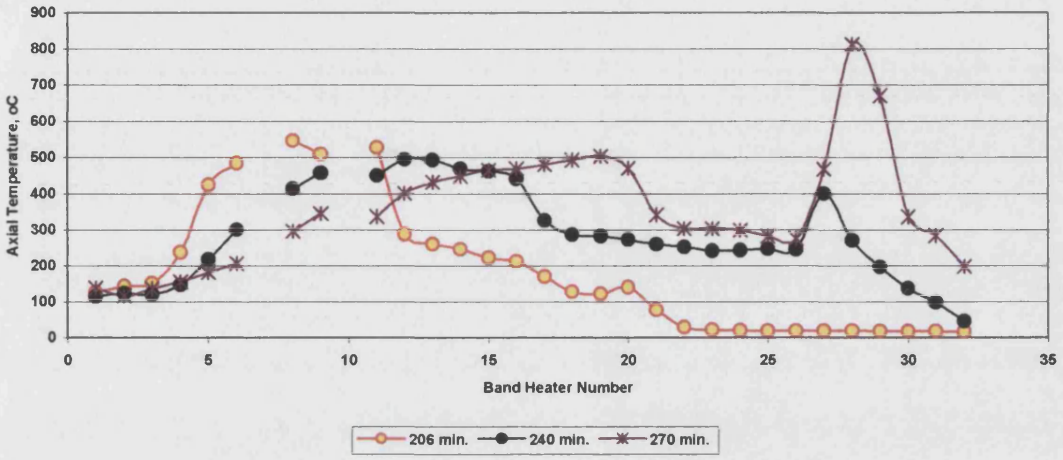

Figure 4.42 Run 8 : Axial Temperature Profile Post-Ignition.

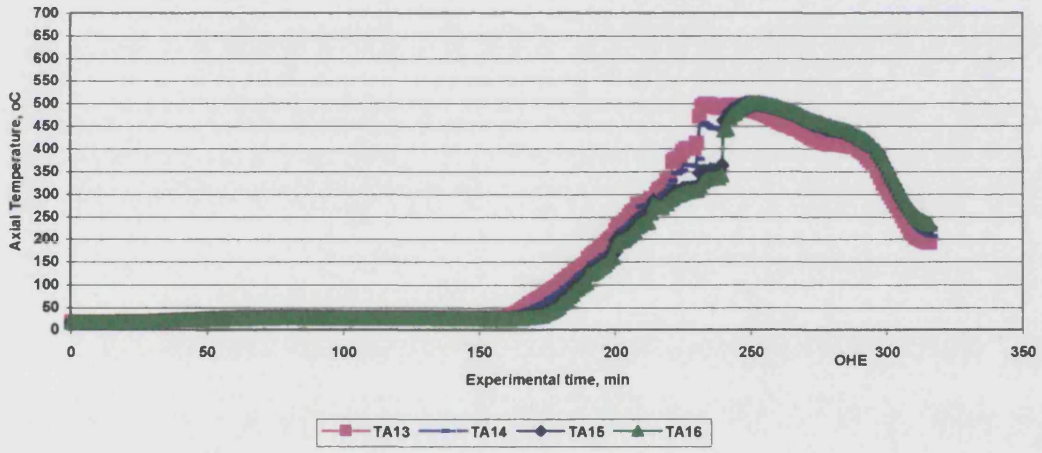

Figure 4.43 Run 8 : Axial Temperature Profile From Band Heater 13 to 16.

The optimum peak temperatures recorded in run 8 are between 500 and 600°C as stated in Figure 4.44. Very high temperatures recorded at the beginning and at the end of the test. The estimated combustion front speed are about 0.5 cm/min mostly in the early stage of the experiment, but higher at the late stage, it reaches 4 cm/min. (Figure 4.45).

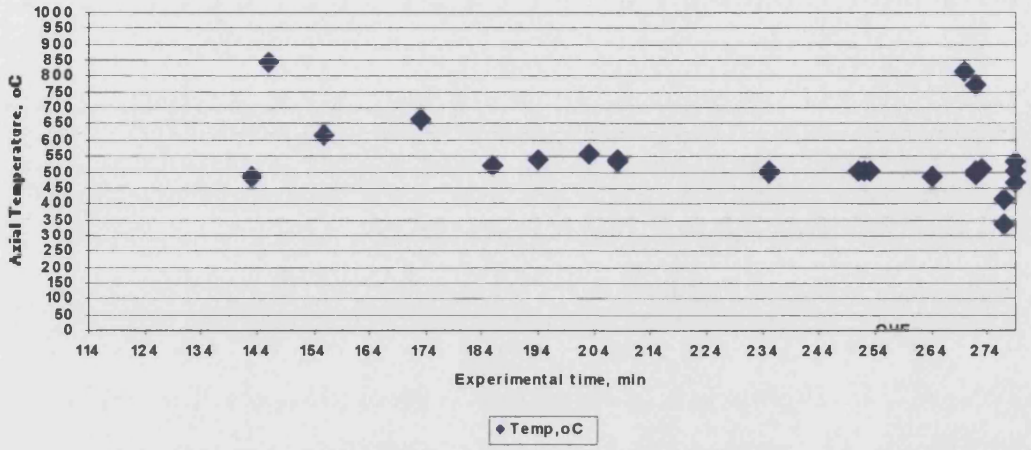

Figure 4.44 Run 4: Axial Temperature Profile, Maximum Peak Temperature.

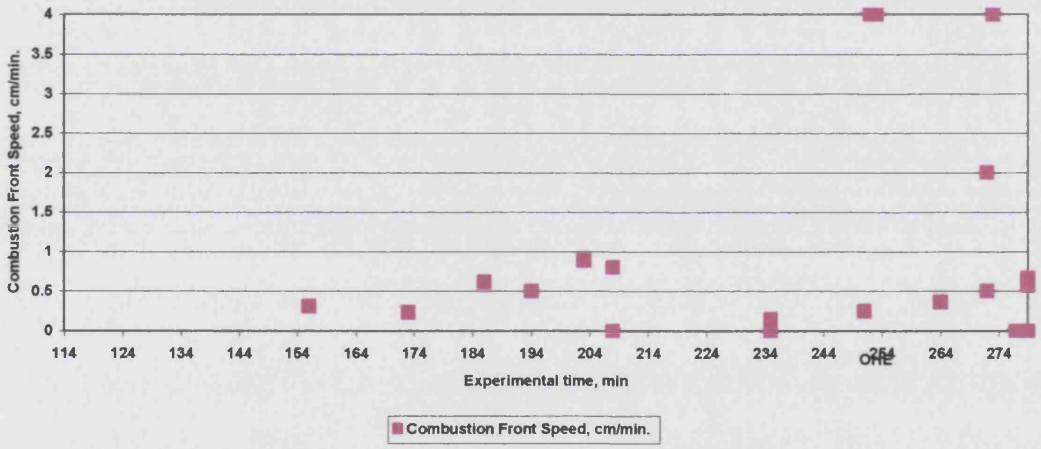

Figure 4.45 Run 8 : Combustion Front Speed.

Produced Gases:

CO_2 concentration build-up gradually in the produced gas as shown in Figure 4.46, eventually it reaches 13-14%. CO reaches a maximum of 2% and then declines during the latter part of the experiment. It is interesting to note that the period during which oxygen is produced is from 214 – 244 minutes. The first observable occurrence of the LTO peak was at 206 minutes at BH20, about 8 minutes before oxygen is first detected in the produced gas.

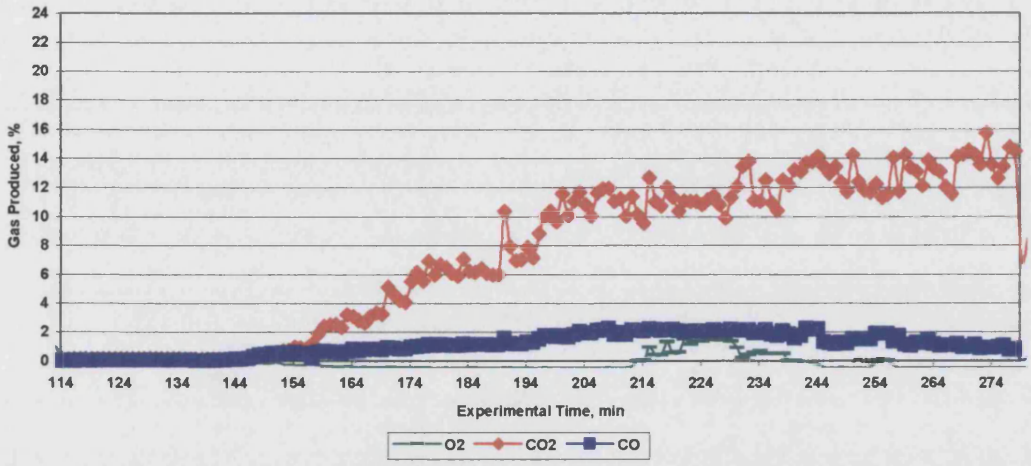

Figure 4.46 Run 8 : Produced Gas Combustion.

Figure 4.47 presents that the gas start produced at time 134 minutes to the end of the test at 279 minutes with continuous and steady produced rate. The total volume of gas produced was 796 liters. However, this will give rate of 5.5 liter/min (42 m^3/m^2 hr).

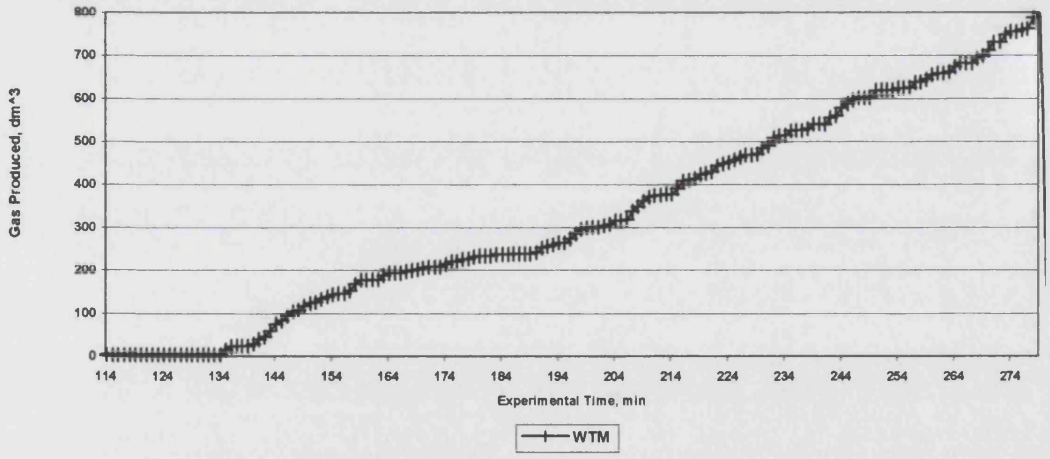

Figure 4.47 Run 8 :Gas Produced Volume

Oil and Water Production:

Oil recovery was 86.7% of the oil originally in place. Most of this was produced during the early period. Water produced throughout the run with 50.5% of original water in place. The production histories are shown in Figure 4.48. In this test oil was leading the water. Correspondingly, It is anticipate that water production will lead, if the initial oil saturation is low.

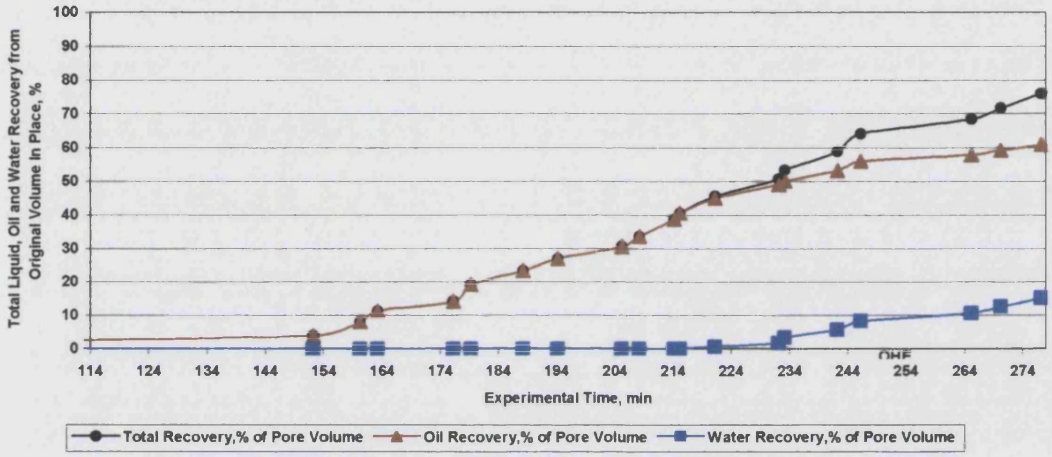

Figure 4.48 Run 8 : Liquid Recovery From Pores Media.

4.5: Run 9:

Run 9 was run at lower pressure of 100 bar, with oil saturation (30%) and water saturation (70%) similar to Run 4 and 6. Faster time of pressure-up the tube (42 minutes) to reach the desired pressure, 100 bar. The iqnitor left on from 43 to 62 minutes, and when the temperature reached 265°C. However, the iqnition then occurred within 2 minutes, causing jump to 430°C. High increase in temperature (800°C) at BH2 and at 68 minutes as shown in Figure 4.49. A second LTO peak begins to form at BH22 at time 95 min. A separate LTO reaction occur between BH20 and BH30, with a peak temp of 180°C. Thereafter, the LTO and HTO peaks were joined together. Hence the combustion zone enlarged, and high temperature observed at BH32, which is eliminate the experiment to continue.

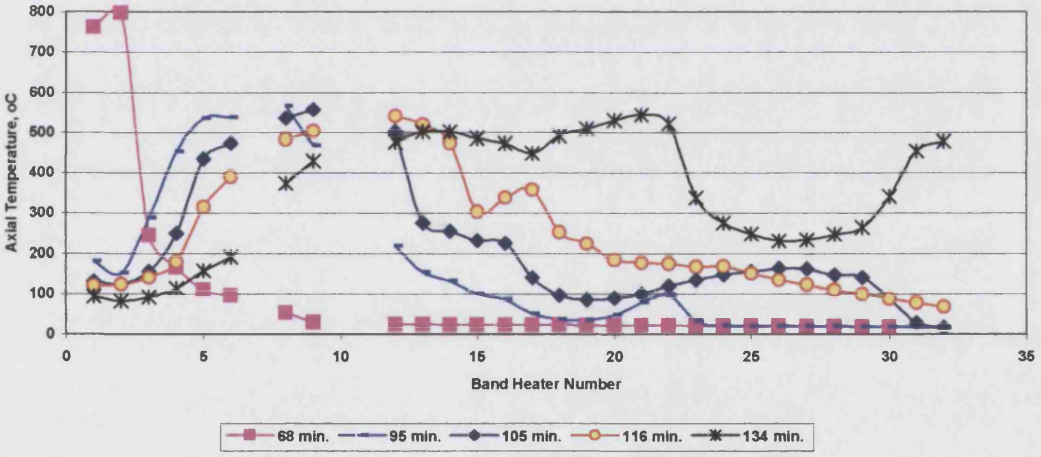

Figure 4.49 Run 9 : Axial Temperature Profile, Post-Ignition.

The movement of the combustion front was steady, but more faster as shown in Figure 4.50.

The maximum peak temperature estimated is show in Figure 4.51. Start from 800°C and then averaged between 500 to 600°C.

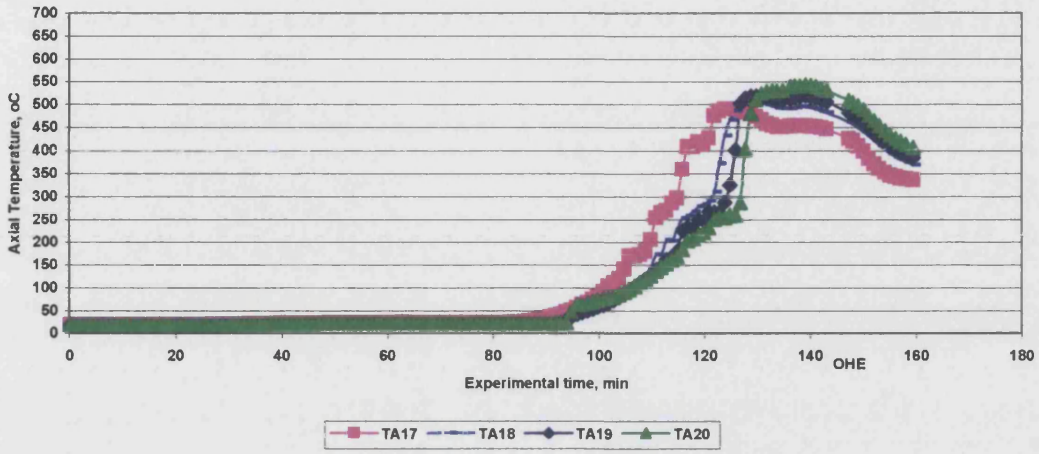

Figure 4.50 Run 9 : Axial Temperature Profile from Band Heaters 17 to 20.

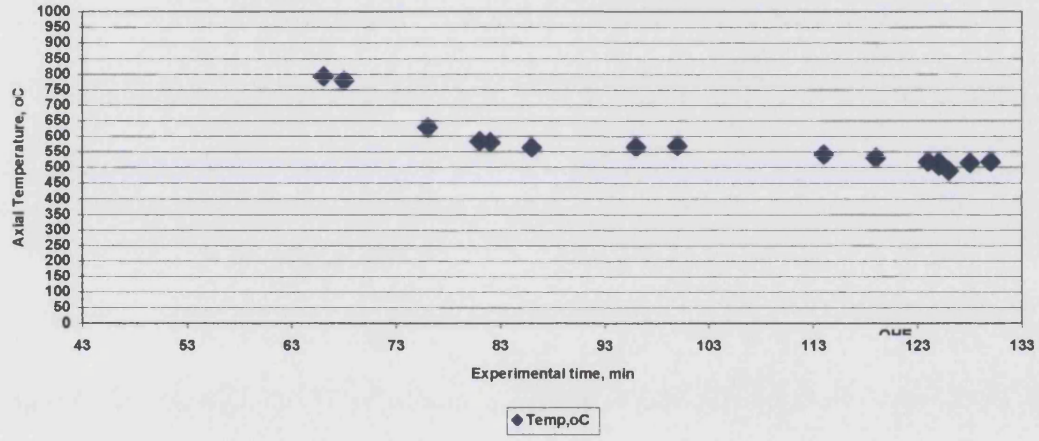

Figure 4.51 Run 9 : Combustion Front Temperature.

The combustion front velocities were faster compared with any previous run, because of lower pressure, and faster control process. Mostly, the combustion front velocity mainly in the range 0.5 - 1 cm/min. little higher at the began and late of the experiment (Figure 4.52).

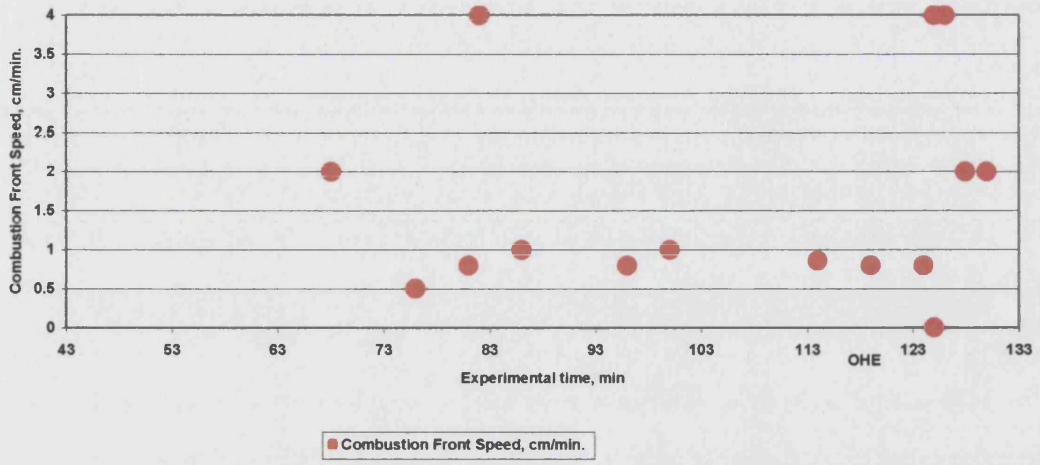

Figure 4.52 Run 9 : Combustion Front Velocity.

Produced Gases:

The value of CO gas was most of the test about 2%. But CO2 reaches values between 10 and 16%. Less than 2%, the oxygen value was also observed as seen in Figure 4.53.

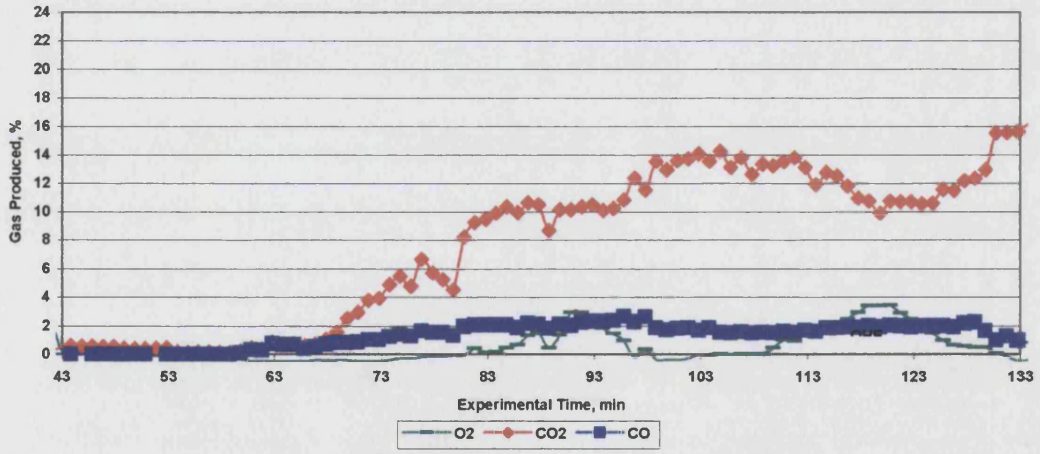

Figure 4.53 Run 9 : Produced Gas Combustion.

Figure 4.54 shows the total volume of gas produced was 653.7 liter with net production time of 80 minutes. The overall producing rate becomes 8.2 liter/min (62.65 m^3/m^2 hr).

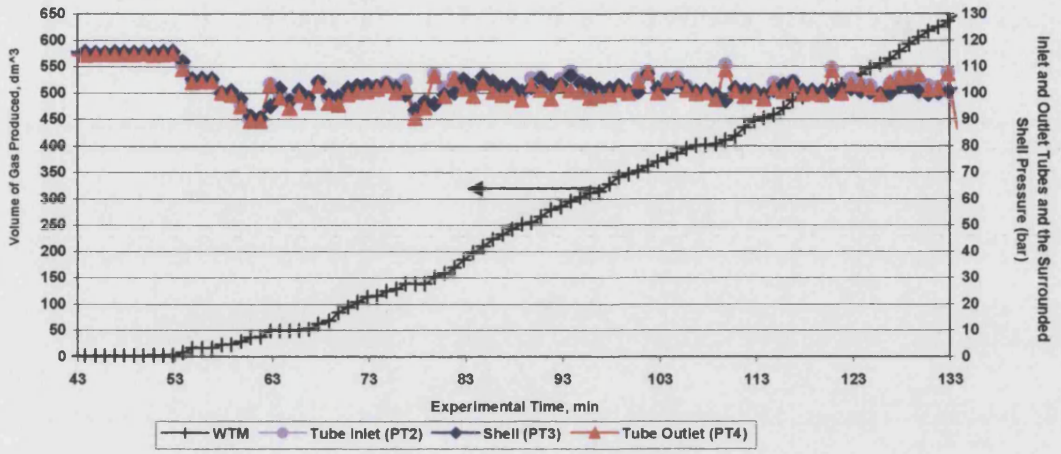

Figure 4.54 Run 9 : Gas Wet Test Meter Measurements (Run Nine).

Oil and Water Production:

Oil production was delayed considerably due to the early production of water, which starts from the beginning of the test (Figure 4.55). Almost all of the oil was recovered (98%). However, since the samples were contaminated with unseparated emulsion, the actual oil recovery may be nearer 80-90%. The water recovery was 74% of water originally in place.

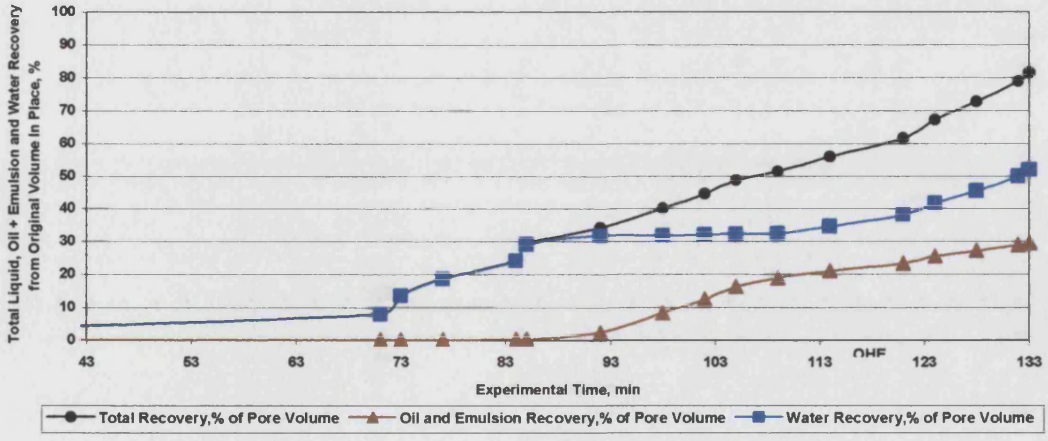

Figure 4.55 Run 9 : Liquid Recovery From Pores Media.

4.6: Post-mortem Photographs of Burned Core from Combustion Tube: Run Four:

This run achieved full, propagating combustion, averaging a combustion front temperature of (400°C). Except for some residual fuel/coke deposited around the tube wall, the core was completely clean, as evidented by it's white colour. A series of photographs was taken at different positions along the combustion tube, in order to examine the state of the MI limestone core, at the end of the experiment. The important features to be noted are:

- Loose, or soft sand.
- White and/or brown and/or black and or light greenish colour.
- The position of burned and unburned media core.
- Rock samples that are consolidated after combustion and oil displacement.
- Position of coke deposits.

The MI Limestone along the tube had a whitish colour, indicating complete combustion had occurred, especially in the middle part.

The loose MI Limestone shown in Figure 4.56, just after to ignition, was present along the tube, up to 19 cm from the inlet.

Some hard pieces of material (agglomerates) (Figure 4.58) where found in the tube after 19 cm. There where mainly near to the tube wall (Figure 4.57), and can be seen more clearly in Figure 4.58. This hard material contained holes, which were connected and interconnected. At the edges of the material, there were some areas having greenish colour, which may indicate reaction of acid with calcium carbonate.

If the MI Limestone becoming white in colour, indicating good or complete combustion had occurred (Figure 4.59). A small amount of gas may have occurred close to the wall as shown at point A.

There was a little variance in to colours of the MI Limestone as shown in Figure 4.60 to 4.62, correspond to distances 35, 51, and 60 cm respectively. This changing, on wavy

colour variation is due to combustion. A more whitish colour is interpreted as more complete combustion occurring. Areas exhibiting a dark colour, indicates the presence of coke, but only small residual amounts. This could be, because the fuel concentration was not uniform or oxygen flow was not well distributed.

At distance of 70 cm, small area of greenish colour appeared at point A in Figure 4.63. This colour effect continued to 76 cm.

A large area of dark colour (black) began to appear, as shown in Figure 4.64 and at point A. This green colour appeared as a coating on a large piece of agglomerated material, which was extended up to 80 cm as shown in Figure 4.65. The cross section of the agglomerated had a whitish colour, meaning that the calcium carbonate had reacted with acid, forming a large hole inside it.

After extraction of the large piece of agglomerate (Figure 4.66), a small amount of coke was seen at 80 cm at point A.

At depth of 82 cm, agglomerated Limestone was found in the middle of the matrix, alongside the axial thermocouple position, as shown in Figure 4.67.

At depth of 95.5 cm (Figure 4.68) some small, slotted holes start appeared almost like a vug. However, There were no green colourations, or agglomerated material, in the remaining section of the MI Limestone, up to 100 cm (Figure 4.69).

The size and shape of the crescent remained similar all the way until the end of the tube, as shown in Figure 4.70.

Figure 4.71 was taken at the screen located at the bottom of the insitu combustion tube. Less than half of the screen contain unburned coke, the rest was burned. The unburned section was due to the effect of cooling, because of the cooler gas entering the shell from the bottom on the same side as the coke deposit. The presence of coke also signifies that the combustion reached the bottom of the tube.

Some of the sealant use on the bottom flange had also managed to seep on to the screen (Figure 4.71).

Figure 4.56 Run 4:Combustion Tube at ignitor.

Figure 4.57 Run 4:Combustion Tube at 19 cm.

Figure 4.58 Run 4:Solid Core at 19 cm.

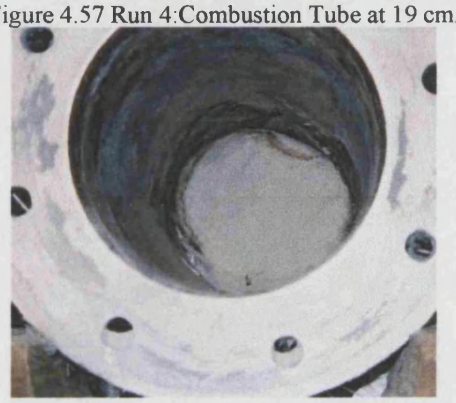

Figure 4.59 Run 4:Combustion Tube at 26 cm.

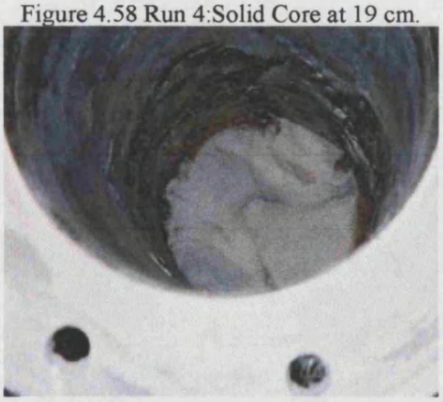

Figure 4.60 Run 4:Combustion Tube at 35 cm.

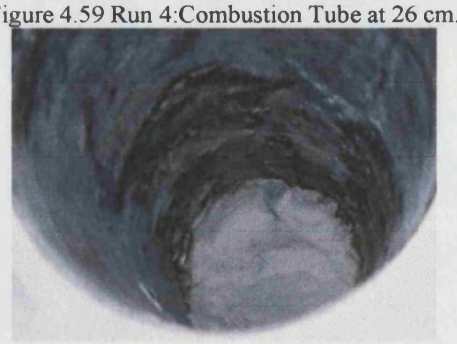

Figure 4.61 Run 4:Combustion Tube at 51 cm.

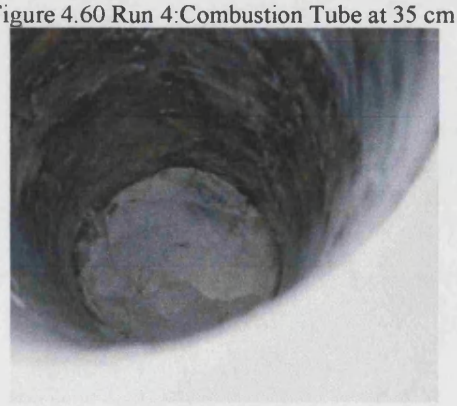

Figure 4.62 Run 4:Combustion Tube at 60 cm.

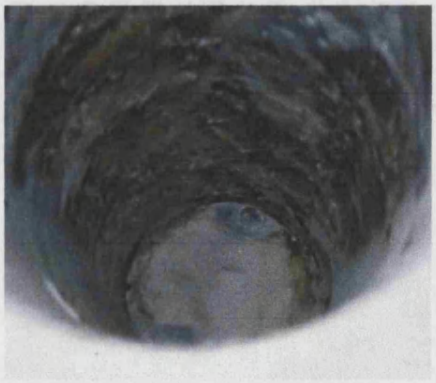

Figure 4.63 Run 4:Combustion Tube at 70 cm.

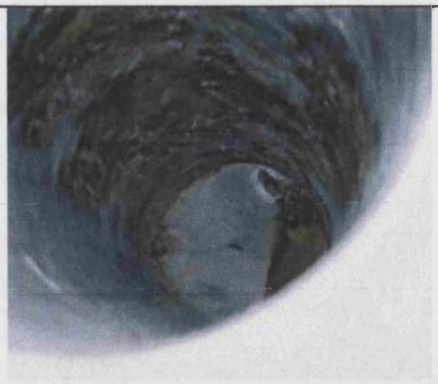

Figure 4.64 Run 4:Combustion Tube at 76 cm.

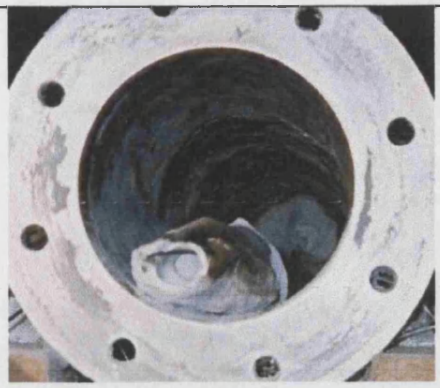

Figure 4.65 Run 4:Solid Core at 76-80 cm.

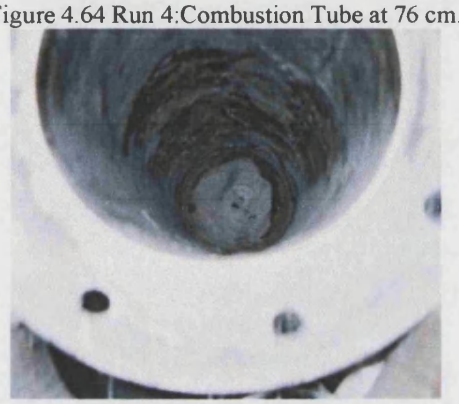

Figure 4.66 Run 4:Combustion Tube at 80 cm.

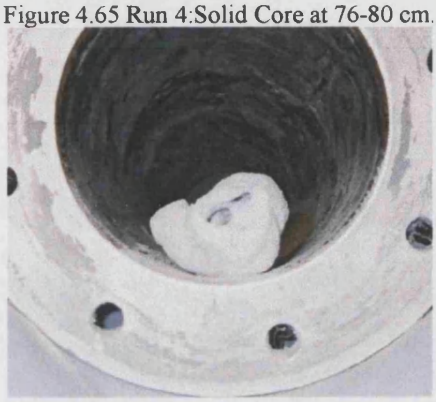

Figure 4.67 Run 4:Solid Core at 82

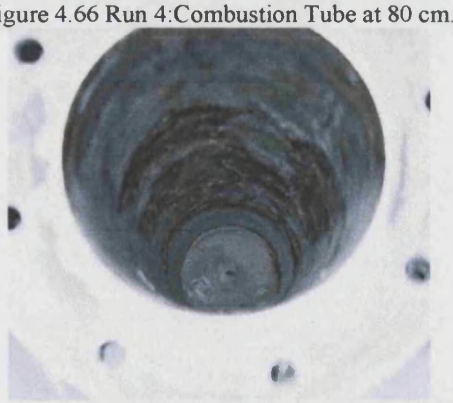

Figure 4.68 Run 4:Coke Solid Coke at 95.5 cm.

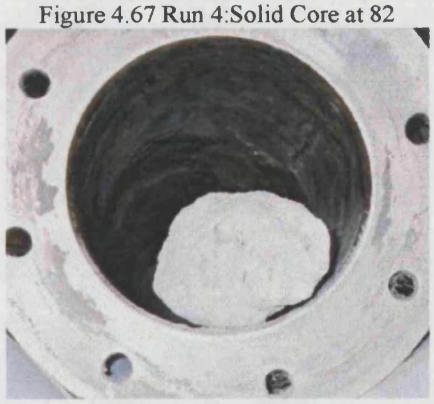

Figure 4.69 Run 4:Solid Core at 95-100 cm.

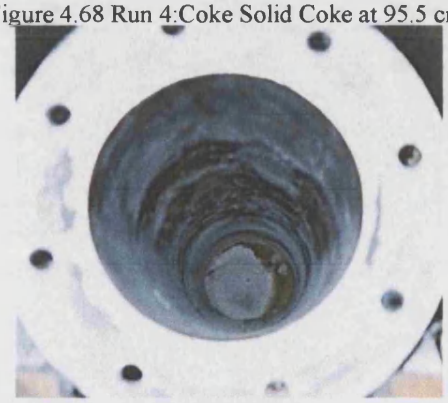

Figure 4.70 Run 4:Combustion Tube at 121.5cm

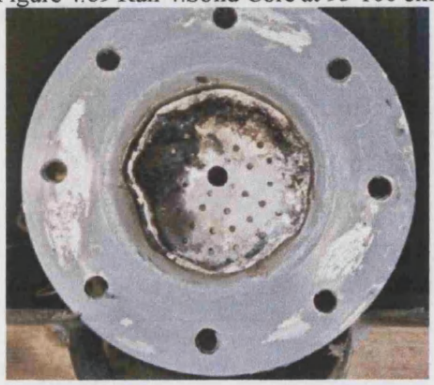

Figure 4.71 Run 4:Combustion Tube Bottom Screen.

Run Five:

Figure 4.72 Shows the condition of the burned calcium carbonate at the ignitor. It shows the presence of linseed oil left behind that was not burnt. It was originally placed beside the ignitor. The clear of MI calcium carbonate indicats 100% combustion.

More than 90 % of the combustion tube cross section shown in Figure 4.73, taken at 8 cm, as burned, and some coke deposited. Some coke as left behind at 12 cm at (Figure 4.74). The coke was located beside the inner tube wall. More burn can be seen at 15 cm as shown in Figure 4.75. The middle hole is for the axial thermocouples prop. Even at 20 cm full combustion occurred as presented in Figure 4.76. Some coke start appears at 24 cm as presented in Figure 4.77.

At 29 cm, as illustrated in Figure 4.73, high percentage of fuel lay down and coke. Small round circle appeared at the middle around the hole of the axial thermocouple probe. At 32 cm, the burnet zone becomes portioned into two, the first one located in the middle as shown in Figure 4.74. The second portion was located beside the combustion tube wall.

The middle burnet media was disappeared at 36 cm as shown in Figure 4.75. More than 90% was unburned. At 42 cm. small circular combusioned zone was appeared as shown in Figure 4.76. The burnet media was stuck to the wall. Figure 4.77 presents a coke deposited at 45 cm.

After 52.5 cm clear white MI calcium carbonate was appeared as shown in Figure 4.78. The round coke still appeared even after 57 cm as it can be seen in Figure 4.79.

At 72 cm from the top of the combustion top, a round circular coke still appeared as shown in Figure 4.80.The circular coke at 72 cm, found latter as a stone as presented in Figure 4.81. This stone consolidated during in-situ combustion process.

Figure 4.72 Run 5:Combustion Tube at Ignitor

Figure 4.73 Run 5:Combustion Tube at 8 cm.

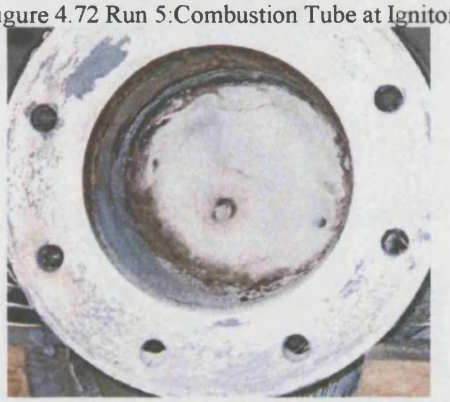

Figure 4.74 Run 5: Combustion Tube at 12 cm.

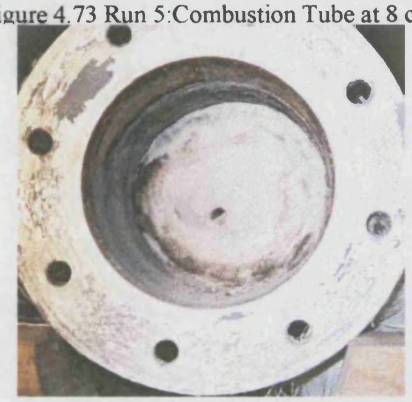

Figure 4.75 Run 5:Combustion Tube at 15 cm.

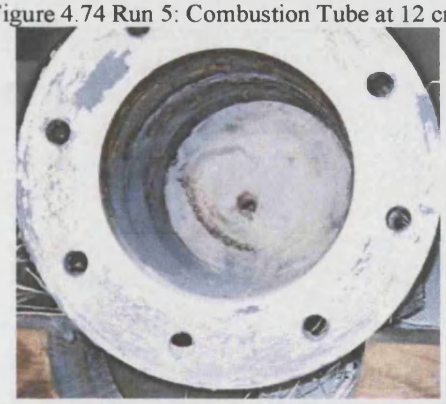

Figure 4.76 Run 5:Combustion Tube at 20 cm.

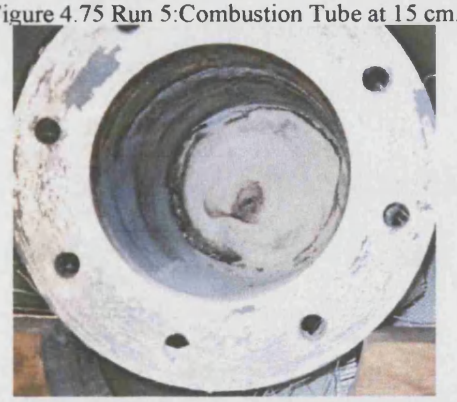

Figure 4.77 Run 5:Combustion Tube at 24 cm.

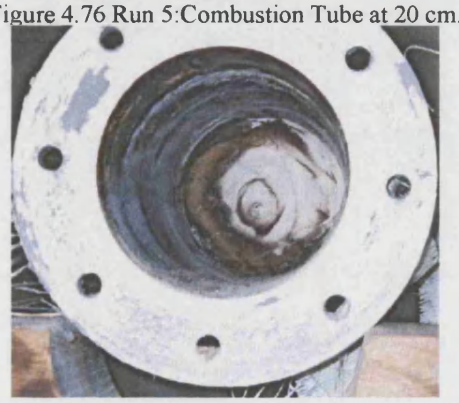

Figure 4.78 Run 5:Combustion Tube at 29 cm.

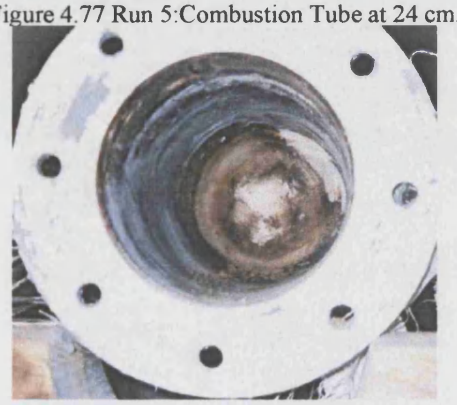

Figure 4.79 Run 5:Combustion Tube at 32 cm.

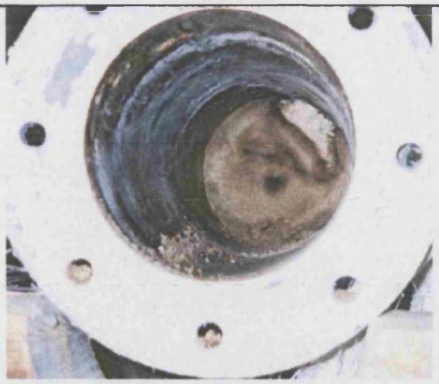

Figure 4.80 Run 5:Combustion Tube at 36 cm.

Figure 4.81 Run 5: Combustion Tube at 42 cm.

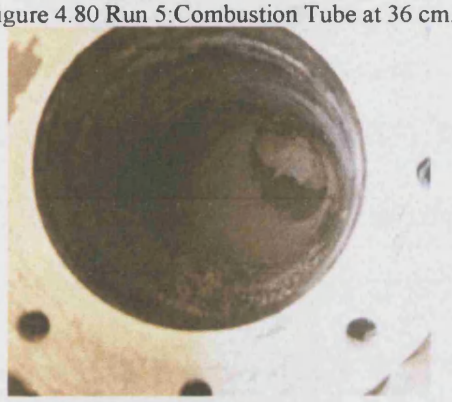

Figure 4.82 Run 5:Combustion Tube at 45 cm.

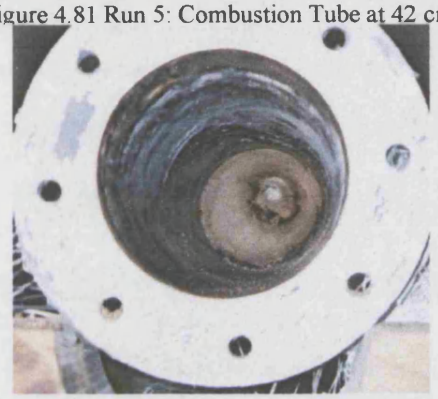

Figure 4.83 Run 5: Combustion Tube at 52.5 cm.

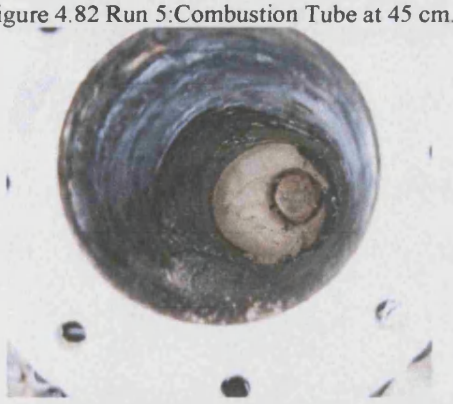

Figure 4.84 Run 5: Combustion Tube at 57 cm.

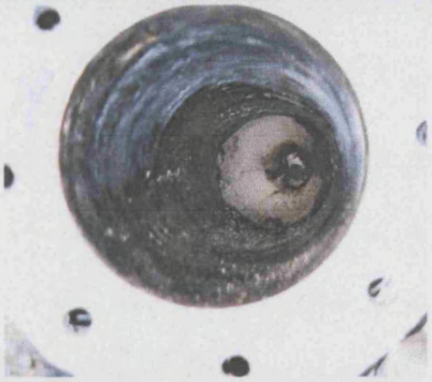

Figure 4.85 Run 5: Combustion Tube at 72 cm.

Figure 4.86 Run 5:Solid Core at 72 cm

Run Six:

The Post mortem photograph of the burned core in the ignitor zone is shown in Figure 4.87. Some coke deposited at the edges closed to the tube wall. Based on the colour of the coke, it seams to be coke created from linseed oil.

More clear burnt media shown at 6.5 cm, as presented in Figure 4.88.Some coke deposited beside the combustion tube inner wall. More clear with very small amount of coke left behind the combustion at distance 17 cm, as shown in Figure 4.89. The soft sand still located at the middle.

The little darkness still appears even at 36 cm as shown in Figure 4.90. Semi circular dark colour still appearing after 46 cm as shown in Figure 4.91. The amount of coke left becomes more than in the previous. Figure 4.92 shows a stone started at 48 cm. The rest of the photo show the media at 51.5 cm. The MI calcium carbonate stone is shown in Figure 4.93. The stone extended from 48 to 53.5 cm. Semi Round shape of coke appeared at 61 cm as shown in Figure 4.94.

A stone was recovered from 61 to 69 cm as shown in Figure 4.95. Square shape of coke and fuel lay down at 69 cm is shown in Figure 4.96. It is also show the interface layer of coke between the fuel lay down and the complete burnt portion.

Figure 4.97 show a big layer of coke located at the middle after 71 cm, with a small area of highly burnet media. After 79 cm, there was no clear burnet media but only coke and fuel as shown in Figure 4.98.

Black round shape of solid cake still observed and extended to 90 cm as shown in Figure 4.99. The solid stone was recovered at 94 cm as shown in Figure 4.100. The total length of the stone was about 11 cm, started from 83 to 94. At the end of the stone (at 94 cm) a square shape of soft coke formed as shown in Figure 4.101. The coke still extended even after 106 cm as shown in Figure 4.102.

Figure 4.87 Run 6:Combustion Tube at Ignitor

Figure 4.88 Run 6:Combustion Tube at 6.5 cm.

Figure 4.89 Run 6:Combustion Tube at 17 cm.

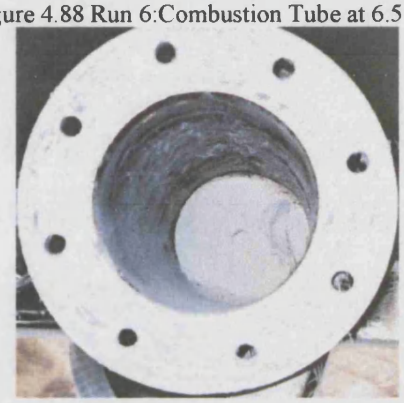

Figure 4.90 Run 6:Combustion Tube at 36 cm.

Figure 4.91 Run 6:Combustion Tube at 46 cm.

Figure 4.92 Run 6:Combustion Tube at 51.5 cm.

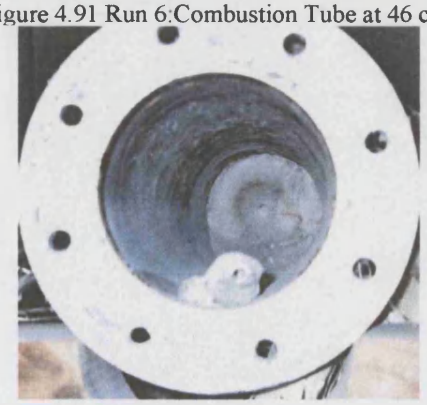

Figure 4.93 Run 6:Solid Core at 53.5 cm.

Figure 4.94 Run 6: Combustion Tube at 61 cm.

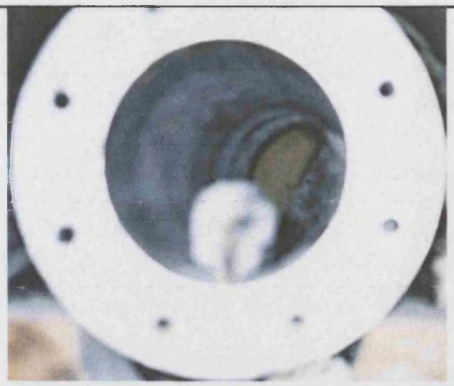

Figure 4.95 Run 6:Solid Core at 61-69 cm.

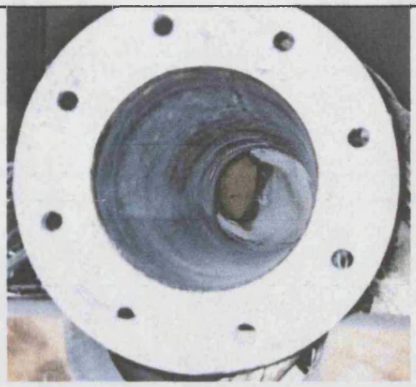

Figure 4.96 Run 6: Combustion Tube at 69.

Figure 4.97 Run 6: Combustion Tube at 71 cm.

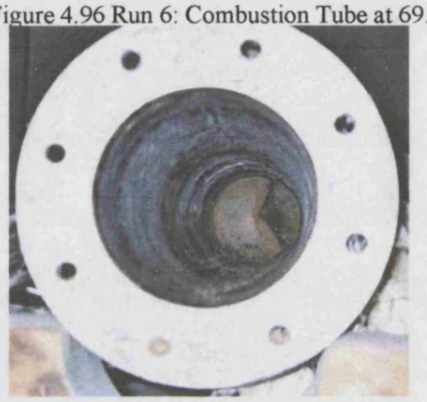

Figure 4.98 Run 6: Combustion Tube at 79 cm.

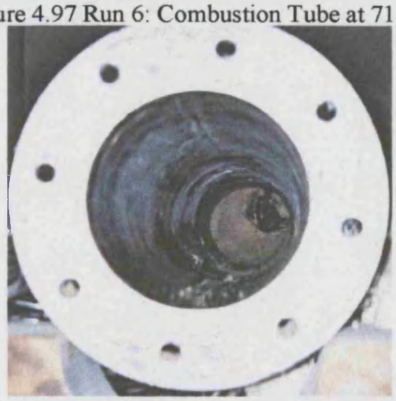

Figure 4.99 Run 6: Combustion Tube at 90 cm.

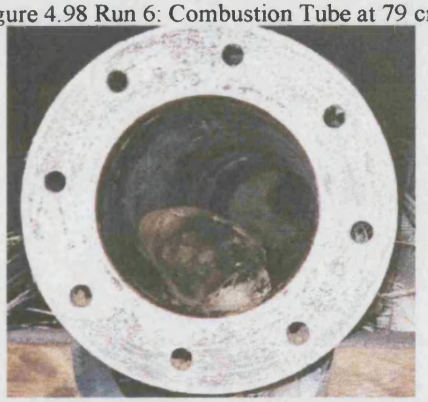

Figure 4.100 Run 6:Solid Core at 94 cm.

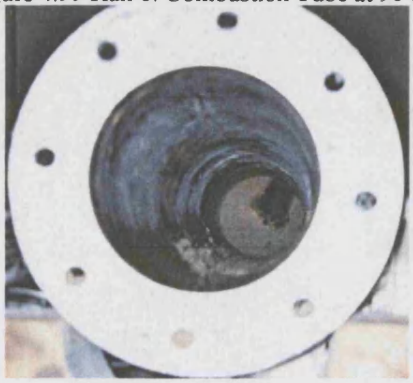

Figure 4.101 Run 6: Combustion Tube at 94 cm.

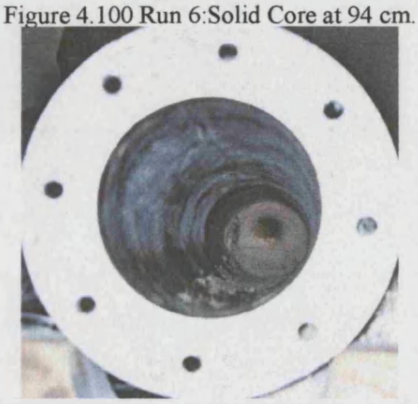

Figure 4.102 Run 6: Combustion Tube at 106 cm.

Run Eight:

Figure 4.103 shows the top part of the core close to the ignitor. The complete burned core extends to 12 cm as shown in Figure 4.104. The centre core represent the position of the axial thermocouples probe, but now filled with soft calcium carbonate particles. Hard consolidated MI calcium carbonate stone was formed 13 cm from the top. It was 5 cm long, with a hole in the middle, as shown in Figure 4.105. Soft white MI calcium carbonate found again at 22 cm, as shown in Figure 4.106. The same clear appearance found again at 32 cm as presented in Figure 4.107.

Soft MI calcium carbonate appears at the middle of the core, as shown in Figure 4.108, at distance of 40 cm. Soft MI calcium carbonate was found up to 53 cm, as illustrated in Figure 4.109. The brightness and clear white coloures an indication of excellent combustion because there was no coke or fuel left behind. Up to a distance of 63 cm, all the fuel and coke in tube had been burned. At 63 cm some dark brown colour starts to appear as shown in Figure 4.110. Round cycle of coke start appears after 72 cm as shown by Figure 4.111. Another observation was saw, where stone just start appearing beside the inner side of the tube wall. The MI calcium carbonate stone discovered can be seen in Figure 4.112. It consists of non uniform shape, with more than 10 cm long. Dark brown colour (fuel)start appear in one edge of the combustion tube circle, as shown in Figure 4.113 and at distance of 82 cm.

The same shape was seen in the previous tests. It is believe that it occur due to high heat loss in that corner cause by cooling effect of shell gas injected from the bottom and it influence the part beside the shell inlet gas portion.The coke and/or the fuel left behind enlarge more at distance 92 cm as shown Figure 4.114. The fuel volume becomes more bigger, more than 50% of cross section area with dark brown colour as it can be seen in Figure 4.115. Small piece of stone recovered at 98 cm.High percentage of fuel lied down at 103 cm as illustrated in Figure 4.116.The presence solid black colour (COKE) which indicate high temperature oxidation and combustion occurred beside the combustion tube wall. The solid coke (MI calcium carbonate) where started at 100.5 cm. The MI calcium

carbonate recovered from 100.5 cm to 114 cm is shown at Figure 4.117, it shows good combustion occurred in the media, which indicate more reactive crude available at 114 cm. It shows location of stone at depth of 100.5 cm, it looks black and solid, with a hole in the middle.

The presence of coke is an indication of less vigorous combustion not fully burnt media. The other end of the stone at 114 cm, is clear white, which means that half the stone was exposed to high temperature, burning all of the fuel. This also can give good knowledge about the oxygen breaking though and availability of fuel and more reactive crude. It was appeared at 114 cm that the combustion front moved forward in non uniform displacement and reactivity. It appear that the pocket of burnt zone can be found farther if the oxygen breaking through and found more reactive oil. At distance 121 cm, the burned area shrinks, becoming smaller, as shown in Figure 4.118.

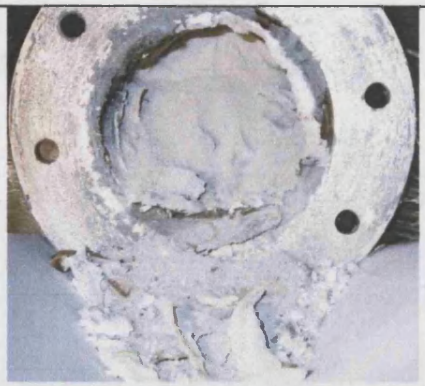

Figure 4.103 Run 8:Combustion Tube at Ignitor

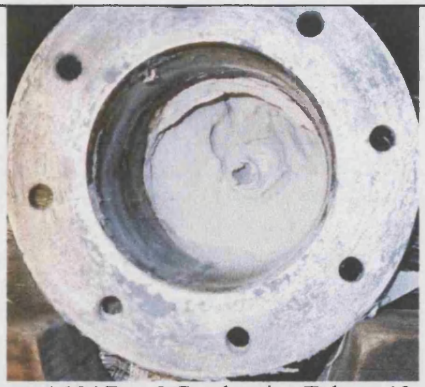

Figure 4.104 Run 8:Combustion Tube at 12 cm.

Figure 4.105 Run 8:Combustion Tube at 13 cm.

Figure 4.106 Run 8:Combustion Tube at 22 cm.

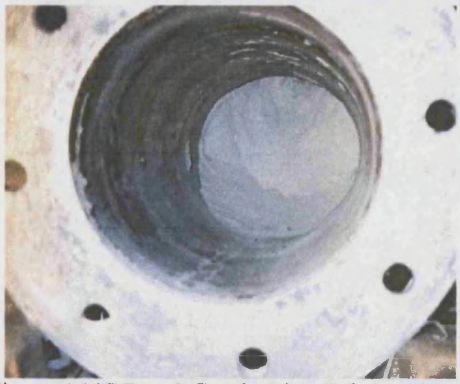

Figure 4.107 Run 8:Combustion Tube at 32 cm.

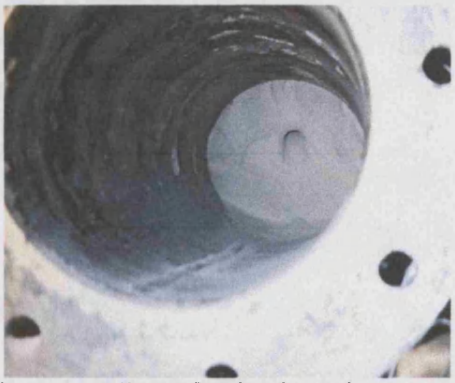

Figure 4.108 Run 8:Combustion Tube at 40 cm.

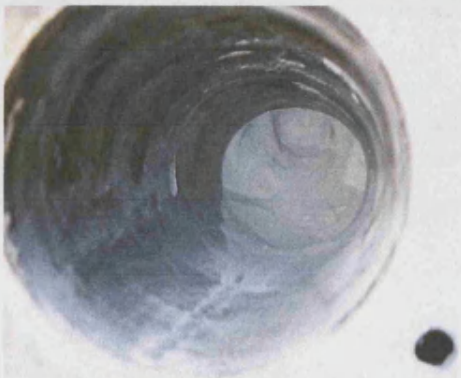

Figure 4.109 Run 8:Solid Core at 53 cm.

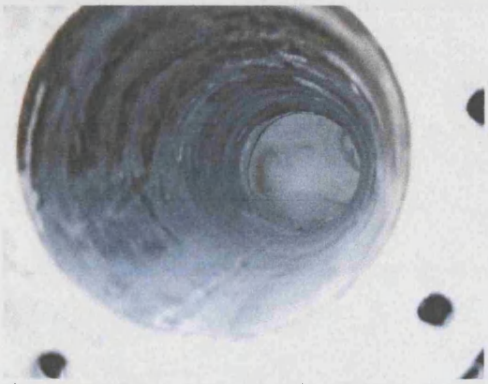

Figure 4.110 Run 8: Combustion Tube at 63 cm.

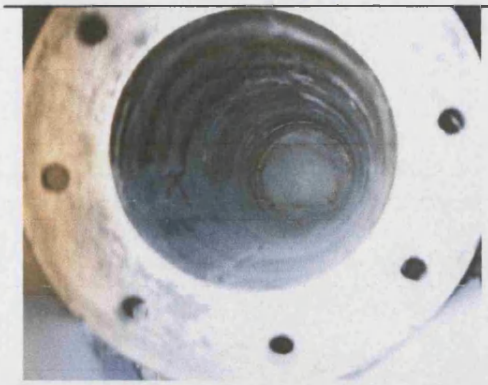

Figure 4.111 Run 8:Combustion Tube at 72 cm.

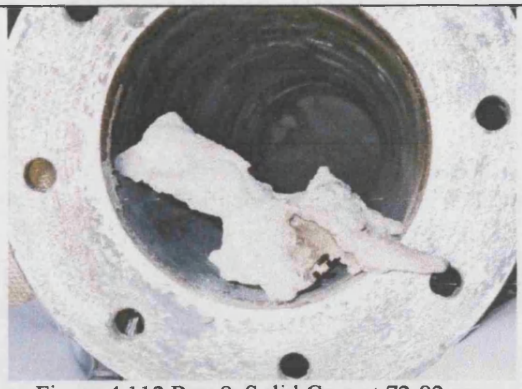

Figure 4.112 Run 8: Solid Core at 72-82 cm.

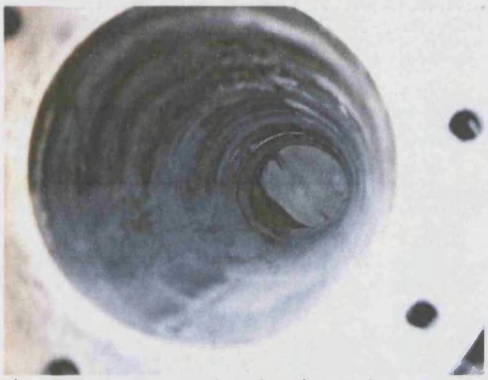

Figure 4.113 Run 8: Combustion Tube at 82 cm.

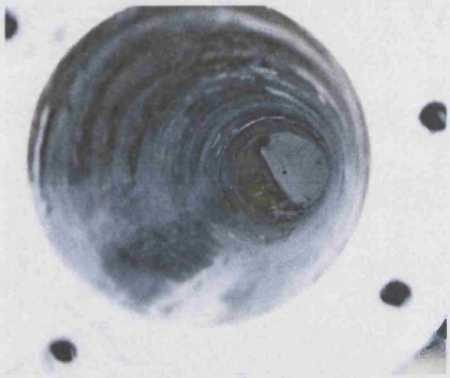

Figure 4.114 Run 8: Combustion Tube at 92 cm.

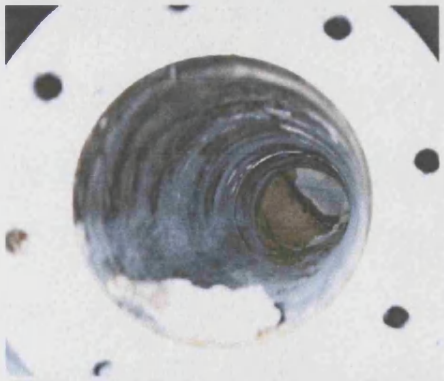

Figure 4.115 Run 8: Solid Core at 98 cm.

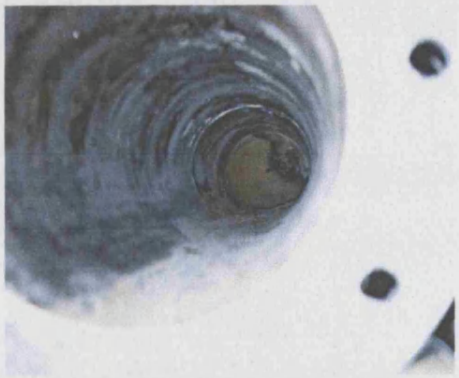

Figure 4.116 Run 8:Solid Core at 103 cm.

Figure 4.117R8: Combustion Tube at 100.5-114

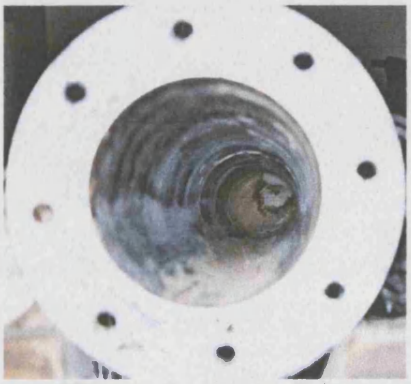

Figure 4.118 Run 8: Combustion Tube at 121 cm.

Run Nine:

The following post mortem photos will show the position and the condition of the core after being exposed to the combustion heat process. Figure 4.119 show the MI calcium carbonate beside the ignitor position. It looks as a loose particle and complete white which indicate whole fuel and coke were burnt completely. All the way from the top of the combustion tube to 15 cm, Figure 4.120 show that the media of MI calcium carbonate burnet completely, presented as loose and completely dry particle. The thermocouple probe located in the middle cross section of the combustion tube can be seen Figure 4.121 after 25 cm with a slightly bigger hole due to presence of loose particle at the middle. At distance 30 cm, 5 cm long stone was discovered as shown in Figure 4.122, it shows clear media with no coke or fuel left behind the combustion front.

Continuation of clean media MI calcium carbonate even at 46 cm as presented in Figure 4.123. A big unsymmetrical stone was discovered at 47 cm. The stone shown in Figure 4.124, extended to 58 cm. The stone exposed to combustion as indicated by the white colour. Some small coke deposited on the top of the stone can be seen as well. Figure 4.125 taken at 72 cm presents a clear fully brunet media, with little small deposition of coke left behind.
Figure 4.126, present the same shape as it has been seen in the previous tests. A portion of fuel lied down at 87 cm. The coke always found and present as an interface between the fuel lay down mainly in light brown colour, and the fully burnt media (MI calcium carbonate). The coke always form in black colour. During extraction of the media to make photo, it can be very easy to distinguish between the coke and the fuel lay down by the hardness. The coke, some times thin but always harder than any other in media.

Figure 4.127 present a thick layer of coke just between the unburnet zone and burned zone. This clearance of interface was taken at 97 cm. Half of the cross section area was burnet. The reason of this partitions is due to high heat losses and cooling effect caused by injecting shell gas (nitrogen) from the bottom, closed to the portion where the unburned fuel presents.

Figure 4.128 was taken at 105 cm, it show high fuel lay down or deposited. Stone of MI calcium carbonate was observed, but it start at about 100 cm. Difficulties where observed to extract that piece from the combustion tube. Figure 4.129 and 4.130 where taken for the consolidated stone extracted from the post mortem combustion tube. Figure 4.129 presents the side (A) where the stone and the coke/fuel deposited. Figure 4.130 shows the other side (Side B) of the consolidated stone. It very clear that (side B) shows the burnet side of the stone. This side sticked to the wall of the combustion tube.

Figure 4.119 Run 9:Combustion Tube at Ignitor

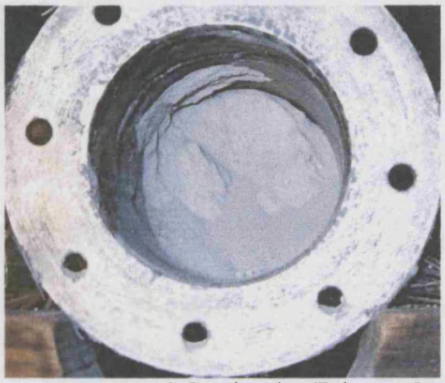

Figure 4.120 Run 9:Combustion Tube at 15 cm.

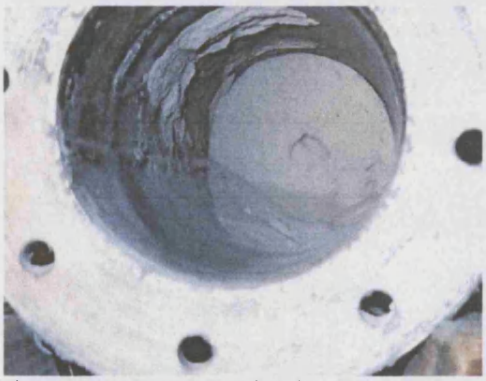

Figure 4.121 Run 9:Combustion Tube at 25 cm.

Figure 4.122 Run 9:Combustion Tube at 30 cm.

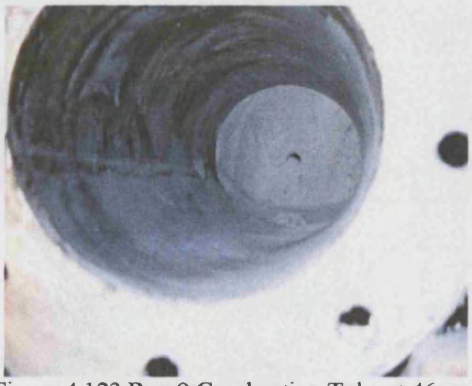

Figure 4.123 Run 9:Combustion Tube at 46 cm.

Figure 4.124 Run 9:Solid Core at 46-58 cm.

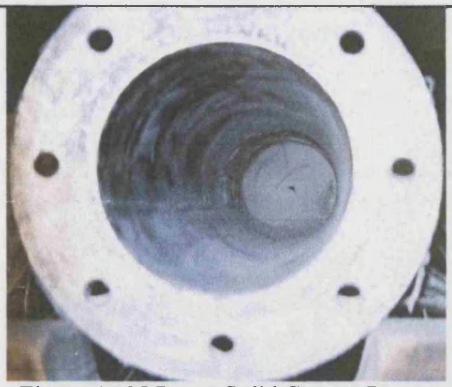

Figure 4.125 Run 9:Solid Core at 72 cm.

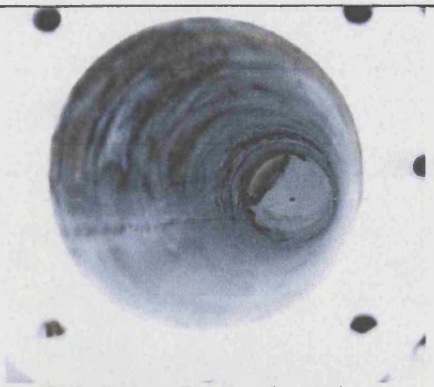

Figure 4.126 Run 9: Combustion Tube at 87 cm.

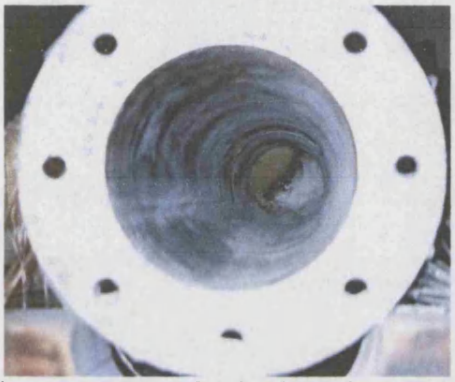

Figure 4.127 Run 9:Combustion Tube at 97 cm.

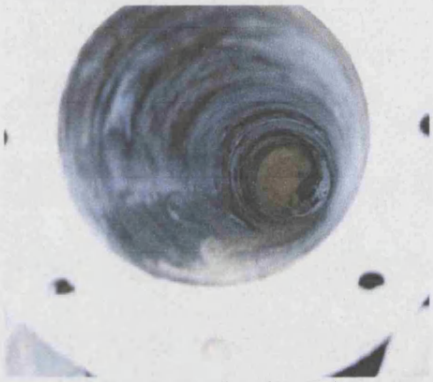

Figure 4.128 Run 9: Combustion Tube at 105 cm.

Figure 4.129 Run 9: Solid Core at 100-125 cm (Side A).

Figure 4.130 Run 9: Solid Core at 100-125 cm (Side B).

Oil and Water Production:

RUN 4:

Samples of the produced liquids taken during Run 4 are shown in Figure 4.131. Figure 4.132 shows the produced liquid which was up to 219 minutes. Prior to this, the produced water was clear. However, there was a small amount of the oil produced close to 219 minutes, with some viscous emulsion adhering to the wall of the glass receiver. The water produced after 219 minutes had a yellowish colour, since it had been affected by the high temperature the combustion front, and resulting oxidation and acid products (Figures 4.133 and 4.134).

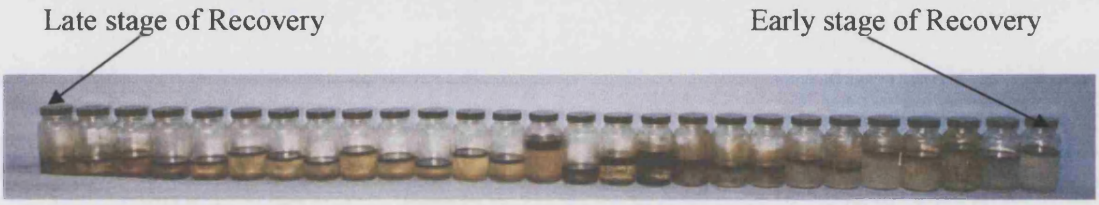

Figure 4.131 : Fluid samples recovered from Run 4.

Figure 4.132 : Produced Oil and Water from Run 4,before 219 minutes
(Water not Affected by Heat Wave)

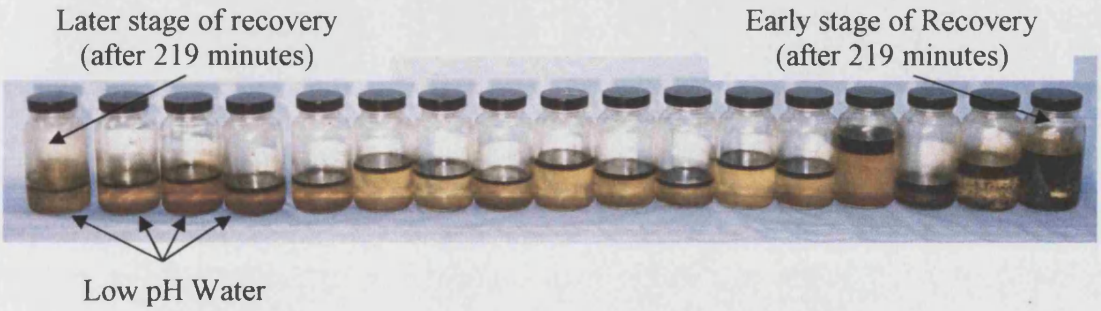

Figure 4.133 : Produced Oil and Water from Run 4, after 219 minutes
(Water Affected by Heat Wave)

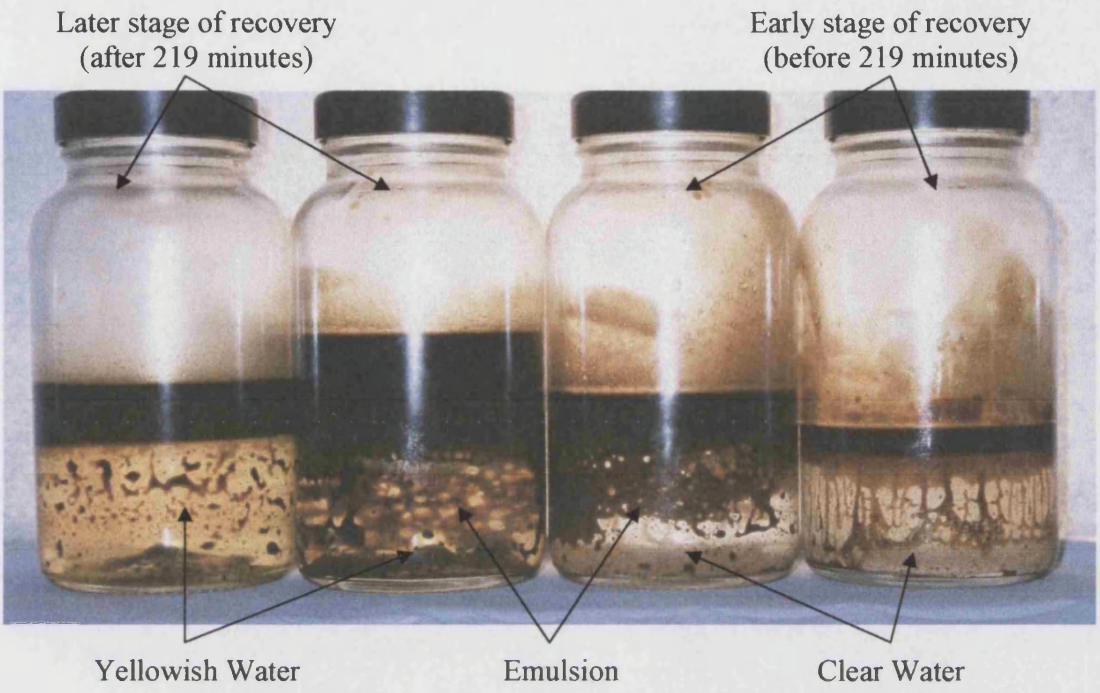

Figure 4.134 : Produced Oil and Water from Run 4.

RUN 5:

The sequence of liquid produced during Run 5 is shown in Figure 4.135. There is a high water content throughout, but more oil is produced during later stages.

Figure 4.135: Total Liquid Recovered from Run 5.

RUN 6:

Figure 4.136 shows the production sequence for Run 6. Early on, with high water cut, tending to diminish later in the experiment. The oil was produced during the test was severely emulsified above the thirds as shown in in Figure 4.137.

Figure 4.136: Liquid Recovery from Run 6.

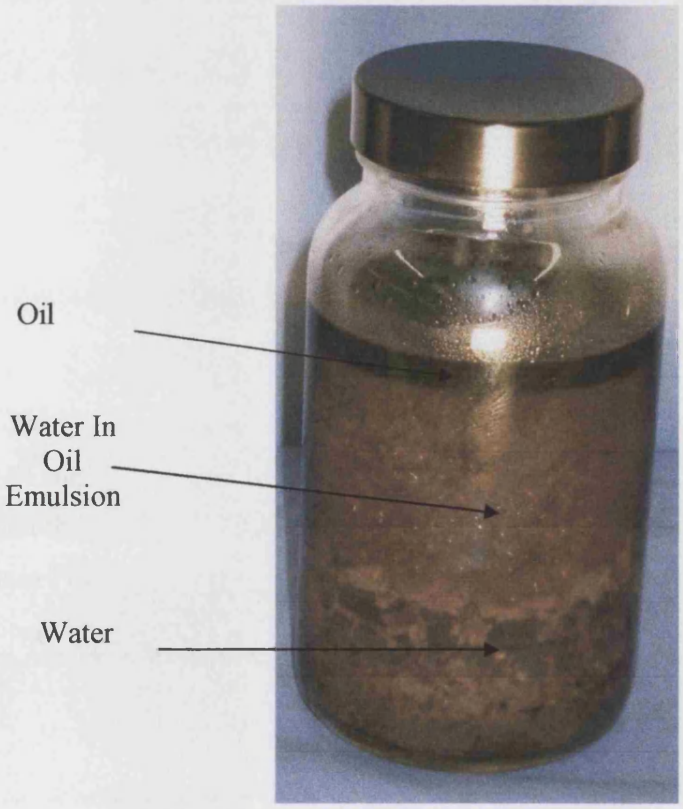

Figure 4.137: Emulsified Oil (Water in Oil Emulsion) in Run 6.

RUN 8:

In Run 8 (Figure 4.138), most of the oil was recovered. The water in the first half of the run is formed emulsion during the middle stage (Figure 4.139). Better separation between water and oil appeared at late stage.

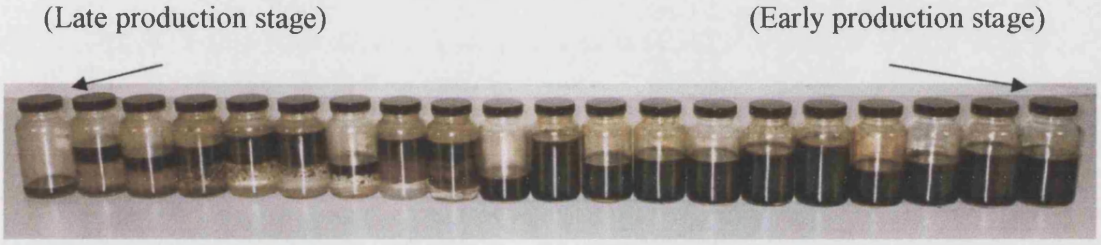

Figure 4.138: Liquid recovery from Run 8.

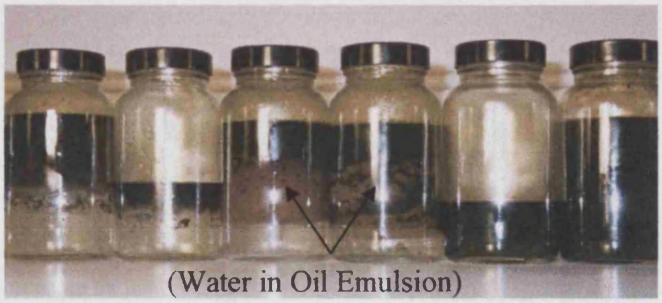

Figure 4.139: Water in Oil Emulsion from Run 8.

Same as what discovered before, Two different water colour recovered. One whitish clear and the other is yellowish. The change of the colours to yellowish is due to heat effect as shown in Figure 4.140.

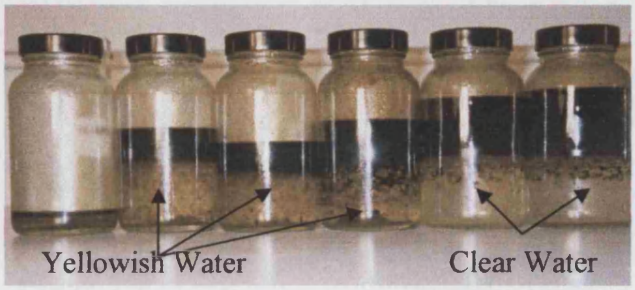

Figure 4.140: Produced Water Affected by Heat in Run 8.

RUN 9:

The sequence of liquid production during Run 9 is shown in Figure 4.141. The water cut initially is very high (Figure 4.142). Followed by production emulsified oil (Figure 4.143). During the transition from mainly water to mainly oil, some deposited material can be seen on the bottom of the sample (Figure 4.144). The change in colour of the water produced also recognized in this test as it can be seen in Figure 4.144.

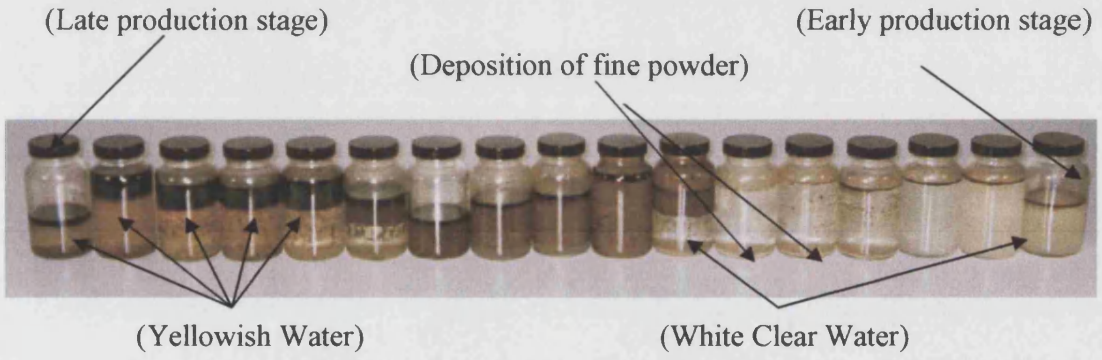

Figure 4.141: Liquid Recovered during Run 9.

Figure 4.142: Clear Water Produced during Early Stages of Run 9.

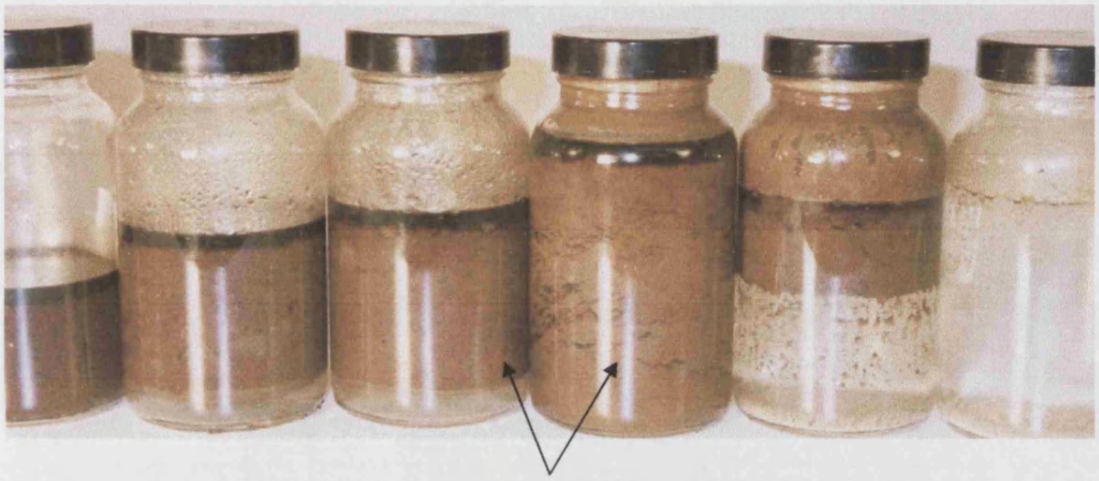

Figure 4.143: Water in oil emulsion (Run 9).

Figure 4.144: Fine Powder Deposit (Run 9).

4.8: Comparison of Some Main Experimental Features

4.8.1: Carbon Oxides:

The amount of CO_2 produced during an experiment changes with time. Since the combustion front only propagate a fraction of the total distance along the combustion tube, it is not possible to know precisely what the instantaneous CO_2 concentration is, unless in-situ samples are obtained.

During the experiments, some CO_2 produced dissolved in crude oil. Hence, CO_2 dissolved in the oil exits with the produced oil, and water. This effect increases with pressure. Figure 4.145 shows the percentage of CO_2 produced versus the volume of produced gas. It is very clear from this plot that, at high air injection rate, the amount of CO_2 produced appears at early stage of the experiment (Run 4). Then is correspondingly, a much more of CO_2 level at lower air injection rates, Run 6, for example. The very important common value of CO_2 produced at the end of the experiment, however, the CO_2 level converges to between 14 and 16 %. A further point to be noted is that the CO_2 measurement at the exit is a 'dry gas' basis. In-situ, the gas is 'wet' i.e. the true instantaneous value, in the combustion tube process atmosphere, is likely to be much lower than 15%, because of the gases, such as steam and a light hydrocarbons.

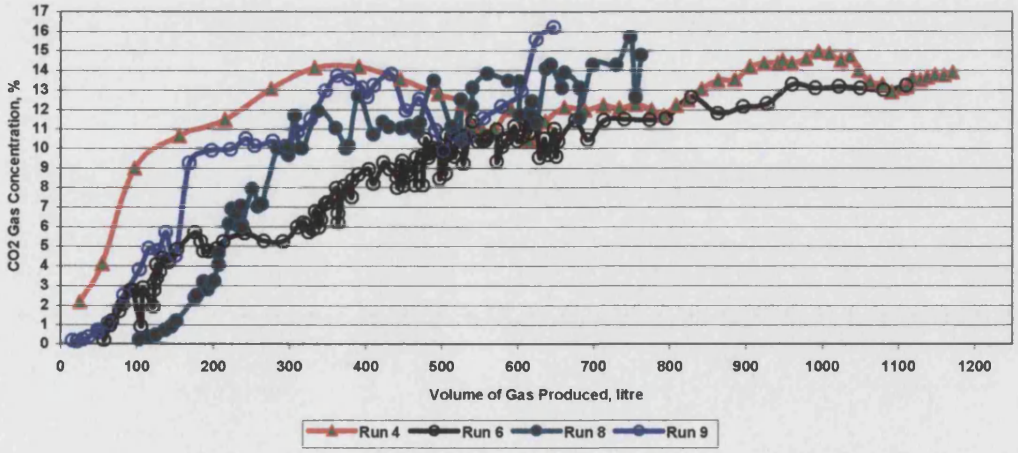

Figure 4.145 : Produced CO_2.

4.8.2: Carbon Monoxide:

The variation of produced CO versus the volume of gas produced is shown in Figure 4.146. The average CO level ranges between 1 to 3%, with average value of about 2%. Runs 6, 8, and 9 show similar trends, starting from zero and then gradually increasing to about 2%. In Run 4, the initial very high value (up to 22%) gradually decrease to amount 2-3%, as the other experiments. The very high values initially are due to high air injection rate used. The effect is indicative of an LTO state. Generally, increasing in CO_2 tends to correspond with reducing values of CO. Since, Run 4 was conducted without band heater control (non-adiabatic), and concequently, it was difficult to establish combustion.

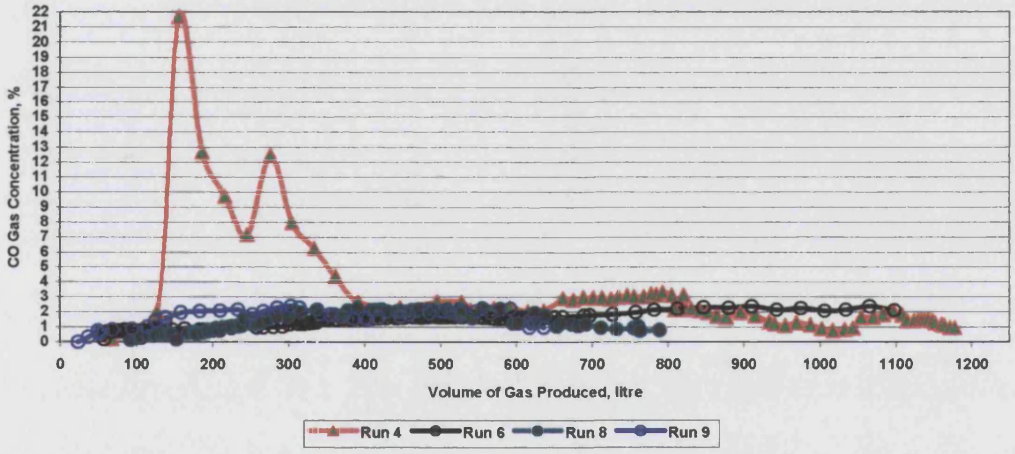

Figure 4.146 : Produced CO.

4.8.3: Oxygen:

From a safety viewpoint, and also economic standpoint, it is not desirable to have channelling of oxygen through the reservoir because:

1. Formation of oxidized oil ahead of combustion front may cause increased fuel laydown and temperatures and subsequently pressure also increased.
2. Increase viscosity of the oxidised oil ahead of the combustion front will reduces oil mobility.
3. Formation of emulsions and tar-like materials plugging of the formation and restrict the fluid flow in the porous media.

One possible benefit of LTO occurrence is that that it improve the reservoir permeability in carbonate media, due the formation of carboxylic acid, downstream of the combustion front.

Figure 4.147 shows the percentage of oxygen produced and not consumed during Runs 4, 6, 8 and 9. It shows that oxygen channelling was recurring, breaking through at an early stage of the experiments. At the same time, CO production is high. The level of gas channelling in Run 6 is particularly severe, resulting in very early breakthrough of oxygen at over 6%. This value then decreases slowly, due to initiation of new separate oxidation zone ahead of the main combustion front. Two periods of minor gas channelling occurred in Run 9, but the produced oxygen level of 3.5% was within tolerable safety limits. Oxygen channelling occurred in practically all of the experiments to high or low degree. This may have been due, in part cooling on one side of the combustion tube caused, by to flow of cold nitrogen in to the shell, inorder to maintain the shell pressures. This effect would lead to quenches combustion reaction near the wall of the combustion tube. Further discussion of this part is given with post mortem analysis.

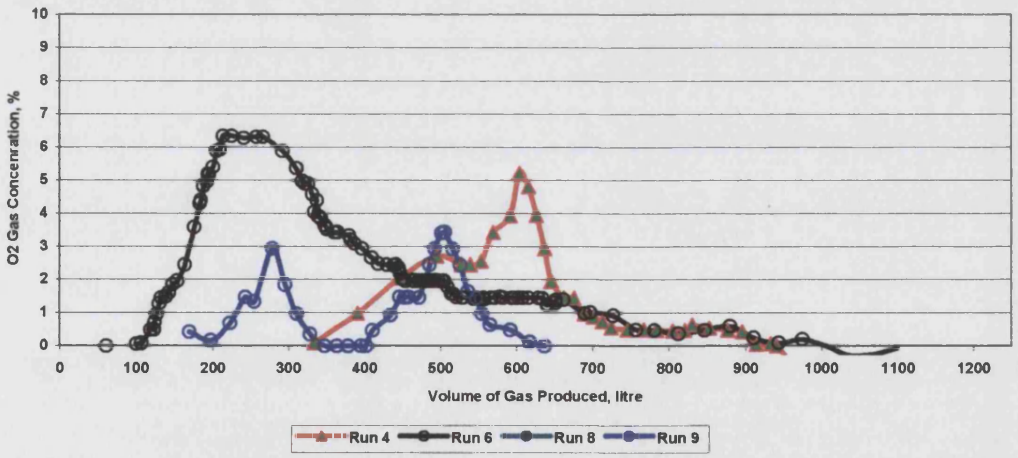

Figure 4.147 : Produced Oxygen.

4.8.4: Gas Molar Ratio:

Gas molar ratio is not considered to be a good indication of combustion performance. Nevertheless, the trends in Figure 4.148 show that the ratio, $(CO/(CO+CO_2))$ is less than

0.2 for most of the experimental period, indicating good combustion. Therefore, with the exception of Run 4, Run 6, 8, and 9 exhibit vigorous combustion.

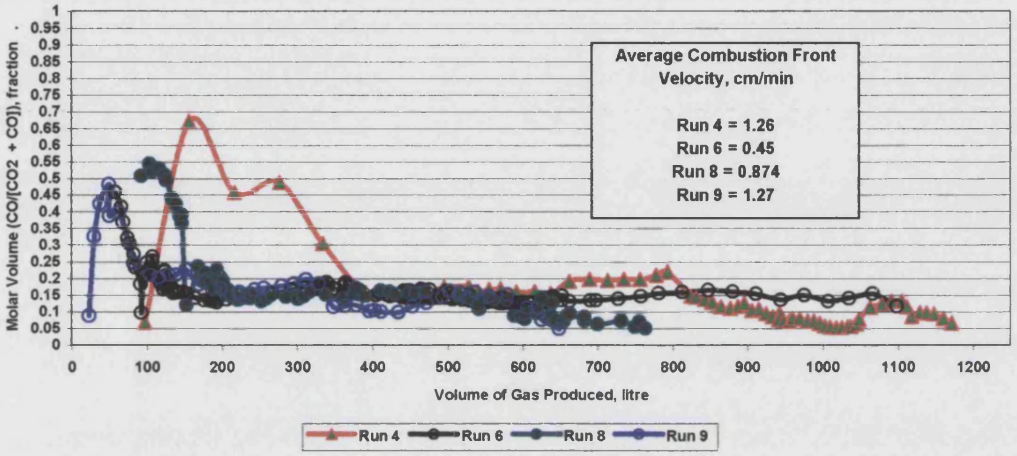

Figure 4.148: Gas Molar Ratio.

4.8.5: Oil Recovery:

Figure 4.149 shows the oil recovery as a function of time. Runs 4, 6, and 8 where conducted at 200 bar, whereas, Run 9 was operated at 100 bar. The initial saturation for all runs 30% oil and 70% water, except Run 8, which was 70% oil and 30% water. Run 9, achieved the highest oil recovery, mainly due to stable combustion front propagation, high combustion front velocity (1.27 cm/min). Another factor enhancing the oil recovery value high is the emulsions inside the core.

Run 4 can be compared with Run 6, because the only varying parameter was air injection flux. Although less oil was recovered in Run 4, the production rate is much faster. This because of the very high air injection rate (~100 m^3/m^2 hr), which creates high combustion front temperature that burning more fuel. Run 6 was conducted at lower rate (~21 m^3/m^2 hr). This affected the oil displacement, cause oil to bank-up just ahead of the combustion front. The control system also worked more effectively, due to less disturbance of pressure. The value of oil recovery is higher, because less fuel is burned.

Run 8 produced a large amount of emulsified oil and water. Three different types of oil were produced. The first oil recovered was virgin oil, i.e. unchanged in composition or density. The second type of oil was emulsified. The third was affected by heat ahead of the combustion front.

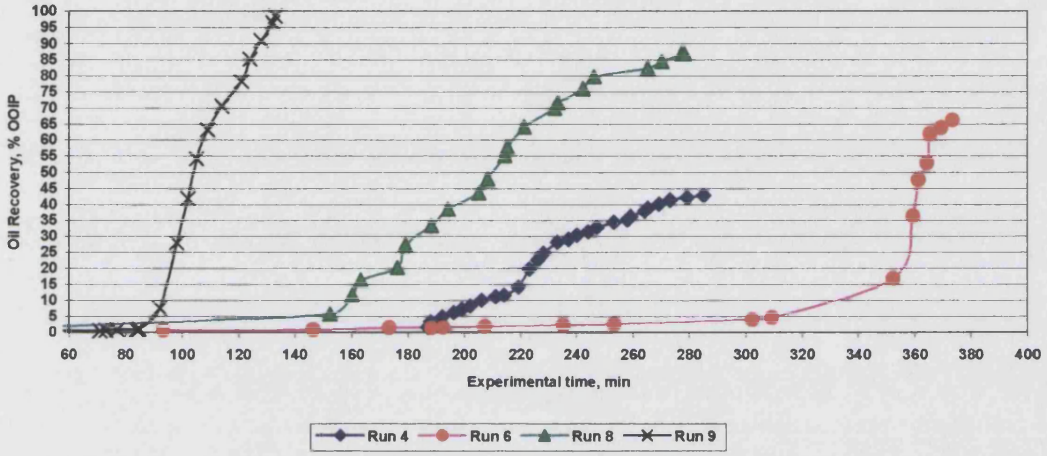

Figure 4.149: Oil Recovery.

4.8.6: Combustion Front Temperature:

The average optimum combustion front temperature for each experiment, started at high temperature, then dropped down to 500 to 600°C. This effect is shown in Figure 4.150. A few lower temperatures, 250 to 300°C, evidencing LTO, are also appeared.

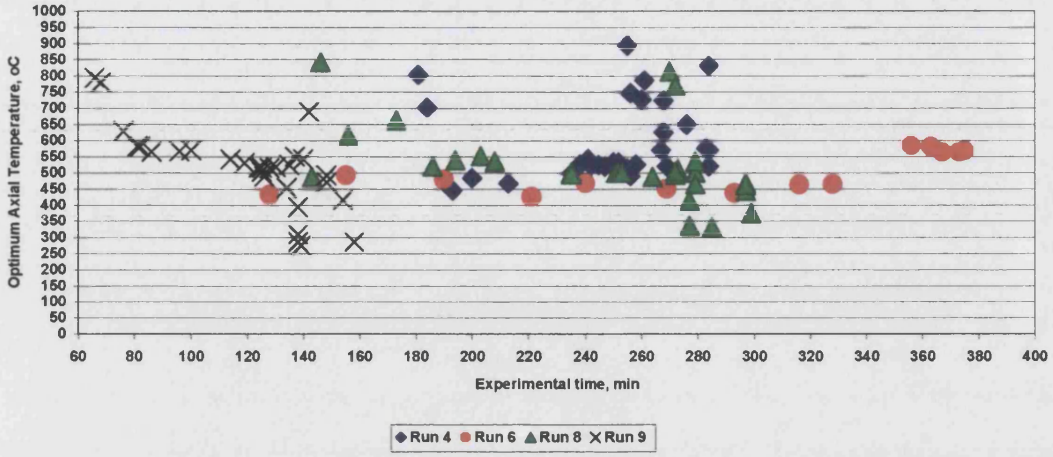

Figure 4.150 : Combustion Front Temperature.

4.8.7: Atomic Hydrogen to Carbon Ratio:

All of the combustion experiments shows similar H/C trends, starting at very high values, then decreasing rapidly with time, as the volume of gas injected increased (Figure 4.151). In all the cases, the H/C stabilises at value of around 2, indicating that vigorous, high temperature combustion was achieved.

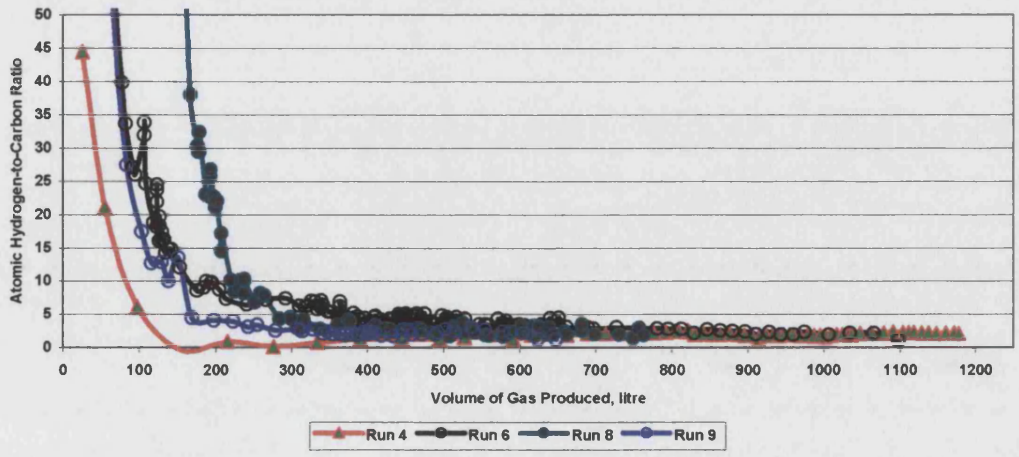

Figure 4.151 : Atomic Hydrogen to Carbon Ratio.

4.8.8: Amount of Fuel Consumed:

Figure 4.152 show that, the rate at which fuel is consumed (per volume of gas produced) is constant at around 0.1 gm/litre.

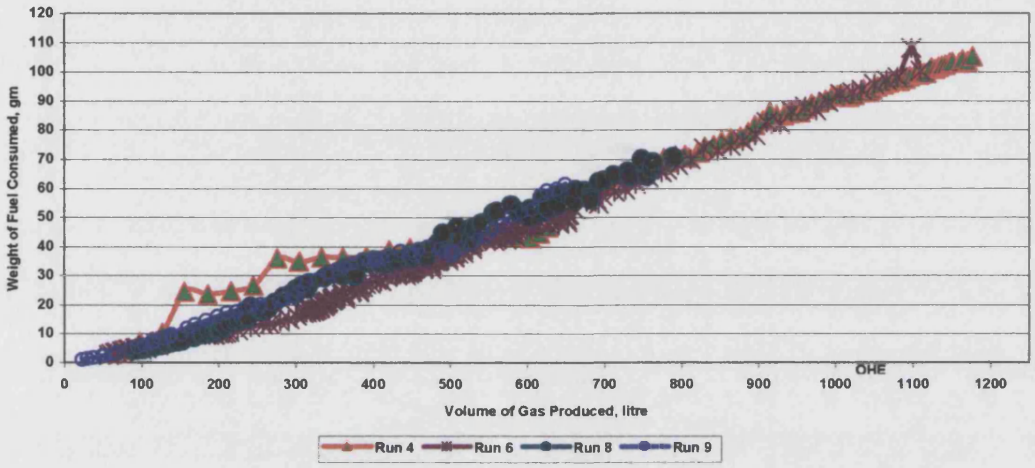

Figure 4.152: Weight of Fuel Consumed.

4.8.9: Fuel Availability:

The fuel availability or amount of fuel deposited are essentially constant for all the experiment, as shown in Figure 4.153. There is some or very little difference due to LTO.

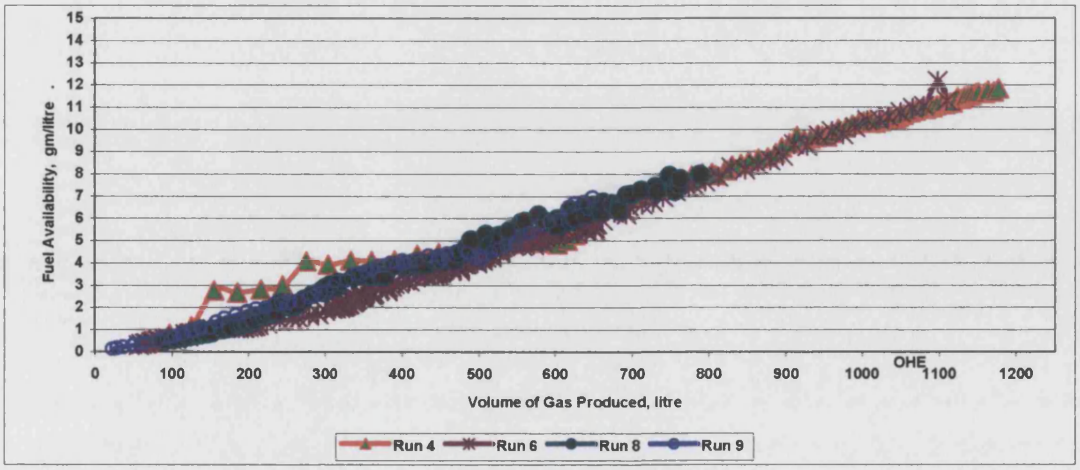

Figure 4.153 : Fuel Availability.

4.8.10: Air Requirement Using Combustion Stoichiometry:

The calculated, air requirement, based on the produced gas composition is shown in Figure 4.154. The graph shows that all runs with same value, as would be expected for the same crude oil.

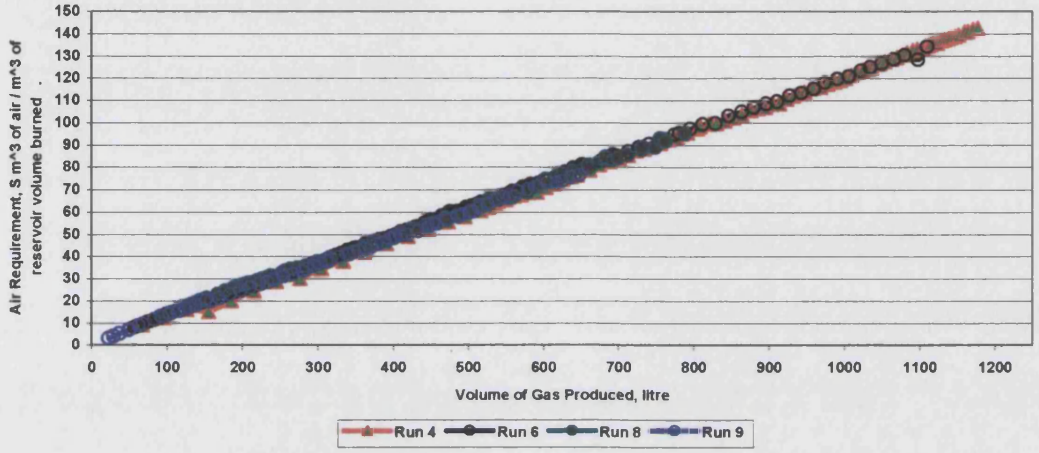

Figure 4.154 : Air Requirement Using Combustion Stoichiometry.

4.8.11: Minimum Air Flux Using Combustion Stoichiometry:

The minimum air flux required to sustain a propagates combustion front is shown in Figure 4.155. The lower value correspond to Run 6, which has the lower combustion front velocity.

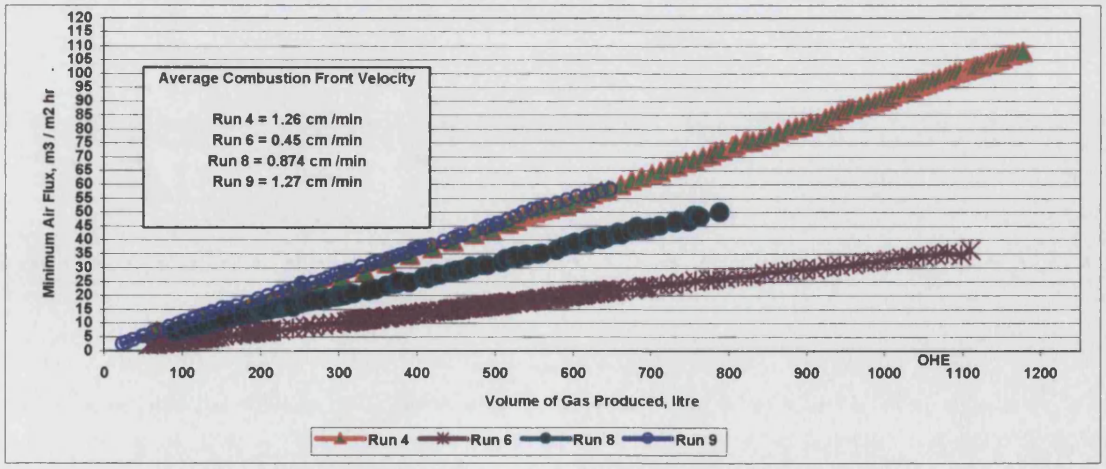

Figure 4.155: Minimum Air Flux from Produced Gas Composition.

Axial and Wall Temperature Difference

Run 4 (Non adiabatic BH control):

As it is shown in Figure 4.156 to 4.160 . The difference between axial temperature and the wall temperature are can be seen clearly. No band heater control or adiabatic control. It even better to test laboratory with out using the band heater if it is possible, to be sure that it will work in field scale. It is also, and some times it is called worst case that may be occur in the field or actual scale. When the band heater where not used, it mean that there are heat losses to the surrounded. Bearing in mind that there are insulate eliminate or minimise the heat losses surround the combustion tube.

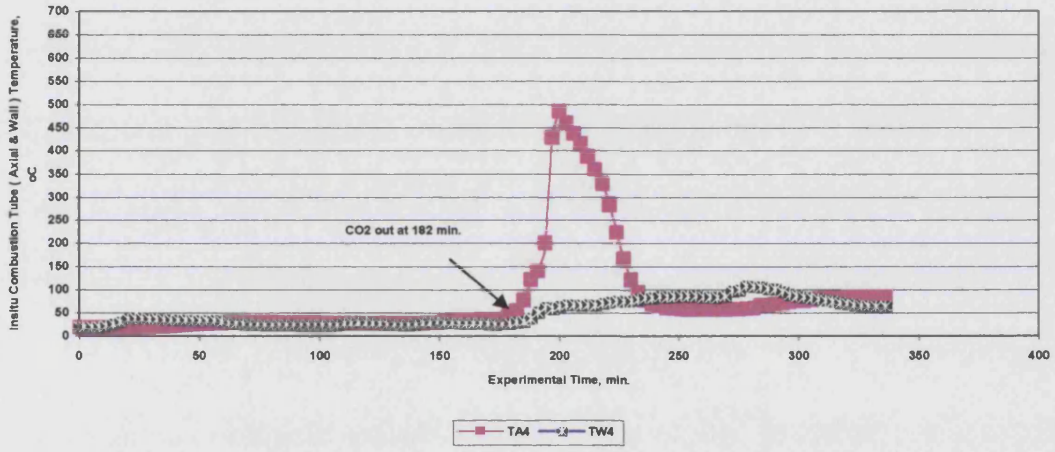

Figure 4.156 Run 4 : Axial and Wall Temperature Difference for TA4 & BH4.

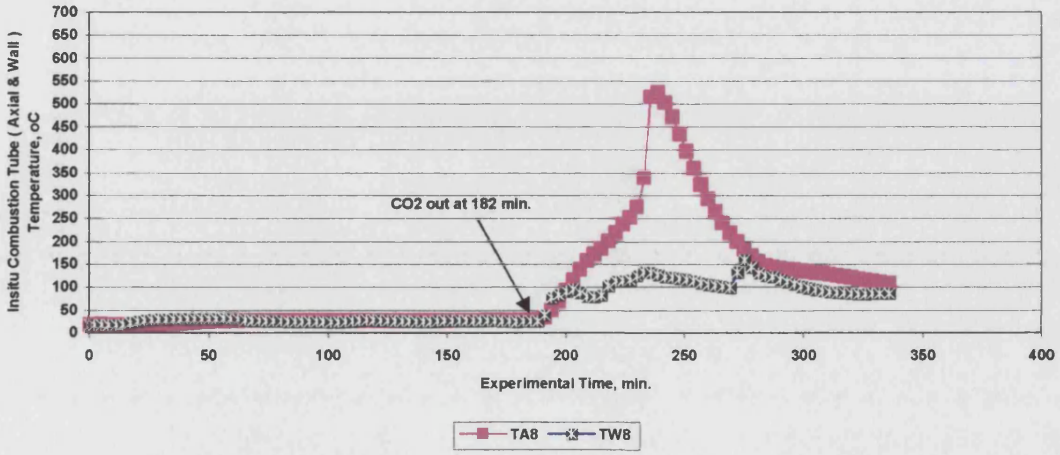

Figure 4.157 Run 4 : Axial and Wall Temperature Difference for TA8 & BH8.

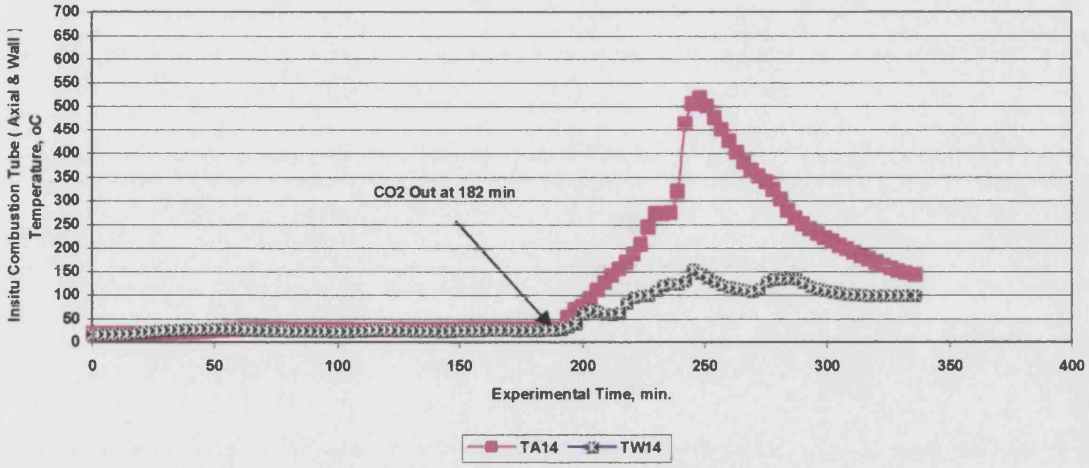

Figure 4.158 Run 4 : Axial and Wall Temperature Difference for TA8 & BH8.

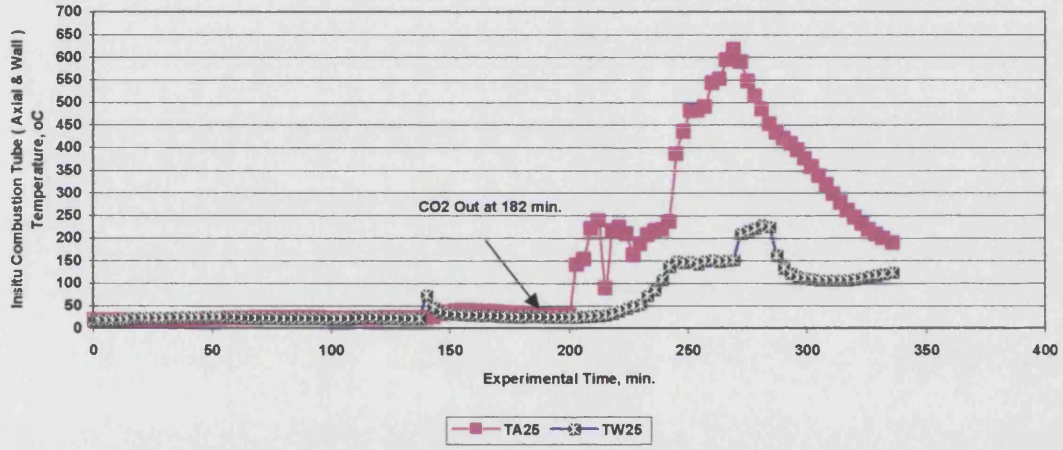

Figure 4.159 Run 4 : Axial and Wall Temperature Difference for TA25 & BH25.

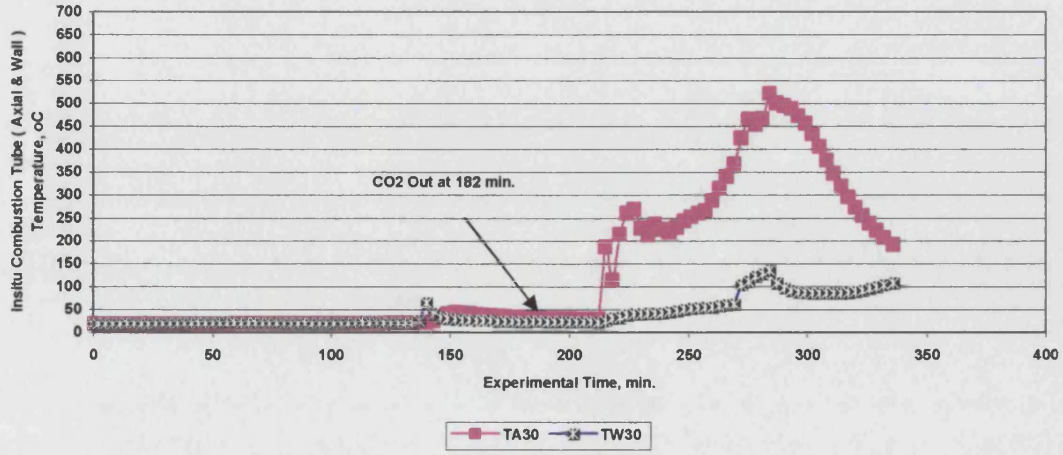

Figure 4.160 Run 4 : Axial and Wall Temperature Difference for TA30 & BH30.

Run 6 (adiabatic BH control):

Figures 4.161 to 4.165 Shown the axial and wall temperature at different locations at BH 4, 8, 14, 25 and 30. Closed to the ignitor, there will be artificial ignition and combustion affected by the ignitor. The figures shows that there are considerable different between the wall and axial temperature, this was due to band heater control problem. The band heater operations can not achieve good control due to computer speed. Most of the time, the system control pressure because it was programmed that the first priority to the pressure and then temperature. There was a lot of disturbance in pressure during the run. However, at location of BH14, as shown in Figure 4.163 better control was achieved.

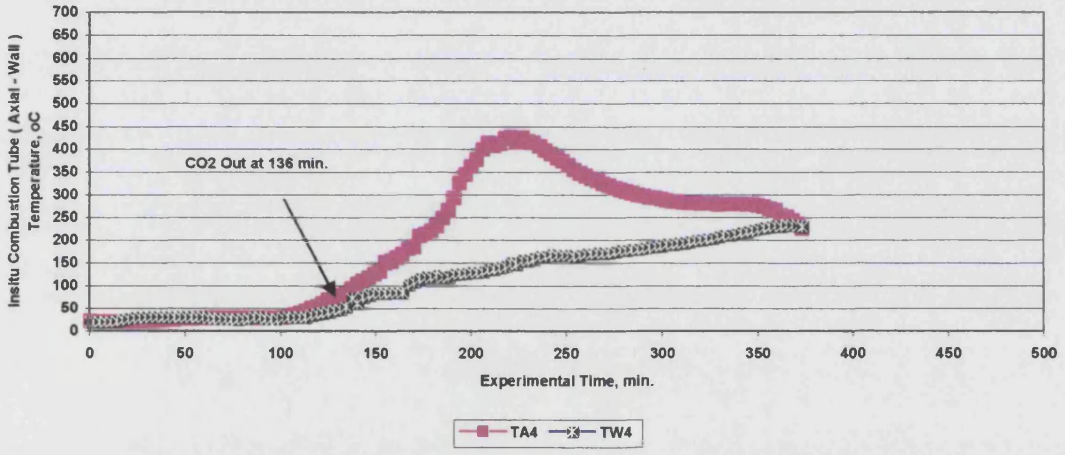

Figure 4.161 Run 6 : Axial and Wall Temperature Difference for TA4 & BH4.

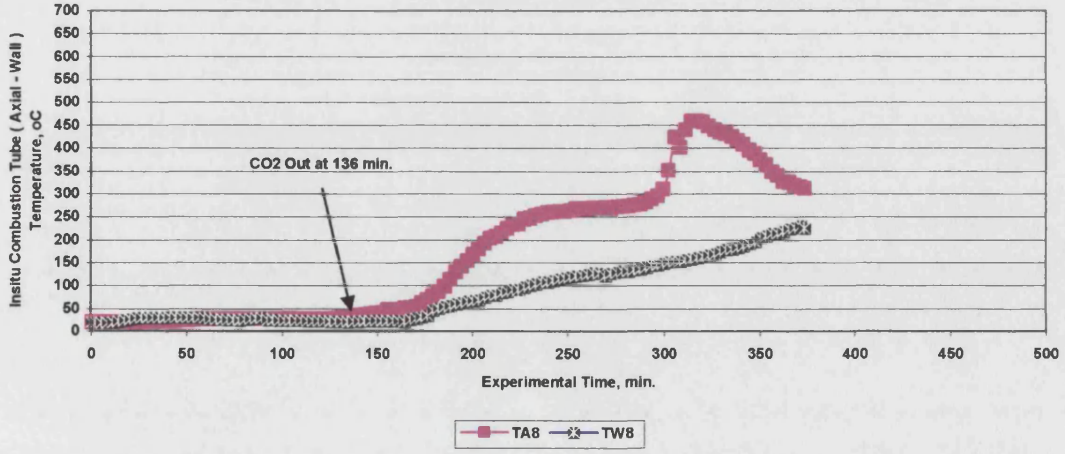

Figure 4.162 Run 6 : Axial and Wall Temperature Difference for TA8 & BH8.

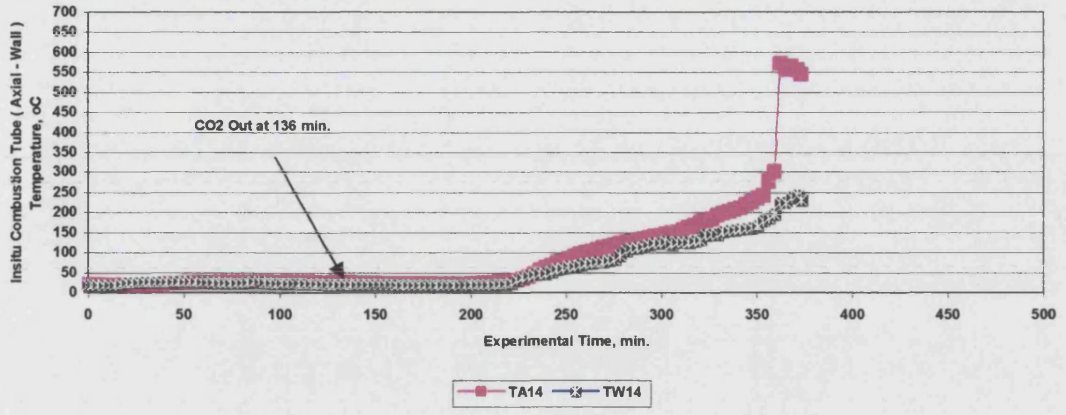

Figure 4.163 Run 6 : Axial and Wall Temperature Difference for TA14 & BH14.

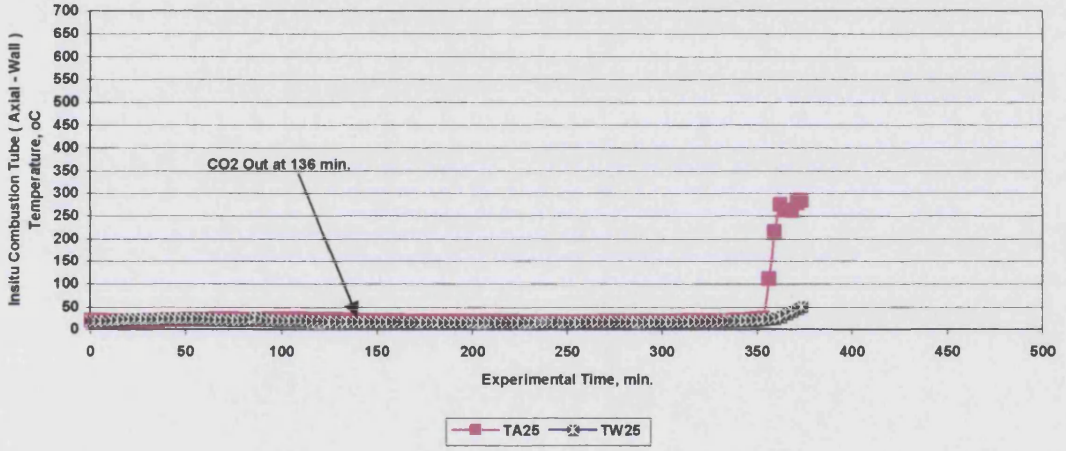

Figure 4.164 Run 6 : Axial and Wall Temperature Difference for TA25 & BH25.

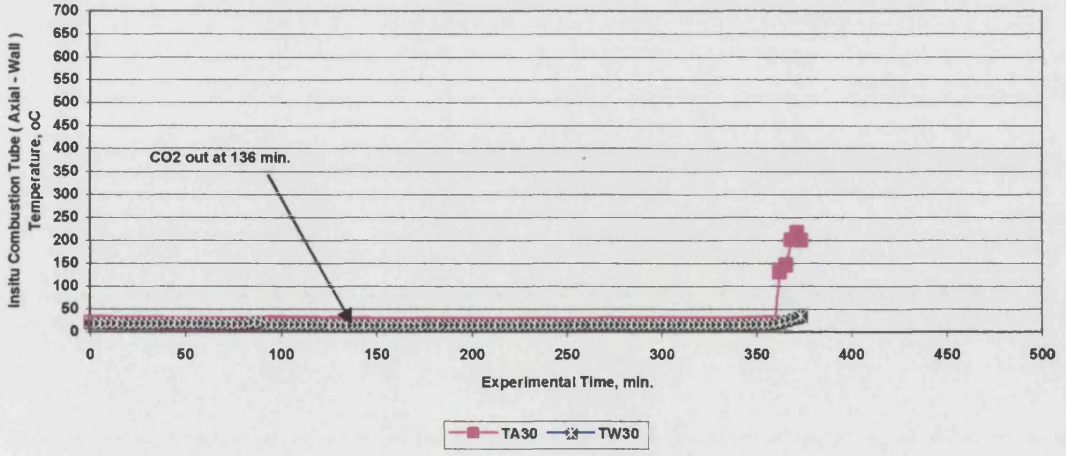

Figure 4.165 Run 6 : Axial and Wall Temperature Difference for TA30 & BH30.

Run 8 and 9 conducted utilizing adiabatic BH's control. Due to the reasons stated previously, the control system was unable to achieve adiabatic control. Generally, the axial temperature always higher than the wall temperature. Then the opposite occur after the combustion moves ahead in the centre more than beside the wall. Run 9 shows that wall temperature was higher than axial temperature at the began of the experiment. Then after, similar trend as run 8 achieved. Better control achieved later at the end of the experiment (see Appendix F). Note that for Run 8, first appearance of CO_2 with the produced gas was at 147 minutes, but in Run 9 was 60 minutes.

SIMULATION OF EXPERIMENTS

Introduction :

A preliminary series of numerical simulations was conducted using the STARS reservoir simulator. The purpose was to understand further the operation of the in-situ combustion process, and also aid in the design of the air injection experiments. The STARS reservoir simulator (Computer Modelling Group, Calgary) can solve steam injection and in-situ combustion problems in three dimensions.

Combustion Tube Model:

The modelled combustion tube which was used in the simulation is shown in Figure 4.166 . It is one dimension, vertical, downwards displacement.

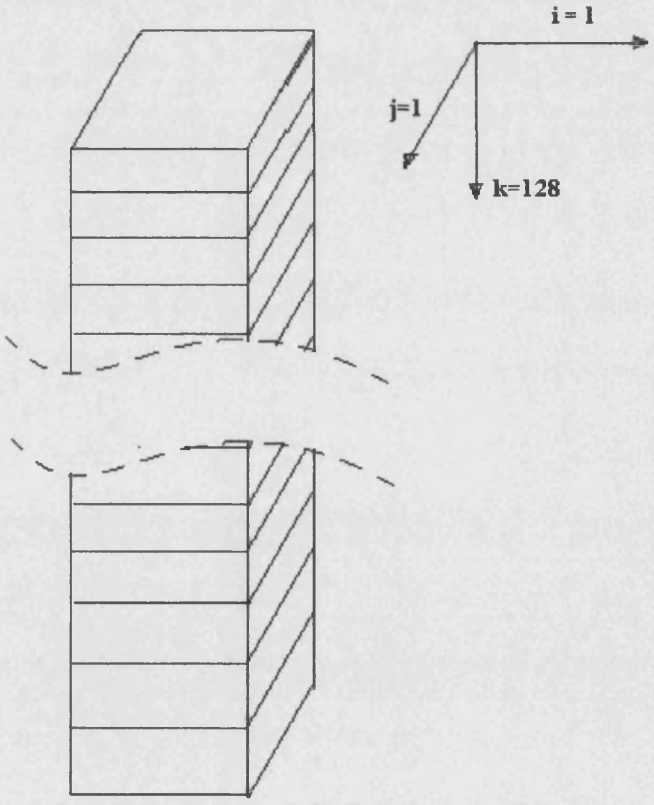

Figure 4.166 : Combustion Tube Simulation Grid.

Input Simulation Features :

The overall features of the simulation can be listed as shown in Table 4.2 (Appendix E). The entire data in the whole runs are same, the only change that made in every simulation runs are that necessary to be matched with the experimental data .

Table 4.2 : Physical Properties and Reactions for Simulation Model Base.

Parameter	Discription
Ekofisk Crude Oil: Pseudo-Component	PC1 : C1 – C5 PC2 : C6 – C10 PC3 : C11+
Reactions:	
1. Heavy Oil Cracking	$C_{11^+} \rightarrow C_6 - C_{10} + \text{Coke}$
2. Heavy Oil Cracking	$C_{11^+} \rightarrow C_1 - C_5 + \text{Coke}$
3. Heavy Oil Burning	$C_{11^+} + O_2 \rightarrow H_2O + CO/CO_2 + \text{energy}$
4. Light Oil Burning	$C_6 - C_{10} + O_2 \rightarrow H_2O + CO + \text{energy}$
5. Hydrocarbon gas Burning	$C_1 - C_5 + O_2 \rightarrow H_2O + CO + \text{energy}$
6. Coke Burning	$\text{Coke} + O_2 \rightarrow H_2O + CO_2 + \text{energy}$
7. Carbon Monoxide Burning	$CO + 0.5O_2 \rightarrow CO_2 + \text{energy}$
Operation Conditions: - Pressure, bar - Temperature, °C	 100 – 200 38
Ignitor	Band Heater 1 – 4 (250°C)
Core	MI Limestone Porosity, 42.8% Permeability 616-1600 md
Fluid Saturation: Water saturation,% Oil Saturation,% Gas saturation,%	 30 - 80% 20 -70 7

Sensitivity Runs:

Several simulation runs were conducted on run 4 result, to understand how the simulation results could be affected by varying certain input parameters. The attempting which were carried out are stated in Table 2 and as follow:

Table 2 : Simulation Tests (Reaction Parameter and Permeability).

Parameter	Changes (from – to)	Effect(Temperature Distribution)
1. Reaction parameters:		
A. Activation Energy, kJ/gm m		
1\ $C_{11+} \rightarrow C_6 - C_{10} + Coke$	27-127	Minor
2\ $C_{11+} \rightarrow C_1 - C_5 + Coke$	25-125	Minor
3\ $C_{11+} + O_2 \rightarrow H_2O + CO/CO_2 + energy$	16.5-116.5	Moderate
4\ $C_6 - C_{10} + O_2 \rightarrow H_2O + CO + energy$	17.5-117.5	Minor
5\ $C_1 - C_5 + O_2 \rightarrow H_2O + CO + energy$	17-117	Minor
6\ $Coke + O_2 \rightarrow H_2O + CO_2 + energy$	6.5-106.5	Major
7\ $CO + 0.5O_2 \rightarrow CO_2 + energy$	7.5-107.5	Major
B. Reaction Enthalpy, kJ/gm m		
1\ $C_{11+} \rightarrow C_6 - C_{10} + Coke$	0-5000	Minor
2\ $C_{11+} \rightarrow C_1 - C_5 + Coke$	0-5000	Minor
3\ $C_{11+} + O_2 \rightarrow H_2O + CO/CO_2 + energy$	8-108	Minor
4\ $C_6 - C_{10} + O_2 \rightarrow H_2O + CO + energy$	3.6-103.6	Minor
5\ $C_1 - C_5 + O_2 \rightarrow H_2O + CO + energy$	0.185-100.185	Minor
6\ $Coke + O_2 \rightarrow H_2O + CO_2 + energy$	0.437-100.437	Major
7\ $CO + 0.5O_2 \rightarrow CO_2 + energy$	283.8-383.8	Minor
$CO + 0.5O_2 \rightarrow CO_2 + energy$	283.8-28.38	Major
2. Permeability,md	616 – 6000	No effect

3. Air Injection Rate :

The air injection rates obtained from STARS required after many trials to obtain a suitable value.The average value of produced gas was essential same as measured values,

4. Liquid Recovery :

Study of recovery mechanisms through changing or relative permeability curves. It was found that STARS simulator programmed into the bases of forming liquid bank (oil or water) just ahead of the combustion front . Also no change in original or initial water or oil saturation farther ahead of the combustion front. It assumes the piston displacement mechanism occur ahead and farther down the combustion tube.

The final predicted relative permeabilities curves used for the simulation are shown in Figure 4.167.

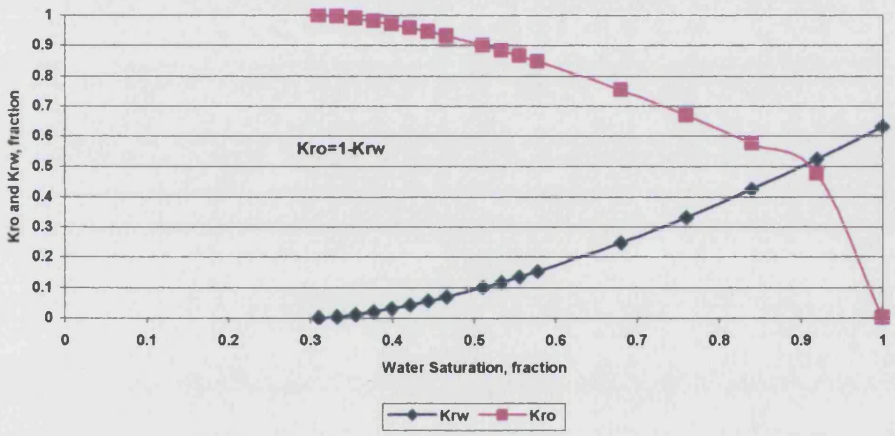

Figure 4.167 : Relative Permeability curves Utilized in STARS.

Produced Gases (CO and CO_2):

The produced CO and CO_2 was adjusted to fit a reaction enthalpy. It was found:

a- The exact and closed values of CO and CO_2 produced can be obtained but the temperature distribution profile cannot be mentained, because of the low temperature predicted, also delay liquid recovery.

b- reasonable values were selected to maintain all CO and CO_2, temperature distribution profile and liquid recovery taken in consideration the challenging of oxygen during through the combustion tube during the experiments.

The other unknown quantity was the volume of nitrogen used to pressurize the oil and water inside the combustion tube, after many trials, a value of 7% was obtained.

A complete simulation runs involved pressurisation, ignition (first 20 minutes) followed by air injection. The initial reservoir temperature was set at 38°C. Finally, the last selected run gained on Run 4 was used as a common on all other runs (6, 8 and 9), with changing the variable parameters. The complete STARS input file can be seen in Appendix (E).

RUN 4 SIMULATION :

History Match (Production Gas Flow Rate):

As it mentioned previously, many simulation trials were performed in order to obtain a match between the experimental results and the STARS simulation prediction. No separate/multipeaks, difficulties of programming channelling, or fingering of fluid. The STARS simulator, basically simulates the displacement ahead of the combustion front as piston like displacement. Nevertheless, driving the liquid (oil + water) farther ahead of the combustion front as a piston displacement with liquid (oil or water) bank accumulated just ahead of the combustion front.

Since the in-situ combustion tube process is not steady (pump with constant air injection rate and pressure), but with more or less constant pressure; the average injection rate estimated by STARS.

The simulated air injection rate was changed many times in order to obtain match with the experimental value. For a produced gas rate of 83.9 m^3/m^2hr, 99.2 m^3/m^2hr of air injection was required.

Axial Temperature Distribution:

Delay of about 29 minutes was detected moreover that the general ignition heating time (20 minutes). The 29 minutes estimated from matching the first time CO_2 and CO produced in the experiment.

Figure 4.168 present the temperature profile along the combustion tube at different time. It is clear from the figure that the combustion zone enlarged and becomes wider with experiment time. The shape of the temperature profile shows that the combustion front temperature is much lower than the maximum gained behind the combustion front due to high fuel (coke) available and deposited behind. This coke is responsible for getting higher temperature as stated before from energy generated due to burning coke.

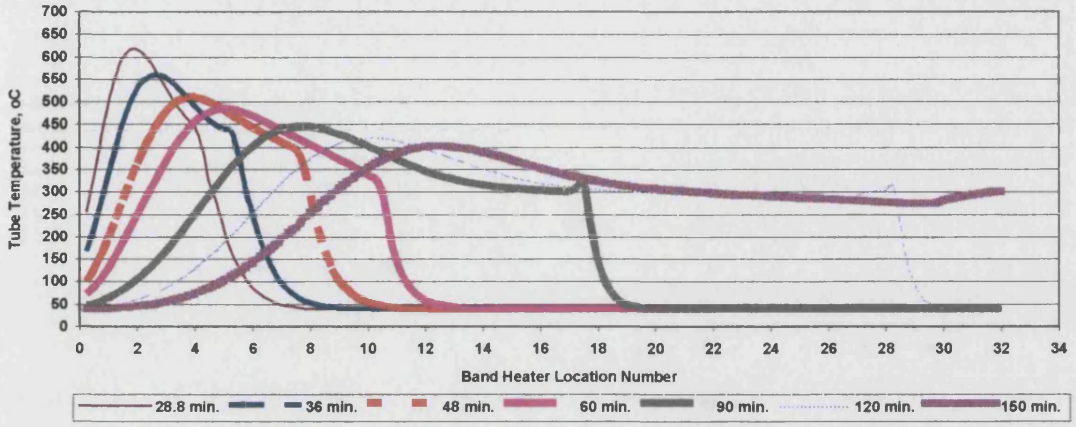

Figure 4.168 : Predicted Temperature Distribution Using STARS (Run 4).

Comparison between experimental results with the simulated, show closed temperature profile between time 28.8 to 48 minutes as shown in Figure 4.169. The late experiment temperature can not be simulated; it was caused due to oxygen breakthrough.

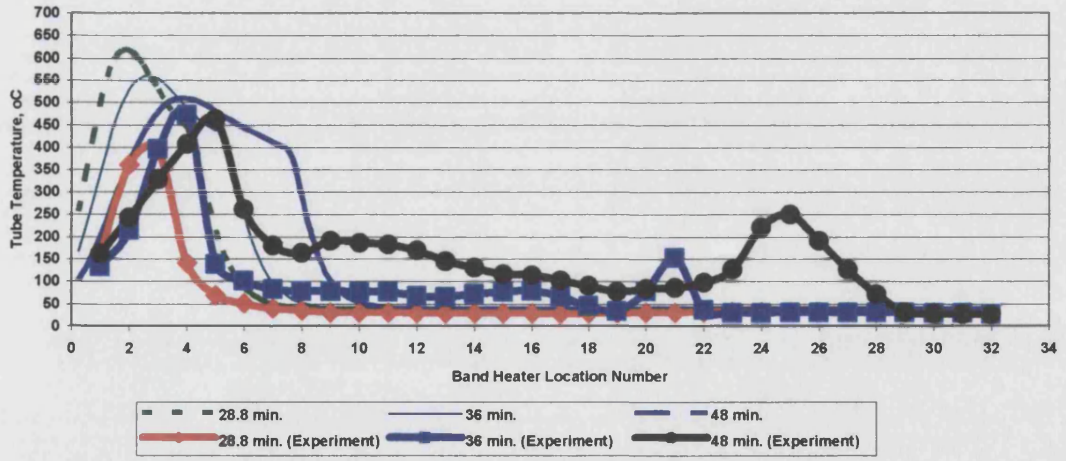

Figure 4.169 : Experimental and Predicted Axial Temperature profile in Limestone Core. Time base-line adjusted by -29 min. at Time 28.8, 36 and 48 minutes.

Figure 4.170 presents that the combustion front moved down faster than the predicted by STARS simulator between time 60 to 90 minutes.

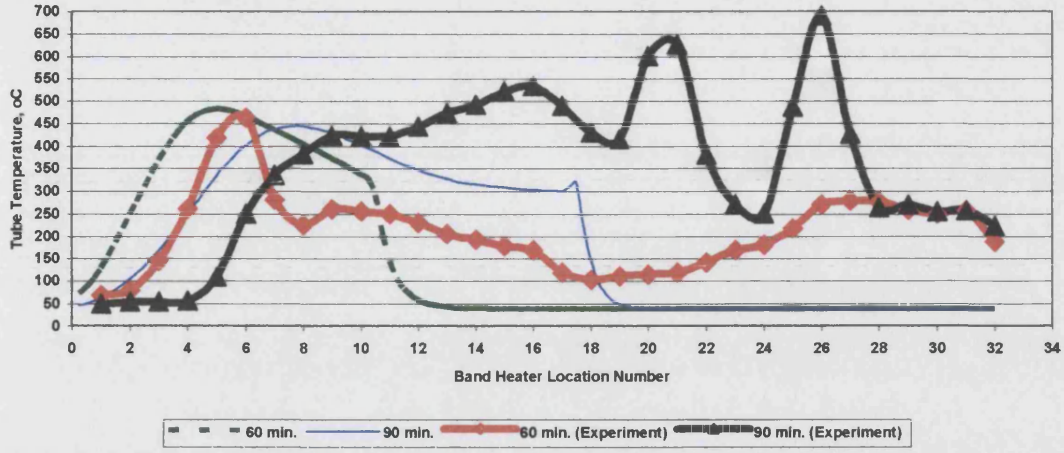

Figure 4.170: Predicted Temperature Distribution Using STARS (Run 4).
Time base-line adjusted by -29 min. at Time 60 and 90 minutes.

The combustion front reach to the end in the experiment and the simulator as shown in Figure 4.171 in time between 120 to 150 minutes. The temperature at BH1 was higher in the experiment than the predicted by the simulator. The simulator predict also high amount of coke deposited at BH10.

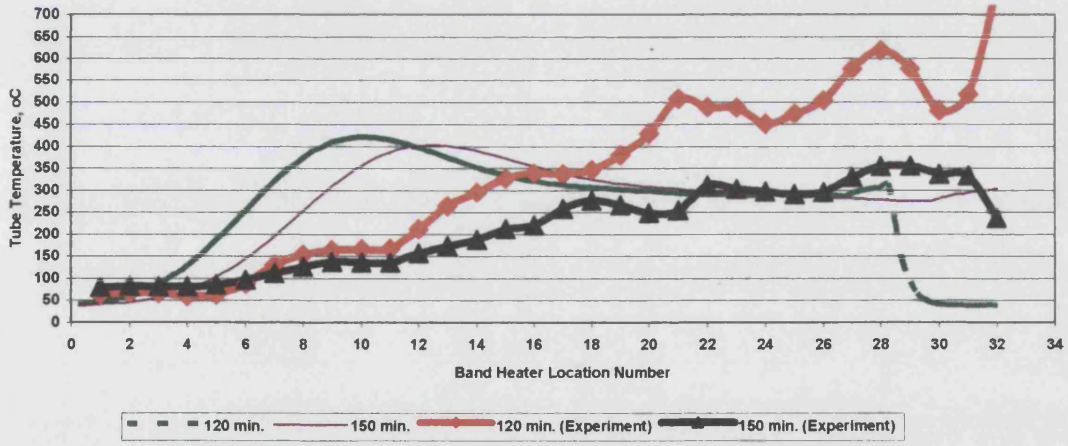

Figure 4.171 : Experimental and Predicted Axial Temperature profile in Limestone Core. Time base-line adjusted by -29 min. at Time 120 and 150 minutes.

The combustion front temperature and the maximum temperature logged can be seen in Figure 4.172, shows a 100°C difference between experiment and predicted. The highest temperature during the simulation, is not necessarily to combustion front temperature but it is function of fuel (coke)availability , reactivity of fuel and air (oxygen) availability. Normally, The highest fuel concentration is found ahead of the combustion front, while

the highest oxygen concentration is located behind the combustion front. The measured and predicted temperatures do not coincide especially at the beginning and toward the end of the experiment.

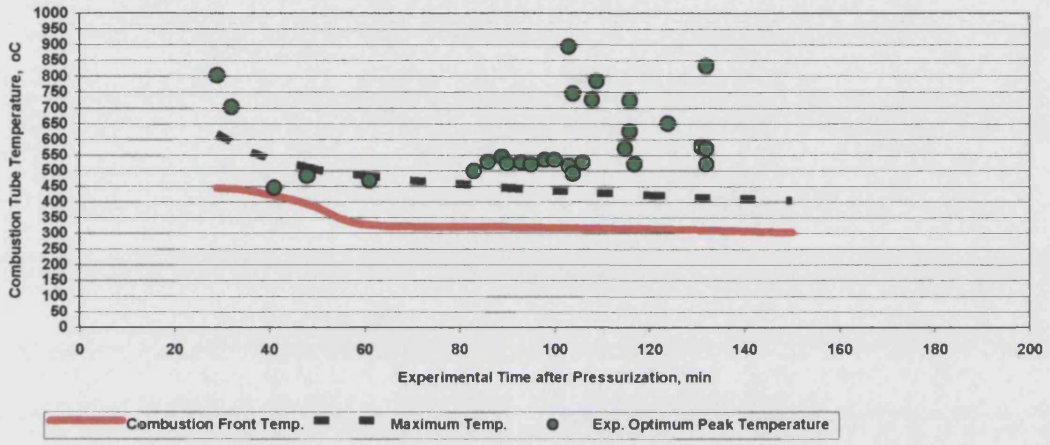

Figure 4.172 : Combustion Front and Maximum Temperature Utilizing STARS Simulator (Run 4).

Combustion front velocity varies between 0.5 to 1.45 cm/min. It reach 0.7 cm/min. after 38 minutes, and 1.45 cm/min. at time 120 minutes finally reduced to about 0.5 cm/min.(Figure 4.173)

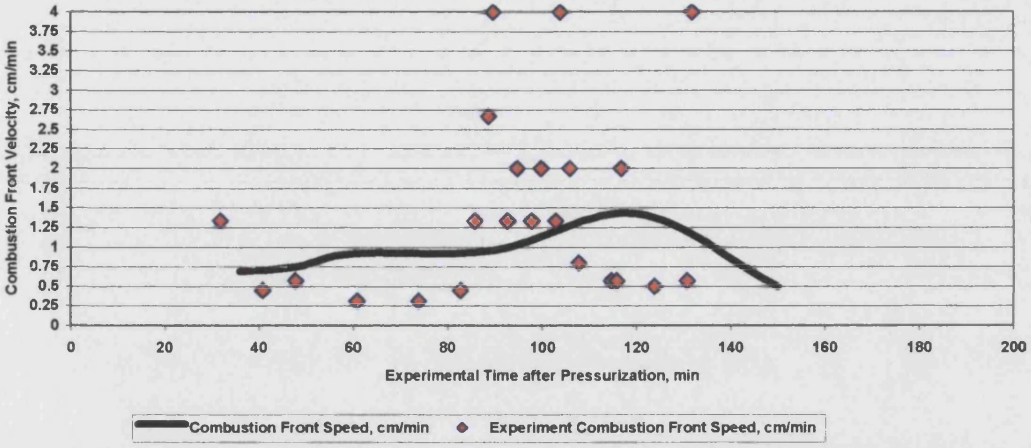

Figure 4.173 : Combustion Front Velocity Utilizing STARS Simulator.

The CO predicted by STARS in Run 4, start at a value (12%), reduces down to 3.5%, as shown in Figure 4.174. The value of CO_2 predicted equal to the produced from the experiment (about 14 %).

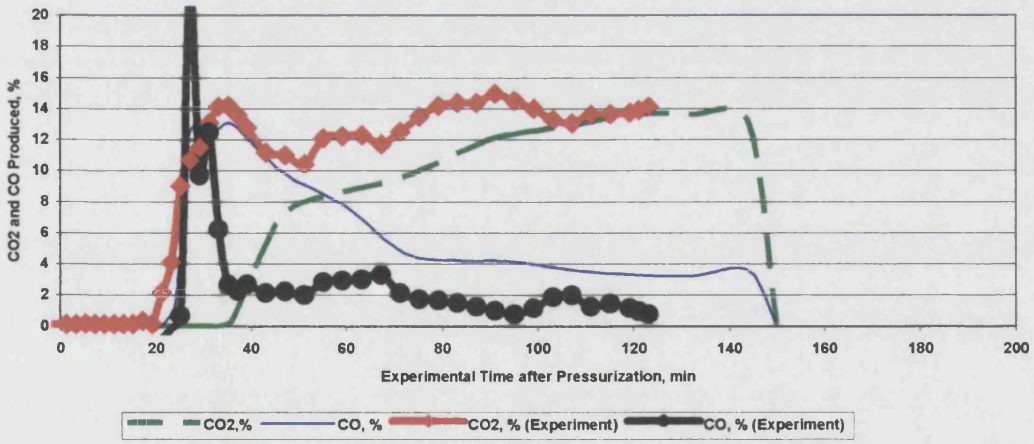

Figure 4.174 : CO_2 and CO Recovered Utilizing STARS Simulator and Experiment (Run 4). Time base-line adjusted by -29 min.

Figure 4.175 shows that there are very closed recovery of oil and water at the end of the experiments when compared with STARS. It is very clear that the oil recovery went gradually to the end of the experiment. But the predicted by the STARS shows that there where an oil bank ahead of the combustion front started to come out after 90 minutes.

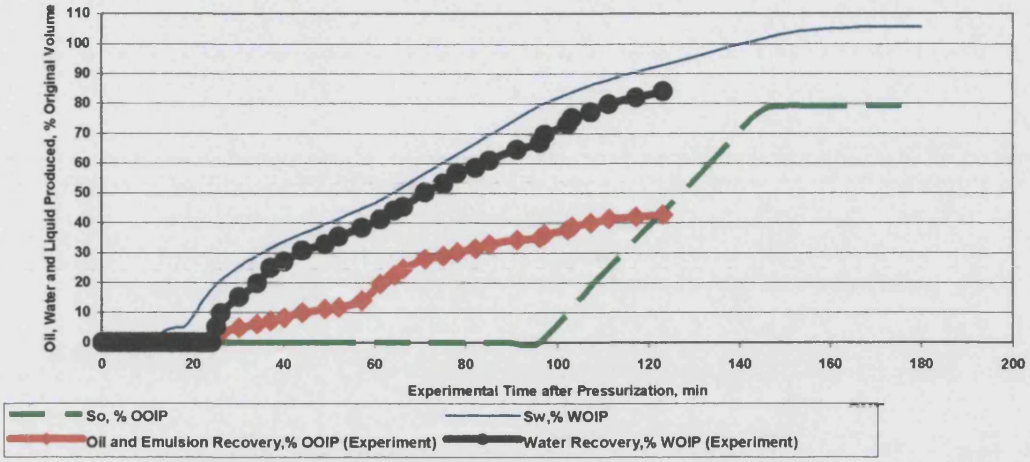

Figure 4.175: Oil and Water Recovery Utilizing STARS and Experiment (Run 4). Time base-line adjusted by -29 min.

RUN 6 SIMULATION :

Run 6 was conducted at low air injection rate. To estimate the average air injection rate used experimentally, STARS used to predict it by adjusting the exact gas produced rate to gain 21 m^3/m^2hr it required 26.3 m^3/m^2hr.

Figure 4.176 shows the temperature distribution profile of run 6 along the combustion tube. The shape of the curves seam to be symmetrical, and maximum peak temperatures just in the middle of the curve.

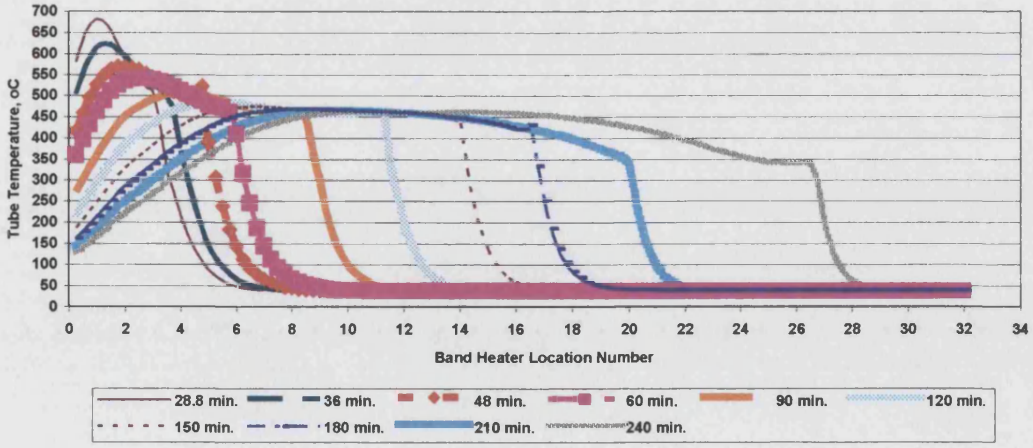

Figure 4.176: Temperature Distribution Utilizing STARS Simulator (Run 6).

From time 28.8 to 48 minutes, the combustion front temperature seam to have the exact start between the experiment and the predicted as shown in Figure 4.177. The simulation maximum peak temperature are much higher than the measured experimentally.

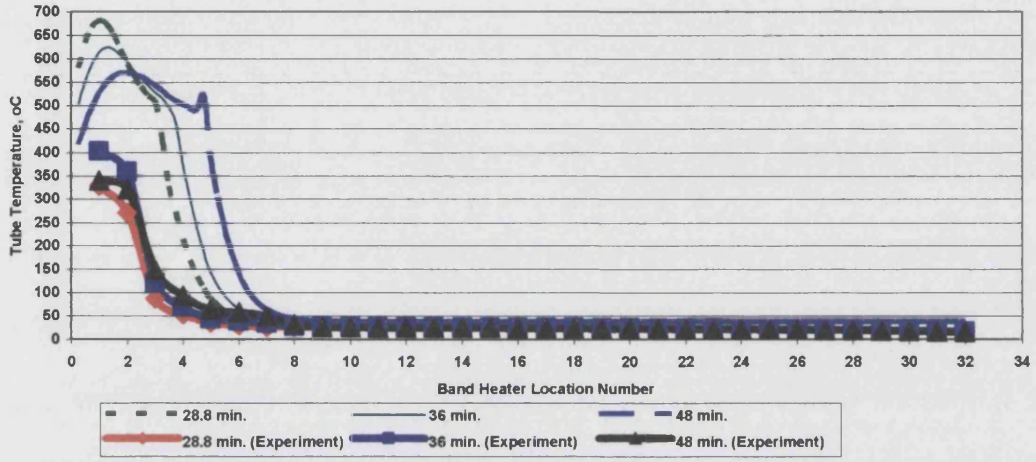

Figure 4.177: Experimental and Predicted Axial Temperature profile in Limestone Core, at Time 28.8, 36 and 48 minutes.

Figures 4.178, 4.179 and 4.176 shows the same phenomena. The start of temperature rising are just about the same between the experimental and STARS temperature profile from time 60 to 180 minutes.

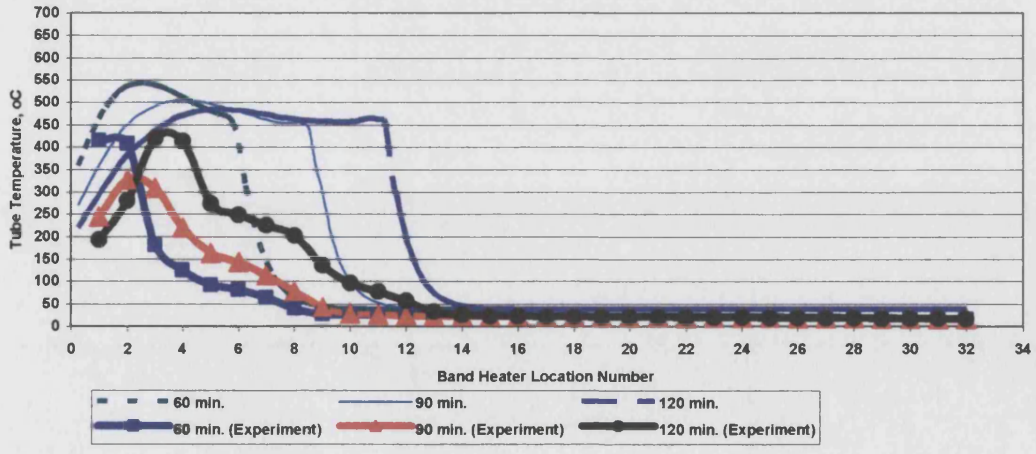

Figure 4.178 : Experimental and Predicted Axial Temperature profile in Limestone Core, at Time 60, 90 and 120 minutes.

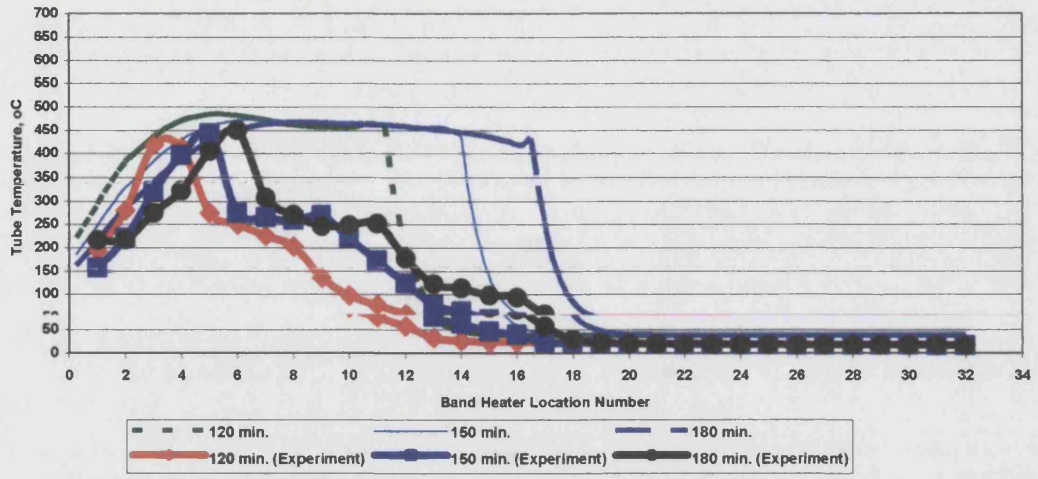

Figure 4.179: Experimental and Predicted Axial Temperature profile in Limestone Core, at Time 120, 150 and 180 minutes.

At time 210 minutes, the start up rising due to combustion front seam to be closed, but fare way at 240 minutes, (Figure 4.180). Generally, if the combustion occur in the edges and not in the middle of the combustion tube where axial thermocouples located; falls prediction can be caused easily.

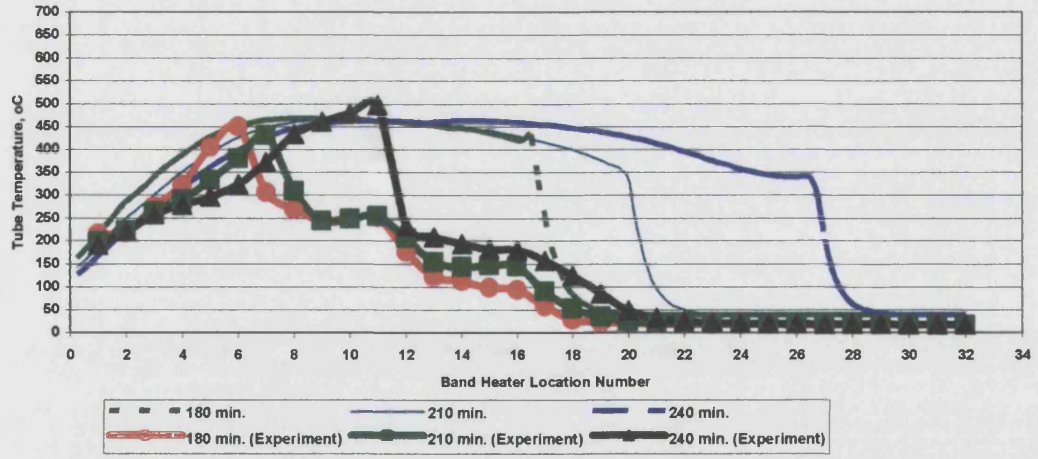

Figure 4.180 : Experimental and Predicted Axial Temperature profile in Limestone Core, at Time 180, 210 and 240 minutes.

The combustion front temperature are much closed to maximum peak temperature due to low air injection rate as illustrated in Figure 4.181. The estimated Combustion front temperature of the actual test and the simulator shows matching each others. The average temperature located between 450 and 500°C.

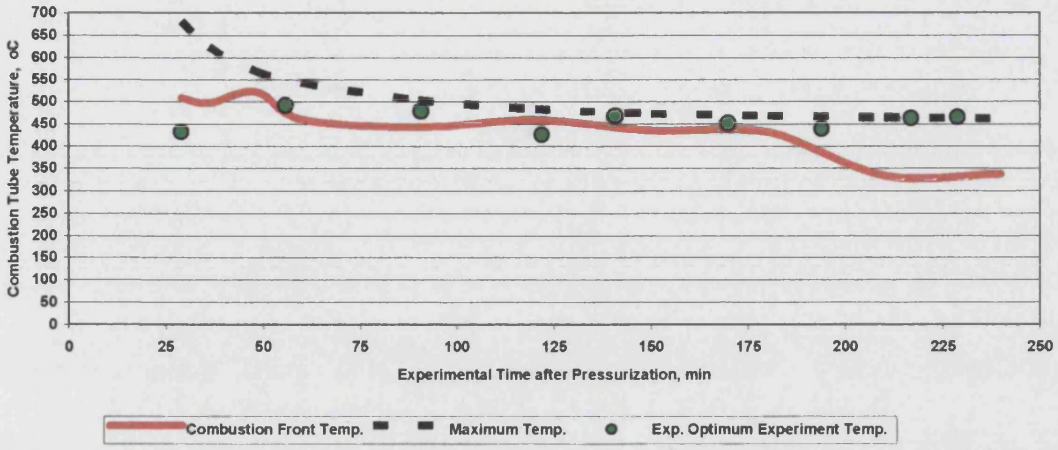

Figure 4.181: Combustion Front and Maximum Temperature Utilizing STARS Simulator and Experiment (Run 6).

Figure 4.182 shows more steady of combustion front velocity (0.38 cm/min.) all the way to time of 200 minutes, then gradual increase to 0,85 cm/min. at the end of the experiment. The estimated velocity of the combustion front seem to be closed to the measured from the test.

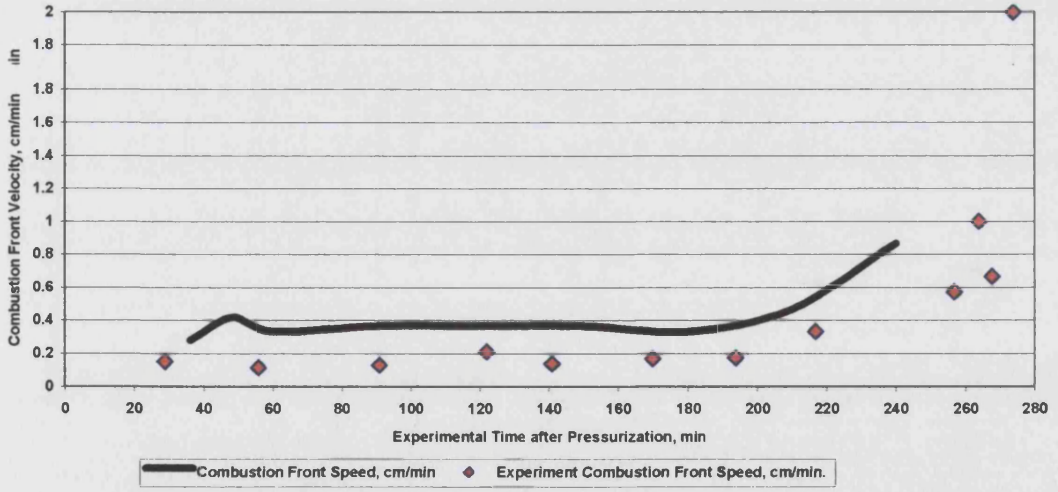

Figure 4.182: Combustion Front Velocity Utilizing STARS Simulator and Experiment (Run 6).

Figure 4.183 shows the value of CO_2 produced similar to the predicted, but different in trend in CO. STARS produce 6.8% while the experiment 2%. As it mentioned previously this values are apart from each others due to adjusting other parameters.

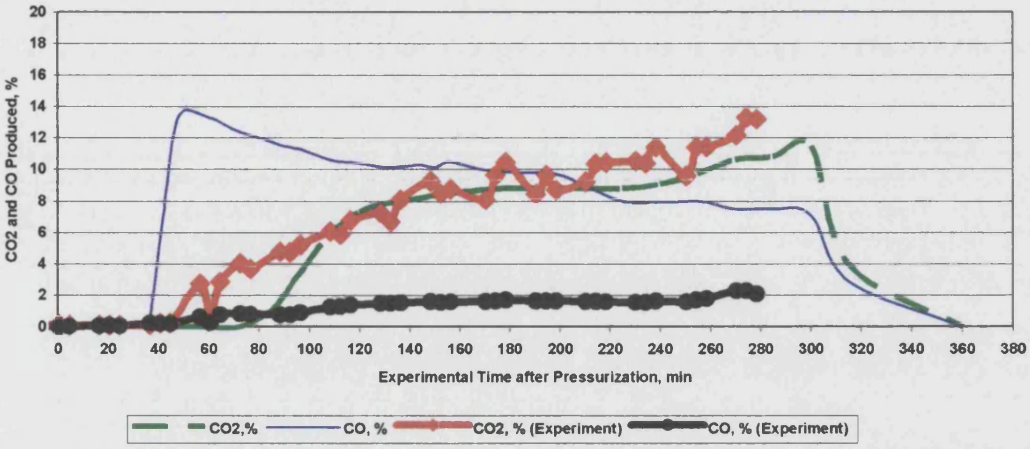

Figure 4.183: CO_2 and CO Recovered Utilizing STARS Simulator and Experiment (Run 6).

The oil recovery in run 6 seems to be exactly as predicted by STARS. Figure 4.184 presents both STARS and experiment oil and water recovery. The predicted water recovery higher than the produced experimentally.

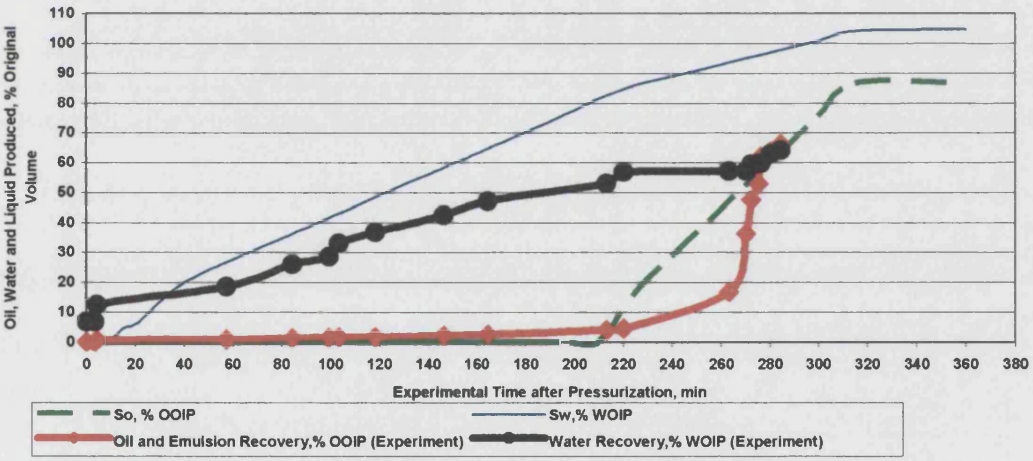

Figure 4.184 : Oil and Water Recovery Utilizing STARS Simulator and Experiment (Run 6).

RUN 8 SIMULATION :

To maintain average gas production rate of 42 m^3/m^2hr, it require 52.3 m^3/m^2hr air injection rate.

The predicted temperature profile of run 8 conducted by STARS can be shown in Figure 4.185. The general shape of the curves similar to run 4.

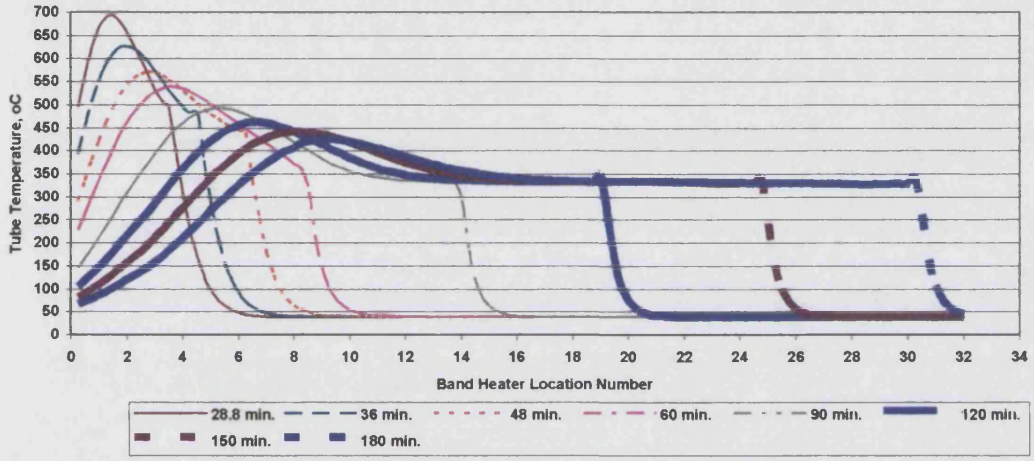

Figure 4.185 : Temperature Distribution Utilizing STARS Simulator (Run 8).

At time 28.8 minutes the combustion front began between BH7 and BH8 for both experiment and STARS, but at 36 minutes the experiment combustion front moved faster than STARS as shown in Figure 4.186.

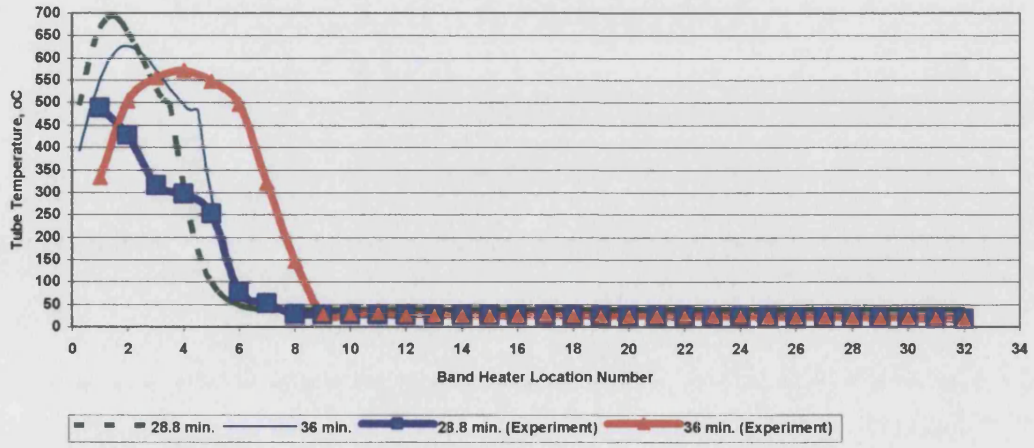

Figure 4.186 : Experimental and Predicted Axial Temperature profile in Limestone Core, at Time 28.8 and 36 minutes.

Similar peak temperatures were gained between 48 to 60 minutes as shown in Figure 4.187, but the combustion front in the experiment moved more faster than the simulator.

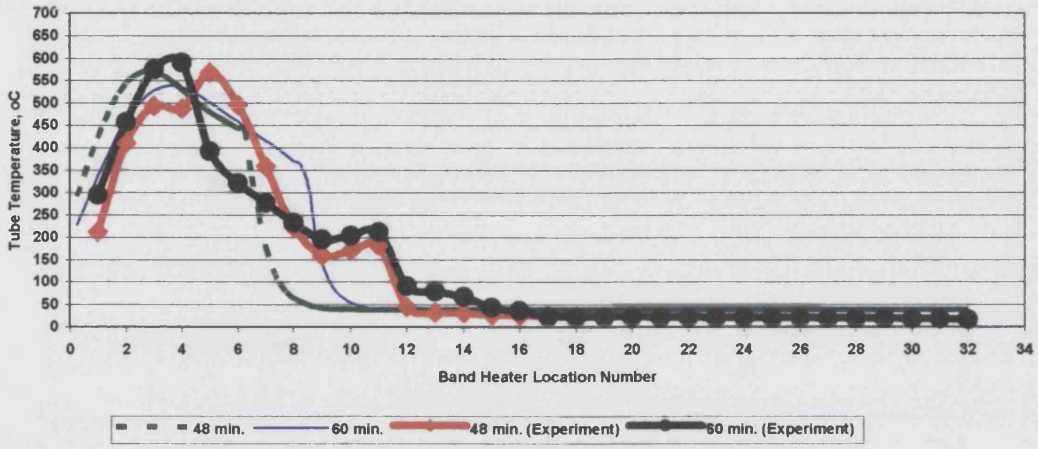

Figure 4.187: Experimental and Predicted Axial Temperature profile in Limestone Core, at Time 48 and 60 minutes.

Same things occurred between 90 and 120 minutes, but the shape of the curves are more or less similar as presented in Figure 4.188.

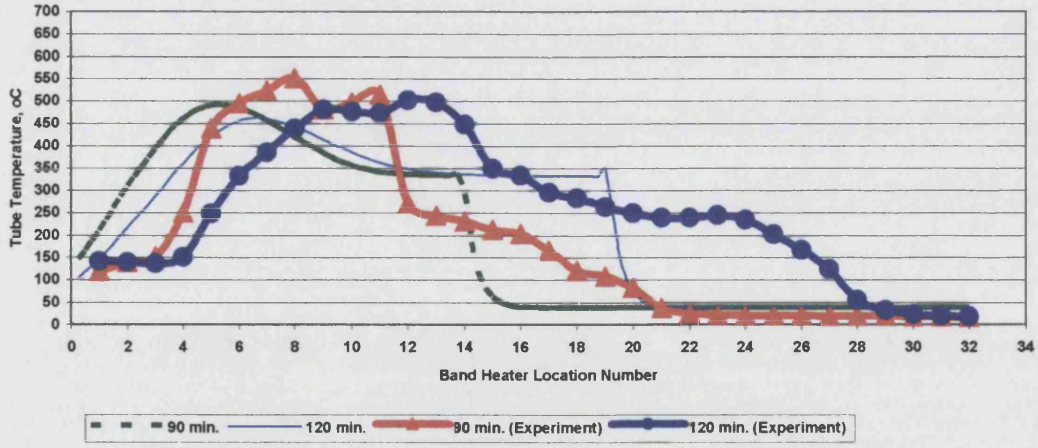

Figure 4.188: Experimental and Predicted Axial Temperature profile in Limestone Core, at Time 90 and 120 minutes.

Figure 4.189 shows that most of the tube still under high temperature due to combustion enlarging (wide).

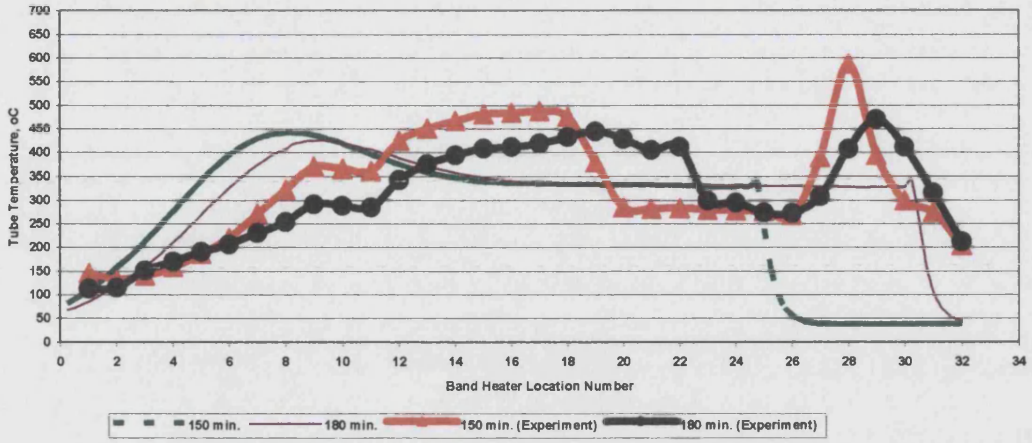

Figure 4.189: Experimental and Predicted Axial Temperature profile in Limestone Core, at Time 150 and 180 minutes.

The combustion front and the maximum peak temperature utilizing STARS are shown in Figure 4.190, it is clear that there are considerable difference specially when the ignition start and the combustion start moving down the tube. The optimum experiment temperature shows very closed agreement with the maximum temperature estimated from STARS.

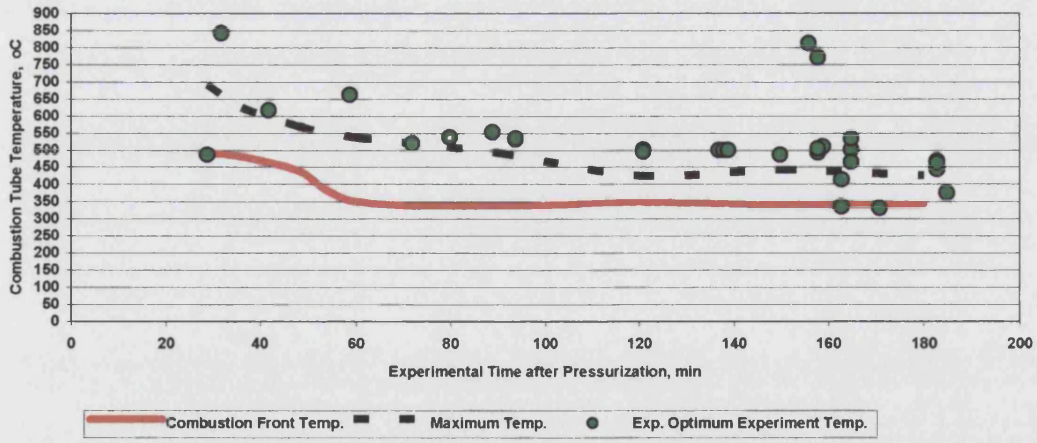

Figure 4.190: Combustion Front and Maximum Temperature Utilizing STARS Simulator (Run 8).

The average combustion front velocity is 0.75 cm/min. as show in Figure 4.191. The estimated combustion front speed are identical with the measured from the experiment.

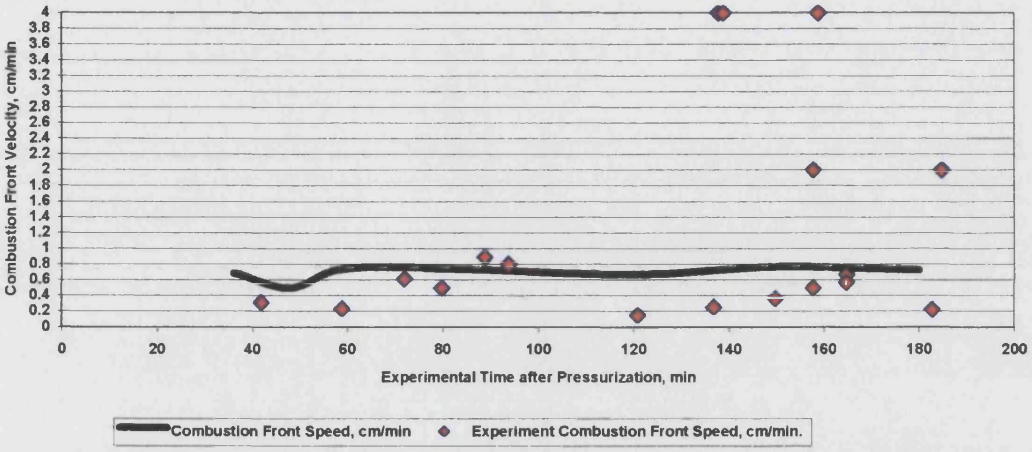

Figure 4.191: Combustion Front Velocity Utilizing STARS Simulator (Run 8).

The CO_2 produced in the experiment seem to breakthrough the combustion tube before what predicted by STARS, as shown in Figure 4.192. The late value of CO_2 produced reach to about 15% in the experiment by the simulator shows only about 12%.

There is about 4 to 5 % difference between the estimated and measured value of CO, also, difference in entire general trend.

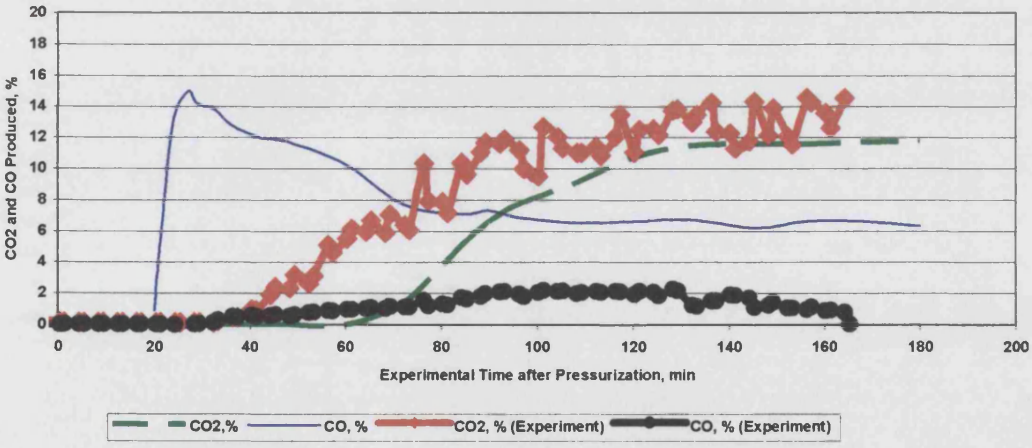

Figure 4.192: CO_2 and CO Recovered Utilizing STARS Simulator and Experiment (Run 8).

The oil recovery experimentally is just about same as predicted by STARS. As it was mentioned before that there was some water in oil emulsion that make the value little higher, see Figure 4.193.

The value of water produced is less than the predicted; it may be due to the end effect of the wetting phase (water). Also the percentage of water used was low, the percentage of error can becomes high in big combustion system.

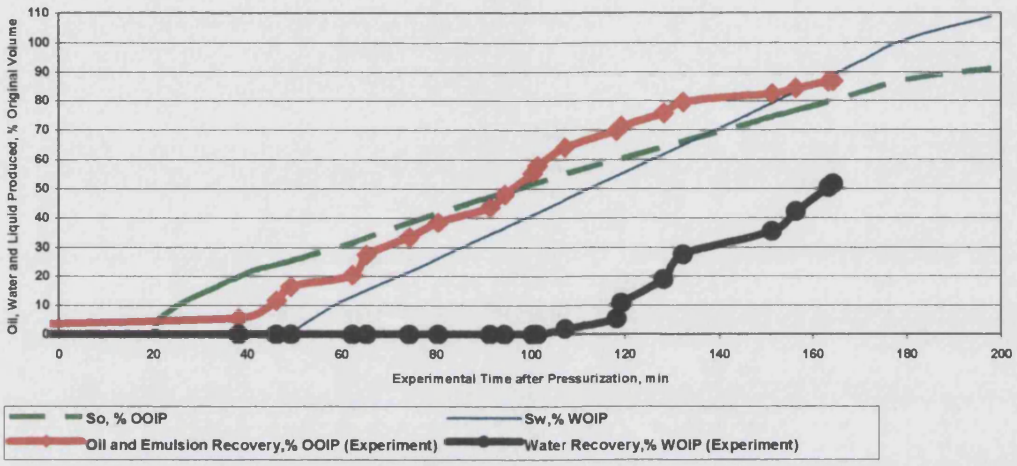

Figure 4.193: Oil and Water Recovery Utilizing STARS Simulator and Experiment (Run 8).

RUN 9 SIMULATION :

Run 9 was conducted at lower pressure of 100 bar. The predicted air injection flow rate as obtained by STARS is 67.8 m^3/m^2hr, which gives 62.65 m^3/m^2hr as average gas mass flow rate similar to experiment. The temperature distributions profile of STARS is shown in Figure 4.194. The maximum peak temperature where delayed at the very rear of the curves. However, it is believed due to the presence of coke left behind and high speed of moving the combustion front.

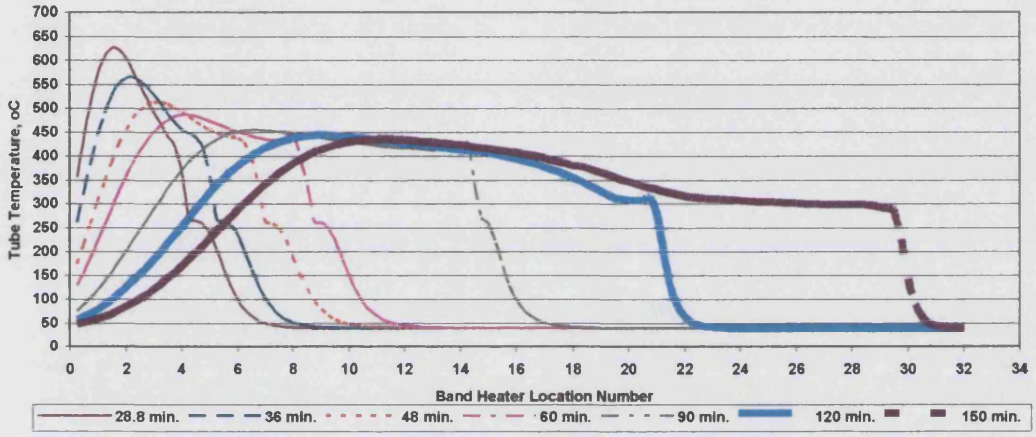

Figure 4.194 : Temperature Distribution Utilizing STARS Simulator (Run 9).

Similar peaks temperatures were predicted during time from 28.8 to 36 as shown in Figure 4.195.

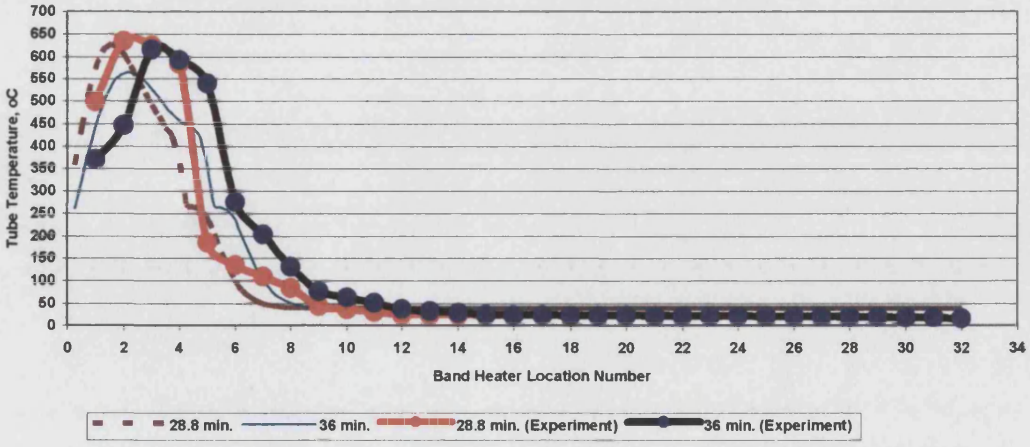

Figure 4.195: Experimental and Predicted Axial Temperature profile in Limestone Core, at Time 28.8 and 36 minutes.

Figures 4.196 and 4.197 presents the temperature profile from time 48 to 120 minutes. It is very clear that the experiment temperature profile moved faster compared to the predicted by STARS. This may be caused by channelling of oxygen causing an extension of fire farther ahead.

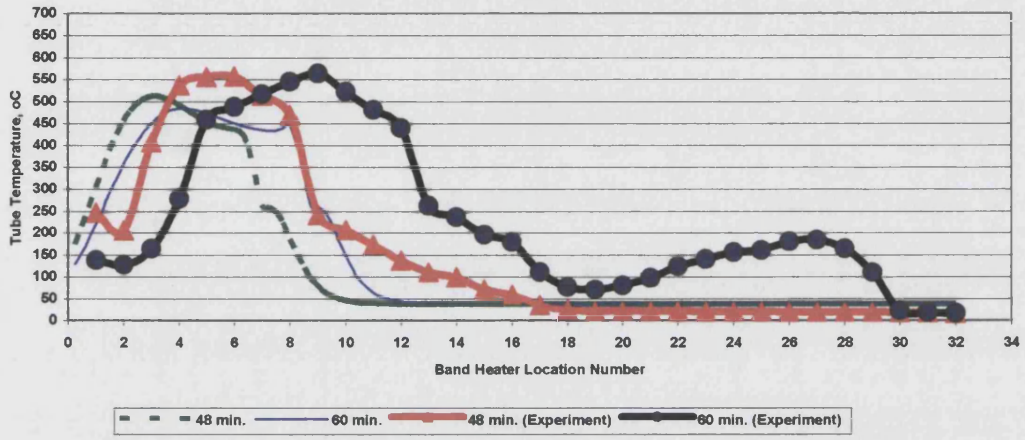

Figure 4.196: Experimental and Predicted Axial Temperature profile in Limestone Core, at Time 48 and 60 minutes.

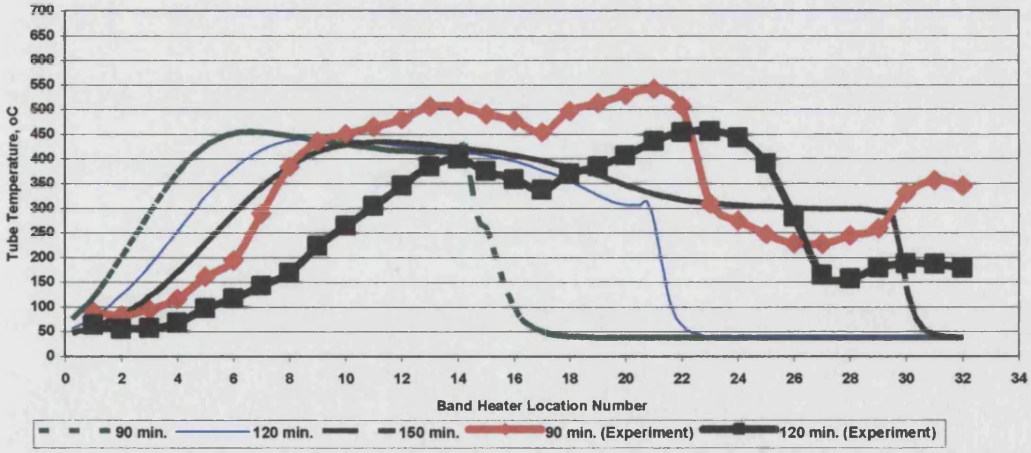

Figure 4.197: Experimental and Predicted Axial Temperature profile in Limestone Core, at Time 90 and 120 minutes.

The difference between the combustion front temperature and maximum peak temperature seem to be high at the beginning of the test and late at the end as shown in

Figure 4.198. The overall trend of the optimum peak temperatre seem to be similar to the estimated by stars. The experimental measurement shows about 50 °C higher than the estimated by STARS.

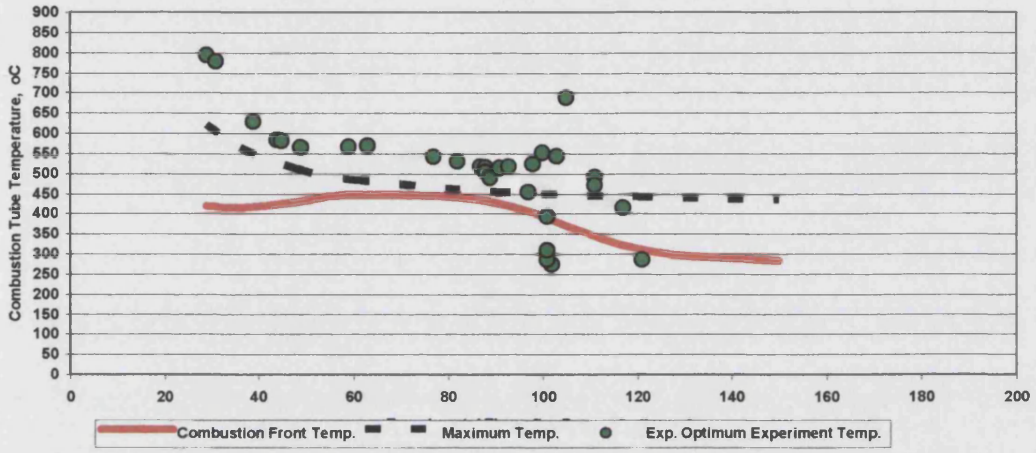

Figure 4.198: Combustion Front and Maximum Temperature Utilizing STARS Simulator (Run 9).

The combustion front velocity was increased rabidly from 0.5 cm/min. to about 1.2 cm/min. at the end of the experiment as shown in Figure 4.199. Experiment combustion front speed shows more fluctuation than the estimated by STARS. However, it should be emphasize that at low pressure, the speed of the combustion move some times faster depend of the permeability and solidification of coke just ahead of front.

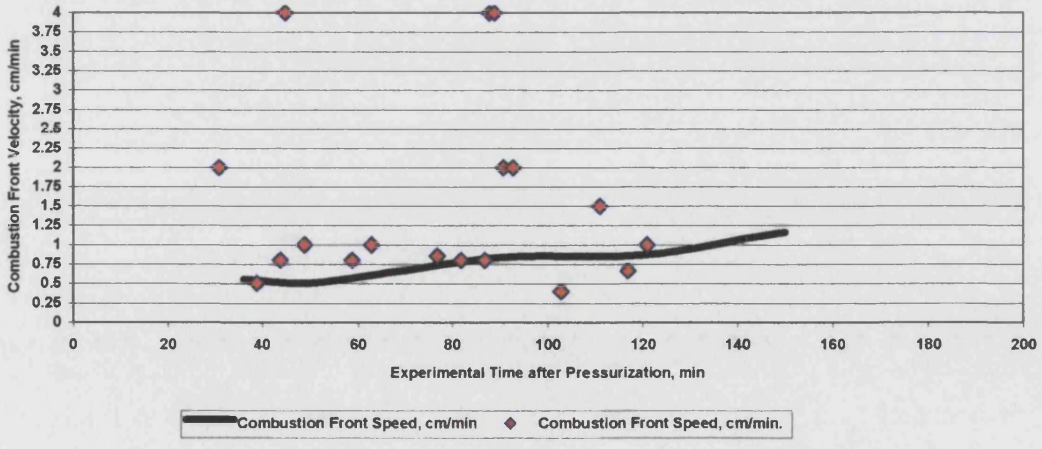

Figure 4.199 : Combustion Front Velocity Utilizing STARS Simulator (Run 9).

Considerable increase in CO_2 produced during experiment then decreased to about 10% which mach the value predicted by STARS, then increase again to about 16%. No similarity in the trends of CO. The last value predicted was about 9% but the produced about 2% as shown in Figure 4.200.

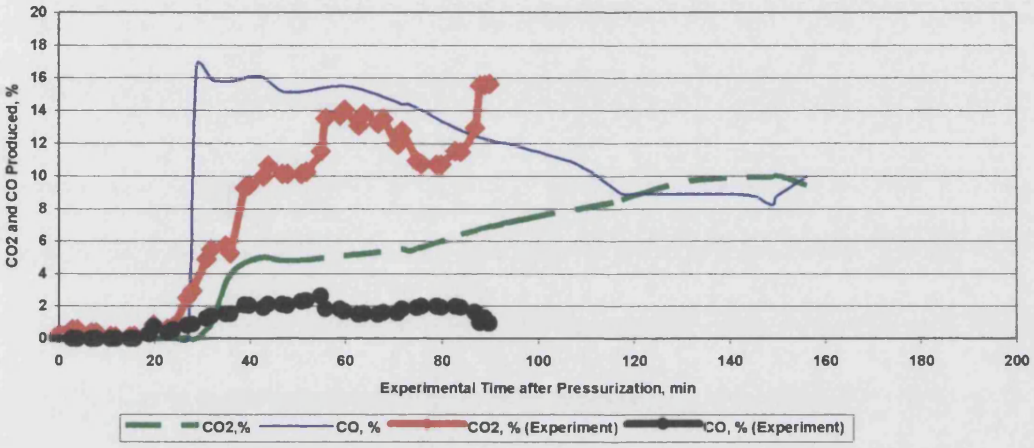

Figure 4.200: CO_2 and CO Recovered Utilizing STARS Simulator and Experiment (Run 9).

The water produced utilizing STARS appear to have the same trend as the produced during the experiment as shown in Figure 4.201. Similar and parallel trend, in the oil recovery between the predicted and the actual recovered experimentally. Here again, the delay of oil recovery by STARS due to the assumption of forming oil bank just ahead of the combustion front and at the end of the displacement (piston displacement).

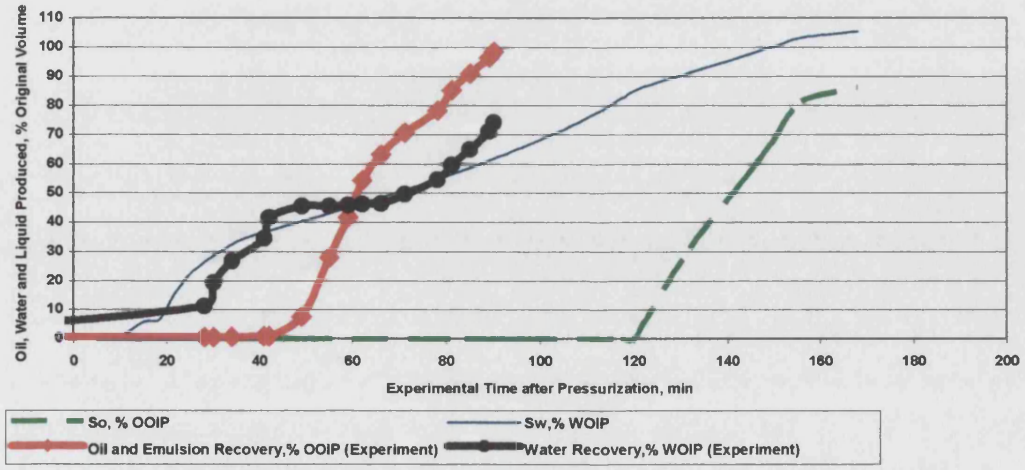

Figure 4.201: Oil and Water Recovered Utilizing STARS Simulator and Experiment (Run 9).

CHAPTER FIVE

CONCLUSIONS AND RECOMMENDATIONS

Conclusions:

The main conclusions arising from the research are:

1. Light Ekofisk crude oil (42°API), contained in a matrix of crushed MI limestone, at high pressure (200 bar) can sustain high temperature, propagating in situ combustion. The combustion tube tests were conducted at relatively high air injection rates, equivalent to range of injection flux of 20 – 100 $m^3/hr\ m^2$. The combustion front temperature varied from 550 – 600°C, as the air injection rate increased. However, none of the combustion tube tests operated adiabatically, because of poor band heater control. The minimum air flux required to sustain combustion front propagation, without band heater compensation, was 21 $m^3/hr\ m^2$.

2. If the air injection flux is too high, then significant channeling of oxygen can occur ahead of the combustion front, giving rise to LTO effects. This was manifested in the formation of viscous, or emulsified oil, very high temperature zones ahead of the combustion front up to 850°C (due to oxygen radicals accumulating in the oil). Low temperature oxidation of the oil produced strong acids, causing dissolution of the MI limestone. The high temperatures produced, calcite agglomerations, which had a very high void porosity. At low air injection fluxes, less than 21 $m^3/hr\ m^2$, oil banking occurred. This primarily acts to delay the start of oil production.

3. Oil recovery depends greatly on the initial oil saturation. At a water flooded oil residual of 30%, the oil recovery was 64%. At Soi = 70%, the oil recovery was 86.7%.

Recommendations:

1. Satisfactory adiabatic control of the combustion tube was not achieved for most of the experiments. This was due to the inability of the present computer to cope with the multitasking requirements of data acquisition , especially the high tasking priority set on pressure control of the shell and combustion tube. Thus band heaters control was assigned a lower priority. Therefore, a more powerful computer is required, with at least 2.5 Mb, or greater. It may be advisable to have a dual processor machine.
2. The LABView software should be updated to the latest edition. Also, all of the signal input card should be checked, and any faulty cards replaced.
3. Although the band heater power supply was thoroughly checked for the present experiment and certain improvement made, i.e. on-off status for each band heater, further detailed testing required to ensure completely satisfactory operation.
4. The axial thermocouples probe needs to be refurbished to replace the two inactive thermocouples.
5. Further tests, under adiabatic control should be controlled to see what the effect of adiabatic versus non-adiabatic states.
6. The band heater control is influenced by the injection of cold nitrogen needed to replace the bleed-off as a result of heating-up during an experiment. One solution could be replaces the 'on-off' solenoid bleed valve on the shell with a continues automatic valve, which should reduce the amount of nitrogen from the shell.

REFERENCES

REFERENCES

1 - Abu-Khamsin S. A., Brigham W. E., and Ramey Jr H. J. " Reaction Kinetics of Fuel Formation for In-Situ Combustion" SPE 15736, Presented at the 5th SPE Middle East Oil Show, Manama Bahrain, March 7-10, 1987.

2 - Adegbesan K. O., Donnelly J. K., Moore R. G., and Bennion D. W. "Low Temperature Oxidation Kinetic Parameters for In-Situ Combustion Numerical Simulation" SPE 12004, presented at the 58th Annual Technical Conference and Exhibition of SPE-AIME, San Francisco, CA, Oct. 5-8 1983.

3 - Alexander J.D., Martin W.L., and Dew J.N. "Factors Affecting Fuel Availability and Combustion During In-situ Combustion", JPT, October 1962, pp 1154-1164.

4 - Al-Saffar H., Price D., Soufi A., and Hughes R. "Distinguishing between Overlapping Low Temperature and High Temperature Oxidation Data obtained From a Pressurised Flow Reactor System Using Consolidated Core Material", Fuel 79(2000) 723-732.

5 - Amoco Energy Group North America "West Hackberry Tertiary Project (Quarterly Technical Progress Report)", Report 1/1/97 – 3/31/97.

6 - Babu D.R., and Cormack D.E. "Effect of Low-Temperature Oxidation on the Composition of Athabasca Bitumen", Fuel 1984, Vol. 63, June pp 858-861.

7 - Bae J. H. "Characterization of Crude Oil for Fireflooding Using Thermal Analysis Methods" Soc. Pet. Eng. J. (June, 1977) pp 211-18.

8 - Bagci A.S., Kok M.V., and Okandan "Combustion Reaction Kinetics in Limestones Containing Heavy Oils", SPE 15737, Paper presented at the Fifth SPE Middle East Oil Show Manama, Bahrain, March 7-10, 1987.

9 - Behar F., Ungere P., and Audibert A., and Villalba M. "Experimental Study and Kinetic Modelling of Crude Oil Pyrolysis in Relation to Thermal Recovery Processes", FOURTH UNITAR/UNDP Conference on Heavy Crude and Tar Sands. Paper No. 97.1988.

10 - Belgrave J. D. M. , Moore R. G., and Benion D. D. " The Thermal Behaviour of Vertically Operated Near Adiabatic In Situ Combustion Tubes" Journal of Petroleum Science and Engineering, 5, 1990, pp 51-65.

11 - Belgrave J.D.M., Moore R.G. and Ursenbach M.G. "Comprehensive Kinetic Models for the Aquathermolysis of Heavy Oils", paper presented in Petroleum Society of CIM, Calgary, Alberat, June 21-15, 1994.

12 - Belgrave J.D.M., Moore R.G., and Ursenbach M. G. "Gas Evolution From The Aquathermolysis of Heavy Oils", The Canadian journal of Chemical Engineering, Volume 72, June, 1994.

13 - Bousaid I.S., and Ramet H.J. "Oxidation of Crude Oil in Porous Media" SPEJ, June 1968, pp137-148.

14 - BP Review "More than Just Hot Air", August 2000.

15 - Briggs P.J., Baron R.P., Fulleylove R.J., and Wright M.S. "2Development of Heavy-Oil Reservoirs", JPT , Feb 1988, pp206-214.

16 - Burger J., Sourieau P., and Combarnous M., "Thermal Methods of Oil Recovery" 1985, Editions Technip, Paris, 1985, pp 247-307.
17 - Burger J.G. and Sahuquent B.C. "Laboratory Research on Wet Combustion", JPT (Oct. 1973) 1137-46.
18 - Burger J.G., and Sahuquet B.C., "Chemical Aspects of In-Situ Combustion-Heat of Combustion and Kinetics", SPEJ, October 1972, pp 410-422.
19 - Buxton T.S., and Craig F. F. " Effect On Injection Air Ratio and Reservoir Oil Saturation on the Performance of a Combination of Forward Combustion and Water Flooding", AIChE Symposium No. 127, Vol. 69, pp 27-30.
20 - Chu C. "State-of-Art Review of Fire Field Projects"SPE of AIME , January 1982, pp 19-25.
21 - Chu C. "Two Dimensional Analysis of a Radial `Heat Wave" Trans. AIME 1964 pp 85-95.
22 - Dabbous M.K., and Fulton P.F. "Low-Temperature-Oxidation Reaction Kinetics and Effect on the In-Situ Combustion Process", SPEJ, June 1974, pp253-262.
23 - Dew J.N., and Martin W.L. " Air Requirements for Forward Combustion", Part2, Petroleum Engineering (Jan. 1965) 82-85.
24 - Dietz D. N. and Weijdema J. "Wet and Partially Quenched Combustion" Journal of Petroleum Technology, April 1968, pp 411-415.
25 - DON W. Green & G.Paul Will Hite, "Enhanced Oil Recovery", Texas, 1998.
26 - Drici O., and Vossoughi S. "Study of the Surface Area Effect on Crude Oil Combustion by Thermal Analysis Techniques" JPT, April 1985, pp731-735.
27 - Dubdud I., Huges R., and Price D. "Kinetics of In situ Combustion of Athabasca Tar Sands Studied in A Differential Flow Reactor" Trans IChemE, Vol. 68, Part A, July 1990.
28 - El Ayadi O. H. "High Pressure In-Situ Combustion Studies- Commissioning Development and Combustion Tests" MPhil Theses, University of Bath, 1993
29 - El-Usta S. "High Pressure combustion tube studies of medium and light oil" PhD thesis, University of Bath, 1998.
30 - Farouq Ali, S. M.: " Redeeming of In-situ Combustion" Proceedings DOE/NIPER Symposium on In-Situ Combustion Practices-Past", paper No ISI 1 Present and Future Applications, Tulsa, Oklahoma, 21-22 April 1994.
31 - Fassihi M. R., Meyers K.O., and Weisbrod K. R. " Thermal Alteration of Viscous Crude Oils", Society of Petroleum Engineers Papers 14225, presented at the SPE Annual Technical Conference and Exhibition, Las Vegas, September 22-25, 1985.
32 - Fassihi M. R., and Gilliham T. H. " The Use of Air Injection to Improve the Double Displacement Processes" SPE 26374, 68th Annual Technical Conference and Exhibition, Houston, Texas, October 3-6, 1993.
33 - Fassihi M. R., Brigham W. E., and Ramey H. J. "The Reaction Kinetics of In-Situ Combustion", SPE 9454: presented at the 55th Annual Technical Conference and Exhibition, Dallas, Texas, 21-24 Sep. 1980.
34 - Fassihi M.R., Brigham W.E., and Ramey H.J. "Reaction Kenetics of Insitu Combustion: Part 1 – Observations" SPEJ, August 1984, pp 399-407.
35 - Fassihi M.R., Brigham W.E., and Ramey H.J. "Reaction Kinetics of In-situ Combustion: Part 2 – Modeling" SPEJ, August 1984, pp 408-416.
36 - Fassihi M.R., Meyers K.O., and Baslle P.F. "Low-Temperature Oxidation of Viscous Crude Oils" SPE Reservoir Engineering, November 1990, pp 609-616.

37 - Fassihi M.R., Yannimaras D.V., and Kumar V.K. "Estimation of Recovery Factor in Light Oil Air Injection Projects" SPE 28733, Paper presented at the SPE International Petroleum Conference & Exhibition of Mexico held in Veracurz, Mexico. 10-13 October 1994.

38 - Fassihi M.R., Yannimaras D.V., Westfall E.E., and Gillham T.H. "Economics of Light Oil Air Injection Projects", SPE/DOE 35393, Paper presented at the 1996 Light Oil Air Injection Projects", SPE/DOE 35393, Paper presented at the 1996 SPE/DOE Tenth Symposium on Improved Oil Recovery held in Tulsa, OK, 21-24 April 1996.

39 - Garon A.M., Kumar M., Lau K.K., and Sherman M.D. "A Laboratory Investigation of Sweep During Oxygen and Air Fireflooding", SPE Reservoir Engineering, Nov. 1986 , pp 565-574.

40 - Germain P., and Geyelin J.L. "Air Injection Into A Light Oil Reservoir: The Horse Creek Project" SPE 37782, Paper presented at the 1997 middle East Oil Show held in Bahrain 15-18 March 1997.

41 - Gillham T.H., Cerveny B.W., Fornea M.A., and Bassiouni Z. "A New/Economically Viable EOR Process for the U.S. Gulf Coast", World Oil/ November 1997, pp47-50.

42 - Greaves M. , Tuwil A. A. and Field R. W. "Horizontal Producers Wells in In-Situ Combustion Processes" CIM/AOSTRA Annual Technical Conference, Banff, Canada 21-24 April 1991.

43 - Greaves M., and Saghr A. M. "A New Horizontal Well Concept for IOR from Light Oil Reservoirs Using Air Injection" the 1997 European Symposium on IOR, The Hague, 20-22 Oct. 1997.

44 - Greaves M., El-Saker A., and Xia T.X. "Thai-New Air Injection Technology for Heavy Oil Recovery and InSitu Upgrading" The Petroleum Society, Paper 99-15.

45 - Greaves M., Field R.W., and Adewusi V.A. "Insitu Combustion Kinetic Studies of Medium Heavy Crude Oil", Chem Eng Res Des, Vol. 66, July 1988.

46 - Greaves M., Field R.W., and Al-Shalabe M.I. "Insitu Combustion Studies of North Sea Forties and Maya Crude Oils", Chem Eng Res Des, Vol. 65, January 1987.

47 - Greaves M., Rathbone R.R., Hughes R., and Price D. "The Exothermicity and Oxidative Kinetics of North SEA Light Crude Oils for Air Injection IOR Processes"Report case for support, University of Bath.

48 - Greaves M., Ren S.R., and Rathbon R.R., Fishlock T., and Ireland R. "Improved Residual Light Oil Recovery by Air Injection (LTO) Process)", Journal of Canadian Petroleum Technology, January 2000, Volume 39, No. 1, pp57-61.

49 - Greaves M., Ren S.R., and Rathbone R.R. "Air Injection for IOR from Light-Oil reservoirs: Oxidation Rate and Displacement Studies", JPT January 1999, pp 46-48.

50 - Greaves M., Ren S.R., and Xia T.X. "New Air Injection Technology for IOR Operations in Light and Heavy Oil Reservoirs" SPE 57295, presented at the 1999 SPE Asia Pacific Imroved Oil Recovery Conference to be held in Kuala Lumpur, Malysia, 25-26 Octobar 1999.

51 - Greaves M., Wilson A., Al-Honi M., and Lockett A.D. "Improved Recovery of Light/Medium Heavy Oils in Hetrigeneous Reservoirs using Air Injection/ Insitu Combustion (ISC)", SPE 35693, Paper at the Western Regional Meeting, Anchorage, Alaska, 22-24 May 1996.

52 - Greaves M., Young T.J., El-Usta S., Rathbone R.R., Ren S.R., and Xia T.X. "Air Injection Into Light and Medium Heavy Oil Reservoirs: Combustion Tube Studies on West of Shetlands Clair Oil and Light Australian Oil", Trans IChemE, Part A, Chem Eng Res Des, 78: 721-730 (2000).
53 - Hansel J.G., Benning M.A., and Fernbacher J.M. "Oxygen In-Situ Combustion for Oil Recovery : Combustion Tests" JPT, July 1984, pp1139-1144.
54 - Hansel J.G., Benning M.A., and Fernbacher J.M. "Oxygen In-situ Combustion For Oil Recovery : Combustion Tube Tests" SPE 11253, January 1984.
55 - Hansel J.G., Benning M.A., and Fernbacher J.M. "Oxygen In-Situ Combustion for Oil Recovery: Combustion Tube Tests" JPR, July 1984, pp1139-1144.
56 - Hardy W. C., Fletcher P. B., Shepard J. C., Dittman E. W., and Zadow D. W. " In-Situ Combustion Performance in a Thin Reservoir Containing High Gravity Oil" Journal of Petroleum Technology, Feb. 1972 pp 199-208.
57 - Hughes R., Dubdub I., and Price D. " Kinetics of In Situ Combustion of Athabasca Tar Sands Studied in a Differential Flow Reactor" Trans IChemE, Vol. 68, part A, July 1990.
58 - Hughes R., Kamath V. M. and Price D. " Kinetics of In-Situ Combustion for Oil Recovery" Chem. Eng. Res Des. Jan. 1987, Vol.(65), pp 23-28.
59 - Hughes R., Kamath V.M., and Price D. "Kinetics of "In-Situ" Combustion for Oil Recovery", Chem Eng Res Des, Vol., 65, January 1987, pp 23-28.
60 - Hughes R., Kazi R., Oklany J. S. and Price D. " The Effect of Formation Type on Fuel Oxidation Relevant to the In Situ Combustion Process for the Recovery of Heavy Oil" IchemE Meeting, Leeds 2-3 April 1996.
61 - Hutchence K., and Freitag N. "An Alternative Approach To The Selction of Psedocomponents for Modelling In-situ Combustion", Petroleum Society of CIM and Canmet, paper No 21, pp21-1 to 21-6.
62 - Hvizdos L.J., Howard J.V., and Roberts G.W. "Enhanced Oil Recovery Through Oxygen-Enriched In-situ Combustion: Test Results from the Forest Hill Field in Texas", JPT, June 1983 pp1061-1070.
63 - Islam M. R., Chakma A., Farouq Ali S. M. "State of the Art In-Situ Combustion Modeling and Operation", SPE 18755, Claifornia Regional Meeting Bakerfield, April 5-7, 1989, pp 105-118.
64 - Islam M.R., and Farouq Ali S.M., Journal of petroleum science and Engineering, 1992,6, 367-379.
65 - Kazi R .A. "A high pressure kinetic study of the in-situ combustion process for oil recovery" PhD Thesis. University of salford, 1995.
66 - Kisler J.P., and Shallcross D.C. "An improved model for the oxidation processes of light crude oil" Trans IchemE 1997; 75:392.
67 - Kisman, K. E., and Lau E. C. "A New Combustion Process Utilizing Horizontal wells and Gravity Drainage", Journal of Canadian Petroleum Technology, 33, No. 3, 1994, pp39-45.
68 - Kok M.V., and C. Keskin "Comparative Combustion Kinetics for In-situ Combustion process", EAGE-10th European Symposium on Improved Oil Recovery, Brighton, UK, 18-20 August, 1999.
69 - Kok M.V., and Karacan O. "Pyrolysis Analysis and Kinetics of Crude Oils" Journal of thermal Analysis, Vol.52 (1998) 781-788.
70 - Kumar M., and Garon A.M. "A Method for Predicting Oxygen and Air Fireflooding Performance", SPE Reservoir Engineering, May 1991, PP 245-251.

71 - Lin C.Y., Chen W.H., Lee S.T., and Culham W.E. "Numerical Simulation of Combustion Tube Experiments and Associated Kinetics of In-Situ Combustion Processes" SPE 11074. and in Soc. Pet. Eng. J. Dec 1984.

72 - Lukyaa A.B.A., Hughes R., Millington A., and Price D. "Evaluation of A North SEA for Recovery by In Situ Combustion using High Pressure Differential Scanning Calorimetry", TransIChemE,Vol.72,Part A, March 1994.

73 - Majerrison D.M., and Fassihi M. R. " Morgan Pressure \Cycling In-Situ Combustion Project – Performance Modeling", 7th European IOR Symposium, Moscow, Russia, Oct. 27-29, 1993.

74 - Mamora D. D., and Brigham W. E. " The Effect of Low Temperature Oxidation on Fuel and Produced Oil During In-Situ Combustion of a Heavy Oil" In-Situ, 19 (4), 1993, pp 341-365.

75 - Mamora D.D., and Brigham W.E. "The Effect of Low-Temperature Oxidation on Fuel and Produced Oil During In-Situ Combustion" DOE/NIPER, paper presented at the DOE/NIPER, Symposium on In situ combustion Practices-Past and Applied in Tulsa, Oklahoma, April 21-22, 1994.

76 - Mamora D.D., and Brigham W.E. "The Effect of Low-Temperature Oxidation on the Fuel and Produced Oil During In-situ Combustion of a Heavy Oil" Marcel Dekker, Inc, 1995, pp341-365.

77 - Mattax Calvin C. and Robert L. " Reservoir Simulation" Dalton, First printing, Henry L. Doherty Memorial Fund of AIME Society of Petroleum Engineers Richardson, TX 1990.

78 - McNeil J. S. and Moss J. T. " In Situ Combustion" Oil and Gas Journal Vol. 56, No. 37 September 1958.

79 - Meyers K.O., Fassihi M.R., Basile P. F. " Low Temperature Oxidation of Viscous Crude Oil" SPE 15648, 61st Annual Technical Conference and Exibition of the SPE, New Orleans, Oct. 5-8, 1986.

80 - Millour J.P., Moore R.G., Bennion D.W., Ursenbach M.G. and Gie D.N. "An expanded compositional model for low-temperature oxidation of athabasca bitumen", Paper published in Journal of Canadian Petroleum Technology, May-June 1987, Montereal (pp 24-31).

81 - Moore R. G., Bennion D. W., Millour J. P., Ursenbach M. G., and Gie D. N. " Comparison of the Effect of Thermal Cracking and Low-Temperature Oxidation on Fuel Deposition During ISC" Proc. 1986 U.S> DOE Tar Sands Symposium Jackson WY July 1986 DOE/METC 87/6073.

82 - Moore R. G., Mehta (Raj) S. A., M. G. Ursenbach, and Laureshen C. J. " Strategies for Successful Air Injection-Based IOR Processes", Presented at the 7th Onternational Conference on Heavy Crude and Tar Sands, Beijing, China, October 27-30, 1998, Paper No. 135

83 - Moore R.G., Benion D.W., Belgrave J.D.M., Gle D.N., and Usenbach M.G. "New Insights into Enriched-Air In-Situ Combustion" JPT, July 1990, pp 916-923.

84 - Moore R.G., Laureshen C.J., Belgrave J.D.M., Ursenbach M.G., and Mehta S.A., "In-Situ Combustion in Heavy Oil Reservoirs: problems and perspectives", IN SITU, 21(1), pp 1-26, 1997.

85 - Moore R.G., Laureshen C.J., Mehta S.A., and Urensenbach M.G. "Observations and Design Considerations for Insitu Combustion Projects" Journal of Canadian Petroleum Technology, Paper:97-100, Special Edition 1999, Volume 38, No. 13.

86 - Moore R.G., Mehta S.A., Belgrave J.D.M., Urenbach M.G., Laureshen C.J., Weissan J.G., and Kessler R.V. "A Downhole Catalytic Upgrading Process for Heavy Oil Using In situ Combustion"The Petroleum Society, Paper 96-72 pp 1-10.

87 - Moss J. T., and Cady G. V. " A Laboratory Investigation of Oxygen Combustion Process for Heavy Oil Recovery", SPE 10706, presented at SPE Annual Technical Meeting, San Francisco, March 1982, pp 55-68.

88 - Naji H.S.A. and Poettman F.H. "Reservoir Engineering Equations for In-Situ Combustion",In Situ (1991) 15, No. 2, 175-94.

89 - Nelson T.W., and McNeil J.S. Jr. "How to Engineer an In-Situ Combustion Project", Oil & Gas J. (June 5, 1961) 58-65.

90 - Nzekwu B. I., Hallam R. J., and Willimas G.J. J. "Interpretation of Temperature Observations from a Cyclic-Steam/In-Situ Combustion Project" paper SPE 17389, March 23-25, 1988.

91 - Onyekonwu K. Pande M.O., and Brigham W.E. "Experimental and Simulation Studies of Laboratory In-Situ Combustion Recovery", SPE 15090, paper presented at the 56th California Regional Meeting of the Society Engineers held in Okland CA, April 2-4 1986

92 - Petit H. " In-Situ Combustion Experiments with Oxygen Enriched Air", In Situ 14 (1), 1997 pp 49-76

93 - Philips C.R. and Hsieh I. "Oxidation Reaction Kinetics of Athabasca Bitumen" Fuel, 1985, Vol.64, July pp985-989.

94 - Popp V.V., Dinulesue V.D. "Dehydration and Desalting of Heavy and Viscous Crude Oil Produced by In-situ Combustion", SPE 28539, presented at the 69th Annual Technical Conference and Exibition held in new Orleans, LA, USA, 25-28 Sept 1994.

95 - Pottaman F. H. , Schilson R. E. and Surkalo H. " Philosophy and Technology of In-Situ Combustion in Light Oil Reservoirs" 7th World Pet. Cong. Mexico City, May 1967 pp 487-498

96 - Prasad R.S., and Salater J.A. "High-Pressure Combustion Tube Tests", SPE/DOE 14919, paper presented at the SPE/DOE 5th Symposium on Enhanced Oil Recovery of the SPE and the DOE held in Tulsa, OK, April 20-23, 1986

97 - Prats M. " Thermal Recovery" , SPE Monograph Series, Society of Petroleum Engineers, Richardson, TX (1982) 7.

98 - Ranjbar M. and Push G. "Experimental Studies of Crude Oil Pyrolysis, Fuel Formation and Combustion in Relation to In-situ Combustion", Paper presented in Heavy Crude and Tar Sands-Hydrocarbons for 21th Centry

99 - Ranjbar M., and Pusch G. "Pyrolysis and Combustion Kinetics of crude oils, Asphaltenes and Resine in Relation to Thermal Recovery Processes" Journal of analysis and Applied Pyrolysis, 20(1991) 185-196, Elsevier Science Publishers B.V.,Amesterdam.

100 - Rashidi F. and Bagci S. "Effect of Pressure and Clay content on Combustion Kinetics of Heavy Oil in Limestone Medium", Presented in Heavy Crude Tar Sands-Hydrocarbons for the 21th Centry

101 - Reed R. L., reed D. W., and Tracht J. H. " Experimental Aspects of Reverse Combustion in Tar Sands", Trans. AIME 219, 1960 pp 99-108.

102 - Ren S.R., Greaves M., Rathbone R.R. "Air Injection LTO Process: An IOR Technique for Light-Oil Reservoirs", SPEJ, March 2002, pp 90-99.

103 - Sakthikumar S., Madaoui K., and Chastang J. "An Investigation of the Feasibility of air Injection Into A Waterflooded Light Oil Reservoir" SPE 29806, Paper presented at the SPE Middle East Oil Show held in Bahrain 11-14 March 1995.

104 - Sarma H.K., Yazawa N.and Kumagai N. "Evaluation of Air Injection Potential for Three Light-Oil Reservoirs"Technology Research Center, Japan National Oil Corporation-Japan.

105 - Schumacher M. M. " Enhanced Recovery of Residual and Heavy Oil" 2nd ed, Noyes Data Corporation, New Jersey, USA (1980).

106 - Shahani G.H. and Gunardson H.H. "Oxygen Enriched Fire Flooding" paper presented at the at the DOE/NiperSymposium on In Situ Combustion Practices, and in Tulsa , Oklahoma, April 21-22, 1994

107 - Shahani G.H., and Hansel J.G. "Oxygen Fireflooding: Combustion Tube Tests With Light, Medium, and Heavy Crude Oils" SPE Reservoir Engineering, November 1987, 583-590

108 - Shallcross D. C., de los Rios C. F., Castanier L. M. and Brigham W. E. "Modifying In-Situ Combustion Performance by the use of Water-Soluble Additives", Soc. Pet. Eng. J., Aug. 1991, pp 287-294.

109 - Sibbald L. R., Moore R. G., and Bennion D. W. "In-Situ Combustion Process Study With a Combined Experimental/Analytical Approach" SPE Paper 18074, Presented at the SPE Annual Technical Conference and Exhibition Houston Oct 2-5, 1988

110 - Soodhoo K., and Philips C.R. "Non-Catalytic Hydrocracking of asphaltenes (Reaction Kinetics)" Fuel, 1988, Vol. 67, April, 521-529

111 - Surguchev L.M., Koundin A., and Yannimaras D. "Air Injection-Cost Effective IOR Method to Improve Oil Recovery from Depleted and Waterflooded Fields" SPE 57296, Paper presented at the 1999 SPE Asia Pacific Improved Oil Recovery Conference (APIORC), 25-26 October 1999.

112 - Tadema H. J. "Mechanism of Oil Production by Underground Combustion" Proc. 5th World Pet. Cong. New York City, May 1959. Sec II Paper No. 22, 279-287.

113 - Terwilliger P.L., Clay R. R., Wilson L. A. Jr., and Gonzalez-Gerth E. " Fireflood of the P_{2-3} Sand Reservoir in the Miga Field of Eastern Venezuela" SPE 4765, SPE – AIME IOR Symposium, Tulsa Apr. 22-24, 1974

114 - Tiffin D.L. and Yannimaras D.V. "The insitu Combustion performance of light Oils as A Function of Pressure (1000 to 6000 psig)" In Situ2, 47-64 (1997)

115 - Tiffin D.L., and Yannimaras D.V. "High Pressure Combustion Tube of Light Oils", Paper Presented at the 8th. Eurobean IOR-Symposium in Viena, Austria, May 15-17,1995, pp265-271

116 - TsuZuki N., Takeda N., Suzuki M., and Yokoi K. "The Kinetic Modeling of Oil cracking by Hydrothermal Pyrolysis Experiments" International Journal of Coal Geology 39(1999) 227-250.

117 - Turta A. "Insitu Combustion – From Pilot to Commercial Application", DOE/NIPER Symposium on In Situ Combustion Practices – Past, Present and Future Application, Yulsa, April 21-22, 1994

118 - Turta A., and Singhal A. K.: "Reservoir Engineering Aspects of Oil Recovery from Low Permeability Reservoirs by Air Injection" SPE 48841, to be presented at 1998 SPE International Conference and Exhibitions, Beijing China, 2-6 Nov. 1998.

119 - Turta A.T., and Ayasse C. "Recent Laboratory Results of THAI and Its Comparison with Other IOR Processes" SPE 59334, Paper presented at the 2000 SPE/Doe Improved Oil Recovery Symposium held in Tulsa, Oklahoma, 3-5 April 2000.

120 - Ungerere P., Behar F., Villalba M., Heum O.R., and Audibert A. "Kinetic Modeling of Oil Cracking", Advances in Organic Geochemistry 1987, Org. Geochem. Vol.13, Nos 4-6, pp.857-868, 1988, printed in Great Britain.

121 - Uran, L.C. "Petroleum Production Engineering" McGraw-Hill Book Company, Inc. Second Edition 1939, pp 433-451.

122 - Vossoughi S., and Said Saim "A Different approach in Generating Kinetic Models for Crude Oil Combustion: Application to an In-Situ Combustion Process" , AOSTRA Journal of Reserch, 8 (1992) 131

123 - Vossoughi S., and Willhite G.P. "Development of a kinetic Model for In-situ Combustion and Prediction of the process Variables Using TGA/DSC Techniques", SPE 11073, paper presented at the 57th Annual Fall Technical Conference and Exhibition of SPE of AIME., held in New Orleans. LA. Sept. 26-29, 1982.

124 - Vossoughi S., Bartlett G. W., and Willhite G. P. "Prediction of In-Situ Combustion Variables by Use of TGA/DSC Technique and the effect of sand grain specific surface area on the process" Soc. Pet. Eng. J. Oct 1985 pp 656-664

125 - Vossoughi S., Willhite G.P., Kritikos W.P., Guvenir I.M., and Shoubary Y.E "Automation of an In-situ Combustion Tube and Study of the Effect of Clay on the In-situ Combustion Process"SPE 10320 presented at the SPE 56th Annual Technical Conference and Exhibition in San Antonio Oct. 5-7, 1981.

126 - Vossoughl S., and El-Shoubary Y. "Kinetic of Crude-Oil Coke Combustion", SPE reservoir Engineering, May 1989, pp 201-206.

127 - Weijedma J. : " Report from Koninklijke, Shell. Exploration and Production, Laboratory, Rijswijk", The Netherlands, 1968.

128 - White P. D., and Moss J. T. " Thermal Recovery Methods", PennWell Books, 1983

129 - White P.D., and Farfield W.H. " Oxygen Fireflood is Source of CO_2" Oil and Gas Journal, July 19, 1982, pp 177-180

130 - Wichert G.C., Okazawa N.E., Moore R.G., and Begrave J.D.M. "In-situ Upgrading of Heavy Oils by Low-Temperature Oxidation in the Presence of Caustic Additives", SPE 30299, Paper presented at the international Heavy Oil Symposium held in Calgary, Albrta, Canada 19-21 June 1995

131 - Wilbur H. S., and Clayton J. R. " Role of Clays in the Enhanced Recovery of Petroleum" SPE 8845, presented at the First Joint SPE/DOE Symposium on EOR, Tulsa Oklahoma April 20-23 1980

132 - Wilson L. A., Reed R. L., Reed D. W., Clay R. R., and Harrison N.H. " Some Effect of Pressure On Forward and Reverse Combustion" Soc. Pet. Eng. J. Sep 1963 pp 127-137.

133 - Wu C. H., and Fulton P.F. " Experimental Simulation of the Zones Preceding the Combustion Front of an In-Situ Combustion Process" Soc. Pet. Eng. J. March 1971 pp38-46

134 - Xia T.X. and Greaves M. "Down hole Upgrading of Athabasca Tar Sand Bitumen Using THAI-SARA Analysis", SPE 69693, Paper presented at the 2001 SPE/DOE International Thermal Operations and Heavy Oil Symposium Held in Margarita, 12 March 2001.

135 - Xia T.X. and Greaves M. "Upgrading Athabasca Tar Sand Using Toe-to-Heel Air Injection" SPE/Petroleum society of CIM 65524, paper presented at the 2000 SPE/Petroleum Society of CIM International Conference on Horizontal Well Technology held in Calgary, Alberta Canada, 6-8 November 2000

136 - Yannimars D. V., and Tiffin D. L. " Screening of Oils from In-Situ Combustion at Reservoir Condition by Accelerating Rate Calorimetery" SPE Res. Eng. Feb. 1995, pp 36

137 - Yoshiki K.S., and Philips C. R. "Kinetics of the Thermo-Oxidative and Thermal Cracking Reactions of Athabasca Bitumen" Fuel, 1985, Vol 64, November pp1591-1597

138 - Young T. J. "The dynamics and Control of In-situ Combustion", PhD Thesis, University of Bath, 1997

APPENDICES

APPENDIX - A

HTO Equations

HTO reactions can be represents by the following equation : Burger *et al* 1985

$$CH_x + (1 - \Gamma/2 + x/4)O_2 \rightarrow (1-\Gamma)CO_2 + \Gamma CO + x/2\, H_2O \quad \ldots\ldots\ldots(2.1)$$

Where :

x = Atomic hydrogen/carbon ratio of the fuel

Γ = Molar Ratio $CO/(CO+CO_2)$

The determination of fuel availability from the analysis of combustion-tube data begins with an analysis of the stoichiometry of the combustion reaction. The composition of the fuel is not known but is assumed to be represented as a hypothetical hydrocarbon with the chemical formula CH_{FHC}. Where FHC is the ratio of hydrogen to carbon in the fuel. The high-temperature combustion of CH_{FHC} when the combustion products are water, carbon dioxide, and carbon monoxide is represented by

$$CH_{F_{HC}} + n_{O_2} O_2 \rightarrow n_{CO_2} CO_2 + n_{CO} CO + \left(\frac{F_{HC}}{2}\right) H_2O \quad \ldots\ldots\ldots(2.2)$$

Where:

n_{O_2} = mole of oxygen reacting, n_{CO_2} = moles of CO_2 in the combustion gases, n_{CO} = mole of CO in the combustion gases, and F_{HC} = atomic ratio of hydrogen to carbon in the fuel.

$$m = \frac{\text{moles } CO_2 \text{ produced}}{\text{moles CO produced}} = \frac{n_{CO_2}}{n_{CO}} = \frac{379 \times n_{CO_2}}{379 \times n_{CO}} = \frac{V_{CO_2}}{V_{CO}} \quad \ldots\ldots\ldots(2.3)$$

Equation (2.2) can be simplified by substituting m as follow.

$$CH_{F_{HC}} + \left(\frac{2m+1}{2m+2}\frac{F_{HC}}{4}\right)O_2 \rightarrow \left(\frac{m}{m+1}\right)CO_2 + \left(\frac{1}{m+1}\right)CO + \left(\frac{F_{HC}}{2}\right)H_2O \quad \text{.....(2.4)}$$

When the oxygen is not totally consumed, an oxygen utilization efficiency can introduced to measure the extent of combustion.

The injected gas is usually air in some cases may be enriched with oxygen. The oxygen utilization efficiency is determined from the analysis of produced gases. From Equation (2.5),

$$E_{O_2} = \frac{\text{moles of oxyen consumed}}{\text{moles of oxyen injected}} = \frac{\left(y_{iO_2} n_i - y_{pO_2} n_p\right)}{y_{iO_2} n_i} = 1 - \left(\frac{y_{iN_2}}{y_{iO_2}}\right)\left(\frac{y_{pO_2}}{y_{pN_2}}\right) \quad \text{.....(2.5)}$$

Where :

y_{iO_2} = average mole fraction of oxygen in the injected gas,

y_{pO_2} = average mole fraction of oxygen in the produced gas,

n_i = moles of gas injected during a specified time interval,

n_p = moles of produced gas during a specified time interval. When the injected gas

y_{iN_2} = mole fraction nitrogen in the injected gas and

y_{pN_2} = mole fraction nitrogen in the produced gas.

If air is the injected gas,

$$E_{O_2} = 1 - \left(\frac{0.79}{0.21}\right)\left(\frac{y_{pO_2}}{y_{pN_2}}\right) \quad \text{.....(2.6)}$$

Naji and Poettman, 1991 show that the oxygen use is given by Equation (2.7) when the injected gas is 100% oxygen.

$$E_{O_2} = 1 - y_{pO_2} \quad \text{.....(2.7)}$$

The hydrogen/Carbon (H/C) ratio is determined from a material balance on the hydrogen and the carbon oxides which are produced by high temperature oxidation. All hydrogen in the fuel reacts with oxygen to produce water, which is not completely recovered or measured. Thus hydrogen consumption is determined by the material balances on

oxygen. The oxygen that is consumed appears as CO_2, CO, and water. Hydrogen consumption is overestimated by this balance because some of the oxygen is consumed in low-temperature reactions where oxygen combines with hydrogen to produce oxygenated compounds. For this reason, hydrogen is referred to as apparent hydrogen consumption. Writing a balance based on the stoichiometry of the compounds, the H/C ratio is given by Naji and Poettman, 1991.

$$F_{HC} = \frac{4\left(\frac{y_{iO_2}}{y_{iN_2}}\right) - \left(\frac{y_{iO_2}}{y_{iN_2}} + 1\right)\left(1 - y_{pN_2}\right) + 2\,y_{pCO}}{y_{pCO}} + y_{pCO} \quad \text{.....(2.8)}$$

For the case where the injected gas is pure oxygen , Equation (2.8) becomes Naji and Poettman, 1991.

$$F_{HC} = \frac{4\left(1 - y_{pO_2} - 0.5\,y_{pCO} - y_{pCO_2}\right)}{y_{pCO_2} + y_{pCO}} \quad \text{.....(2.9)}$$

When air is injected , ($y_{iO_2} = 0.21$ and $y_{iN_2} = 0.79$) the apparent H/C ratio can be computed directly from combustion gas analysis with Dew and Metin, 1965.

$$F_{HC} = \frac{106.3 + 2CO - 5.06(CO_2 + CO + O_2)}{CO_2 + CO} \quad \text{.....(2.10)}$$

Where:

CO_2 = mole % CO_2 in produced gas ,
CO = mole % CO in produced gas, and
O_2 = mole % O_2 in produced gas.

2.12.1 : Fuel Availability:

Fuel availability can be computed from the analysis of combustion-tube data over a specified period of time. The fuel availability from the combustion-tube experiment is defined by

$$m_E = \frac{w_f}{V_b} \quad \text{.....(2.11)}$$

Where :

w_f = mass of carbon and hydrogen consumed when V_b (in cubic feet) of reservoir was y_{PCO} burned. In a combustion-tube run, n_P moles of gas with an average composition of y_{PCO_2}, y_{PCO}, and y_{PO_2} are produced during a time interval, Δt, when the combustion front is a propagated through V_b. It is assumed that the combustion tube is operating under steady state conditions so that the velocity of the combustion front is constant. Under these conditions,

$$V_b = (x_2 - x_1)A = v_f (t_2 - t_1)A \quad \text{.....(2.12)}$$

Where:

x_1 and x_2 = locations of the combustion front at times t_1 and t_2, respectively; A = cross-sectional area of the tube , and v_f = average velocity of the combustion front. v_f may be determined by plotting the location of the peak temperature in the combustion tube vs. time. The slope of this graph is the velocity of the combustion front.

2.12.2 : Fuel Consumed:

The fuel consumed is the sum of the mass of carbon and hydrogen consumed. Appling a material balance to the produced gases, the mass of carbon and hydrogen consumed is given by

$$w_f = (12 + F_{HC})(y_{pCO_2} + y_{pCO})n_P = (12 + F_{HC})(m+1)y_{pCO}n_P \quad \text{.....(2.13)}$$

2.12.3 : Air Requirement:

The combustion front can advance only by consuming fuel . Thus, the air required will be directly proportional to the fuel availability. Oxygen (pure or in a mixture of air) is required to burn fuel, because air is the common source of oxygen. The air required for

dry forward combustion is defined as the standard volume of air required to burn a unit volume of reservoir. In common oilfield units, the air requirement is defined as

$$a_R = \frac{\text{scf}}{\text{ft}^3 \text{ reservoir volume burned}} \quad \text{.....(2.14)}$$

2.12.3.A - Combustion Stoichiometry.

The air requirement is calculated from combustion stoichiometry from the apparent H/C ratio of the fuel. From Equation,

$$m_R = \text{lbm fuel / ft}^3 \text{ reservoir volume burned}$$

The fuel availability determined from combustion-tube runs, m_E, must be adjusted to reservoir conditions when the porosity of the porous material in the combustion tube is not equal to the porosity of the reservoir rock. [Nelson and Mc Neil, 1961][89] introduce the correction factor given by Equation 2.15 to account for differences the reservoir porosity, ϕ_R , and that of the combustion-tube experiment, ϕ_E .

$$m_R = \left(\frac{1-\phi_R}{1-\phi_E}\right) m_E \quad \text{.....(2.15)}$$

Therefore,

$$\frac{m_R}{1-\phi_R} = \frac{m_E}{1-\phi_E} = \frac{\text{lb fuel}}{\text{ft}^3 \text{ sand grain}}$$

The fuel has an apparent molecular formula $CH_{F_{HC}}$. And the apparent molecular weight of the fuel is (12 + F_{HC}). Thus, the moles of fuel burned when 1 ft^3 of reservoir rock is burned is given by

$$\frac{\text{moles fuel}}{\text{ft}^3} = \frac{m_R}{12 + F_{HC}} \quad \text{.....(2.16)}$$

The air requirement as scf/ft^3 of reservoir volume burned is given by

$$a_R = \frac{379}{y_{IO_2} E_{O_2}} \left(\frac{2m+1}{2m+2} + \frac{F_{HC}}{4}\right)\left(\frac{m_R}{12 + F_{HC}}\right) \quad \text{.....(2.17)}$$

Where E_{O_2} = combustion efficiency of oxygen, fraction, and y_{iO_2} is mole fraction oxygen in the injected gas .

Some of the injected air is stored in the burned volume and does not contribute to the combustion efficiency. This is not a factor when the pressure is low. However, at high pressures, the stored air should be considered. If the burned volume is assumed to be at the injection pressure p_i, then the air requirement at p is approximated by Naji and Poettman, 1991 .

$$a_R^* = a_R + \left(\frac{\phi_R}{B_{gi}}\right) \quad \text{.....(2.18)}$$

Where:

a_R^* = air requirement at p_i, scf/ft^3 rock; E_{O_2} = Oxygen consumption efficiency, B_{gi} = Gas Formation Volume Factor (FVF) for air at injection pressure and temperature of the region behind the combustion front, ft3/scf, and p_i = BHP of the air in the injection well, psi. At high pressures, the air requirement is increased considerably by storage in the burned zone.

2.12.3.B - Material Balance:

The air requirement can be determined experimentally during steady-state combustion by measuring the injected air rate and the combustion front velocity. The air requirement is given by

$$a_R^* = \frac{u_a}{v_f} \quad \text{.....(2.19)}$$

Where :

u_a = injected air flux, scf/ft^2-hr = G_i/A.

Note that the air requirement determined from the measured gas injection rate includes storage in the burned zone. The air requirement computed from stoichiometry should be

in reasonable agreement with that determined from combustion stoichiometry when storage in the burned zone is accounted for.

2.12.4 : Displacement From Burned Zone :

Combustion stoichiometry for HTO may also be used to estimate the volume of oil displaced by the moving combustion front, the volume of water displaced and produced by the combustion gases produced. However, the rates of fluid production cannot be predicted from stoichiometry.

A combustion front displaces all oil and water that is not consumed by the combustion process. Thus, a material balance can calculate oil displacement from the burned region. The material balance requires that the oil displaced equal the oil initially present minus oil burned.

$$V_{ob} = \phi V_{Rb} (S_{oi} - S_{oF}) \quad \text{.....(2.20)}$$

Where :

V_{ob} = Oil displaced from the burned volume, ft^3;

V_{Rb} = Bulk volume burned, ft^3;

S_{oF} = Oil saturation equivalent to fuel consumed, and

S_{oi} = Initial oil saturation.

The equivalent oil saturation is given by

$$S_{oF} = \frac{m_R}{\phi \rho_F} \quad \text{.....(2.21)}$$

Where :

The equivalent oil saturation requires an estimate of the density of the fuel. As discussed earlier, the fuel has a composition that is quite different from the original crude oil. Consequently, the density of the fuel is not known accurately. Nelson and McNeil, 1961 suggest using a specific gravity of 1.0 (ρ_F=62.4 Ibm/ft^3) for the fuel to recognize the change in the crude oil as a result of coking and cracking that occurs during the fuel deposition process. Parts1 assumes that the density of the fuel is equal to that of the oil.

Water displaced by the is-situ combustion process comes from the initial water saturation and the water produced by the combustion reaction. The volume of water displaced from the burned volume is given by

$$V_{wb} = \phi V_{Rb} (S_{iw} - S_{wF}) \quad \text{.....2.22}$$

Where :

S_{wF} = Water saturation equivalent to water produced by the combustion reaction, and

V_{wb} = Water (liquid equivalent) displaced from the burned volume plus water produced in the reaction, ft^3.

The water produced by the combustion reaction is derived from the stoichiometry. There is $F_{HC}/2$ mol water produced per mole of fuel ($CH_{F_{HC}}$) burned. The volume of water produced per cubic foot of reservoir volume burned is given by

$$V_w = \frac{9.0\, m_R\, F_{HC}}{\rho_w (12 + F_{HC})} \quad \frac{ft^3\ H_2O}{ft^3\ \text{reservoir burned}} \quad \text{.....(2.23)}$$

Thus,

$$S_{wF} = \frac{9.0\, m_R F_{HC}}{\rho_w \phi (12 + F_{HC})} \quad \text{.....(2.24)}$$

The economics of in-situ combustion is controlled by the cost of air combustion. The air/oil ratio is a measure of the effectiveness of the combustion process and can be computed from combustion stoichiometry . Considering only the burned zone, the ratio of the air injected to oil displaced (**AOR**)is given by

$$F_{AOb} = 5.615 \left[\frac{a_R^*}{\phi_R (S_{oi} - S_{oF})} \right] \left(\frac{scf}{bbl} \right) \quad \text{.....(2.25)}$$

The volume of combustion gases is a useful parameter in the evaluation of the operation of a combustion project. Expressions for estimating the volume of combustion gases are derived from the combustion stoichiometry, assuming that the project is operating in the HTO regime.

$$n_{pCO_2} + n_{pCO} + n_{pH_2O} = \left(1 + \frac{F_{HC}}{2}\right) \quad \left(\frac{\text{moles}}{\text{mole fuel consumed}} \right) \quad \text{.....(2.26)}$$

$$n_{pO_2} = \left(1 - E_{O_2}\right)\left(\frac{n_{O_2}}{E_{O_2}}\right)\left(\frac{\text{moles}}{\text{mole fuel consumed}}\right) \quad \text{.....(2.27)}$$

and $$n_{pN_2} = \left(\frac{1 - y_{iO2}}{y_{iO2}}\right)\left(\frac{n_{O_2}}{E_{O_2}}\right)\left(\frac{\text{moles } N_2}{\text{mole fuel consumed}}\right) \quad \text{.....(2.28)}$$

Thus, the total amount of combustion gases per mole fuel consumed is given by

$$n_{pf} = \left[1 + \frac{F_{HC}}{2} + \left(\frac{1 - y_{iO2}\, E_{O_2}}{y_{iO2}\, E_{O_2}}\right) n_{O_2}\right]\left(\frac{\text{moles } N_2}{\text{mole fuel consumed}}\right) \quad \text{.....(2.29)}$$

The combustion gas volume in SCF/ft^3 Reservoir burned:

$$G_{pF} = \left(\frac{379\, m_R}{12 + F_{HC}}\right)\left[1 + \frac{F_{HC}}{2} + \left(\frac{1 - y_{iO_2}\, E_{O_2}}{y_{iO_2}\, E_{O_2}}\right) n_{O_2}\right] \times \left(\frac{2m + 1}{2m + 2} + \frac{F_{HC}}{4}\right) \quad \text{.....(2.30)}$$

Equation (2.30) may be used to estimate the burned-zone volume from the produced gas analysis, assuming that all combustion gases are produced. Equation 8.269 must be modified to account for an increase in gas saturation in the unburned region of the reservoir.

2.12.5 : Heat Release by In-Situ Combustion:

In-situ combustion releases considerable quantities of heat to the reservoir and surrounding formations. The amount of energy released can be estimated from heat of combustion data. Dew and Mertin, 1965, and Burger and Sahuquent, 1973.Equation (2.31) gives the heat of reaction, Prats, 1982 and Burger and Sahuquent, 1973 assuming water produced by the combustion reaction condenses :

$$\Delta h_a = \frac{94.0 - 67.9\, m' + 31.2\, F_{HC}}{1 - 8.5\, m' + 0.25\, F_{HC}} \quad \textbf{Btu/scf air} \quad \text{.....(2.31)}$$

Where :

$$m' = \frac{CO}{CO + CO_2} \text{ in the influent gas.}$$

Equation (2.31) does not account for the oxygen utilization efficiency because $E_{O_2} = 1.0$

APPENDIX - B

Equipment Components

Item Description	Specifications	Manufacturer/Supplier
AAV1 – AAV6 **AAV11 – AAV12** **AAV16 – AAV18** **AAV20 – AAV23**	HB Series Air Operated, Packless Bellows valve. Normally Closed. Actuation pressure 75-110 psi, Operating pressure 3500 psi Operating temperature 40-65°C	Nupro Corp./ Swagelok Co. Bristol Valve & Fitting Co. Ltd. Fourth Way Avonmouth Bristol BS11 8DG
AAV15 – AAV19 **AAV1 – AAV6** **AAV11 – AAV12** **AAV16 – AAV18** **AAV20 – AAV23**	HB Series Air Operated, Packless Bellows valve. Normally Open. Actuation pressure 75-110 psi, Operating pressure 3500 psi Operating temperature 40-65°C	Nupro Corp./ Swagelok Co. Bristol Valve & Fitting Co. Ltd. Fourth Way Avonmouth Bristol BS11 8DG
AC	Air Compressor Hunter Air 50 Flow – 12 cfm Capacity – 50 litre Pressure – 150 psi	Clarke International Lower Clapton Road London E5 ORN
AOFMV	Air Operated Fine Metering Valve Actuated Pressure 60-100 psi	High Pressure Equipment Co.
O_2 Analyser	Servomex 570 A 0-100 %	Servomex (UK) Ltd. Crowborough Sussex, TN6 3 DU
CO_2 Analyser	Servomex 1400 series 0-100 %	Servomex (UK) Ltd. Crowborough Sussex, TN6 3 DU
CO Analyser	Servomex 1400 series 0-25 %	Servomex (UK) Ltd. Crowborough Sussex, TN6 3 DU
CAR	Manual Operated, see CPC	Watson Smith Ltd.
CPC 1 – CPC 10	Current to Penumatic Converter Input Signal 4-20 mA Output (pressure) 0-150 psi	Watson Smith Ltd. Cross Chancellor St. LEEDS LS6 2 RT
CVs	Check Valves Rated to 3000 psi	Nupro Corp./Swagelok Co.
DPT	Differential Pressure Transducer Model 11510 Output 4-20 mA	Rosemount Ltd. Heat Place Bognot Regis West Sussex PO22 9 SH
F1-F8	"TF" Series in-line filters	Nupro Corp./Swegelok Co.
LMF1	Brooks 5850TR Mass Flow Controller 0-1000 ml/min	Flotech Ltd. Horsfield Way, Bredbury Stockport SK6 2SR
PG1 – PG 14	High Pressure Gauge Rated to 3700 psi	Budenberg Gauge Co Ltd.
PPRV1 – PPRV4, PPRV10	54-2300 series Air Activated Precision Pressure Regulator (Normal Closed)	Tescom Corporation Pressure Control Division

	Range 20-10,000 psi	
PPRV5, PPRV6, and PPRV8	54-2300 series Air Activated Precision Pressure Regulator (Normal Closed)	Tescom Corporation Pressure Control Division
PRVG1	44-220 series Spring loaded Pressure Reducing Regulator Max op Press. 3000 psi	Tescom Corporation Pressure Control Division
PRVG2	44-220 series Spring loaded Pressure Reducing Regulator Max op Press. 400 psi	Tescom Corporation Pressure Control Division
PRVL1	44-220 series Spring loaded Pressure Reducing Regulator Max op Press. 4000 psi	Tescom Corporation Pressure Control Division
PRVL2	44-220 series Spring loaded Pressure Reducing Regulator Max op Press. 125 psi	Tescom Corporation Pressure Control Division
PT1 – PT4	Super THE Ultra Precision Absolute Pressure Transducer Range 10 – 3000 psi	RDP Electrics Ltd. Grove Street Heat Town Wolvehampton WV10 OPY
PT5	PDCR 900 series Pressure Transducer Rang 0-60 bar	Druck Ltd. Fur Tree Lane Groby Leicester
PT6	PDCR 900 series Pressure Transducer Rang 0-350 bar	Druck Ltd. Fur Tree Lane Groby Leicester
PT7, PT8	P1000 series pressure transducer Range 0 – 250 psi	Lucas Schaevitz Ltd. 543 Ipswitch Road Slough SL1 4 EG
PT9	P1000 series pressure transducer Range 0 – 25 psi	Lucas Schaevitz Ltd. 543 Ipswitch Road Slough SL1 4 EG
PT10, PT11	P1000 series pressure transducer Range 0 – 75 psi	Lucas Schaevitz Ltd. 543 Ipswitch Road Slough SL1 4 EG
SV	3 Way Direct acting Solenoid Valves 240V AC actuation	ASCO Uk Coppas Controls Ltd. Aldermoor Wey Industrial Estate Longwell Green Bristol BS15 7DA
TC	K-Type minerally insulation, thermocouple	TC Ltd. PO 130 Cowley Mill Trading Estate Uxbridge UB8 2 YS
WTM	DM3D Wet Tests Meter 600 dm^3/hr Max Op. Press. 100 mbar	Alexandra Wright Co Unit 1-3 Kimpton Link Business Centre Sutton SM3 9OP

Check Results of Solenoid Valves

SV No.	Terminal Wire No.	Port	Line	Relay Board Wiring	Status	Comment
SV0						
SV1	36	3	6	6 Red	O.K.	
SV2	15	2	0	3 Blue	O.K.	
SV3	46	3	1	5 Orange	O.K.	
SV4	13	2	1	3 Purple	O.K.	
SV5	40	3	4	5 Blue	O.K.	
SV6	38	3	5	5 Purple	O.K.	
SV7	17	1	7	3 Green	O.K.	
SV8	29	1	1	2 Blue	O.K.	
SV9					Not available	
SV10	34	3	7	6 Orange	O.K.	
SV11	1	2	7	4 Purple	O.K.	
SV12	25	1	3	2 Purple	Not used	
SV13	31	1	0	2 Yellow	O.K.	
SV14	43	0	2	1 Yellow	O.K.	
SV15	23	1	4	3 Red	Not used	
SV16	9	2	3	4 Orange		
SV17	11	2	2	4 Red	Not used	
SV18	7	2	4	4 Yellow	O.K.	
SV19	28	4	2	6 Blue	O.K.	
SV20	42	3	3	5 Green	O.K.	Ball Valve 3
SV21	26	4	3	6 Purple	Not used	
SV22	5	2	5	4 Green	O.K.	
SV23	48	3	0	5 Red	O.K.	
SV24	44	3	2	5 Yellow	Not used	
SV25	3	2	6	4 Blue	O.K.	
SV26	21	1	5	3 Orange	O.K.	
SV27	35	0	6	2 Red	O.K.	
SV28	33	0	7	2 Orange	Not used	
SV29	19	1	6	3 Yellow	O.K.	
SV30	27	1	2	2 Blue	O.K.	
SV31	30	4	1	6 Green	O.K.	Ball Valve 4
SV32	47	0	0	1 Red	Not used	
SV33	32	4	0	6 Yellow	O.K.	

SV34	39	0	4	1 Blue	Not used	
SV35	16	5	0	7 Red		
SV36	37	0	5	1 Purple		
SV37	14	5	1	7 Orange		
SV38						

APPENDIX - C

Check Status of Pressure Transducers

PT Number	Status	Comment, Scale Reading	Specifications	Manufacturer/ Supplier
PT1	O.K.	Bar	Super the Ultra Precision Absolute Pressure Transducer **Range 10-3000 psi (211 bar)**	RDP Electronics Ltd Grove Street Heat Twon Wolvehampton WV10 OPY
PT2	O.K.	Bar		
PT3	O.K.	Bar		
PT4	O.K.	Bar		
PT5	O.K.	Bar	PDCR 900 series Pressure transducer **Range 0-60 bar**	Druck Ltd Fur Tree Lane Groby Leicester
PT6	O.K.		PDCR 900 series Pressure transducer **Range 0-350 bar**	Druck Ltd
PT7	O.K.		P1000 series pressure transducer **Range 0-250 bar**	Lucas Schaevitz Ltd 543 Ipswitch Road Slough SL1 4EG
PT8	O.K.	Bar		
PT9	O.K.	Bar (Not available in flow diagram)	P1000 series pressure transducer **Range 0-25 psi (1.8 bar)**	Lucas Schaevitz Ltd
PT10	O.K.	Psi	P1000 series pressure transducer **Range 0-75 psi (5.3 bar)**	Lucas Schaevitz Ltd
PT11	O.K.	Psi		

APPENDIX - D

LabVIEW Computer Tasks

LabVIEW©:

Within LabVIEW © any program or subroutine is made up of two parts : a front panel and a program diagram. The front panel contains the control (inputs) and the indicators (output). Using these, a virtual instrument (VI) is built as the graphical user interface (HUI). The program diagram links the inputs and outputs using a graphical language ("G") which is icon based and objected. These icons have input and output terminals which are linked together with data lines or "wires". These wires have different colours to represent the type of data being carried e.g. an array of double precision numbers, a string , a Boolean etc.

Once a program has been written an icon may be designed for it. A pattern of terminals can then be designed with which to write its control and indicators. This program or VI may then be used as a subroutine, or sub-VI, in a larger program.
"G" allow one to escape from the line by line sequential execution order of conventional programming language in a unique style of multitasking; Where a wire branches so too does the program's operation, each branch sharing the computer's CPU time. Importantly this sharing can be weighted toward certain tasks. It is therefore a perfect medium for the process control, where numerous tasks must be carried out simultaneously.

In-Situ Combustion Tube Experiment Program Description:

IscView implements the following series of tasks:

1. The user enters the conditions for the experiment. The position and state of all valves is initiated.
2. The front panel for the experiment is called and the Data acquisition (DAQ) and safety monitoring are started.

3. The combustion tube is then slowly brought up to operating pressure (1 bar at a time).
4. Data logging is commenced. This continues throughout the experiment, all important data being saved to disk.
5. Nitrogen injection is commenced, first to flux-out oxygen from the system. The nitrogen flow rate is increased slowly to the required value.
6. The BHs are activated to heat the limestone up to its reservoir temperature. There is now flow through the tube, at this stage HPS, LPS, control of the Back Pressure, Injection Pressure and Tube and Shell differential pressure is initiated.
7. The ignition of the tube takes place : BH operation is switched to control adiabatically. Power to the ignitor is increased to achieve the required iqnition temperature. Air injection is started to commence iqnition.
8. Once ignition has taken place, the combustion front is allowed to propagate down the tube. Sampling of produced liquid is done whenever liquid produced.
9. Shut down, and finally cooling. The experiment is terminate before the combustion front reach the end of the tube, when T/C 30 reach 280°C.

Computer Tasks Modification:

In-Situ Combustion Tube Experiment Test set-up : 

: *"ISC Tube Experiment.vi"*

Table D-1 show a front panel and Figure D-1 show a program diagram of "ISC Tube Experiment.vi" . All important check messages and valves setting changing of the whole experiment run showed in the table. Message (1) and (2) remind the operator to make pre-experiment check and confirm it each and every time to the computer. There are four sets in the program as shown precisely in Table D-1 . Set (1) perform the set-up valve position during initial pressurization until the desired set pressure reached. Then, set (2) will commenced to heat-up the reservoir (bed) to initiate reservoir temperature, simultaneously ignitor start. Set (3) and (4) programmed to control the injection gas system, where O_2 and N_2 mass flow meter initiated to increase and control flux to the required fluxes.

Msg1

- Compressed air on 80psi
- Manual Control Station Air supply on
- Turn on trace heating
- Turn on CPC, PT power supply
- Turn on External Fan
- Turn on cooling water supply for gas knock out
- Open Valve at Base of Tube

Msg2

- Turn on SV power via the watchdog controller
- Turn on SCXI power
- Turn BH transformers
- Turn on ignitor power
- Plug in Rotating Sampler
- Set mass flow meters for run and remote
- Make Sure Signs are post ! Are you ready to begin the

Set 1

Valve Type	Number	State	Description
SV	25	open	Separate Shell & Tube
SV	5	open	close main vent
SV	6	open	open injection line
SV	3	open	open N2 supply line
SV	4	open	allow PPRV2 control
SV	27	open	allow PPRV3 control
SV	30	open	allow PPRV6 control
SV	13	open	open high to low pressure sides
SV	1	open	open O2 supply line
SV	19	open	by pass LMF1
SV	11	open	by pass LMF2

Set 2

Valve Type	Number	State	Description
SV	31	open	open tube top to bottom
SV	4	close	close PPRV 2
CPC	7	10.00	allow gas venting via AAV21

Set 3

Valve Type	Number	State	Description
SV	19	close	put LMF1 on line
SV	11	close	put LMF2 on line

Set 4

Valve Type	Number	State	Description
SV	2	open	open PPRV1
SV	4	open	open PPRV2

Table D-1 : IscView Initialisation (T.Yang, 1997) (Front Panel).

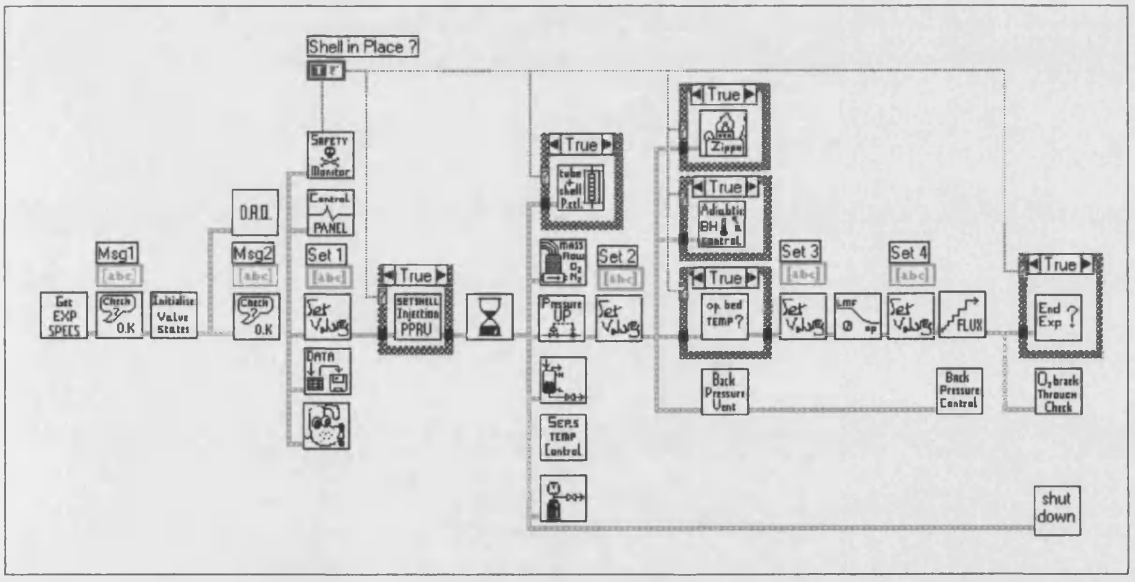

Figure D-1 : IscView Initialisation Graphics (T.Yang, 1997) .

The program flow chart Figure D-1 has been upgraded to fulfil the commissioning requirement. The modified flow chart is shown in Figure D-2. The modification is made

to the initial reservoir temperature initiation. Heating-up of the limestone core during pressurization of the system, occurs for two reasons . First, mimic the exact operation in practice. Second, to distribute the tasks that will help control during displacement and combustion process.

Second modification was to pressurise the tube and shell simultaneously for the following reasons :

1. to prevent venting during pressurization of the shell, and reducing the amount of gas needed.
2. Avoid over-pressuring the combustion tube.
3. Nitrogen is used to pressurise the tube and pressure shell.
4. Perform controllable pressurization time.
5. Prolong the life of valves used for venting and pressurizing. i.e. AAV22 and AAV4.

Table D-2 present the modification made on previous sets shown in Table D-1. These modifications allow the system to pressurize without venting.

Msg1

- Compressed air on 80psi
- Manual Control Station Air supply on
- Turn on trace heating
- Turn on CPC, PT power supply
- Turn on External Fan
- Turn on cooling water supply for gas knock out
- Open Valve at Base of Tube

Msg2

- Turn on SV power via the watchdog controller
- Turn on SCXI power
- Turn BH transformers
- Turn on ignitor power
- Plug in Rotating Sampler
- Set mass flow meters for run and remote
- Make Sure Signs are post ! Are you ready to begin the

Set 1

Valve Type	Number	State	Description
SV	**25**	**close**	**Communicate Shell & Tube**
SV	5	open	close main vent
SV	6	open	open injection line
SV	3	close	**open N2 supply line
SV	2	open	allow PPRV1 control
SV	**27**	**close**	**No PPRV3 control**
SV	30	open	allow PPRV6 control
SV	13	open	open high to low pressure sides
SV	1	open	open O2 supply line
SV	19	open	by pass LMF1
SV	11	open	by pass LMF2

Set 2

Valve Type	Number	State	Description
SV	**25**	**open**	**Separate Tube & Shell**
SV	**27**	**open**	**Allow PPRV3 control**
SV	31	open	Close Tube Top to bottom
SV	4	close	Close PPRV2
CPC	7	10.00	Allow gas venting via AAV21

Set 3

Valve Type	Number	State	Description
SV	19	close	put LMF1 on line
SV	11	close	put LMF2 on line

Set 4

Valve Type	Number	State	Description
SV	2	open	open PPRV1
SV	4	open	open PPRV2

Table D-2 : Modified IscView program (Front Panel).

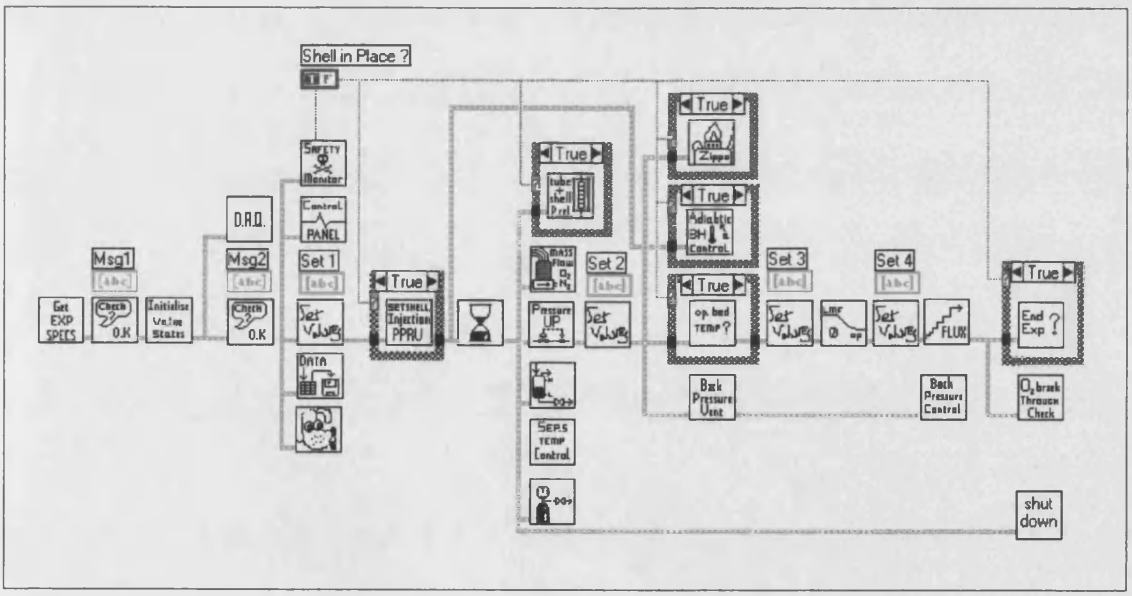

Figure D-2 : Modified main test set-up (Diagram).

APPENDIX - E

STARS Input Data File

```
***------------------------------------------------------------------------------------------
**      1D Combustion TUBE TEST No.RUN-4 EKOFISK light oil.
**      ==================================================
**------------------------------------------------------------------------------------------

** Special Features :
** 1) 1D Vertical Combustion Tube
** 2) Four Hydrocarbon Components: three liquid C11+,C6-10,C1-5 and one solid.
**    Stocktank stabilized oil is used and CH4 composition is negligible.
** 3) Two non-condensible gases: Oxygen & CO gases.
** 4) Four chemical reactions:
**    (a) Cracking of Heavy Oil to Light Oil and Coke,
**    (b) C11+ Heavy Oil burning,
**    (c) C6-10 light oil burning,
**    (d) Coke burning.
** 5) High initial pressure ( 200 bar, 20000 Kpa, 2900 psia) and 23oF ( 73.4 °F)
Temperature.
** 6) Injection end is heated externally, ignition temperature 350oC (662oF).
** 7) Porosity: 42.8 % Permeability : 1600 md
** 8) Water saturation: 70%                Oil Saturation : 25 % and
**    5% gas saturation assumed nitrogen the initial conditions.
** 9) Simulation stop when producing ends after 12 hours or
**    when the combustion front reaches the end  of the combustion Tube.

**
==========================================================================
**      INPUT/OUTPUT CONTROL
**
==========================================================================

filename output index-out main-results-out  **Use defaults names

*title1 '1D Light Oil Combustion Tube Test Run No. 4'
*title2 'EKOFISK Oil PVT Characterization'

*inunit field except 1 1 ** hrs instead of days
      except 11 1 ** ft3 instead of bbl
*OUTUNIT LAB
**CHECKONLY
```

```
*outprn *grid pres sw so sg temp y x solconc obhloss viso
*outprn *well *all
*wrst 300 *wprn *grid 300 *wprn *iter 300

outsrf grid pres sw so sg temp y x w solconc obhloss
        masdenw masdeno masdeng pcow pcog visw viso visg
        Krw kro krg kvalyw kvalyx cmpdenw cmpdeno cmpvisw
        cmpviso cmpvisg cchloss

outsrf well component 5 7 8

outsrf special blkvar temp 0 1   ** T history, block 1

blkvar temp 0 4          ** "   block 4
blkvar temp 0 8          ** "  block 8
blkvar temp 0 12     ** "  block 12
blkvar temp 0 20     ** "  block 20
blkvar temp 0 24     ** "  block 24
blkvar temp 0 28     ** "  block 28
blkvar temp 0 32     ** "  block 32
blkvar temp 0 36     ** "  block 36
blkvar temp 0 40     ** "  block 40
blkvar temp 0 44     ** "  block 44
blkvar temp 0 48     ** "  block 48
blkvar temp 0 52     ** "  block 52
blkvar temp 0 56     ** "  block 56
blkvar temp 0 60     ** "  block 60
blkvar temp 0 64     ** "  block 64
blkvar temp 0 68     ** "  block 68
blkvar temp 0 72     ** "  block 72
blkvar temp 0 76     ** "  block 76
blkvar temp 0 80     ** "  block 80
blkvar temp 0 84     ** "  block 84
blkvar temp 0 88     ** "  block 88
blkvar temp 0 92     ** "  block 92
blkvar temp 0 96     ** "  block 96
blkvar temp 0 100    ** "  block 100
blkvar temp 0 102    ** "  block 102
blkvar temp 0 104    ** "  block 104
blkvar temp 0 106    ** "  block 106
blkvar temp 0 108    ** "  block 108
blkvar temp 0 110    ** "  block 110
blkvar temp 0 112    ** "  block 112
blkvar temp 0 114    ** "  block 114
blkvar temp 0 116    ** "  block 116
blkvar temp 0 118    ** "  block 118
```

blkvar temp 0 120	** "	block 120
blkvar temp 0 121	** "	block 121
blkvar temp 0 122	** "	block 122
blkvar temp 0 123	** "	block 123
blkvar temp 0 124	** "	block 124
blkvar temp 0 125	** "	block 125
blkvar temp 0 126	** "	block 126
blkvar temp 0 127	** "	block 127
blkvar temp 0 128	** "	block 128
avgvar temp 0	**	Average T in tube
blkvar sw 0 1	**	Sw history, block 1
blkvar sw 0 4	**	Sw history, block 4
blkvar sw 0 8	**	Sw history, block 8
blkvar sw 0 16	**	Sw history, block 16
blkvar sw 0 24	**	Sw history, block 24
blkvar sw 0 32	**	Sw history, block 32
blkvar sw 0 40	**	Sw history, block 40
blkvar sw 0 48	**	Sw history, block 48
blkvar sw 0 56	**	Sw history, block 56
blkvar sw 0 64	**	Sw history, block 64
blkvar sw 0 72	**	Sw history, block 72
blkvar sw 0 80	**	Sw history, block 80
blkvar sw 0 88	**	Sw history, block 88
blkvar sw 0 96	**	Sw history, block 96
blkvar sw 0 104	**	Sw history, block 104
blkvar sw 0 112	**	Sw history, block 112
blkvar sw 0 120	**	Sw history, block 120
blkvar sw 0 128	**	Sw history, block 128
blkvar so 0 1	**	So history, block 1
blkvar so 0 4	**	So history, block 4
blkvar so 0 8	**	So history, block 8
blkvar so 0 16	**	So history, block 16
blkvar so 0 24	**	So history, block 24
blkvar so 0 32	**	So history, block 32
blkvar so 0 40	**	So history, block 40
blkvar so 0 48	**	So history, block 48
blkvar so 0 56	**	So history, block 56
blkvar so 0 64	**	So history, block 64
blkvar so 0 72	**	So history, block 72
blkvar so 0 80	**	So history, block 80
blkvar so 0 88	**	So history, block 88
blkvar so 0 96	**	So history, block 96
blkvar so 0 104	**	So history, block 104
blkvar so 0 112	**	So history, block 112
blkvar so 0 120	**	So history, block 120
blkvar so 0 128	**	So history, block 128

blkvar sg 0 1	**	Sg history, block 1
blkvar sg 0 4	**	Sg history, block 4
blkvar sg 0 8	**	Sg history, block 8
blkvar sg 0 16	**	Sg history, block 16
blkvar sg 0 24	**	Sg history, block 24
blkvar sg 0 32	**	Sg history, block 32
blkvar sg 0 40	**	Sg history, block 40
blkvar sg 0 48	**	Sg history, block 48
blkvar sg 0 56	**	Sg history, block 56
blkvar sg 0 64	**	Sg history, block 64
blkvar sg 0 72	**	Sg history, block 72
blkvar sg 0 80	**	Sg history, block 80
blkvar sg 0 88	**	Sg history, block 88
blkvar sg 0 96	**	Sg history, block 96
blkvar sg 0 104	**	Sg history, block 104
blkvar sg 0 112	**	Sg history, block 112
blkvar sg 0 120	**	Sg history, block 120
blkvar sg 0 128	**	Sg history, block 128
blkvar pres 0 128	**	Block Pressure, 128
blkvar pres 0 90	**	Block Pressure, 90
blkvar pres 0 60	**	Block Pressure, 60
blkvar pres 0 30	**	Block Pressure, 30
blkvar pres 0 4	**	Block Pressure, 4
blkvar pres 0 1	**	Block Pressure, 1
blkvar solconc 9 16	**	Coke Conc, "
blkvar x 1 1	**	y(Water), 1"
blkvar x 2 1	**	y(C11+), 1"
blkvar x 3 1	**	y(C6-C10), 1"
blkvar x 4 1	**	y(C1-C5), 1"
blkvar y 5 1	**	y(CO2), 1"
blkvar y 5 32	**	y(CO2), 32"
blkvar y 5 64	**	y(CO2), 64"
blkvar y 5 96	**	y(CO2), 96"
blkvar y 5 128	**	y(CO2), 128"
blkvar y 7 1	**	y(O2), 1"
blkvar y 7 32	**	y(O2), 32"
blkvar y 7 64	**	y(O2), 64"
blkvar y 7 96	**	y(O2), 96"
blkvar y 7 128	**	y(O2), 128"
blkvar y 8 1	**	y(CO), 1"
blkvar y 8 32	**	y(CO), 32"
blkvar y 8 64	**	y(CO), 64"
blkvar y 8 96	**	y(CO), 96"
blkvar y 8 128	**	y(CO), 128"

```
** ==========GRID AND RESERVOIR DEFINITION
==========

*GRID *CART 1 1 128        **      Blocks in K direction ( Normal Vertical )
** Tube I.D. = 10 cm. Cross-section area is pi*(d/2)**2
** = 78.54 cm2 = L*L. So equivalent block side is
** L= 8.86227 cm ( 0.28708 ft ).
** Total Tube Length is 125 cm;
** block size = 125/128 = (0.976563*0.032808=0.032039 ft)
*DI *CON 28708E-05
*DJ *CON 0.28708
*DK *CON 0.032039

*POR *CON 0.428
*permi *con 616
*permj *equalsi
*permK *equalsi

*END-GRID

*ROCKCP 35.02 *THCONR 1 *THCONW 0.36 *THCONO 0.077 *THCONG 0.0833
** *cpc 4.06

** ==========FLUID DEFINITIONS ==========

*model 9 8 6          **      Number of noncondensible gases is numy-numx = 2
                      **      Number of solid components is ncomp-numy = 1
                      **      N2 & CO2 soluble in the liquid petroleum phase
                      **      O2 & CO only the gas phase insoluble in the liquid
petroleum phase

*compname 'WATER'  'C11+' 'C6-10' 'C1-5'  'CO2'  'N2'  'O2'    'CO'   'COKE'
**
*cmm       18   329.36  115.98  72.15   44.01  28.01   32    28.01  13
*pcrit    3155   196.90  363.09  488.1  1071.0  500   730    507.5
*tcrit    705.7   1478.9  548.2  385.47  87.56 -232.84 -181.72 -220.78

*avg      0 3.926e-6 3.926e-6 2.166e-6 2.1267e-4 2.1960e-4 2.1960e-4 2.1960e-4
*bvg      0 1.102  1.102  0.943  0.721  0.721  0.702  0.702
*avisc    0 4.02e-4 4.02e-04 4.02e-4 4.02e-4 4.02e-4
*bvisc     0 6121.6 6121.6 6121.6 6121.6 6121.6

*molden   0 0.2024 0.1309 0.0481 0.6623 0.6944   ** LBMOLE/FT3
*cp       0 4e-6  4.5e-6  5e-6  7e-6  7.5e-6
*ctl      0 1.496e-4  2.839e-4 2.839e-4 2.839e-4 2.839e-4
                      ** 55.191  44.189  39.368     LB/FT3
```

```
                    ** 11.6   39.1   44.8  API

** *SOLID_CP 'COKE' 16.9984 0
** *SOLID_DEN 'COKE' 916.256 0 0

*SOLID_CP 'COKE' 4.06 0
*SOLID_DEN 'COKE' 4.4 0 0

**
** CHEMICAL REACTION 1 - Cracking : C11+--> C6-C10+ Coke
*compname 'WATER'  'C11+' 'C6-10' 'C1-5' 'CO2'  'N2'  'O2'    'CO'   'COKE'
**
** *storeac        0        1        0       0       0     0     0       0      0
** *stoprod        0        0     2.80       0       0     0     0       0     13
** *freqfac  4.167E5 *eact 62802    *renth 93040

** *storeac        0        1        0       0       0     0     0       0      0
** *stoprod        0        0     3.88       0       0     0     0       0  60.92
** *freqfac  4.167E5 *eact 27000    *renth 40000

*storeac     0         1       0       0       0      0     0       0       0
*stoprod     0         0  0.30735      0       0      0     0       0  21.93749
*freqfac  2.0e05       *eact 27000   *renth 0

**
**CHEMICAL REACTION 2 - Cracking : C11+--> C1-C5 + Coke
*compname 'WATER'  'C11+' 'C6-10' 'C1-5' 'CO2'  'N2'  'O2'    'CO'   'COKE'
**
*storeac   0     1     0     0     0     0     0       0      0
*stoprod   0     0     0  0.3356   0     0     0       0   23.0613
*freqfac  2.1e05       *eact 125000  *renth 0

**
**CHEMICAL REACTION 3 - Heavy Oil Burning: C11+ + O2-->
H2O+CO/CO+energy
*compname 'WATER'  'C11+' 'C6-10' 'C1-5' 'CO2'  'N2'  'O2'    'CO'   'COKE'
**
*storeac   0     1     0     0     0     0  20.94472    0      0
*stoprod 18.93632  0     0     0     0     0     0    22.95311    0
*freqfac  3.020e10    *eact 16500    *renth 8774.06
**

**
**CHEMICAL REACTION 4 - Light Oil Burning: C6-C10 + O2 -->H2O + CO + energy
*compname 'WATER'  'C11+' 'C6-10' 'C1-5' 'CO2'  'N2'  'O2'    'CO'   'COKE'
```

```
**
*storeac   0      0     1     0     0     0  8.970302   0      0
*stoprod  10.35473  0    0     0     0     0     0    7.585879   0
*freqfac   3.020e10    *eact 17500    *renth 3685.33
**
```

```
**
**CHEMICAL REACTION 5 - Hydrocarbon Gas Burning: C1-C5 + O2-->
H2O+CO+energy
*compname 'WATER'  'C11+'  'C6-10'  'C1-5'  'CO2'  'N2'  'O2'    'CO'   'COKE'
**
*storeac   0      0     0     1     0     0  5.792082   0      0
*stoprod  6.685998  0     0     0     0     0     0    4.898167   0
*freqfac   3.020e10    *eact 17000    *renth 185.3466
**
```

```
**
**CHEMICAL REACTION 6 - Coke Burning : Coke + O2--> H2O+CO2 +energy
*compname 'WATER'  'C11+' 'C6-10' 'C1-5'  'CO2'  'N2'  'O2'    'CO'   'COKE'
**
*storeac   0      0     0     0     0     0     1.4      0      1
*stoprod   0.8     0     0     0     1     0     0        0      0
*freqfac   3.0e5         *eact 150000   *renth 100437.19
**
```

```
**
**CHEMICAL REACTION 7 - Hydrocarbon Gas Burning: CH4 + 2O2-->
2H2O+CO2+energy
** *compname 'WATER'  'C7+' 'C2-C6' 'CH4'  'CO2'  'O2'   'COKE'
**
** *storeac   0      0     0     1     0     2      0
** *stoprod   2      0     0     0     1     0      0
** *freqfac   3.020e10
** *eact 59450
** *renth 502.533              ** Recation Enthalpy BTU/lbmole
**
```

```
**
**CHEMICAL REACTION 8 - Carbon Dioxide Burning: CO + 0.5O2--> CO2+energy
*compname 'WATER'  'C11+' 'C6-10' 'C1-5' 'CO2' 'N2' 'O2' 'CO' 'Coke'
**
*storeac   0   0   0   0   0   0   0.5    1      0
*stoprod   0   0   0   0   1   0     0    0      0
*freqfac   1.5e5
** *freqfac 8.064E8
*eact 7550
```

*renth 1.8E5
** *solden 4.4
**
**
** Pseudocomponent K value tables for pressures 500 psi & 6500 psi 100oF to 1300oF be deg intervals
*kvtablim 500 3250 100 1300

*kvtable 2 ** K value table for C11+
1.320E-07 8.800E-08 6.600E-08 5.280E-08 4.400E-08 3.772E-08 3.300E-08 2.933E-08
2.640E-08 2.400E-08 2.200E-08 2.031E-08
5.453E-06 3.635E-06 2.727E-06 2.181E-06 1.818E-06 1.558E-06 1.363E-06 1.212E-06
1.091E-06 9.915E-07 9.088E-07 8.389E-07
8.461E-05 5.641E-05 4.230E-05 3.384E-05 2.820E-05 2.417E-05 2.115E-05 1.880E-05
1.692E-05 1.538E-05 1.410E-05 1.302E-05
6.938E-04 4.626E-04 3.469E-04 2.775E-04 2.313E-04 1.982E-04 1.735E-04 1.542E-04
1.388E-04 1.262E-04 1.156E-04 1.067E-04
3.671E-03 2.447E-03 1.835E-03 1.468E-03 1.224E-03 1.049E-03 9.176E-04 8.157E-04
7.341E-04 6.674E-04 6.118E-04 5.647E-04
1.418E-02 9.454E-03 7.090E-03 5.672E-03 4.727E-03 4.052E-03 3.545E-03 3.151E-03
2.836E-03 2.578E-03 2.363E-03 2.182E-03
4.340E-02 2.893E-02 2.170E-02 1.736E-02 1.447E-02 1.240E-02 1.085E-02 9.644E-03
8.679E-03 7.890E-03 7.233E-03 6.676E-03
1.112E-01 7.413E-02 5.560E-02 4.448E-02 3.707E-02 3.177E-02 2.780E-02 2.471E-02
2.224E-02 2.022E-02 1.853E-02 1.711E-02
2.481E-01 1.654E-01 1.241E-01 9.925E-02 8.271E-02 7.089E-02 6.203E-02 5.514E-02
4.962E-02 4.511E-02 4.135E-02 3.817E-02
4.960E-01 3.307E-01 2.480E-01 1.984E-01 1.653E-01 1.417E-01 1.240E-01 1.102E-01
9.920E-02 9.018E-02 8.267E-02 7.631E-02
9.073E-01 6.048E-01 4.536E-01 3.629E-01 3.024E-01 2.592E-01 2.268E-01 2.016E-01
1.815E-01 1.650E-01 1.512E-01 1.396E-01
1.543044 1.029E+00 7.715E-01 6.172E-01 5.143E-01 4.409E-01 3.858E-01 3.429E-01
3.086E-01 2.806E-01 2.572E-01 2.374E-01
2.470692 1.647E+00 1.235E+00 9.883E-01 8.236E-01 7.059E-01 6.177E-01 5.490E-01
4.941E-01 4.492E-01 4.118E-01 3.801E-01
*KVTABLE 3 ** K VALUE TABLE FOR C6-C10
0.0019 0.0013 0.0010 0.0008 0.0006 0.0005 0.0005 0.0004 0.0004 0.0003 0.0003 0.0003
0.0147 0.0098 0.0073 0.0059 0.0049 0.0042 0.0037 0.0033 0.0029 0.0027 0.0024 0.0023
0.0655 0.0437 0.0328 0.0262 0.0218 0.0187 0.0164 0.0146 0.0131 0.0119 0.0109 0.0101
0.2068 0.1378 0.1034 0.0827 0.0689 0.0591 0.0517 0.0459 0.0414 0.0376 0.0345 0.0318
0.5135 0.3424 0.2568 0.2054 0.1712 0.1467 0.1284 0.1141 0.1027 0.0934 0.0856 0.0790
1.0743 0.7162 0.5372 0.4297 0.3581 0.3070 0.2686 0.2387 0.2149 0.1953 0.1791 0.1653
1.9790 1.3193 0.9895 0.7916 0.6597 0.5654 0.4947 0.4398 0.3958 0.3598 0.3298 0.3045
3.3085 2.2057 1.6542 1.3234 1.1028 0.9453 0.8271 0.7352 0.6617 0.6015 0.5514 0.5090
5.1286 3.4190 2.5643 2.0514 1.7095 1.4653 1.2821 1.1397 1.0257 0.9325 0.8548 0.7890
7.4866 4.9911 3.7433 2.9946 2.4955 2.1390 1.8716 1.6637 1.4973 1.3612 1.2478 1.1518

10.4114 6.9410 5.2057 4.1646 3.4705 2.9747 2.6029 2.3137 2.0823 1.8930 1.7352
1.6018
13.9149 9.2766 6.9575 5.5660 4.6383 3.9757 3.4787 3.0922 2.7830 2.5300 2.3192
2.1408
17.9943 11.9962 8.9972 7.1977 5.9981 5.1412 4.4986 3.9987 3.5989 3.2717 2.9991
2.7684
*kvtable 4 ** K VALUE TABLE FOR C1-C5
0.0318 0.0212 0.0159 0.0127 0.0106 0.0091 0.0079 0.0071 0.0064 0.0058 0.0053 0.0049
0.1479 0.0986 0.0739 0.0591 0.0493 0.0422 0.0370 0.0329 0.0296 0.0269 0.0246 0.0227
0.4590 0.3060 0.2295 0.1836 0.1530 0.1311 0.1147 0.1020 0.0918 0.0834 0.0765 0.0706
1.0947 0.7298 0.5473 0.4379 0.3649 0.3128 0.2737 0.2433 0.2189 0.1990 0.1824 0.1684
2.1785 1.4523 1.0893 0.8714 0.7262 0.6224 0.5446 0.4841 0.4357 0.3961 0.3631 0.3352
3.8075 2.5383 1.9038 1.5230 1.2692 1.0879 0.9519 0.8461 0.7615 0.6923 0.6346 0.5858
6.0438 4.0292 3.0219 2.4175 2.0146 1.7268 1.5110 1.3431 1.2088 1.0989 1.0073 0.9298
8.9153 5.9435 4.4576 3.5661 2.9718 2.5472 2.2288 1.9812 1.7831 1.6210 1.4859 1.3716
12.4202 8.2801 6.2101 4.9681 4.1401 3.5486 3.1050 2.7600 2.4840 2.2582 2.0700
1.1908
16.5347 11.0231 8.2674 6.6139 5.5116 4.7242 4.1337 3.6744 3.3069 3.0063 2.7558
2.5438
21.2194 14.1463 10.6097 8.4878 7.0731 6.0627 5.3049 4.7154 4.2439 3.8581 3.5366
3.2645
26.4251 17.6168 13.2126 10.5701 8.8084 7.5500 6.6063 5.8723 5.2850 4.8046 4.4042
4.0654
32.0977 21.3985 16.0488 12.8391 10.6992 9.1708 8.0244 7.1328 6.4195 5.8359 5.3496
4.9381
*kvtable 5 ** K VALUE TABLE FOR CO2
2.4914 1.6609 1.2457 0.9966 0.8305 0.7118 0.6229 0.5536 0.4983 0.4530 0.4152 0.3833
6.8249 4.5500 3.4125 2.7300 2.2750 1.9500 1.7062 1.5167 1.3650 1.2409 1.1375 1.0500
14.3411 9.5607 7.1705 5.7364 4.7804 4.0975 3.5853 3.1869 2.8682 2.6075 2.3902
2.2063
25.3553 16.9035 12.6776 10.1421 8.4518 7.2444 6.3388 5.6345 5.0711 4.6101 4.2259
3.9008
39.8103 26.5402 19.9052 15.9241 13.2701 11.3744 9.9526 8.8467 7.9621 7.2382 6.6351
6.1247
57.4057 38.2705 28.7029 22.9623 19.1352 16.4016 14.3514 12.7568 11.4811 10.4374
9.5676 8.8317
77.7156 51.8104 38.8578 31.0862 25.9052 22.2045 19.4289 17.2701 15.5431 14.1301
12.9526 11.9562
100.2720 66.8480 50.1360 40.1088 33.4240 28.6491 25.0680 22.2827 20.0544 18.2313
16.7120 15.4265
124.6166 83.0777 62.3083 49.8466 41.5389 35.6047 31.1541 27.6926 24.9233 22.6576
20.7694 19.1718
150.3284 100.2189 75.1642 60.1314 50.1095 42.9510 37.5821 33.4063 30.0657 27.3324
25.0547 23.1274
177.0362 118.0241 88.5181 70.8145 59.0121 50.5818 44.2590 39.3414 35.4072 32.1884
29.5060 27.2363

204.4214 136.2809 102.2107 81.7685 68.1405 58.4061 51.1053 45.4270 40.8843
37.1675 34.0702 31.4494
232.2161 154.8107 116.1080 92.8864 77.4054 66.3475 58.0540 51.6036 46.4432
42.2211 38.7027 35.7256
*kvtable 6 ** K VALUE TABLE FOR N2
27.0188 18.0125 13.5094 10.8075 9.0063 7.7197 6.7547 6.0042 5.4038 4.9125 4.5031
4.1567
38.0483 25.3655 19.0241 15.2193 12.6828 10.8709 9.5121 8.4552 7.6097 6.9179 6.3414
5.8536
48.9645 32.6430 24.4822 19.5858 16.3215 13.9898 12.2411 10.8810 9.7929 8.9026
8.1607 7.5330
59.4225 39.6150 29.7113 23.7690 19.8075 16.9779 14.8556 13.2050 11.8845 10.8041
9.9038 9.1419
69.2638 46.1759 34.6319 27.7055 23.0879 19.7897 17.3160 15.3920 13.8528 12.5934
11.5440 10.6560
78.4340 52.2893 39.2170 31.3736 26.1447 22.4097 19.6085 17.4298 15.6868 14.2607
13.0723 12.0668
86.9345 57.9563 43.4672 34.7738 28.9782 24.8384 21.7336 19.3188 17.3869 15.8063
14.4891 13.3745
94.7952 63.1968 47.3976 37.9181 31.5984 27.0843 23.6988 21.0656 18.9590 17.2355
15.7992 14.5839
102.0592 68.0395 51.0296 40.8237 34.0197 29.1598 25.5148 22.6798 20.4118 18.5562
17.0099 15.7014
108.7741 72.5161 54.3871 43.5097 36.2580 31.0783 27.1935 24.1720 21.7548 19.7771
18.1290 16.7345
114.9876 76.6584 57.4938 45.9951 38.3292 32.8536 28.7469 25.5528 22.9975 20.9068
19.1646 17.6904
120.7452 80.4968 60.3726 48.2981 40.2484 34.4986 30.1863 26.8323 24.1490 21.9537
20.1242 18.5762
126.0891 84.0594 63.0445 50.4356 42.0297 36.0254 31.5223 28.0198 25.2178 22.9253
21.0148 19.3983

** Reference Conditions
*prsr 14.7 *temr 77 *psurf 14.65 *tsurf 62

** ==========ROCK-FLUID PROPERTIES==========
*rockfluid

*swt **Water-Oil Relative Permeabilities

** Sw Krw Kro
** — — —

0.31 0 1.0
0.3323 0.0037 0.9963
0.3547 0.0104 0.9896

```
0.3769 0.0191 0.9809
0.3992 0.0294 0.9706
0.4215 0.041  0.959
0.4439 0.0539 0.9461
0.4662 0.068  0.932
0.5108 0.0991 0.9009
0.5331 0.116  0.884
0.5554 0.1339 0.8661
0.5777 0.1525 0.8475
0.68   0.2479 0.7521
0.76   0.3325 0.6675
0.84   0.425  0.575
0.92   0.5247 0.4753
1      0.6313 0.0

**     0.31   0.0    1.0
**     0.3323 0.0037 0.8869
**     0.3547 0.0104 0.7784
**     0.3769 0.0191 0.6747
**     0.3992 0.0294 0.576
**     0.4215 0.041  0.4828
**     0.4439 0.0539 0.3951
**     0.4662 0.068  0.3136
**     0.5108 0.0991 0.1707
**     0.5331 0.116  0.1109
**     0.5554 0.1339 0.0603
**     0.5777 0.1525 0.0213
**     0.6800 0.2479 0.00
**     0.7600 0.3325 0.00
**     0.8400 0.425  0.00
**     0.9200 0.5247 0.00
**     1.0000 0.6313 0.00

**     0.752  0.256  0.0

*slt        ** Liquid-gas relative permeabilities

**     Sl     Krg    Krog
**
       0.31   0.49   0.00
       0.43   0.3344 0.00
       0.5909 0.1722 0.0008
       0.7139 0.0844 0.0481
       0.8364 0.0276 0.2577
       0.9591 0.0017 0.7513
       1.000  0.000  1.000
```

```
** *swr 0.25 *sorw 0.25 *sgr 0.12 *sorg 0.2
** ═══════════════════════IINITIAL CONDITIONS ═══════════════════
*initial
*pres *con 2900              ** High initial pressure 70 bar ( 7000 kPa or 1015.266 psi)
*sw *con 0.70                    ** Initial water saturation is 0.70
*so *con 0.23                ** initial gas saturation is 0.05

*temp *con 100                   ** Reservoir Bed Temperature 23 oC ( 73.4oF)
Minimum 100

** Gas in tube at the initial conditions is N2 with small concentration of C1-C5
** at equilibrium with the liquid petroleum phase (99.7% N2 & 0.3% C1-C5).

*MFRAC_GAS 'N2' *CON 0.997
*MFRAC_GAS 'C1-5' *CON 0.003

**                    **          'WATER'  'C11+' 'C6-10' 'C1-5'  'CO2'  'N2'  'O2'
'CO'  'COKE'
**                                *molefrac *gas *con        3*0.0        0.003  0.0
0.997 0.0    0.0

**                                ** *molefrac &gas *con             5*0.0
0.79  0.21   0.0
**        ** Initial petroleum phase fraction are : C11+ = 0.419300  C6-C10 = 0.276600
C1-c5= 0.304100
**                ** After equilibization with the N2 gas phase the Nitrogen fraction in
the oil phase is 0.04 and
**                ** the hydrocarbon frcaction are : C11+=0.402528  C6-C10 =0.265536
C1-C5= 0.291936

** This is the new run for Ekofisk oil, X-31
*MFRAC_OIL 'C11+' *CON 0.6139565
*MFRAC_OIL 'C6-10' *CON 0.292828
*MFRAC_OIL 'C1-5' *CON 0.0432535
*MFRAC_OIL 'N2' *CON 0.05
**                                **          'WATER'  'C11+'  'C6-10'  'C1-5'  'CO2'
'N2'  'O2'   'CO'   'COKE'
**                                    *molefrac *oil *con 0.0   0.385756 0.254472
0.279772 0.0   0.08
**                                  ** *MOLEFRAC *OIL *CON 0.0 0.419300
0.276600 0.304100 0.0 0.0

** ═══════════════════ NUMERICAL CONTROL ═══════════════════

*numerical ** All these can be defaulted. The definitions
```

```
                ** here match the previous data.

*maxsteps 1800 *north 10 *newtoncyc 20 *itermax 15

*norm  press 15  satur .1 temp 40 y .1  x .1
*converge press .15 satur .002 temp .5 y .002 x .002
**ncuts 30
*run

** ========== RECURRENT DATA ==========

time 0 dtwell .005


well 1 'INJECTOR' injector 1
*incomp gas 5*0.0 0.79 0.21 0.0

*TINJW 100                                  ** the recomended is 70 oF but the k
value start at 100 oF
operate gas 27.50954          **23.27176*12.983/10.983   ** Injection Rate 23.27176
ft3/hr (83.9 m3/m2hr)
** 100 cm3/min               ** Injection Rate 2.219 ft3/hr (8m3/m2hr)
perf 1  ** i j  k  wi(gas)
          1  1  128  5.54
**incomp gas 5*0.0 0.79 0.21 0.0
**incomp water 1.0 0.0 0.0 0.0
**tinjov 73.4
**tinjw 70

well 2 'PRODUCER' producer 2
operate bhp 2900
monitor temp 1800 stop
geometry k 1 1 1 0            ** Linear pressure drop at tube end
*PERF *Tube-END 2 ** i j k
        1 1 1 1.0



**perf geo 2 ** i j k
**          1 1 1
*shutin 1

heatr ijk 1 1 122:128 350           ** Use external heaters to raise the temperature
**heatr ijk 1 1 63 550         ** USe external heaters to raise the temperature
**heatr ijk 1 1 126 550             ** Use external heaters to raise the temperature
time 0.083
```

```
outsrf grid pres sw so sg temp y x w solconc obhloss
              masdenw masdeno masdeng pcow pcog visw viso visg
time 0.15
outsrf grid pres sw so sg temp y x w solconc obhloss
              masdenw masdeno masdeng pcow pcog visw viso visg
time 0.25
outsrf grid pres sw so sg temp y x w solconc obhloss
              masdenw masdeno masdeng pcow pcog visw viso visg
time 0.30

open 1

time .3333

heatr con 0                    ** Shut off external heters

time 0.35

outsrf grid pres sw so sg temp y x w solconc obhloss
              masdenw masdeno masdeng pcow pcog visw viso visg
time 0.4
outsrf grid pres sw so sg temp y x w solconc obhloss
              masdenw masdeno masdeng pcow pcog visw viso visg
time 0.45
outsrf grid pres sw so sg temp y x w solconc obhloss
              masdenw masdeno masdeng pcow pcog visw viso visg
time 0.48
outsrf grid pres sw so sg temp y x w solconc obhloss
              masdenw masdeno masdeng pcow pcog visw viso visg
time 0.53
outsrf grid pres sw so sg temp y x w solconc obhloss
              masdenw masdeno masdeng pcow pcog visw viso visg



time 0.55
outsrf grid none
time 0.6
outsrf grid pres sw so sg temp y x w solconc obhloss
              masdenw masdeno masdeng pcow pcog visw viso visg
time 0.7
outsrf grid none
time 0.8
outsrf grid pres sw so sg temp y x w solconc obhloss
              masdenw masdeno masdeng pcow pcog visw viso visg
time 1.0
```

```
outsrf grid none
time 1.2
outsrf grid pres sw so sg temp y x w solconc obhloss
        masdenw masdeno masdeng pcow pcog visw viso visg
time 1.4
outsrf grid none
time 1.5
    outsrf grid pres sw so sg temp y x w solconc obhloss
        masdenw masdeno masdeng pcow pcog visw viso visg
        krw kro krg kvalyw kvalyx cmpdenw cmpdeno cmpvisw
        cmpviso cmpvisg cchloss
time 1.6
outsrf grid none
time 1.8
    outsrf grid pres sw so sg temp y x w solconc obhloss
        masdenw masdeno masdeng pcow pcog visw viso visg
        krw kro krg kvalyw kvalyx cmpdenw cmpdeno cmpvisw
        cmpviso cmpvisg cchloss
time 2.0
outsrf grid none
time 2.2
outsrf grid none
time 2.4
    outsrf grid pres sw so sg temp y x w solconc obhloss
        masdenw masdeno masdeng pcow pcog visw viso visg
        krw kro krg kvalyw kvalyx cmpdenw cmpdeno cmpvisw
        cmpviso cmpvisg cchloss
time 2.5
    outsrf grid none
time 2.6
outsrf grid none
time 2.8
    outsrf grid pres sw so sg temp y x w solconc obhloss
        masdenw masdeno masdeng pcow pcog visw viso visg
        krw kro krg kvalyw kvalyx cmpdenw cmpdeno cmpvisw
        cmpviso cmpvisg cchloss
time 3.0
outsrf grid none
time 3.3
    outsrf grid pres sw so sg temp y x w solconc obhloss
        masdenw masdeno masdeng pcow pcog visw viso visg
        krw kro krg kvalyw kvalyx cmpdenw cmpdeno cmpvisw
        cmpviso cmpvisg cchloss
time 3.5
outsrf grid none
time 3.75
```

```
        outsrf grid pres sw so sg temp y x w solconc obhloss
                masdenw masdeno masdeng pcow pcog visw viso visg
                krw kro krg kvalyw kvalyx cmpdenw cmpdeno cmpvisw
                cmpviso cmpvisg cchloss
time 4.0
outsrf grid none
time 4.25
        outsrf grid pres sw so sg temp y x w solconc obhloss
                masdenw masdeno masdeng pcow pcog visw viso visg
                krw kro krg kvalyw kvalyx cmpdenw cmpdeno cmpvisw
                cmpviso cmpvisg cchloss
time 4.5
outsrf grid none
time 4.75
        outsrf grid pres sw so sg temp y x w solconc obhloss
                masdenw masdeno masdeng pcow pcog visw viso visg
                krw kro krg kvalyw kvalyx cmpdenw cmpdeno cmpvisw
                cmpviso cmpvisg cchloss
time 5.0
outsrf grid none
time 5.25
        outsrf grid pres sw so sg temp y x w solconc obhloss
                masdenw masdeno masdeng pcow pcog visw viso visg
time 6.0
stop
```

APPENDIX - F

Axial and Wall Temperature Differences

Run 8:

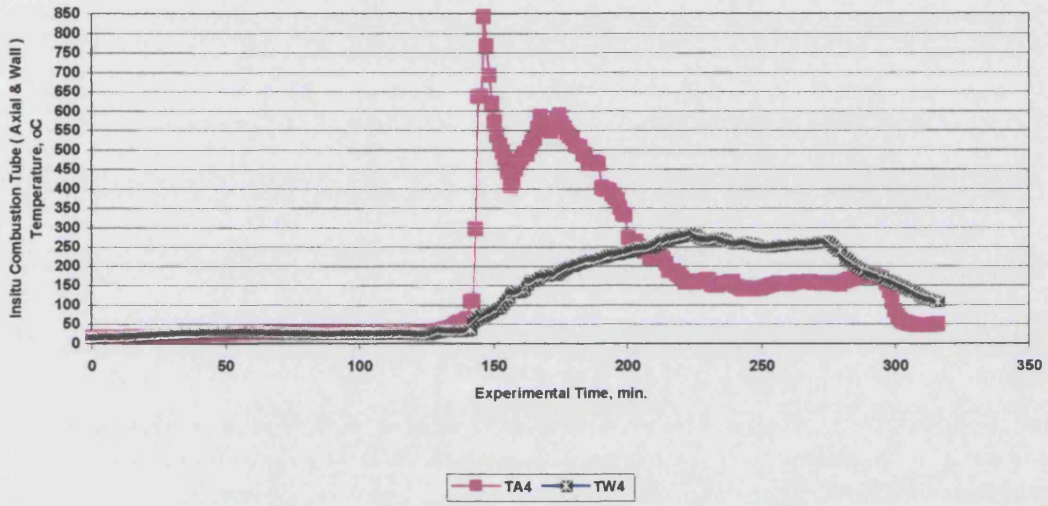

Figure F-1 Run 8 : Axial and Wall Temperature, TA4 and BH4.

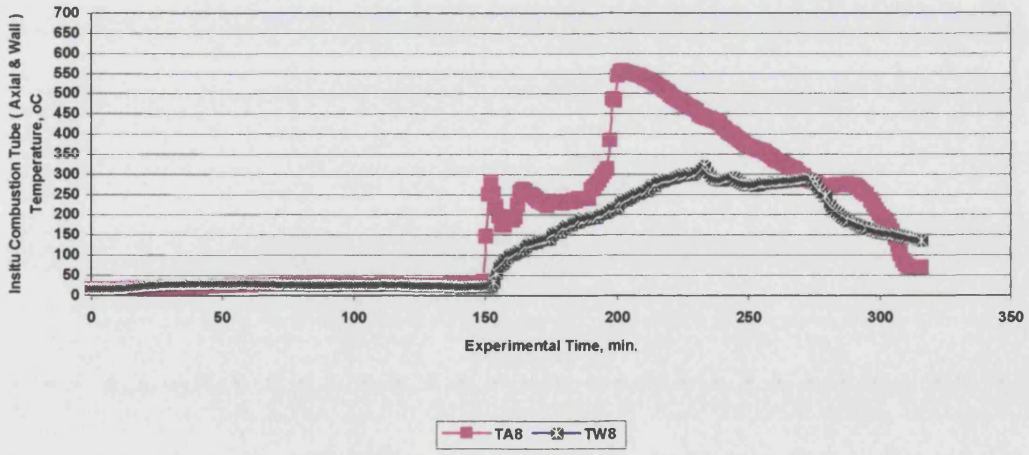

Figure F-2 Run 8 : Axial and Wall Temperature, TA8 and BH8.

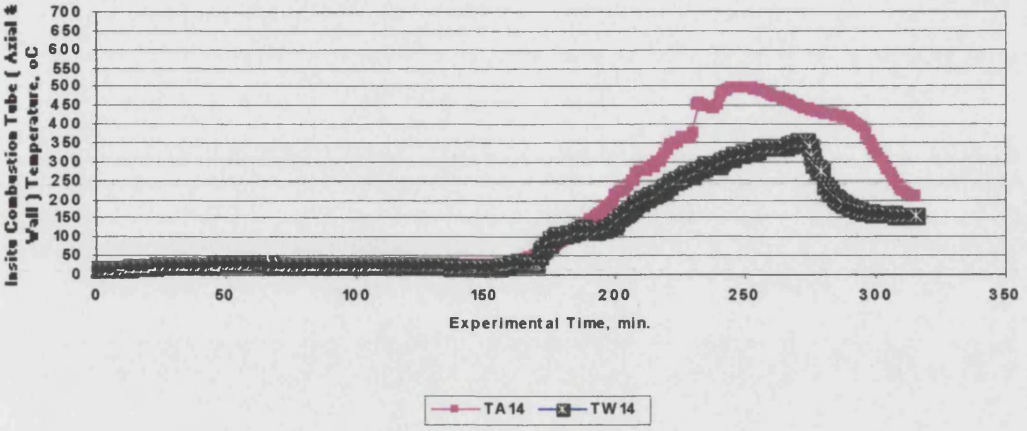

Figure F-3 Run 8 : Axial and Wall Temperature, TA14 and BH14.

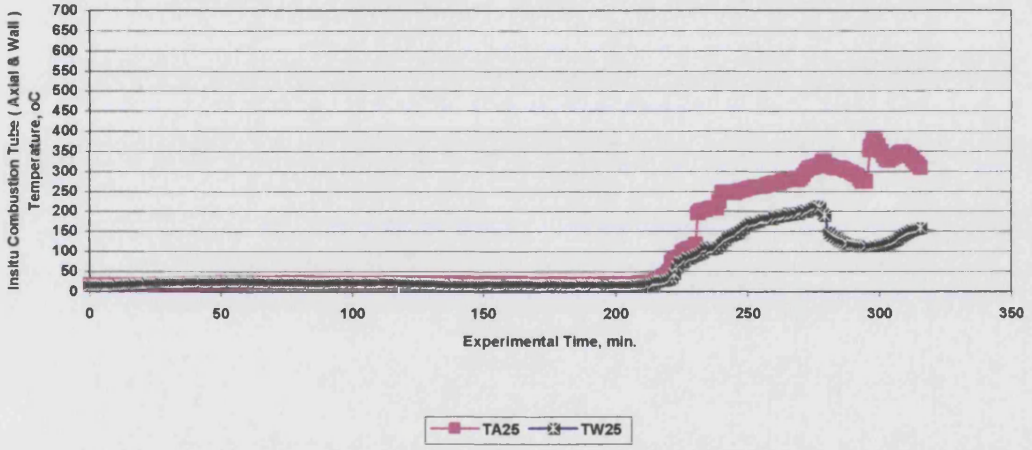

Figure F-4 Run 8 : Axial and Wall Temperature, TA25 and BH25.

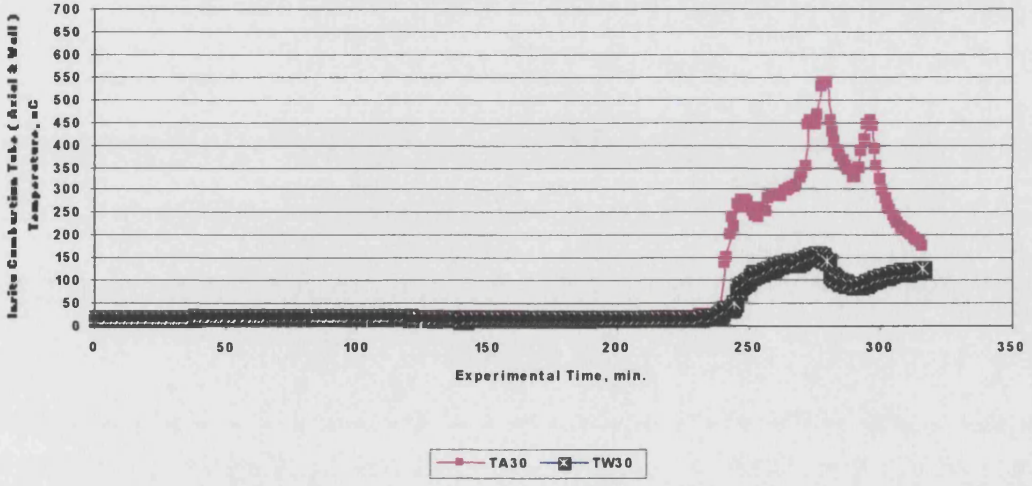

Figure F-5 Run 8 : Axial and Wall Temperature, TA30 and BH30.

Run 9:

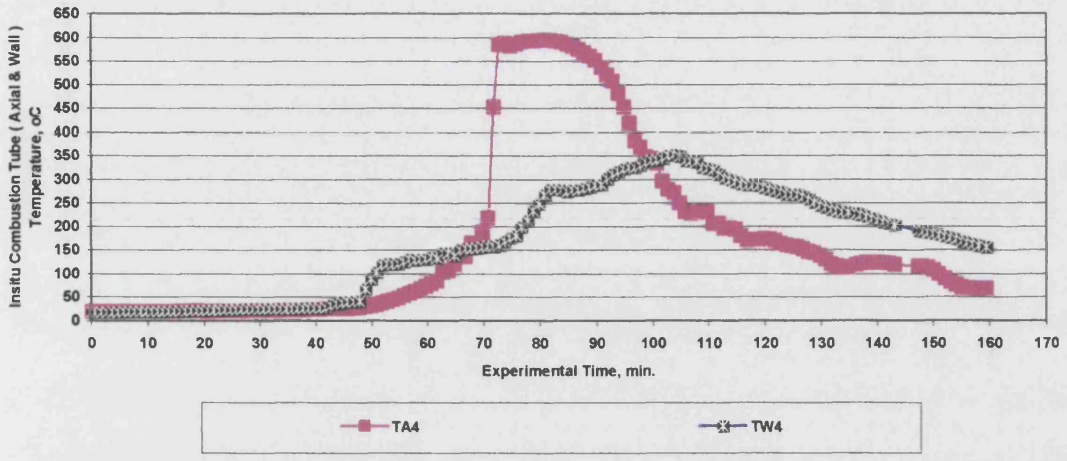

Figure F-6 Run 8 : Axial and Wall Temperature, TA4 and BH4.

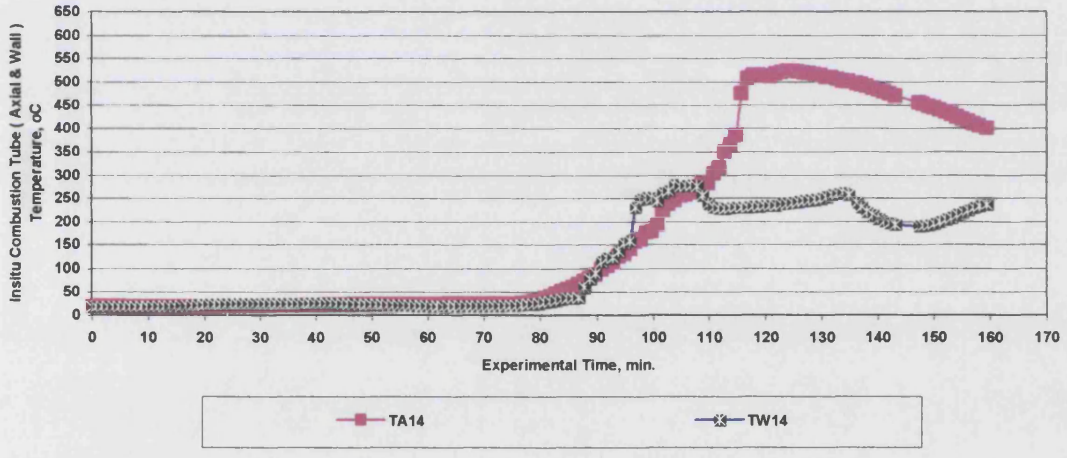

Figure F-7 Run 9 : Axial and Wall Temperature, TA14 and BH14.

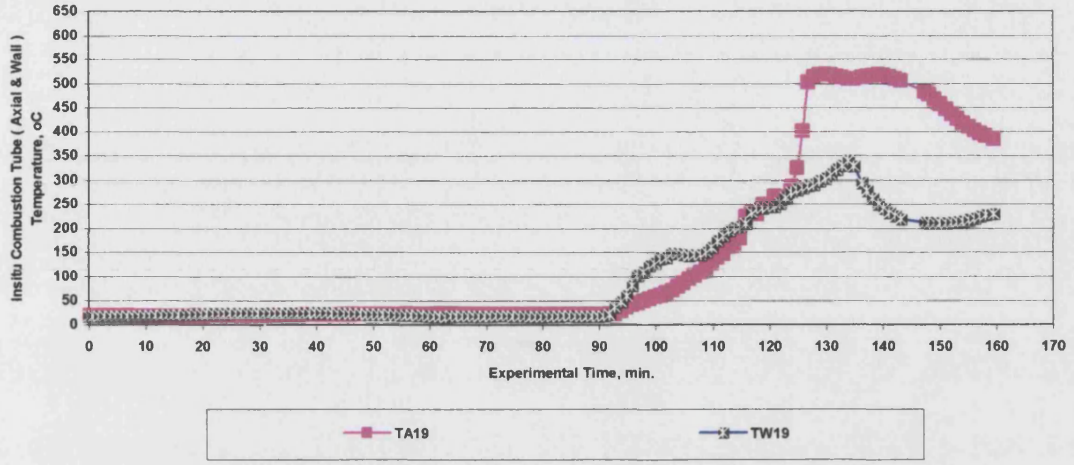

Figure F-8 Run 9 : Axial and Wall Temperature, TA19 and BH19.

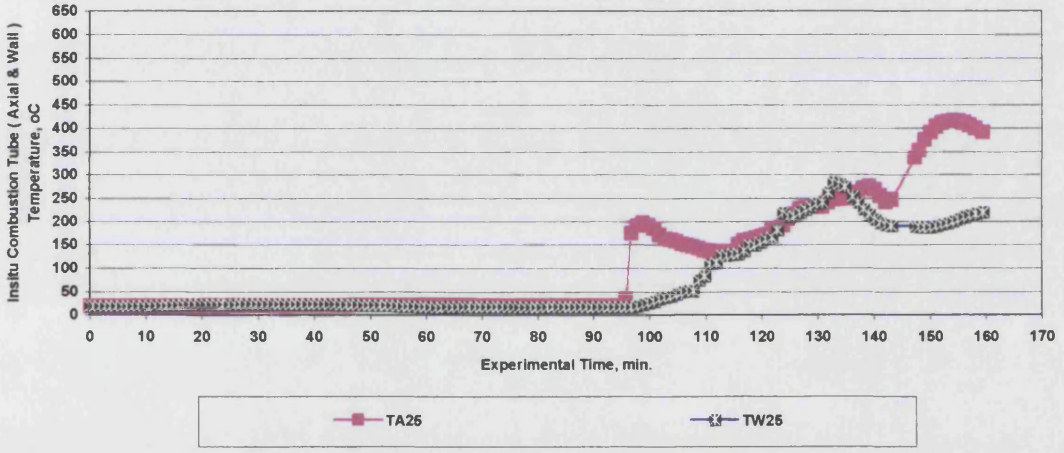

Figure F-9 Run 9 : Axial and Wall Temperature, TA25 and BH25.

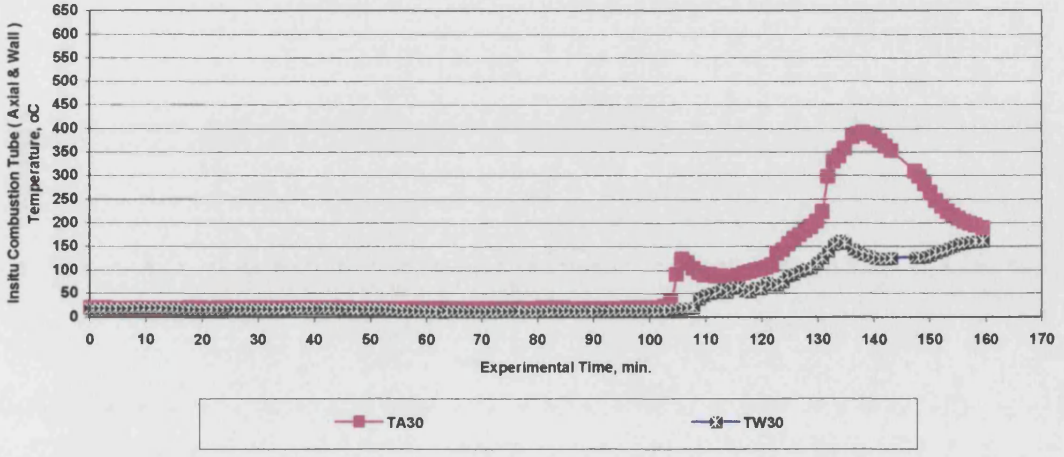

Figure F-10 Run 9 : Axial and Wall Temperature, TA30 and BH30.

Published Papers

IOR-B023

AIR INJECTION INTO DEEP LIGHT OIL RESERVOIRS: COMBUSTION TUBE STUDIES

AUTHOR(S)
M. GREAVES,R.R. RATHBONE.O. EL AYADI AND M.EL ABIDI
Address
Improved Oil Recovery Group,Department of Chemical Engineeering,University of Bath,Bath BA2 7AY,England

Abstract

Water flooding can leave more than 30% residual oil,with some areas of the reservoir containing much higher Sor's in tighter zones,or trapped beneath shale lenses. How to access this oil residual? Air injection may be a good candidate and could be operated either in a low temperature oxidation (LTO) mode, at the reservoir temperature,or in a high temperature oxidation mode (HTO),i.e. in-situ combustion. Or even a combination of the two. Does it matter which? Only if the oxygen in the injected air is not consumed ,before reaching the production well,or if undesirable oxygenated products are formed.

Two high pressure combustion tube tests (200 bar) were performed on a North Sea light crude oil,using MIL (mud industry limestone) to represent the chalk matrix. The residual oil saturation was Sor = 30 %,with Swr = 70 %. With such a large amount of water present in the reservoir,an economic recovery process must be capable of mobilizing the residual oil at a high enough rate,without excessive,or prolonged,water production. The air injection flux is a critical parameter,both technically and economically.

In one of the tests,sustained propagation of the combustion front was achieved,traversing the full length of the 1.2 m combustion tube. However,the second test,which used a lower air injection flux,did not sustain combustion front propagation. Generally,combustion temperatures were around 450 °C,but some 'high peaks' were observed for short periods. Cumulatives oil recoveries varied from 10 % to 70 %,depending on the air flux. *Post mortem* inspection of the combusted matrix showed that it was largely clean,with no residual oil or coke. Some solid inclusions were also found.

Introduction

Maturing oil provinces in the North Sea,USA and other areas of the world face dimishing propects,unless new techniques are developed in time. In tight,very low permeability reservoirs,gas injection may be the only answer. Where to get sufficient gas to inject? In Western Europe and North America,market forces usually dictate that the hydrocarbon gases are sold. Carbon dioxide is only available from natural sources in a few areas and may frequently require pipelining. The same can be said of flue gas,which will usually require collection.. Most IOR (Improved Oil Recovery) methods require the 'Injection of an 'Expensive Fluid' and the options available for a suitable process in the field tend to reduce sharply. One gas which is cheap,available in large quantities,everywhere,is air. Fassihi et al. **(Ref. 1)** estimated the economics for small gas injection projects to be approximately $2-4 capital and $3-5 operating expense per barrel of incremental oil produced.

Air injection into light reservoirs can be either a secondary or tertiary recovery process. Light oil reservoirs are usually deep enough and therefore at sufficiently high temperature for spontaneous ignition of the oil to occur. This is because the reactivity of the oil increases rapidly with temperature. Yannimaras et al. **(Ref. 2)** employed accelerating rate calorimetry to determine the exothermicity characteristics of different oils. This provides a type of fingerprint identity for each oil,indicating whether the oil is sufficiently reactive in the LTO region (reservoir temperature up to 250 °C) to autoignite,and whether also,there will be a smooth transition to the in situ combustion (ISC) region,and HTO of the oil. For a light oil,LTO can be sufficient **(Ref.3,4)** to create a safe process,i.e. remove all of the oxygen in the injected air by reaction with the oil. As the oxidation zone (LTO) or combustion zone (HTO) moves through the reservoir,stripped HC gases,steam and flue gas (mainly CO2 and N2) displace the oil,consuming about 5% to 8% of the oil as fuel. Combustion tube studies are used to determine how much air is required and also whether a self-sustaining,combustion front can be propagated through the reservoir core **(Refs 5,6,7).** Although combustion tube experiments mimic the sub-processes,i.e. formation of a steam bank,condensed water and oil bank,and show that only about one-third of the core needs to be swept inorder to recover most of the oil,because they are 1-D and the moving front is artificially stabilized,they cannot provide any useful information on sweep efficiency and scale-up. This requires 3-D experiments **(Ref.8).** Combustion tube data is also useful for validating reaction kinetic models that need to be incorporated into numerical simulators.

Experimental

The arrangement of the combustion tube facility is shown in Fig. 1. The combustion tube is 1.2 m long and 0.1m in diameter. It is surrounded by 32 band heaters. Temperature is measured by an axial probe with a thermocouple at each band heater position. The band heaters may be controlled individually to maintain adiabatic conditions. The combustion tube assembly is contained within a pressure shell to allow operation to 240 bar pressure. The produced fluids are separated and gas flowrate and CO, CO_2, O_2 composition is monitored.

The matrix material used in the runs reported here was MI limestone which was chosen to simulate the chalk matrix in the Ekofisk field and provide sufficient injectivity to operate the combustion tube. The matrix material was premixed with oil and water before packing into the combustion tube. Experimental conditions for both runs are given in Table 1. Both tests were operated without bandheater control,so causing significant heat loss.

Run 4 – High Air Flux

This test was run without bandheater (BH) control,i.e non-adiabatically,and therefore respresents a pessimistic case compared to the reservoir. Following nitrogen injection and preheating of the inlet section of the core,immediate ignition was achieved at 215 °C (178 minutes) when air injection started. The core temperature increased rapidly to 614 °C (180 minutes) and the combustion front then propagated outwards from the inlet face to reach BH2 location at 184 minutes. The combustion front temperature then steadied at around 450 °C,as shown in Fig. 2. Heating of downstream sections of the core occurred due to fluid transport and LTO. This created two secondary fronts at BH20 (213 minutes) and BH 23 (215 minutes),with temperatures between 260 – 280 °C. During this time the main combustion front became stalled at BH5 for 17 minutes,remaining at 465 °C. A new secondary front started at BH 20 at (225 minutes). The main combustion front reactivated with a temperature of 450 - 500°C and advanced to the middle of the tube,as shown in Fig. 3. Although the secondary fronts were still propagating up to this point,the more dramatic effect subsequently,was the sudden appearance of the two very high temperature peaks. For a light oil,such high temperatures (700 – 900 °C) were not anticipated. This high temperature effect was also confirmed by the bluish temper colour of the stainless steel axial thermocouple probe when it was inspected after the test. The leading edge of the combustion front continued to propagate to the end of the tube at a temperature of 807 °C ,when combustion was terminated (285 minutes).

For most of Run 4,the air injection rate was maintained at 10.81 litres/min (82.59 m3/h m2),but the rate was reduced to 5.2 litres/min towards the end of the run (272 – 284 minutes). The composition of the produced gas is shown in Fig. 4. The high carbon monoxide concentration,initially,is due to LTO,but it falls rapidly as the combustion front becomes more stabilized. The carbon dioxide concentration remains at a high level,around 12 %,or more,throughout the run. When the combustion front stalled for a short period during the early part of the test,the oxygen was not totally consumed,and significant amounts of were produced. Oxygenated oil,containing free-radicals may have concentrated in the oil in the downstream sections of in the core,causing the high combustion temperatures (see previous section). In the field there would be sufficient residence time for the oxidation reactions to go to completion,so long as the reservoir temperature is high enough (> 90 °C).

Fig. 5 shows the variation of the combustion front velocity during the test. Before the occurrence of the secondary front(s),the velocity is in the range 0.3 – 0.5 cm/min (0.18 – 0.3 m/h). This is to be expected with such high air injection rates in the combustion tube. However,if the injection rate is scaled to reservoir condition,wherein the actual rock permeability is only few mD,compared to 1D (approximately) for the crushed MI limestone,it will be reduced by a large factor. Similarly,the combustion front velocity in a homogeneous reservoir will be of the order of fraction of a m/day,because the air injection flux will be of the order of 1m3/h m2,or less.

Run 5 – Low Air Flux

The objective of this test was to see if combustion could be sustained with a lower air injection flux compared to over 80 m3/h m2 in Run 4. In the later period of the test,the air flux was increased to 93.8 m3/h m2,but this lasted for only about 10 per cent of the total period of air injection. As can be seen in Fig. 6, oxygen breakthough occurs at the production end of the combustion tube soon after ignition,at 119 minutes. However,combustion is not fully established and there is a rapid deterioration in performance leading to severe oxygen breakthrough. The situation was only recovered somewhat by heating the tube to 150 °C. This is entirely artificial,since the reservoir should operate close to adiabatic. Although much improved carbon dioxide levels are achieved,oscillating about the 10 % level,a self-sustained combustion front was never achieved and the produced oxygen levels remained high.

The conclusion to be gained from the two tests combustion tests,is that,inorder to propagate a stable combustion front with this light oil,the air injection rate needs to be above a certain minimum value. This figure appears to be correspond to a minimum air injection flux of approximately 40 m3/h m2. Because s the combustion front velocity was quite high in Run 4,the heat losses in the combustion front region were not sufficient to reduce the reaction intensity significantly. If full-adiabatic control had been employed to minimize heat losses (mimicking the reservoir) the minimum air injection flux required would,actually,be significantly lower than 40 m3/h m2.

Oil and Water Production Rates

The final oil recovery from Run 4 was 40 % OOIP,compared to only 9 % OOIP for Run 5. Although Run 5 was far from ideal,it underlines the important effect of air injection rate on the oil recovery. In Fig. 7, it is also apparent that,in Run 4,a large amount of water wasw produced along with the oil. This is to be expected,since the initial amount of water in the core was high at 70 %. The produced water-cut averaged just over 70 % before the oil was contacted by the combustion front (218 minutes),but then decreased down to about 43 % for the remainder of the test. It is important to remember that a 1-D combustion tube resultt cannot provide any reliable indication as to what the true oil recovery will be in the reservoir. This is because the combustion front is artificially stablilised – the tube was mounted vertically,and air i

was injected at the top. The combustion tube results (adiabatic preferably) may,however,be used to validate a suitable oil oxidation kinetics model,which can then be employed in a reservoir simulator.

Post mortem on Burned Core

After each test,the combustion tube and its contents were allowed to cool down to room temperature. The combustion tube was then placed in a horizontal position and the top flange plate was removed. A *post mortem* inspection of the burned MIL matrix was performed by carefully removing small quantities each time. In Run 4,virtually all of the MI limestone core had been swept by the combustion front. Consequently,the burned matrix was essentially clean,having a whitish appearance and loose structure. However,there were also some inclusions found at different distances along the tube. Pieces of hard material,or agglomerate,a few centimeters in size,were discovered 0.2 m along the MIL core,near to the wall. They contained interconnecting holes and some areas of the surface had a greenish colour,suggesting that the MIL may have been attacked by acidic, Approximately three-quarters distance along the tube (0.75 m),an unusual piece of material was found (Fig. 8). It was similar in appearance to a Conche shell,some 4 cms long. The outer shell was probably calcined material (calcite),due to the high combustion temperatures during that period (>800 °C). Another possible explanation for the disappearance of the interior is dissolution of the carbonate matrix by organic acids formed during LTO of the oil when the main combustion front became stalled.

In Run5,the MIL was mainly of whitish appearance for about one-third of the core,reflecting that it had been contacted by the combustion front. However,from the early stages of air injection the matrix shows unburnt areas near the wall. The dark,unburnt,or partially combusted areas increase across the core until,at 0.36 m from the top,it extends to approximately 80 %. There was also coke deposited at 0.42 m distance. At 0.72 m ,a hardened,shell-like agglomerate was discovered. It was surrounded by coke and the interior may have been dissolved by organic acid,as in Run 4.

Concluding Remarks

1. Comparing the combustion performance of Run 4 (high flux) against Run 5 (low flux) indicates that for the light crude oil,there is a minimum air injection rate needed to sustain propagation of a stable combustion front. This corresponded to an air injection flux of about 40 Sm3/h m2,when no band heater compensation was applied (non-adiabatic operation).
2. Stable in situ combustion was achieved at combustion temperatures of 450 °C. There were also short periods of very high combustion temperatures (>800 °),because more fuel was produced (locally) in downstream sections of the core. This was caused by LTO of the oil, arising from temporary stalling of the main combustion front.
3. The appearance of the burned MIL matrix from Run 4 (high flux) was white in colour with no residue or coke. Therefore,virtually all of the core had been contacted by the combustion front. A hard,calcited shell-like agglomerate was discovered at a distance of 0.75 m from the top of the core. The interior of the agglomerate was dissolved away,possibly due to the formation of organic acids (LTO condition) and also because of carbonate decomposition at the high combustion temperatures (HTO condition).
4. Oil recovery was strongly affected by the air injection rate,varing from 40% OOIP at high flux in Run 4 to only 9 % OOIP at low flux in Run 5.

References

1. Fassihi M. R.,Yannimaras D.V.,Westfail E.E. and Gilham T.H.,"Economics of Light Oil Air Injection",SPE Paper No. 36393,March 1996.

2. Yannimaras D.V. and Tiffin D.L ,"Screening of Oils for In-Situ Combustion at Reservoir Conditions by Accelerating Rate Calorimetry",SPERE,February 1995,pp 36-39.
3. Ren R.S.,Greaves M. and Rathbone,R.R.," Oxidation Kinetics of Noth Sea Light Crude Oils",Trans IChemE,Vol 77,Part A,1999,pp 385-394.
4. Ren S.R.,Greaves M. and Rathbone,R.R.,"Air Injection LTO Process: An IOR Technique for Light Oil Reservoirs",SPE Journal,March 2002,pp 90-99.
5. Tiffen D.L. and Yannimaras D.V.,"High Pressure Combustion Tube Performance of Light Oils",8th European Symposium on IOR,Vienna,Austria,May 15-17,1995.
6. Greaves M.,Young T J,El-Usta,S.,Rathbone R.R.,Ren,S.R. and Xia,T.X.,"Air Injection into Light and Medium Heavy Oil Reservoirs",Trans IChemE,Vol 78,Part A,2000,pp 721-730.
7. Juan E.S.,Sanchez A.,del Monte A.,Moore R.G.,Mehta S.A. and Ursenbach M.G.,"Laboratory Screening of Air Injection-Based IOR in Two Waterflooded Light Oil Reservoirs",Paper 2003-215: The Petroleum Society's Canadian International Petroleum Conference,Calgary,Canada,June 10-12,2003.
8. Wilson A,Shallcross D.C. and Greaves M,"Three-Dimensional Studies of In-Situ Combustion Process with Reservoir Heterogeneities",INSITU,Vol 24,No. 4,2000,pp 251-276.

Acknowledgement

The authors are grateful to the Joint Management Committee of the AIROIL Project for permission to publish the results contained in this paper. We are also grateful to the European Community for supporting the research via Contract No. NNE5/1999/20071,under the RTD and Demonstration activity on "Energy,Environment and Sustainable Development – Part B Energy Program".

O. El Ayadi is grateful to the Libyan Education Ministry for funding his PhD studies at the University of Bath and similarly,M. El Abidi gratefully acknowledges support from Veba Oil Company,whilst studying for his MPhil degree.

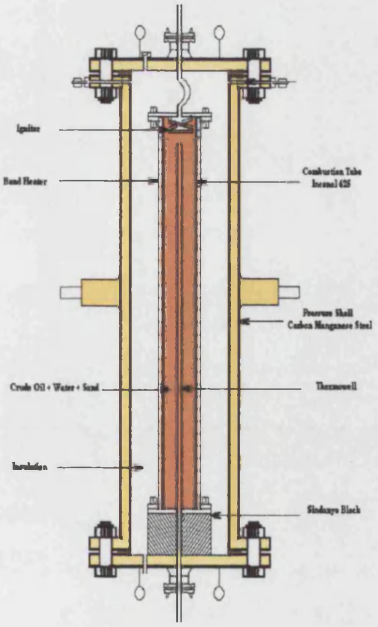

Figure 1 Combustion Tube Schematic

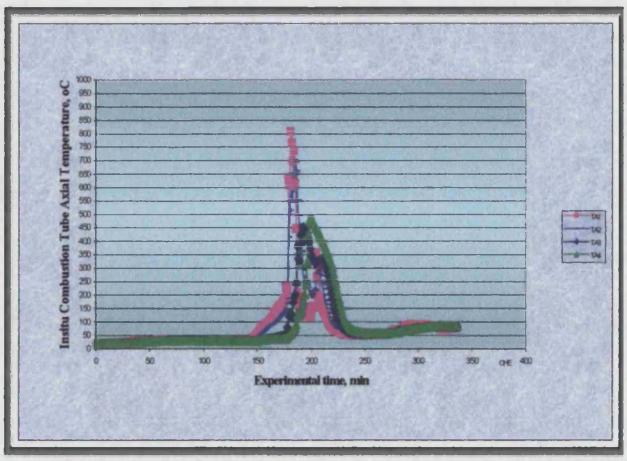

Figure 2 Temperatures near the top of the combustion tube during Run 4

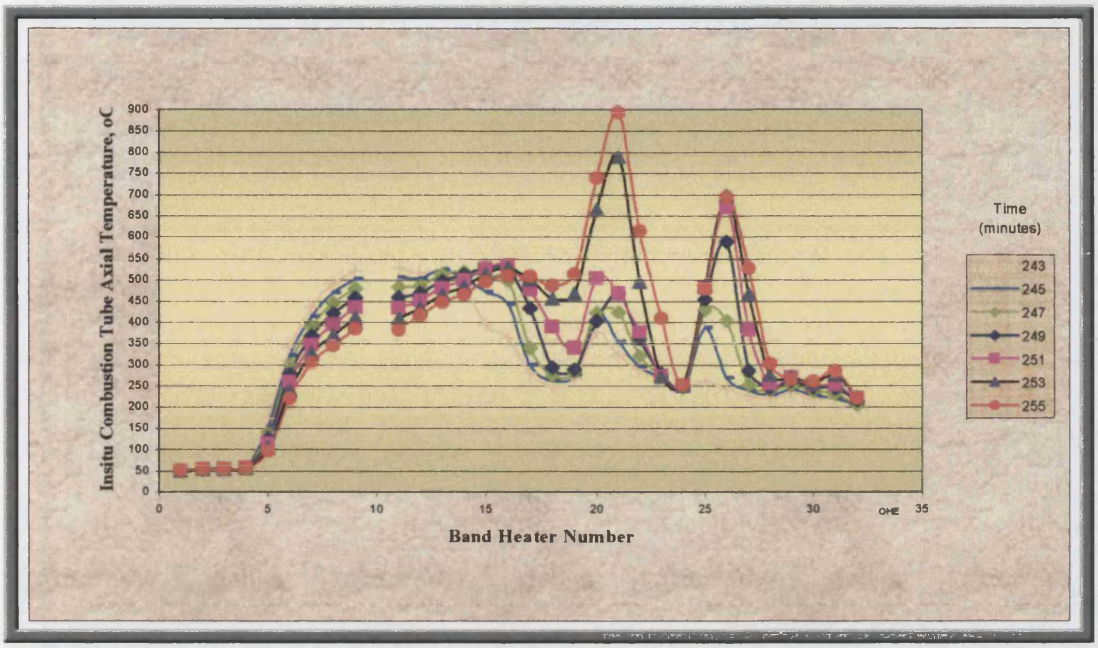

Figure 3 Variation of temperature with position 243 to 255 minutes into Run 4

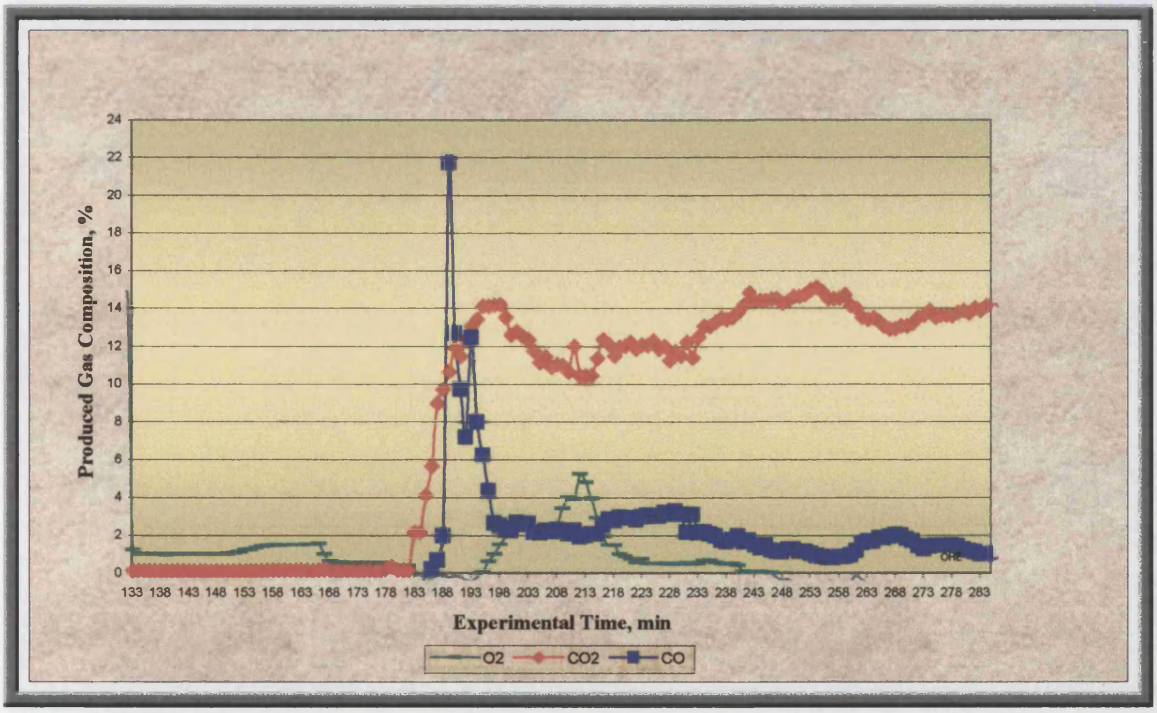

Figure 4 Produced Gas Composition in Run 4

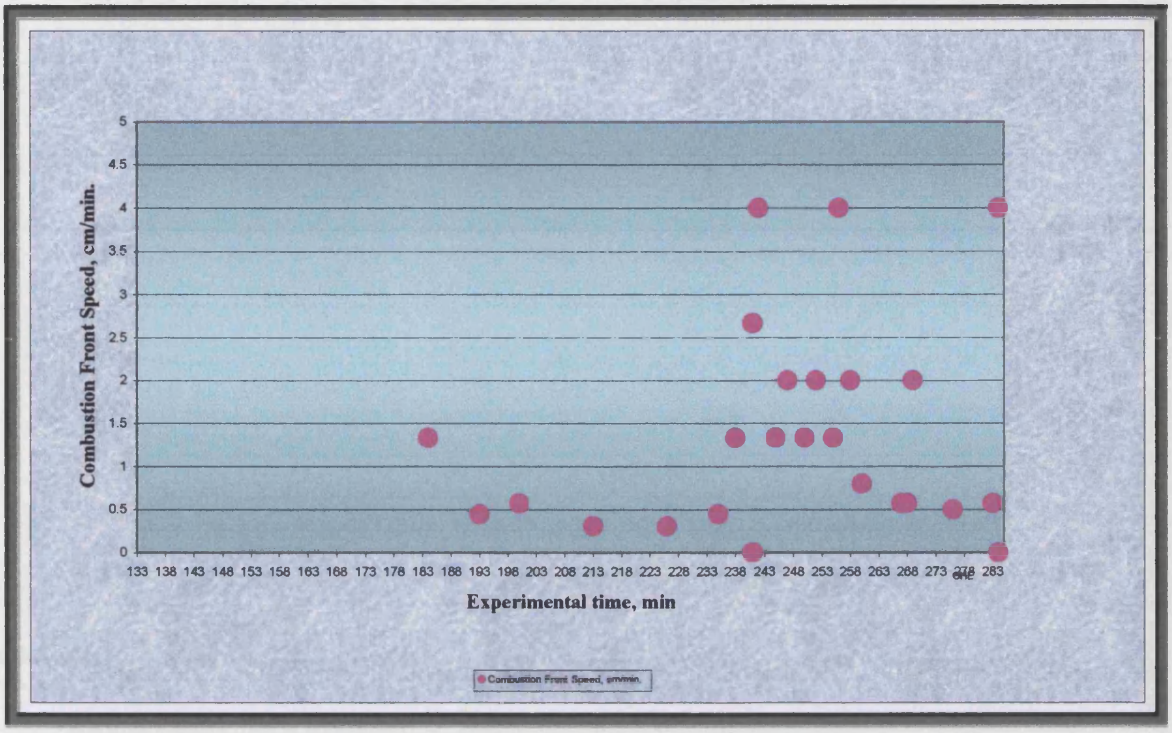

Figure 5 Combustion Front Velocity in Run 4

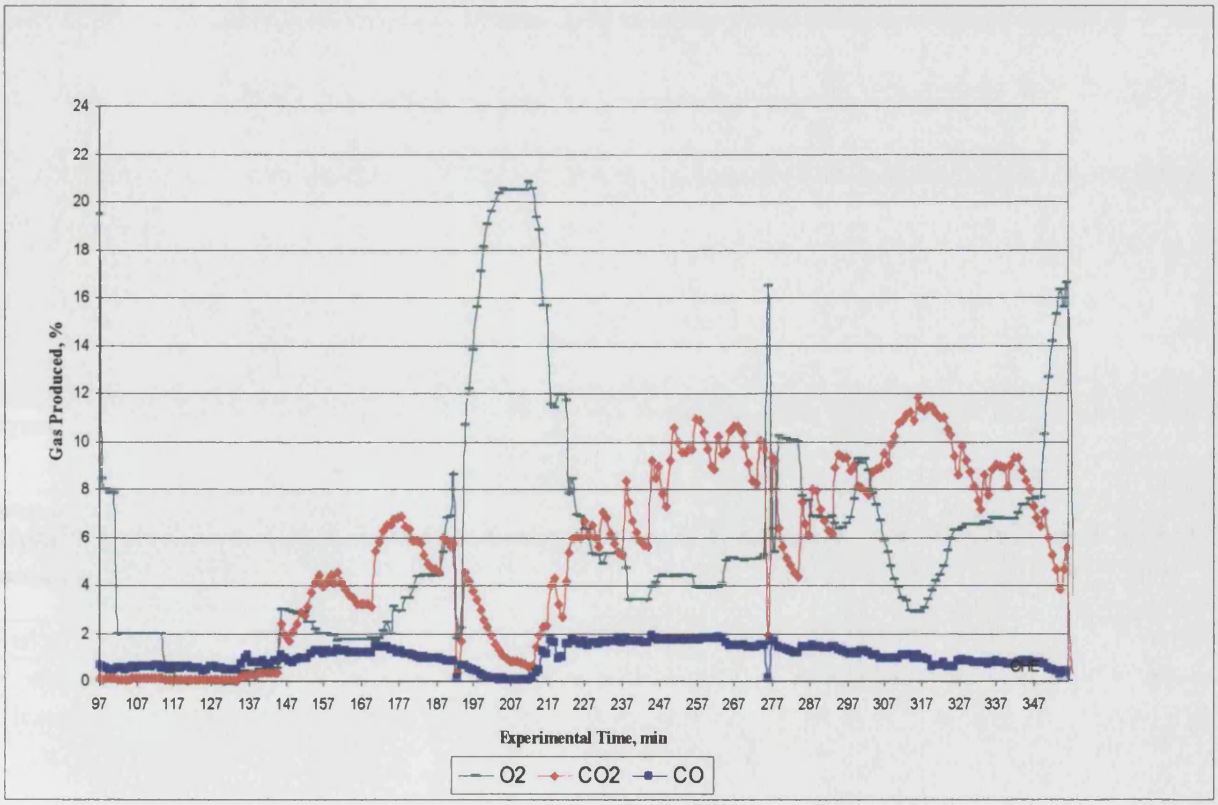

Figure 6 Produced Gas Composition in Run 5

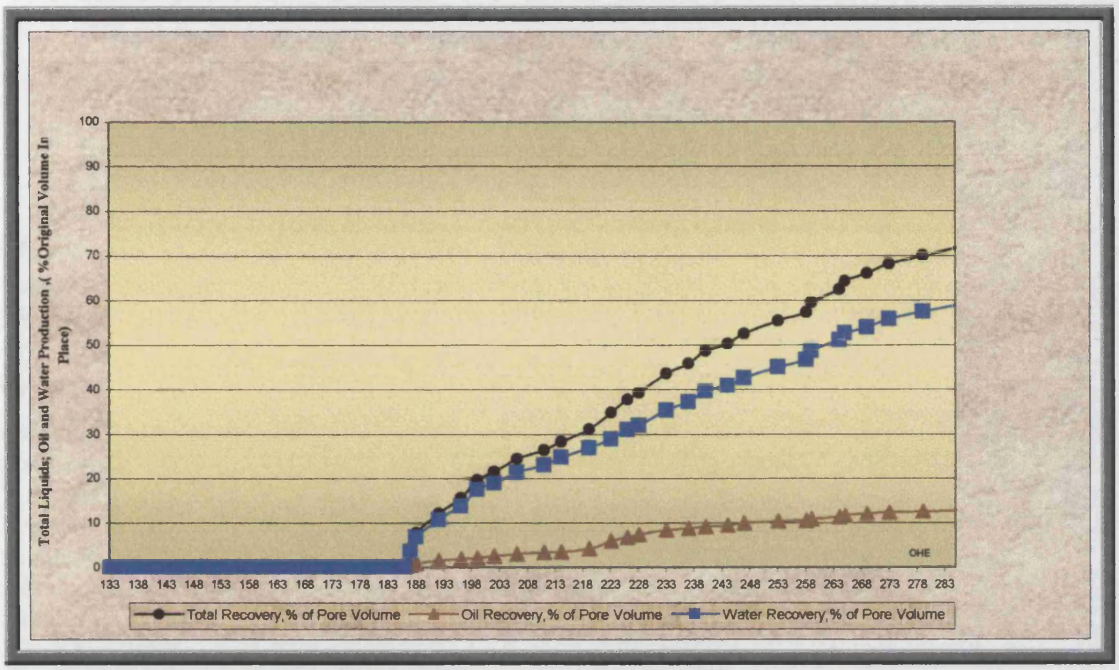

Figure 7 Produced Fluids during Run 4

Figure 8 Post-mortem of Run 4

Condition/Experiment	Run 4	Run 5
Pressure, bar	200	200
Initial Temperature, °C	18-28	18-22
Initial Oil Sat., %	30	27.6
Initial Water Sat., %	70	64.4
Initial Gas Sat., %	-	8.0
Gas rate,m3/m2hr	83.9	30.8 93.8 36.4

Table 1 Experimental Conditions

The 8th Mediterranean Petroleum Conference and Exhibition,
Tripoli, Libya, 20 -22 January, 2004

AIR INJECTION PROCESSES FOR IMPROVED OIL RECOVERY - LIGHT OIL AND HEAVY OIL RESERVOIRS

M. Greaves, T. X. Xia, O. El Ayadi and M. G.A.S El Abidi
Improved Oil Recovery Group, Department of Chemical Engineering, University of Bath, BATH BA2 7AY,England

Abstract

Water flooding can leave more than 30% residual oil, with some areas of the reservoir containing much higher S_{or}'s in tighter zones, or trapped beneath shale lenses. How to access this oil residual? Air injection may be a good candidate and could be operated either in a low temperature oxidation (LTO) mode, at the reservoir temperature, or in a high temperature oxidation mode (HTO), i.e. in-situ combustion. Two high pressure combustion tube tests (200 bar) were performed on a North Sea light crude oil, using MIL (mud industry limestone) to represent the chalk matrix. The residual oil saturation was S_{or} = 30 %, with S_{wr} = 70 %. With such a large amount of water present in the reservoir, an economic recovery process must be capable of mobilizing the residual oil at a high enough rate, without excessive, or prolonged, water production. The air injection flux is a critical parameter, both technically and economically. In one of the tests, sustained propagation of the combustion front was achieved, traversing the full length of the 1.2 m combustion tube. However, the second test, which used a lower air injection flux, did not sustain combustion front propagation. Generally, combustion temperatures were around 450 °C, but some 'high peaks' were observed for short periods. Cumulative oil recoveries varied from 10 % to 70 %, depending on the air flux. *Post mortem* inspection of the combusted matrix showed that it was largely clean, with no residual oil or coke. Some solid inclusions were also found.

One of the most important advances affecting in-situ heavy oil recovery is the advent of horizontal well technology. The integration of reservoir processes and horizontal wells has led to the development of 'short-distance oil displacement processes'. In effect this creates a short-path for oil displacement, since mobilised heavy oil or bitumen 'drains' directly into the horizontal producer well. The distance between he 'active' front and the horizontal well is only a few metres, compared with 100's of metres for conventional displacement. A shortened pathway, compared to conventional displacement processes, and creates significant operational advantages. Heavy oil and bitumens present special difficulties compared to conventional light oil. Principally, this is due to the very high, in-situ oil viscosities, which can vary from a few thousand to millions of mPas. Unless the oil can be mobilised sufficiently, by substantially reducing its in-situ viscosity, the oil recovery efficiency will be seriously eroded. Since heavy oil and bitumens usually contain more than 50% heavy residue, a successful process needs to recover a significant portion of this, preferably with some degree of in-situ upgrading. A new process called THAI – 'Toe-to-Heel Air Injection' [1] is a more advanced variant of conventional in-situ combustion (ISC), but it operates as a short-distance displacement process. Since THAI operates at HTO mode, prompting thermal cracking of heavy residual oil, it can achieve significant in-situ upgrading, which also maximizes oil recovery. The THAI process is now the subject of a pilot development at Christina Lake, Canada (2005). Other 'short-distance oil displacement' processes have also been proposed, including TTHW and TTHS – respectively, 'Toe-to-Heel Waterflood' and 'Toe-to-Heel Steamflood' [2]. Turta et al. [3] provides an overview of 'short-distance displacement processes, classifying them into (i) those with the displacement front quasi-parallel to the horizontal producer and (ii) those with the displacement front quasi-perpendicular to the horizontal producer. This paper will focus on THAI, in which the displacement is quasi-perpendicular to the horizontal producer.

AIR INJECTION FOR LIGHT OIL RESERVOIRS

Introduction

Maturing oil provinces in the North Sea, USA and other areas of the world face diminishing prospects, unless

new techniques are developed in time. In tight, very low permeability reservoirs, gas injection may be the only answer. Where to get sufficient gas to inject? In Western Europe and North America, market forces usually dictate that the hydrocarbon gases are sold. Carbon dioxide is only available from natural sources in a few areas and may frequently require pipelining. The same can be said of flue gas, which will usually require collection. Most IOR (Improved Oil Recovery) methods require the 'Injection of an Expensive Fluid' and the options available for a suitable process in the field tend to reduce sharply. One gas which is cheap, available in large quantities, everywhere, is air. Fassihi *et al.* [4] estimated the economics for small gas injection projects to be approximately $2-4 capital and $3-5 operating expense per barrel of incremental oil produced.

Air injection into light oil reservoirs can be either a secondary or tertiary recovery process. Light oil reservoirs are usually deep enough and therefore at sufficiently high temperature for spontaneous ignition of the oil to occur. This is because the reactivity of the oil increases rapidly with temperature. Yannimaras *et al.* [5] employed accelerating rate calorimeter to determine the exothermicity characteristics of different oils. This provides a type of fingerprint identity for each oil, indicating whether the oil is sufficiently reactive in the LTO region (reservoir temperature up to 250 °C) to autoignite, and whether also, there will be a smooth transition to the in-situ combustion (ISC) region, i.e. HTO of the oil. For a light oil, LTO can be sufficient [6, 7] to create a safe process, i.e. remove all of the oxygen in the injected air by reaction with the oil. As the oxidation zone (LTO) or combustion zone (HTO) moves through the reservoir, stripped HC gases, steam and flue gas (mainly CO_2 and N_2) displace the oil, consuming about 5% to 8% of the oil as fuel. Combustion tube studies are used to determine how much air is required and also whether a self-sustaining, combustion front can be propagated through the reservoir core [8-10]. Although combustion tube experiments mimic the sub-processes, i.e. formation of a steam bank, condensed water and oil bank, and show that only about one-third of the core needs to be swept in order to recover most of the oil. Because they are 1-D and the moving front is artificially stabilized, they cannot provide any useful information on sweep efficiency and scale-up. This requires 3-D experiments [11]. Combustion tube data is also useful for validating reaction kinetic models that need to be incorporated into numerical simulators.

Experimental

The arrangement of the combustion tube facility is shown in **Fig. 1**. The combustion tube is 1.2 m long and 0.1m in diameter. It is surrounded by 32 band heaters. Temperature is measured by an axial probe with a thermocouple at each band heater position. The band heaters may be controlled individually to maintain adiabatic conditions. The combustion tube assembly is contained within a pressure shell to allow operation to 240 bar pressure. The produced fluids are separated and gas flowrate and CO, CO_2, O_2 composition is monitored.

The matrix material used in the runs reported here was MI limestone which was chosen to simulate the chalk matrix in the Ekofisk field and provide sufficient injectivity to operate the combustion tube. The matrix material was premixed with oil and water before packing into the combustion tube. Experimental conditions for both runs are given in **Table 1**. Both tests were operated without bandheater control, so causing significant heat loss.

Run 4 – High Air Flux

This test was run without bandheater (BH) control, i.e non-adiabatically, and therefore represents a pessimistic case compared to the reservoir. Following nitrogen injection and preheating of the inlet section of the core, immediate ignition was achieved at 215 °C (178 minutes) when air injection started. The core temperature increased rapidly to 614 °C (180 minutes) and the combustion front then propagated outwards from the inlet face to reach BH2 location at 184 minutes. The combustion front temperature then steadied at around 450 °C, as shown in **Fig. 2**. Heating of downstream sections of the core occurred due to fluid transport and LTO. This created two secondary fronts at BH20 (213 minutes) and BH 23 (215 minutes), with temperatures between 260 -280°C. During this time the main combustion front became stalled at BH5 for 17 minutes, remaining at 465°C. A new secondary front started at BH20 at 225 minutes. The main combustion front reactivated with a temperature of 450 - 500°C and advanced to the middle of the tube, as shown in **Fig. 3**. Although the secondary fronts were still propagating up to this point, the more dramatic effect subsequently, was the sudden appearance of the two very high temperature peaks. For a light oil, such high temperatures (700 - 900°C) were not anticipated. This high temperature effect was also confirmed by the bluish temper colour of the stainless steel axial thermocouple probe when it was inspected after the test. The leading edge of the

combustion front continued to propagate to the end of the tube at a temperature of 807 °C, when combustion was terminated (285 minutes).

For most of Run 4, the air injection rate was maintained at 10.81 litres/min (82.59 m^3/m^2h), but the rate was reduced to 5.2 litres/min towards the end of the run (272 – 284 minutes). The composition of the produced gas is shown in **Fig. 4**. The high carbon monoxide concentration, initially, is due to LTO, but it falls rapidly as the combustion front becomes more stabilized. The carbon dioxide concentration remains at a high level, around 12 %, or more, throughout the run. When the combustion front stalled for a short period during the early part of the test, the oxygen was not totally consumed, and significant amounts of oxygen were produced. Oxygenated oil, containing free-radicals may have concentrated in the oil in the downstream sections of in the core, causing the high combustion temperatures (see previous section). In the field there would be sufficient residence time for the oxidation reactions to go to completion, so long as the reservoir temperature is high enough (> 90 °C).

Fig. 5 shows the variation of the combustion front velocity during the test. Before the occurrence of the secondary front(s), the velocity is in the range 0.3 – 0.5 cm/min (0.18 – 0.3 m/h). This is to be expected with such high air injection rates in the combustion tube. However, if the injection rate is scaled to reservoir condition, wherein the actual rock permeability is only few mD, compared to 1D (approximately) for the crushed MI limestone, it will be reduced by a large factor. Similarly, the combustion front velocity in a homogeneous reservoir will be of the order of fraction of a m/day, because the air injection flux will be of the order of 1 m^3/m^2h, or less.

Run 5 – Low Air Flux

The objective of this test was to see if combustion could be sustained with a lower air injection flux compared to over 80 m^3/m^2h in Run 4. In the later period of the test, the air flux was increased to 93.8 m^3/m^2h, but this lasted for only about 10 per cent of the total period of air injection. As can be seen in **Fig. 6**, oxygen breakthrough occurs at the production end of the combustion tube soon after ignition, at 119 minutes. However, combustion is not fully established and there is a rapid deterioration in performance leading to severe oxygen breakthrough. The situation was only recovered somewhat by heating the tube to 150 °C. This is entirely artificial, since the reservoir should operate close to adiabatic. Although much improved carbon dioxide levels are achieved, oscillating about the 10 % level, a self-sustained combustion front was never achieved and the produced oxygen levels remained high.

The conclusion to be gained from the two tests combustion tests, is that, in order to propagate a stable combustion front with this light oil, the air injection rate needs to be above a certain minimum value. This figure appears to be correspond to a minimum air injection flux of approximately 40 m^3/m^2h. Because the combustion front velocity was quite high in Run 4, the heat losses in the combustion front region were not sufficient to reduce the reaction intensity significantly. If full-adiabatic control had been employed to minimize heat losses (mimicking the reservoir) the minimum air injection flux required would, actually, be significantly lower than 40 m^3/m^2h.

Oil and Water Production Rates

The final oil recovery from Run 4 was 40 % OOIP, compared to only 9 % OOIP for Run 5. Although Run 5 was far from ideal, it underlines the important effect of air injection rate on the oil recovery. In **Fig. 7**, it is also apparent that, in Run 4, a large amount of water was produced along with the oil. This is to be expected, since the initial amount of water in the core was high at 70 %. The produced water-cut averaged just over 70 % before the oil was contacted by the combustion front (218 minutes), but then decreased down to about 43 % for the remainder of the test. It is important to remember that a 1-D combustion tube result cannot provide any reliable indication as to what the true oil recovery will be in the reservoir. This is because the combustion front is artificially stabilized – the tube was mounted vertically, and air was injected at the top. The combustion tube results (adiabatic preferably) may, however, be used to validate a suitable oil oxidation kinetics model, which can then be employed in a reservoir simulator.

***Post mortem* on Burned Core**

After each test, the combustion tube and its contents were allowed to cool down to room temperature. The combustion tube was then placed in a horizontal position and the top flange plate was removed. A *post mortem* inspection of the burned MIL matrix was performed by carefully removing small quantities each time. In Run 4, virtually the entire MIL core had been swept by the combustion front. Consequently, the burned matrix was essentially clean, having a whitish appearance and loose structure. However, there were also some inclusions

found at different distances along the tube. Pieces of hard material, or agglomerate, a few centimeters in size, were discovered 0.2 m along the MIL core, near to the wall. They contained interconnecting holes and some areas of the surface had a greenish colour, suggesting that the MIL may have been attacked by acidic. Approximately three-quarters distance along the tube (0.75 m), an unusual piece of material was found (**Fig. 8**). It was similar in appearance to a Conche shell, some 4 cm long. The outer shell was probably calcined material (calcite), due to the high combustion temperatures during that period (>800 °C). Another possible explanation for the disappearance of the interior is dissolution of the carbonate matrix by organic acids formed during LTO of the oil when the main combustion front became stalled.

In Run 5, the MIL was mainly of whitish appearance for about one-third of the core, reflecting that it had been contacted by the combustion front. However, from the early stages of air injection the matrix shows unburned areas near the wall. The dark, unburned, or partially combusted areas increase across the core until, at 0.36 m from the top, it extends to approximately 80 %. There was also coke deposited at 0.42 m distance. At 0.72 m, a hardened, shell-like agglomerate was discovered. It was surrounded by coke and the interior may have been dissolved by organic acid, as in Run 4.

HEAVY OIL RECOVERY AND UPGRADING USING THAI

Introduction

In-situ combustion (ISC) was conceived out of high theoretical promise, and because the process generated its own energy via reactions between the oil and injected oxygen (compressed air), the reaction heat, at high temperature, would efficiently mobilise the heavy oil. The theoretical aspects are well-discussed in Burger's et al. book [12]. The original ISC concept was developed over 50 years ago. The idea was to start a combustion front in the reservoir, either spontaneously, or by using some form of downhole burner, electrical device, or chemical oxidant, and then to propagate the front from one well to another. The well configuration used was VIVP (vertical injector-vertical producer), before the advent of horizontal well technology. In principle, the ISC process operates by burning a small fraction of the oil, around 10 wt% typically, and producing the rest. It should, conceptually, be applicable for oils having an in-situ viscosity greater than about 100 mPas, but extending all the way up to heavy oil and tar sands bitumens - if adequate gas communication can be established. By virtue of the high temperature cracking, or bond scission reactions, substantial upgrading of the oil should also occur. As shown in **Fig. 9**, mobilised oil and gases ahead of the combustion front necessarily have to flow through the cold oil region downstream, in order to reach the production well. This gives rise to many operational difficulties, which have plagued conventional ISC heavy oil operations. Despite more than 130 field operations worldwide, during the 1960's and early1980's, conventional ISC failed to gain general acceptance due to many apparent failures. In some cases, this was often due to poor choice of reservoir, but one of the main reasons was poor control of the process. These experiences are extensively documented in the NIPER Conference volume [13].

The operational reality in the field is shown schematically in **Fig. 9**. The most significant operational problems affecting recovery from heavy oil reservoirs, using conventional well patterns, are the following:

(1) gravity segregation, i.e. gas overriding, due to the difference between the oil and gas densities
(2) gas channelling, due to unfavourable reservoir heterogeneity
(3) unfavourable mobility ratio
(4) tendency to slip into LTO (low temperature oxidation) mode

Reservoir engineers also tended to view results obtained from 1-D combustion tube tests perhaps too optimistically. Infact, logic dictates that this type of test is far from reality, because it is idealised by the constrained flow path and forced stability. Which of the above problems is the most serious? It depends on the particular reservoir, but in practice they are all serious. Severe gas overriding, unless controlled (how?), will rapidly lead to gas breakthrough at the production wells, and may also cause burn-out of the well, or even an explosion. The ISC process suffers from severe adverse mobility ratio, typically of the order of 100's or 10,000's, depending on the oil viscosity. So, large frontal instabilities will lead to gas channelling, becoming more severe if the reservoir heterogeneity is unfavourable, especially towards the top of the oil layer. There is a universal consensus now, that ISC must be operated in a vigorous HTO mode. This means that the temperature of the combustion front should be above about 450 °C. Moore *et al.* [14-16] has commented

extensively on this critical aspect of the process. Inability to ensure that there is sufficient oxygen flux reaching the combustion front guarantees that the process will lock into an LTO mode from which it is very difficult, or impossible, to recover. One of the main reasons why conventional ISC fails to sustain vigorous HTO is that the process needs to maintain gas communication over the full-extent of the reservoir, because it is long-distance displacement. Inevitably, therefore, exposure to the full geological-effect of the reservoir creates complexity, but this is not peculiar to ISC. Any process that operates as long-distance displacement, and that includes virtually all normal conventional oil recovery processes, will suffer, because it is at the mercy of the reservoir geology. For example, banking of fluids in the cold regions ahead of the combustion front, or emulsion blocking, spells disaster for ISC, because it reduces the gas injectivity. Inevitably, this leads to the process becoming locked in a downward spiral from which it may be impossible to recover. Thus, there are too many inherent problems with conventional ISC, as applied to heavy oil reservoirs, to warrant much serious interest – except for the 'ideal reservoir'!

A new ISC process is therefore required, which avoids all of the above major operational difficulties and is also stable and robust. A new heavy oil recovery process will also be required to extend the horizon beyond that reached by SAGD (Steam Assisted Gravity Drainage) and VAPEX (Vapour Extraction).

THAI – 'Toe –to-Heel Air Injection'

Short-distance Displacement

The application of horizontal well technology, as far as ISC was concerned, some 15 years ago, appeared to be a 'wild chance'. At the time, the technology was beginning to demonstrate a measure of (claimed) success for thermal heavy oil operations, but more especially, it was more about the future potential of SAGD. It was very uncertain, therefore, whether the application of horizontal wells for ISC could have any possible benefits. Even more critical, whether a 'new process' could possibly work at all.

The essence of short-distance oil displacement processes is depicted in **Fig. 10**. Unlike conventional oil processes, which use a standard well pattern (usually with vertical wells), the pathway for oil displacement in short-distance oil displacement processes (SAGD, VAPEX, THAI) is quite different. The mobilized fluids do not have to displace through the cold (high viscosity) oil region, as it would in the conventional ISC process (long-distance displacement), but instead, it takes the shortest pathway to the horizontal producer in the lower part of the oil layer.

Early Research and Process Stability

Research on an integrated ISC-Horizontal Wells process was first initiated by the Improved Oil Recovery Group at Bath University in 1988-89. ISC experiments were conducted in a low pressure, rectangular combustion cell, measuring 0.4m × 0.4m × 0.1m (later experiments used a 0.6 m long cell). A 3-D geometry was chosen in order to capture the essential flow behaviour around the horizontal producer well, which was located in the bottom of the oil layer. The initial experiments [17, 18] were very successful, insofar as the combustion front could be propagated along the length of the combustion cell, achieving very respectable oil recoveries of around 50-60 % OOIP. In the succeeding years, more than fifty 3-D combustion cell experiments were performed, using a variety of heavy oils, including Athabasca Tar Sands bitumen, and also medium heavy oil. All of these experiments were successful. Specifically, there was never any occurrence of oxygen breakthrough at the production well, broadly confirming that the process was stable.

During the early research phases, much emphasis was placed on the role of the cold oil layer, existing ahead of the combustion front. In **Fig. 11**, it is quite clear from the areal temperature profiles in the sandpack, that the temperature some distance ahead of the combustion front is much lower than in the upstream regions. That this can occur, even after 6 hours of operation, is quite remarkable. The explanation is basically that the oil region downstream of the combustion zone is relatively immobile, and does not readily drain into the HP. Because the oil viscosity in this colder region is very high, it prevents any gas communicating/displacing through it. This is exactly the opposite of what happens in the old conventional ISC process. Of course, the cold oil also serves to provide a seal around part of the perforated HW. However, this is not a convincing argument for complete stability of the process.

It was quite evident that the air injection rate, or flux, was a critical factor influencing the stability of the process, as it is in conventional ISC. Stability of the ISC process is defined as the ability to propagate a high temperature combustion front in a steady, stable manner,

so that most, or all of the oxygen in the injected air is consumed in the process. The ISC process is self-sustaining, so long as the supply of compressed air is not interrupted. If the process is maintained in a HTO mode (> 450 °C), then the heavy residue left behind from the distillation process, is thermally cracked, and a coke-like material is deposited onto the surface of the reservoir sand. This coke is the fuel which sustains the process.

Another feature present in the vertical plane temperature profiles in **Fig. 11** is a condition called 'Controlled Gas Override'. It is evident that the shape of the temperature profile in the vicinity of the combustion front (~500 °C) is more or less constant. The front is more advanced in the top part of the sandpack, but it does not accelerate ahead and create uncontrolled gas overriding. This is an important stabilising feature for the new 'Air Injection-Horizontal Wells' process. It is clear that, in addition to any gravity stabilising effect, there must also be a forced flow into the HW, to counter the gas buoyancy.

One aspect of the process which remained of continuing concern to the reservoir engineering community was - 'How was it possible that oxygen (injected air) did not bypass directly into the toe of the horizontal producer, and breakthrough at the production well?' This was especially intriguing, because the toe of the HW is offset slightly (about 0.05 m) from the line of the vertical injector. Infact, in the earliest experiments, the VI was placed in the middle of the oil layer and still the oxygen did not breakthrough! Hence, although all of the experimental evidence indicated that the new ISC-Horizontal Wells process was stable, the precise mechanism governing the overall stability was not well understood. New experimental evidence for the stabilizing mechanism was discovered recently [18], and will be discussed later.

THAI Process

THAI is an integrated reservoir-horizontal wells process, which uses air injection to propagate a combustion front from the toe-position of the horizontal producer to the heel of the production well. **Fig 12** is a schematic representation of the salient features of the process. Air is injected in the top part of the reservoir, either in direct line drive (VIHP), denoting a single vertical injector and a single horizontal producer, or staggered line drive (2VIHP), wherein two vertical injectors are placed at an offset position with respect to the HP, in the top corners of the section. The HP is placed low in the oil layer, so that the toe is offset from the line of the vertical injector. In the experimental combustion cell this was 0.05 m, but it may scale to about 10 to 15 m in an actual reservoir. The combustion front is shown tilted, i.e. quasi-vertical, although, as mentioned previously, the experiments actually show it to be a composite profile, so that it is more advanced in the top part of the oil layer. There is a temperature gradient across the oil layer, so that the temperature of the combustion front nearer to the HP is 100-150 °C lower that it is at the top. Ahead of the combustion front is the coke zone, where the heaviest residue fractions undergo thermal cracking. This extends through to the MOZ (mobile oil zone). The width of the MOZ extends possible as far as the draining interface, defining the boundary between the upstream MOZ and the downstream 'cold', immobile oil region. The detailed dynamics of the MOZ are very complex and not well understood. However, it is a very important part of the process. Firstly, it is where the precursor processes to coke formation occur and secondly, and most importantly, it is the region which determines oil productivity. If there is a cold, immobile oil region (Cold Heavy Oil), as the experimental temperature profiles suggest (**Fig. 11**), then ahead of the combustion front there is only a finite zone from which oil can be produced. This is the MOZ, or the open 'active' section of the HP. This open-section of the HP is approximately 20 to 30% of the total well length. Therefore, if THAI is to achieve the same, or higher, well productivities, compared say to SAGD, the flow of mobilized oil though the MOZ into the open-section of the HP must be high. This is possible, depending on the pressure draw-down in the well, but also because of the high temperature in this zone. At around 500 °C, the oil viscosity will be very low, and lower still because the oil draining into it has been thermally cracked to a lighter oil. Typically, the oil recovery in the 3-D THAI experiments is about **80 % OOIP**, and may as high as 85 % OOIP. This is principally due to the very efficient thermal sweep of the hot gases ahead of the combustion front, approaching nearly 100% of the sandpack.

Stability of THAI

During startup, it is very important that high temperature ignition is achieved, at least 500 °C (**Fig. 13**). This is necessary to ensure that during the startup period, the oxygen utilization is high and combustion also takes place at high temperatures, in the top part of the oil layer. While the combustion zone is growing in size and expanding downwards, high combustion temperatures (450 – 600 °C) ensure that the rate of oxidation is rapid and the injected oxygen is completely consumed.

Therefore, during this period, hot combustion gases flow directly into the toe of the HP, but the gas contains virtually no oxygen. Hence, bypassing of oxygen directly into the toe of the HP does not occur. After the combustion front has propagated beyond the toe-position, it becomes 'anchored' onto the HP. The stability of the THAI process then depends on two key factors: (1) a high temperature burning zone, which is more advanced in the top part of the oil layer, exhibiting controlled (stable) gas override behaviour, and (2) deposition of coke, or heavy residue, inside the HP. The coke which is deposited inside the HP acts as a gas seal.

It is postulated that the heavy residue, or coke, prevents air (oxygen) channelling from behind the combustion front, through to the toe of the HP. A test (Run 2002-03) was stopped half-way, and after allowing the sandpack to cool down, the HP was removed and cut-open, as shown in **Fig. 14**. The photograph shows that there is a very substantial coke deposit about 3.5 cm long formed inside the HP. The deposit is formed ahead of the combustion front, at a temperature of 400 - 450°C, which is sufficient to form coke. Coke formation in the HP is a dynamic process, continuously forming ahead of the front and then being burned-off behind as the combustion front approaches nearer to the HP. The process continues right up the production end of the HP, but precautions may have been taken in the field before this situation is reached. The process of coke deposition in the HP has also been predicted using the STARS reservoir simulator (Computer Modelling Group) [19].

In-Situ Upgrading

THAI achieves very high oil recoveries, greater than 80 % OOIP (primary or secondary), and also very significant in-situ upgrading. This is due to extensive thermal cracking of the large heavy oil molecules as the oil contacts the hot reservoir matrix in the coke and MOZ. The cracking surface is provided by the reservoir clays, such as kaolinite and illite. The trend shown in **Fig. 15** is typical for a heavy crude oil (Wolf Lake) having an API gravity of 10.5 [20]. The upgrading effect seen at the start of the test is an artefact of the startup-ignition procedure, but as the combustion front begins to propagate outwards, away from the ignition zone, the API gravity falls slightly due to dilution with original crude oil. This effect depends on the offset of the toe of the HW, and the full-effect of the THAI process does not occur until the combustion front becomes 'anchored' onto the HP. Thereafter, the trend of downhole upgrading (thermal) is on a continuously upwards trend. The average upgrading achieved is about 6-7 API points, reaching a maximum API gravity of nearly 18 °API. There is not much difference between dry and wet combustion, except towards the end of the experiment. The region of higher upgrading corresponds to the period of water injection, and may have benefited from production of hydrogen via the water-gas shift reaction. It is postulated that part of the upgrading is due to transfer of hydrogen from larger molecules having side branches, creating an upgraded oil which is rich in saturates [20]. The viscosity of the upgraded oil is in the region of 50 mPas, but as low as 10 – 20 mPas. Further downhole upgrading can be achieved if a catalyst is used. This modification of the THAI process is called CAPRI. In CAPRI, a standard refinery catalyst is gravel-packed around the HP, forming what is in effect a 'radial inflow reactor'. The reservoir provides the reactor 'for free'.

CONCLUDING REMARKS

Air Injection into Light Oil Reservoirs

1. Comparing the combustion performance of Run 4 (high flux) against Run 5 (low flux) indicates that for the light crude oil, there is a minimum air injection rate needed to sustain propagation of a stable combustion front. This corresponded to an air injection flux of about 40 Sm^3/m^2h, when no band heater compensation was applied (non-adiabatic operation).
2. Stable in situ combustion was achieved at combustion temperatures of 450 °C. There were also short periods of very high combustion temperatures (>800 °), because more fuel was produced (locally) in downstream sections of the core. This was caused by LTO of the oil, arising from temporary stalling of the main combustion front.
3. The appearance of the burned MIL matrix from Run 4 (high flux) was white in colour with no residue or coke. Therefore, virtually allof the core had been contacted by the combustion front. A hard, calcited shell-like agglomerate was discovered at a distance of 0.75 m from the top of the core. The interior of the agglomerate was dissolved away, possibly due to the formation of organic acids (LTO condition) and also because of carbonate decomposition at the high combustion temperatures (HTO condition).
4. Oil recovery was strongly affected by the air injection rate, varing from 40% OOIP at high flux in Run 4 to only 9 % OOIP at low flux in Run 5.

Heavy Oil Recovery and Upgrading using THAI

1. Short-distance oil displacement processes provide a pathway for success for heavy oil recovery, as exemplified by the success of SAGD. The THAI process provides an additional route to higher recovery and also substantial in-situ upgrading for heavy oil and bitumens.
2. THAI is a stable and robust in-situ combustion process, as defined by the absence of oxygen breakthrough at the production well and no tendency for severe gas overriding.
3. During startup of THAI, the maintenance of an expanding, high temperature combustion zone and the existence of a 'controlled gas override' condition ensure overall stability and combustion gases flow directly into the toe of the horizontal producer.
4. Coke is deposited inside the HP when the temperature near the producer reaches 400- 450 °C, sufficient to thermally crack heavy residue which has drained through. The coke provides a gas seal, so that injected air cannot bypass into the toe. The formation of coke inside the HP is a dynamic process, occurring ahead of the combustion front and then being burn-off behind it.
5. THAI uniquely achieves substantial in situ upgrading of heavy oil and bitumen via thermal cracking and possible molecular transfer of hydrogen to produce an upgraded oil rich in saturates.

REFERENCES

1. Xia T X, Greaves M., Turta A T, and Ayasse C.: "THAI – A 'Short-Distance Displacement' In Situ Combustion Process for the Recovery and Upgrading of Heavy Oil", *Trans. IChemE,* (2003) *March*, 81(A) pp295-304
2. Turta A. T, and Singhal A. K.: "Overview of Short-Distance Oil Displacement Processes", SPE 66791, Canadian International Petroleum Conference, Calgary, Canada, June 8-10, 2002.
3. Xia T. X. and Greaves, M.: "Upgrading Athabasca Tar Sand Using Toe-to-Heel Air Injection", *J. Can. Pet. Tech.*, (2002) **41**, No. 8, 51-57.
4. Fassihi M. R., Yannimaras D.V., Westfail E.E. and Gilham T.H., "Economics of Light Oil Air Injection", SPE Paper No. 36393, March 1996.
5. Yannimaras D.V. and Tiffin D.L, "Screening of Oils for In-Situ Combustion at Reservoir Conditions by Accelerating Rate Calorimetry", SPERE, February 1995, pp 36-39.
6. Ren R. S., Greaves M. and Rathbone, R. R., "Oxidation Kinetics of North Sea Light Crude Oils", Trans IChemE, Vol 77, Part A, 1999, pp 385-394.
7. Ren S.R., Greaves M. and Rathbone, R. R., "Air Injection LTO Process: An IOR Technique for Light Oil Reservoirs", SPE Journal, March 2002, pp 90-99.
8. Tiffen D.L. and Yannimaras D.V., "High Pressure Combustion Tube Performance of Light Oils", 8th European Symposium on IOR, Vienna, Austria, May 15-17, 1995.
9. Greaves M., Young T J, El-Usta, S., Rathbone R.R., Ren, S. R. and Xia, T. X., "Air Injection into Light and Medium Heavy Oil Reservoirs", Trans IChemE, Vol 78, Part A, 2000, pp 721-730.
10. Juan E.S., Sanchez A., del Monte A., Moore R.G., Mehta S.A. and Ursenbach M.G., "Laboratory Screening of Air Injection-Based IOR in Two Waterflooded Light Oil Reservoirs", Paper 2003-215: The Petroleum Society's Canadian International Petroleum Conference, Calgary, Canada, June 10-12,2003.
11. Wilson A, Shallcross D.C. and Greaves M, "Three-Dimensional Studies of In-Situ Combustion Process with Reservoir Heterogeneities", INSITU, Vol 24, No. 4, 2000, pp 251-276.
12. Burger J G, Sourieau P and Combarnous M.: "Thermal Methods of Oil Recovery", Institut Francais du Petrole Publications (1985).
13. Sarathi P, and Olsen D.: "Field Application of In-Situ Combustion – Past Performance and/Future Application", NIPER/BDM – 0086, BDM-Oklahoma, Inc., NIPER, Bartlesville, OK, USA, Jan. 1999.
14. Moore R. G, Laureshen C J, Mehta S. A. and Ursenbach M. G.: "Observations and Design Considerations for In Situ Combustion Projects", *J. Can. Pet. Tech.*, (1999) **38**, No. 13, 97-100
15. Moore R. G , Laureshen C J, Mehta S A and Ursenbach M G.. "Air Injection Recovery of Cold Produced Heavy Oil Reservoirs", Paper 2001-018, Canadian International Petroleum Conference, Calgary, Canada, 12-14 June, (2001)
16. Moore R. G, Mehta S A and Laureshen C J.: "Air Injection for Oil Recovery", *J. Can. Pet. Tech.*, (2002) **41** No. 6, 16-19.
17. Greaves M. and Tuwil A. A.: "Horizontal Producer Wells in In-Situ Combustion Processes", CM/AOSTRA Technical Conference, Banff, Canada, April (1991).
18. Greaves M, Tuwil A. A. and Bagci A. S.: "Horizontal Producer Wells in In-Situ Combustion Processes", *J. Can. Pet. Tech.*, (1993) **34**, No. 4, 58-67.
19. Xia T. X, Greaves M. and Turta A.: "Main Mechanism for Stability of THAI –'Toe-to- Heel Air Injection', Paper 2003-30, Canadian International Petroleum Conference, Calgary, Canada, 10-12 June (2003).
20. Xia T. X. and Greaves M.: "3D Physical Model Studies of Downhole Catalytic Upgrading of Wolf Lake Heavy Oil Using THAI", *J. Can. Pet. Tech.*, (2002) **42**, No. 8, 58-64.

ACKNOWLEDGEMENTS

The authors are grateful to the Joint Management Committee of the AIROIL Project for permission to publish the results contained in this paper. We are also grateful to the European Community for supporting the research via Contract No. NNE5/1999/20071, under the RTD and Demonstration activity on "Energy, Environment and Sustainable Development – Part B Energy Program". We would like to thank the Engineering and Physical Sciences Research Council (EPSRC), United Kingdom, for supporting the THAI and CAPRI research at the University of Bath, via Research Grants: GL/L71773 and GR/M93017.

O. El Ayadi is grateful to the Libyan Education Ministry for funding his PhD studies at the University of Bath and similarly, M. El Abidi gratefully acknowledges support from Veba Oil Company, whilst studying for his MPhil degree.

Table 1 Experimental Conditions of Combustion Tube Tests

Condition/Experiment	Run 4	Run 5
Pressure, bar	200	200
Initial Temperature, °C	18-28	18-22
Initial Oil Sat., %	30	27.6
Initial Water Sat., %	70	64.4
Initial Gas Sat., %	-	8.0
Gas rate,m3/m2hr	83.9	30.8 93.8 36.4

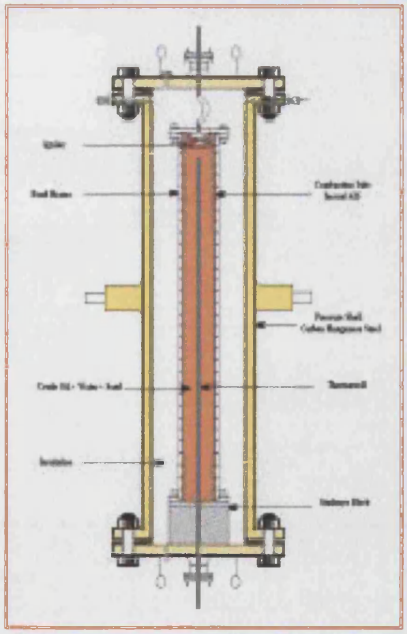

Figure 1 Combustion Tube Schematic

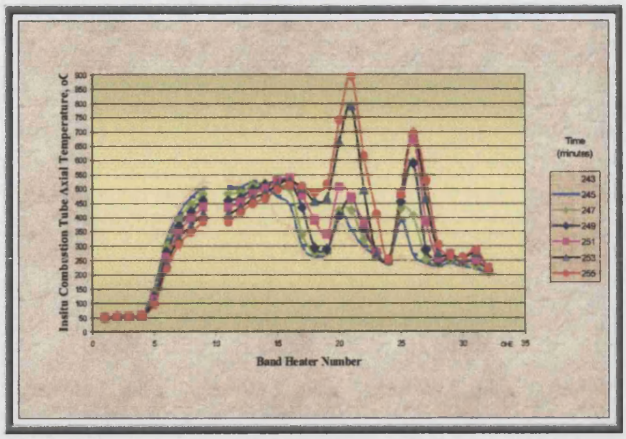

Figure 2 Temperatures near the top of the combustion tube during Run 4

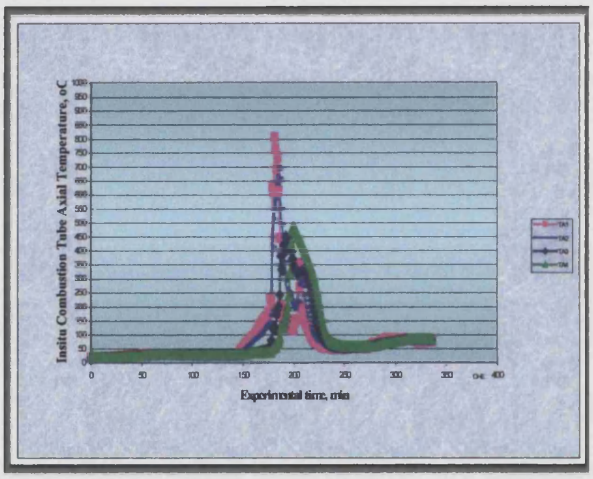

Figure 3 Variation of temperature with position 243 to 255 minutes into Run 4

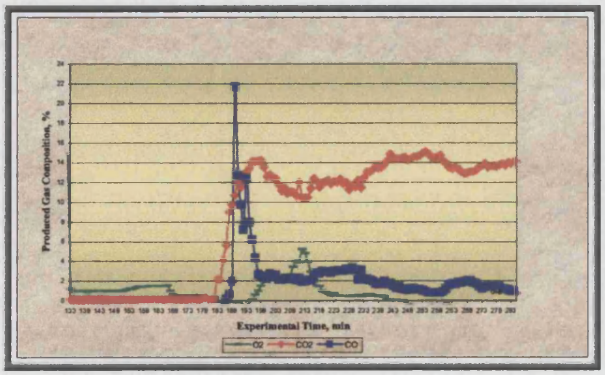

Figure 4 Produced Gas Composition in Run 4

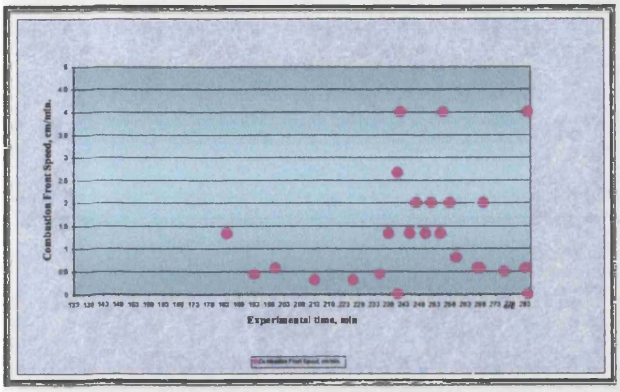

Figure 5 Combustion Front Velocity in Run 4

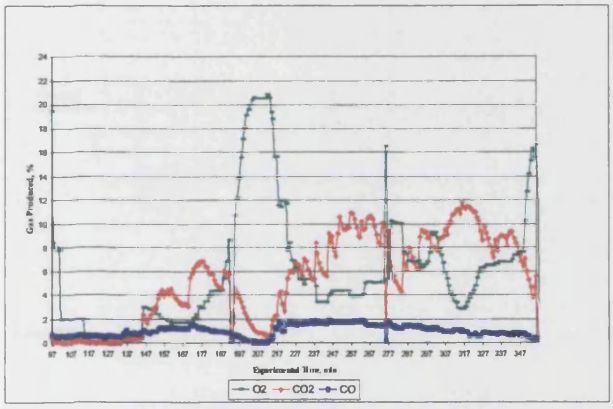

Figure 6 Produced Gas Compositions in Run 5

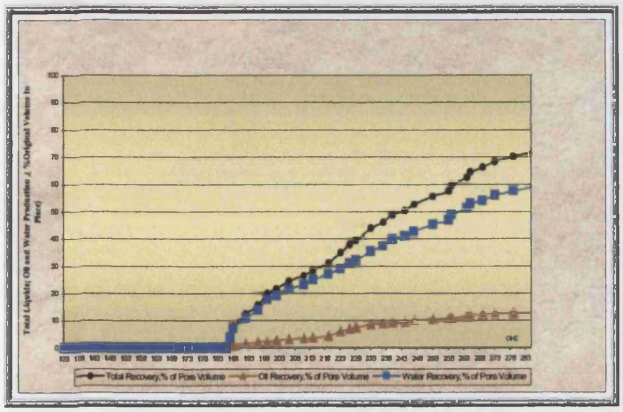

Figure 7 Produced Fluids during Run 4

Figure 8 Post-mortem of Run 4

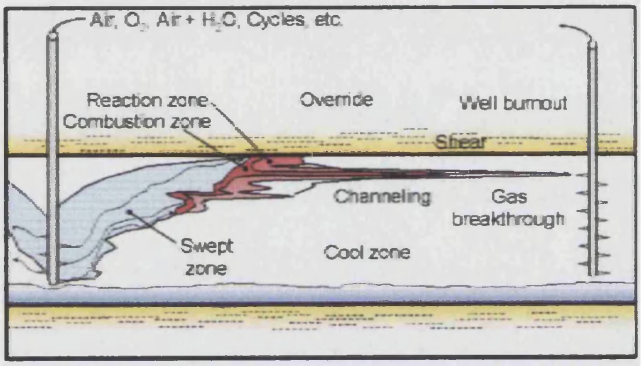

Figure 9 The reality of Conventional ISC Process (Courtesy Prof. M. Dusseault)

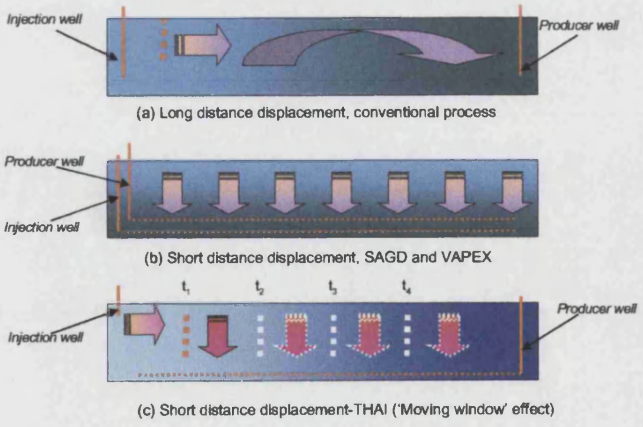

Figure 10 Long-distance and Short-distance Displacement Processes

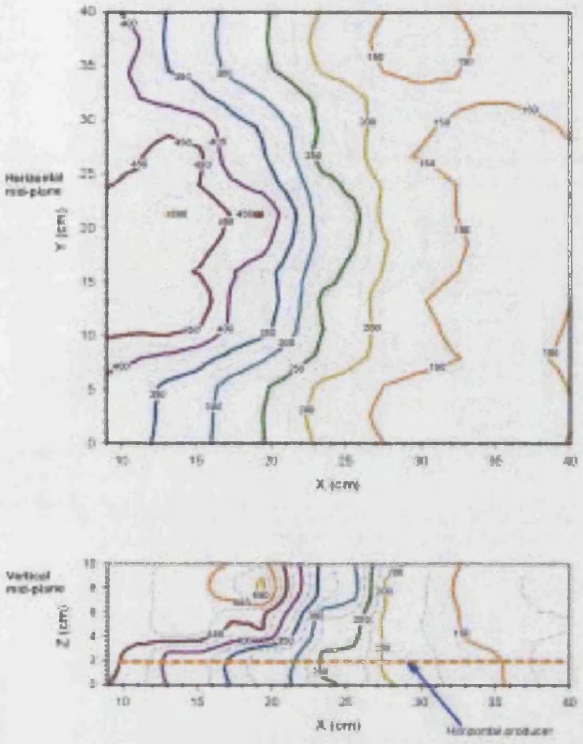

Figure 11. Typical 3-D Temperature Profiles (t = 6 hrs)

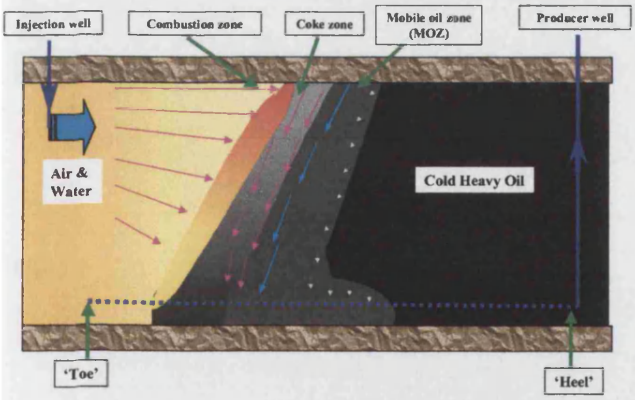

Figure 12. THAI – 'Toe-to-Heel Air Injection' Process

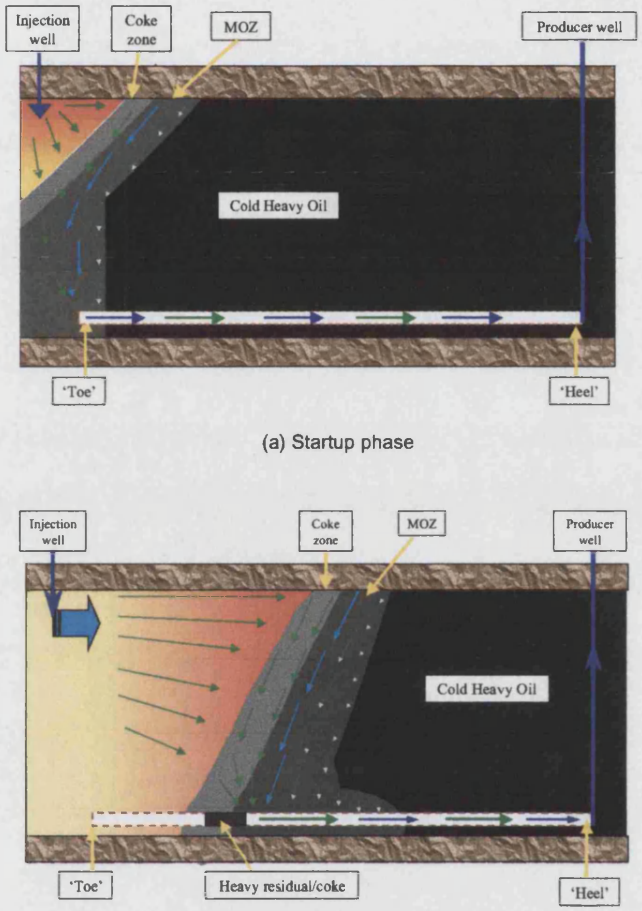

Figure 13. THAI: Startup and Stabilized Operating Periods

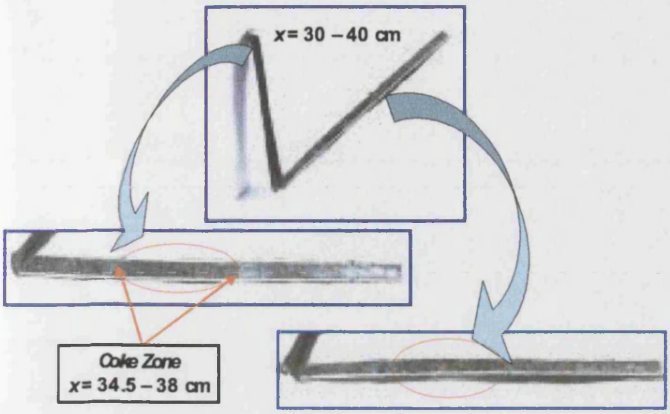

Figure 14. 3-D THAI Experiment: Post-mortem Pictures of Coke Deposition in the Horizontal Producer (Run 2002-03, Wolf Lake heavy oil)

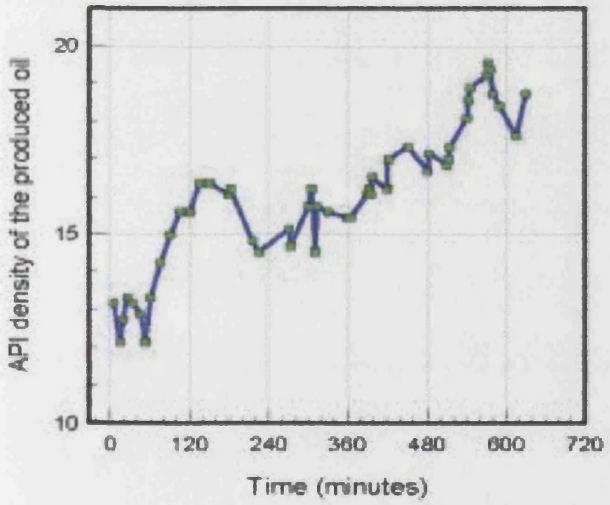

Figure 15. THAI: Heavy Oil Upgrading